High frequency linear friction welding

by

Achilles Vairis

A thesis submitted to the University of Bristol in accordance with the requirements of the degree of Doctor of Philosophy in the Department of Mechanical Engineering in the Faculty of Engineering,

October 1997

Abstract

Linear friction welding is a solid state process for joining materials together through intimate contact of a plasticised interface, which is generated by frictional heat produced as one component is moved under pressure in a direct reciprocating mode relative to another.

The main objective of this research was to explore the frequency range below 120 Hz in linear friction welding of Ti 6Al 4V and guide industry towards design of linear friction welding machines. The effects of frequency and amplitude of oscillation, friction and forging pressure, were studied using a welder purposely built.

Linear friction welding is a self-regulating process. Successful welds depend on process parameters and show appreciable extrusion of plastic matter, while unsuccessful attempts demonstrated a different extrusion behaviour. It was found that the minimum power required to achieve welding conditions increases with frequency due to the strain rate sensitivity of Ti 6Al 4V. Forging at the end of the process can help to produce joints when the energy input is lower than required, although it does not improve weld quality. The impact strength of the welds depends on the size of the heat affected zone and low friction pressures are beneficial to weld integrity.

A two-dimensional finite element model was employed to simulate the early stages of the process. It used coefficient of friction data from frictional behaviour experiments. Results agreed qualitatively with experiments on the increased need for power required at higher frequencies, and quantitatively for temperature and stress conditions at the first phase of the process. The model revealed the interface conditions favourable to welding and provided explanation to the extrusion patterns observed.

A heat flow model was used to predict the temperature pattern of the early stages of the process. The strain rate distribution across the heat affected zone was estimated in a material flow model with a series of kinematically admissible velocity equations describing the material flow fields.

Στους γονείς μου, Αλέκο και Ιωάννα

Acknowledgements

I would like to thank the following :

Dr.Martin Frost for his enthusiastic supervision. He has been a source of much support and guidance for which I am truly grateful and for accepting the unenviable task to review this manuscript.

The Commission of the European Communities for the support provided in the form of a Research Fellowship within the Human Capital Mobility Programme.

The University of Bristol for providing laboratory facilities.

Members of the workshop of the Mechanical Engineering Department who helped in the experimental work of this thesis.

Celia Hollingworth for looking at the English of this thesis and being a good friend.

Dr.Nasos Mitropoulos for the very interesting discussions all these years, and Yianna Euthikrati for being good friends.

Dr.George Tsoulos and Dr.Georgia Athanassiadou for being good friends all these years in Bristol.

Vangelis Karachalios for his never-ending enthusiasm and being a good friend.

Marialena Trivella for her statistics knowledge, her excellent meals and being a good friend.

Mileva Radonjic and Dave Baker for their materials information, and Tim Parker for his TEX assistance.

I am extremely grateful to my mother for her continuous and unconditional support.

Author's Declaration

This thesis, submitted for the degree of Doctor of Philosophy at the University of Bristol, is entirely the work of the author. No work is the result of collaboration, nor is any work of other researcher used, except were clearly referenced.

The views and opinions expressed in this thesis are solely those of the author and not the University of Bristol.

A.Vairis

October 1997

Contents

List of Figures

List of Tables

Nomenclature

Roman notations :

a	Constant
a_1, a_2 ,a_3, a_4	Specific heat model coefficients
A	Process parameter (frictional behaviour model)
B	Stress exponent (frictional behaviour model)
c	Specific heat
C	Temperature exponent (frictional behaviour model)
d	Distance of pin attached to the load cell plate from centre of rotation
erfc	Error function complementary
E	Young's modulus
f	Frequency of oscillation
F	Force
h	total width of the plastic zone
k	Constant
K	Thermal conductivity
ℓ	Length of extruded matter
L	Length of specimen
L_o	Length of specimen (overhang)
m	Strain rate sensitivity
N	Exponent

P	Pressure
q_o	Heat input rate
r	Radius of cylindrical specimen
t	Time
t_t	Axial shortening time
T	Period of oscillation
u,v	Displacement components
υ	Rubbing velocity
υ_y	Velocity component in the axial direction
υ_x	Velocity component in the direction of oscillation
υ_z	Velocity component in the direction perpendicular to movement
υ_0	Axial shortening velocity
w	Specific power input parameter
W	Width of specimen
x	Distance from interface
y_{pl}	Width of the plastic section

Subscript notations :

fr	Frictional
f	Flow
N	Normal
x,y,z	Cartesian co-ordinatesystem

Greek notations :

α	Amplitude of oscillation
α_s	Dimensionless term characterising velocity distribution
γ	Fluidity parameter
Γ	Euler gamma function
δ	Thickness of cylindrical specimen walls
Δh_T	Heat of formation at temperature T
ε	Strain
$\dot{\varepsilon}$	Strain Rate
$\dot{\bar{\varepsilon}}^{vp}$	Viscoplastic flow rate
θ	Temperature
ξ	Dimensionless term characterising strain rate distribution
κ	diffusivity ($\kappa=K/\rho\ c$)
μ	Coefficient of friction
ρ	Density
ρ_s	Dimensionless term characterising the flash shape
σ	Stress
σ_y	Yield stress
σ^2	Variance
τ	Shear stress
ω	Angular velocity

1. Introduction Into Friction Welding

1.1. The Friction Welding Process

1.1.1. Joining Processes

It has been known for a long time, since Joule's experiments, that mechanical energy can be partially transformed into heat generated from friction and much effort has gone into reducing friction by lubrication to prevent seizure. There are some examples of applying sliding friction usefully, as for example in automobile brakes. In most circumstances the thermal energy generated by rubbing contact of surfaces is regarded as undesirable, but recently it has been shown that it can be used to join materials by encouraging seizure in a controlled way which leads to efficient welding.

Current welding methods fall into two classes, fusion welding or pressure welding. In fusion welding the components to be welded are melted at their edges by the local input of heat, and a joint forms as the weld pool cools and unites into a single body, as for example in arc welding. Pressure welding, on the other hand, joins through mechanical plastic deformation in the weld zone brought about by the application of large forces. Contact surfaces are first brought into intimate contact by breaking down surface asperities and contaminants, so that subsequently the inter-atomic forces provide the bond. Friction welding which is the topic of this thesis belongs to the pressure welding category. Friction provides the means to remove asperities by the mechanism of wear, and is used to generate heat to soften the materials to be joined before deforming them plastically. This dynamic mode of heat generation depends on a number of process parameters to be successful, in contrast to fusion welding where the primary component of heat input to the weld, is directly controlled.

1.1.2. Friction Welding Methodology

In pressure welding, the parameters that control the process are pressure, temperature and time. Friction welding requires the addition of relative velocity between the workpieces as a fourth parameter whereby heat is introduced at the interface. It is thus solid state process for joining matcrials together, through intimate contact of a plasticised interface which does not require melting conditions. The plastic interface is generated by heat produced from frictional contact as one component is moved relative to, and in pressure contact with, the mating surface. The weld is usually consolidated by a forging force, usually applied after the cessation of relative motion. The joint created, has a confined heat affected zone, and typically exhibits plastically deformed material extruded from the weld which forms a "flash". Many combinations of geometry and dissimilar materials have been successfully joined by this method.

There are three basic variations of friction welding : rotary, orbital and linear friction welding (see Figure 1). Of these, rotary friction welding is by far the oldest process and linear versions are only recently being investigated. In rotary friction welding one workpiece is rotated as the two axisymmetric workpieces are brought together under friction pressure. Orbital friction welding, can be used to weld non-axisymmetric parts by rotating both components in the same direction at the same speed but with their axes offset, resulting in uniform unidirectional relative motion between the two workpieces over the total interface area. When motion of the components ceases, the parts are aligned mechanically to form a weld. In linear friction welding parts move relative to each other in a direct reciprocating mode produced by a linear mechanism.

1.1.3. Advantages And Limitations Of Friction Welding

The main advantage of the friction welding process is that thermal energy is input directly at the joint interface in contrast to arc welding. Maximum temperatures thus occur in the region where intimate plastic contact between the surfaces is taking place. The temperature gradients in this area can be very high, so that only a small volume of surface material is affected, and this

results in fast joining times, of the order of seconds. Additionally, during the last phases of the process, including the forging phase, hot plastic material is extruded from the joint in all directions, which ensures in most cases that surface contaminants are removed, and a high integrity weld is achieved. As this process is solid state for most metals, i.e. melting is not necessitated, it is immune to defects due to solidification, such as porosity (**Maykuth,1971**) etc. Providing suitable parameters are maintained, it is highly repeatable, producing joints with properties comparable with those of the unwelded parts, where welding distortion is kept minimum due to the small size of the heat affected zone. Often combinations of materials that can be friction welded cannot be joined by other welding processes because of the formation of brittle phases, as in the case of Zircaloy and 410 stainless steel which produces eutectics, or cracking that would make such joints unserviceable. Materials that are good dry-bearing metals are difficult to friction weld. The alloying elements that provide dry lubrication prevent the rubbing interface from being heated by friction, as in the cases of cast iron and free-machining steels possessing high concentration of sulphur, or materials with highly directional properties such as beryllium, or materials that do not seize under normal operating conditions without lubricants. All friction welding processes require minimum surface preparation, and generally are found to be economical in total energy requirements, requiring as low as 10% of power required for butt welding (**Hodge,1964**). The friction welding process can easily be automated, requires low operator skill and produces no harmful by products, as fluxing agents are not generally needed. Surface preparation effects are usually insignificant for many materials, as surface films are broken during the process and extruded from the interface (**Hodge,1964**) (**Smith,1992**), but can be critical for some combinations (CP copper to Ti 6Al 4V (**Crooks,1990**)). Similarly, the atmosphere under which welding is attempted does not influence the process, whether it is air, an inert gas or vacuum (**Smith,1992**).The majority of metals can be friction welded by the rotary friction welding process (Figure 2) to themselves, but some combination of dissimilar materials appear to be impossible to join. In principle, there are no geometric or physical limitations on the pieces to be joined, so that, in practice, the rotary and linear variants of the process can be employed to weld parts of any specific geometry.

The friction welding process however does have some limitations. Rotary friction welding can only join axisymmetric components or axisymmetric to plane as in stud welding. One workpiece must be circular at the interface, while both must have concentric masses as the workpiece revolves at high speeds. The size and shape of the workpiece should be such that it can be clamped and rotated. Rotary friction welding is restricted to flat butt welds that are concentric with the axis of rotation. Workholding devices must be strong enough to withstand heavy shock and torque loads, while workpieces must be able to withstand the torque and axial pressure imposed during the friction and forging phases. For workpieces that must have final angular alignment, provision must also be made for synchronised rotation at the forging stage.

1.1.4. Applications Of Friction Welding

Rotary friction welded parts are found in production applications in a wide variety of industries, from marine, agricultural and automotive to aerospace and oil industries. In the automotive industry parts which are often rotary friction welded include gears, engine valves, axles, drive-line components and shock absorbers. Hydraulic piston rods, track rollers, gears, bushing and similar parts are joined by rotary friction welding in the agricultural industry. In the electrical industry aluminium to copper joints are used for electrical switch gear to reduce cost and weight, while stainless to carbon steel welds are used in marine drive systems and water pumps to conserve expensive materials. Assemblies which have been friction welded are usually used to replace expensive castings and forgings. In the last few years, rotary friction welding has been investigated (**Smith,1992**) as an alternative method for repairs and assembly in space stations for its cleanliness, simplicity, low power requirements and lack of additional consumables. In contrast, linear friction welding has only recently found its first industrial applications in the welding, at low frequency of oscillation, of turbine blades to disks (**Benn,1995**), which improves stress distribution, reduces weight and hence increases power-to-weight ratio for engines.

Friction welding, with its variants, is one of the few applications where friction generated heat is used in a constructive way. Its history as a joining process, is more than a 100 years old, but it has been limited to certain geometries. The development of linear friction welding removes this restriction, and as research into the process progresses, more applications are expected to make use of this approach.

2. Literature Review

2.1. History Of Friction Welding

The first attempt to utilise frictional heat as a joining process appears in 1894 when the first patent for joining the ends of a wire cable was issued in the U.S.A to Moore (US Patent No. 517,807). The next work which produced a patent occurred in Germany in 1929 (**Fritz,1974**), where the concept of using the heat from friction to join was patented (DR patent No. 477084), and further research in the United Kingdom produced a series of patents between 1941 and 1944 on the same subject. In particular, (**Klopstock,1941**) claims protection for the rotary friction welding process for joining any kind of metal, where one of the examples he is describing is known today as stir friction welding. During the second world war rotary friction welding was used in Germany to butt weld thermoplastic pipe and in the US to assemble floating compasses. In 1956, a patent for friction welding was issued in the U.S.S.R. for friction welding of tubes using a rotating intermediate object. Following these early efforts the rotary version of the process has been utilised in Europe, in Japan and in the U.S.A. for a wide range of automotive and aerospace components.

Linear friction welding on the other hand has been explored to a much lesser extent partly due to the complexity of generating the motion, compared to rotary friction welding. In (**Vill,1962**) the process was proposed to cover the need for joining non-circular parts using linear motion. Although linear friction welding received less attention in the early days, it has been covered more recently by patents such as (**Searle,1972**), which describes an arrangement of holding workpieces (similar to the one described in this thesis in chapter 4 on page 30) and the mechanism to apply movement, and in (**Searle,1975**) which describes a mechanism to produce the linear movement. More recently (**Searle,1989**) and (**Roberts,1988**) cover aspects of the reciprocating mechanism needed to produce linear motion, employing hydraulics or eccentric driven shafts. Patents have been granted for applications of the process such as (**Ritter,1973**) where crossed wires are joined to form a mesh by oscillating with a small amplitude, while keeping the

wires under tension and compression in different places. In (**Martens,1971**) the application of translational movement to welding of plates and sheets is described, with no particular claim to a mechanism to apply the linear movement. Linear friction welding is also used in the joining of non-fusible workpieces, such as polymeric thermoplastic materials to polymeric thermosetting materials, (**Summo,1977**) where the melted material is moved into a recess in the mating surface of the workpiece. Recently, rotary friction welding has been used to weld transverse bars between steel plates, and form double skinned composite panels (**Greek,1997**).

2.2. Rotary Friction Welding

2.2.1. Process Variants

Rotary friction welding is by far the most popular of all friction welding processes for joining similar, axisymmetric components, both plastics and metals. There are two basic types of rotary friction welding.

The first one is known as *continuous drive*, where the power input is controlled by regulating rotational speed and axial force throughout the process. The rotating specimen is driven at a constant speed and forced against the stationary specimen. This generates heat at the rubbing interface, and the combined effect of heat and pressure causes plastic deformation. When a certain amount of deformation is achieved or the rotating phase of the process reaches a predetermined time, the rotating component is rapidly stopped and an increased axial force is applied for a specified amount of time, producing a weld. This version of the process can be used to join small pieces to larger structures (for instance in the automotive industry) as it can supply energy continuously as required. Heat usually develops relatively slowly. As a result of the low heat input rates, significant amounts of heat are dissipated beyond the immediate rubbing interface.

The other type of rotary friction welding is called *inertia welding*, where a fixed amount of energy is stored in a rotating flywheel. Instead of a long rubbing phase succeeded by a stationary forging stage, the rotating assembly is accelerated to a predetermined speed, without friction, at which the flywheel is disconnected from the power supply. The frictional resistance to rotation is produced by forcing the specimens together which decelerates the flywheel, converting kinetic energy to heat energy at the weld interface. A forging phase may be applied before rotation stops. Again, once the interface is sufficiently deformed by the process, the weld is consolidated after the specimen rotation has stopped. As energy is delivered to the interface much quicker than in the continuous type, temperature gradients are sharper producing narrow heat affected zones. It must be noted that in the inertia process, the speed of rotation is continuously changing during the welding cycle, producing a variable heat input to the rubbing interface. Inertia welding

allows much bigger components (**Sluetz,1968**), than continuous friction welding, to be welded due to the large amount of energy provided (for instance motor shafts in the aerospace industry) (**MTI,1993**).

Rotary friction welding has been studied more extensively than any other form of friction welding due to the relative simplicity of the process machinery. There is a wealth of information on the process, but a large proportion of it is of an empirical nature. Both inertia and continuous drive types, have wide acceptance, and recommended practices have been issued (**Aws,1989**), with process fundamentals, basic equipment requirements, joint design guidelines, material compatibilities and common welding defects documented, to serve as a guide for those using these variations.

2.2.2. Previous Work On Rotary Friction Welding

Much published work, from the late 1950s up to today, covers aspects such as practical problems up to experimental and theoretical considerations.

2.2.2.1. Process Model For Rotary Friction Welding

Study of the process has lead to theories where it is proposed that it consists of three separate phases (**Vill,1962**) in the friction heating period. The initial phase is characterised by dry friction, with low friction coefficient of about 0.1, the second stage with increasing asperity contact area, and the third phase where steady state conditions are reached at high temperatures. These three separate phases are consecutive, as the two materials are brought into ccntact under pressure. Heat generated from dry friction, leads to an increase in surface contact area during the second phase. This leads to the plastic flow conditions in the last phase which occur more or less uniformly across the entire interface and which are essential for a high integrity weld.

These phases are connected to parameters such as axial shortening and torque (Figure 3). During the initial phase, wear is not uniform across the rubbing interface due to variations in velocity and interfacial pressure. Rubbing and seizing is limited to the annular area where wear fragments are largest. As temperature increases the size of individual junctions increases as well, producing a continuously increasing torque. The material becomes plastic due

to thermal softening and starts to behave like a viscous fluid (**Duffin,1976**). A layer of plastic material forms at the rubbing interface, which reduces the frictional force and decreases torque to a steady state value for extrusion.

2.2.2.2. Process Variables In Rotary Friction Welding

There are three basic variables that can be manipulated in the process : mean surface velocity, time of contact and the axial pressure as the majority of research indicates (**Duffin,1973**) (**Hollander,1962**) (**Vavilov,1968**). These variables determine the amount of energy input to the weld and the rate of heat generation at the interface. It must be emphasised that the rate of heat generation is not uniform across the rubbing interface and that it changes during the different stages of the process. The interfacial pressure arises due to the axial force exerted on the components and is usually applied in steps during the process. The first step requires relatively low contact pressure during heating of the components. The latter stage, usually involves higher pressures, and is effected immediately after cessation of movement to forge the components together. The mean surface velocity is usually stated, since the relative sliding velocity is proportional to radius. This variable is more representative of the velocity condition in the rubbing interface than angular speed, as the velocity changes across the surface.

Although (**Vill,1962**) stated unequivocally that slow speeds and high axial pressures are most efficient, it was based on experiments with solid plain low carbon steel bars. However, there is no evidence to support this view for all materials. From what is available on inertia welding it is indicated that slow speeds can be very effective in the formation of a sound joint.

Other process variables are time, surface condition, specimen geometry, material properties, axial shortening rate and the coefficient of friction. Each of these optimised parameters is found to differ for different materials. The time of contact variable can be directly related to the amount of flash present at the weld interface (**Kobayashi,1989**) (**Oh,1995**). In the former paper, the axial shortening produced is proportional to the friction pressure as well. Process parameters have been studied to produce empirical relationships between time and flash size (**Kobayashi,1989**), but no theoretical explanation

as to the optimum length of axial shortening was given, or any prediction for other materials than the ones studied.

2.2.2.3. Process Monitoring

In an attempt to monitor the process, acoustic emissions generated throughout the process have been used to assess the tensile strength of steels **(Oh,1995)** **(Oh,1996)**. These emissions originate from the workpieces, due to plastic deformation and increases in contact area, as well as the machinery itself. Acoustic emissions are also emitted during the cooling period after forging, due to formation of martensite. Results indicate a statistical correlation between the total acoustic emission count and tensile strength of the joints. As two-thirds of the emissions counted are generated during the cooling stage, this parameter cannot be used for on-line monitoring of the process. Experiments in **(Oh,1996)** indicate that high friction pressures at high rotating speeds produce higher acoustic emission counts, but with a lower tensile strength, which contradicted earlier trends. Another monitoring system has been described in literature **(Ellis,1974)** where the axial shortening rate has been correlated with bending tests of En3B steels. Although, no numerical values for the desirable rate are quoted, it is stated that high axial shortening rates, the result of slow speeds and high friction pressures, produce small heat affected zones. These are detrimental to the strength of the joint, while larger heat affected zones, the result of slow axial shortening rates, are more beneficial.

Machine instrumentation has been documented **(Lebedev,1986)** to measure the torque generated during friction welding, for use in controlling the process as well as the quality of the joints, although this quality control method has not been followed by other researchers.

2.2.2.4. Frictional Behaviour

Although the frictional behaviour of materials in rotary friction welding influences the power generated it has been investigated very little, despite an enormous amount of literature related to static friction.

According to (**Vill,1962**) relative speed, the temperature of the rubbing interface, the nature of material and the presence of surface films, normal pressure and the rigidity of the friction surfaces are factors which influence the coefficient of friction in a quantitative manner.

The rotational speed and the presence of surface oxides are shown to have a critical effect on the coefficient of friction between rubbing surfaces of carbon steel and Monel K-500 (**Zhu,1988**). Although it has been stated in the first book written on friction welding (**Vill,1962**) that an inversely proportional relationship exists between velocity and power produced, theoretical models and experimental results (**Vavilov,1968**) prove the opposite, as high quality joints were achieved at high rubbing velocities. In (**Sluetz,1968**) it is observed that the integrity of steel welds is influenced considerably by the rubbing velocity, while friction pressure is secondary in effect. In (**Duffin,1973**) and (**Duffin,1976**) the influence of rubbing velocity on the torque exerted during the extrusion phase was also commented. The equilibrium torque, as well as the corresponding shear stress exerted on the components, had a maximum value at a specific rubbing speed (0.7 m/sec) for different axial pressures during friction welding En3B. This behaviour could be more correctly attributed to constant power flux during that stage of the process, and may not be an indication of a complex friction behaviour as suggested. Velocity dependence of the friction coefficient was also verified in (**Hollander,1963**) for dissimilar stainless steel workpieces, where the torque changes with rotational speed, indicating an inversely proportional relationship. Increasing the rotating speed does not increase the power input, and there is an optimum speed for each pressure, for which the heat flux is maximum. This relationship enabled (**Hollander,1962**) to postulate that the total power is proportional to the rubbing surface and independent of speed, which is in contrast to experiments which show that with a dependence on speed. This discrepancy could be attributed to the fact that velocity is different for different points along the rubbing interface. A more complex dependence of the coefficient of friction and sliding speed as well as axial pressure has been recorded in literature (**Seregin,1986**) for inertia friction welding of steels. The velocity dependence of the coefficient of friction has also been observed in (**Hasui,1968**), while axial pressure changes produced

little effect on the temperature of the rubbing interface. All these indicate that the friction coefficient is indeed influenced by rubbing speed, but to a greater extent than (**Bowden,1964**) suggests.

In (**Squires,1966**) it was observed that the steady state torque, which is related to the stress state at the interface, is inversely proportional to temperature. Similarly (**Gel'man,1959**) confirmed this for high temperatures, as well as friction pressure and speed. Contrary to that, increasing the applied pressure decreased the coefficient of friction (**Hollander,1963**). However, these may not be accurate as the torque recorded depends on the size of the plastic zone present at the interface. As the extent of that plasticised zone is inversely proportional to pressure, then the plastic work occurring in that stage should contribute more to the torque than the friction coefficient at the rubbing interface.

It is important to note that most of the above postulated expressions for the coefficient of friction have not been experimentally verified to any degree of generality. These dependencies of the friction coefficient on normal load and temperature have to be investigated experimentally for each material and each set of welding conditions.

2.2.2.5. Joining Mechanism

The joining mechanism of friction welding has been studied by some authors. It has been suggested (**Hazlett,1967**), (**Cola,1992**) that the mechanism of bonding in friction welding is high temperature diffusion, especially for dissimilar metal joints such as aluminium / titanium and iron / nickel. Diffusion can have a positive or a negative effect on the properties of a dissimilar metal joint. If mild steel is welded to a high carbon steel, the reduced carbon concentration gradient across the weld may increase the ductility of the joint. But, in a case where the materials to be joined form intermetallics, like iron and aluminium, the hard interlayer may make the joint more brittle. Some evidence of diffusion was shown (**Sassani,1988**) in certain cases of aluminium to nickel joints where there was long frictioning stages. Diffusion must have been present also during the cooling stage of iron into

titanium (**Hashui,1968**), as there are high iron concentration areas away from the bond line.

It seems unlikely for diffusion to be the cause of joint formation in friction welding due to the short process time but conversely it may be the consequence (**Gel'man,1965**), due to the relatively long cooling period. Forging pressure undoubtedly aids that and the rate of material extrusion is much higher than the diffusion rates, but the effects can vary according to position from the centre of the interface. Other evidence against diffusion, as the primary mechanism contributing to friction welding, is the existence of a sharp interface between the various materials.

It has also been suggested in (**Cola,1992**), (**Hollander,1963**), (**Jones,1965**) and (**Sluetz,1968**) that joints are the result of mechanical mixing of a thin layer of molecules on each side of the interface, as they claim to have observed this. This was confirmed during work done at the University of Bristol with linear friction welding of Nimonic 90 (**Crooks,1990**), and inertia friction welding of Al-9Fe-3Mo-1V and 2024-T351 aluminium (**Koo,1992b**).

From a thermodynamic point of view it is expected that a joint will form between smooth and clean polycrystalline bodies when brought together. The free energy at the boundaries of grains will be much less than the total energy of the surfaces that disappear (**Gel'man,1965**). The friction welding process assists in joining the two surfaces by levelling the roughness on the surface due to asperities, and by breaking down oxide films and adsorbed gases that inhibit bonding. The latter factor being most important, as bonding can occur without substantial plastic deformation under vacuum, as diffusion welding demonstrates. Increasing the temperature, assists the bonding process further as might be expected. Joints between similar materials can always be achieved, while "joinability" between dissimilar materials may depend on the difference between the atomic diameters of atoms. If that is large, then no bonds form due to lack of space in the lattice (**Golego,1965**). Energy absorption tests showed that weld integrity could be a function of the extent of mutual solubility between different materials (**Weiss,1965**), pointing to high temperature solid state diffusion as the mechanism. It is worth noting that (**Rabinowicz,1971**) established an experimental relationship between

metallurgical compatibility, based on binary phase diagrams, and the static coefficient of friction. Soft metals had higher coefficient of friction than harder metals, and at the same microhardness level there was a tendency to have lower friction coefficient for the more incompatible materials. Another measure of "joinability" could be the difference of the strength of the dissimilar materials at high temperatures. If this is large enough, it is unlikely that welding conditions will be achieved (**Jones,1965**). To overcome this restriction a third material can be used as an interlayer, with properties between the two materials.

It is widely accepted in the welding industry that flash deformation is related to the quality of the weld. This originates from the assumption that large deformations will remove contaminated material from the original interface which will be succeeded by virgin material from the bulk, free of oxides, oil films and similar contaminants. Although joining is believed to be achieved with the aid of the forging pressure, as (**Gel'man,1965**) stated earlier, it has been demonstrated that it may happen during the heating phase (**Rich,1969**), where extrusion of hot material appears as a result of the movement of the workpieces. The possible insignificant effect of forging has been reported (**Vavilov,1965**) as the forging time barely affected the amount of upset or the joint strength, which could lead to the possible exclusion of the forging phase.

In one of the very few PhD thesis available on friction welding, (**Rich,1969**) the dispersion of the interfacial matter was suggested as a parameter to judge good welds, as it is a function of the axial shortening during forging and the plastic zone size. Unfortunately, this method was not utilised in that work. Temperature profiles similar to the ones observed in metals were attempted to be replicated using plexiglas rods with tempilstick powder and embedded nylon fibres. It was indicated by the embedded nylon fibres patterns that at low speeds bonding may occur, while the specimens were still rotating. However, this observation cannot be conclusive as localised melting may appear at the interface.

Depending on the process parameters used weld integrity can vary. In cases where the heat input is not sufficient the joint cross sectional area may not extend to cover the whole of the interface area, producing a weaker joint. This

area extends from the centre to the periphery. The reason for this may lie (**Sluetz,1968**) in the fact that the velocity has to decrease below a certain value during inertia friction welding, before a bond begins to form while still rubbing. As the centre and areas close to it are at a lower velocity than the periphery, they are the first to join provided there is plastically deformed material. As the rotating workpieces slow down bonding extends towards the periphery.

2.2.2.6. Interface Temperatures

Melting at the interface has remained a question from the beginning of research in this joining technique. Scientists influenced by the Russian school of thought (**Gel'man,1965**) followed the assumption that there is no melting on the interface, while in the western world under the influence of (**Hollander,1962**) the view that melting occurs has been assumed as it was stated early (**Hazlett,1962**) "the frictional heat created by the relative motion, when combined with a controlled axial pressure between the pieces, causes melting of the interface". In spite of these observations, it is strongly suggested from experimental data in all types of metal friction welding that there is no melting at the interface (**Sluetz,1968**) (**Fritz,1974**) (**Duffin,1976**) and (**Hasui,1968**) for similar materials, with the exception of dissimilar material joints (**Hasui,1968**) or in some cases of aluminium alloys and Al-Sic metal matrix composites (**Midling,1994**). This is based on metallographic analysis, temperature measurements and calculations. Analysis of process data such as torque recordings would reveal melting as it would be indicated by a discontinuity in the torque / time curve. If there is any liquid present at near-solidus temperatures it would be so weak that it would be extruded prior to onset of melting and would not contribute significantly to consideration of the thermal field of the weld. Because neither melting or localised regions of liquidation have been observed in the welds, this indicates that temperatures were below the solidus temperature of the material.

Due to the velocity differential on the rubbing interface as well as other parameters like the flywheel energy and friction pressure, different heating patterns appear at the rubbing interface. In certain cases (**Sluetz,1968**) areas in the middle of the workpiece do not heat up at all, or the heat affected zone

created is thinner towards the periphery than at the centre, leading possibly to retainment of contaminants at the interface, and weld defects occurring at the end of the process. The size of the heat affected zone can be reduced with high friction pressures and minimise the time to weld. This can be useful for materials with high thermal conductivity or dissimilar combinations with substantially different melting temperatures. While increases in friction pressure produce thinner heat affected zones with the area at the centre becoming small to the point where it disappears (**Koo,1992b**), velocity produces a more complex response. Low speeds employed can produce heating patterns where the heat affected zone does not exist at the centre of the workpiece, which was also observed by (**Duffin,1976**), (**Hasui,1968**) and (**Squires,1966**). Increasing the speed affects the area in the centre to the point where it is thicker at the centre than the periphery (**Squires,1966**).

2.2.2.7. Analytical Models For Rotary Friction Welding

Despite the wealth of papers on friction welding limited progress has been made in constructing satisfactory theoretical models. In the majority of work it has been assumed that heat is generated from friction at the rubbing interface. As this occurs at the early stages of the process, during subsequent phases plastic work must contribute significantly to the high temperatures encountered. Therefore friction models cannot apply to all phases of the process. Early suggested models (**Vill,1962**) (**Rich,1971b**) using frictional heating do not produce consistent temperature traces compared to experimental data for the whole process. By employing the theory of heat conduction and applying certain simplifying assumptions (**Cheng,1963**) used a finite difference model to estimate the temperature distribution for finite length workpieces during friction welding of AISI 4140 alloy steel and 304 stainless steel. The heat input used in the model was based on experimental torque curves, and there was agreement between the predicted and the recorded temperatures at the beginning of the process. It was observed that the temperature reached during the steady state phase of the process will depend on the heat input during the initial stage of the process. Predicted steady state temperatures are lower than the experimental, despite the fact that there were no heat losses assumed in the model.

A closed form solution of the infinite rod was published in **(Rykaling,1959)**. The power input to the interface was assumed constant and equal to the average energy input over the initial phase of the process, as was estimated from the power consumption of the machine. Although agreement did appear between the temperatures predicted and the experimental values, axial shortening was not taken into account. Extrusion of plastic material from the rubbing interface would move the thermocouples closer to the interface. Taking this into account, the temperatures predicted must be lower than those observed experimentally.

In **(Rich,1971b)** a closed form solution was also presented for temperatures developed during friction welding for workpieces of finite length. The power input model chosen was an approximation of experimental power traces. In contrast to both **(Rykaling,1959)** and **(Cheng,1963)**, where no heat losses were assumed to the chucks, heat sinks at the ambient temperature were assumed to exist at the chucks. Instead of assuming that melting is reached at the interface **(Cheng,1963)**, wear is assumed as the mechanism for dissipating energy. Despite the different reasoning, the boundary condition that temperature is constant at melting is employed during modelling of the extrusion phase. Temperatures predicted did not match closely the experimental data, which was attributed to the fact that material properties were assumed to remain constant, as well as the influence of experimental errors.

All three studies have reduced the three-dimensional heat conduction problem to an one-dimensional analysis estimating the average temperatures across the cross-section during the process for various times. In spite of these efforts, analytical models to predict temperature without resorting to empirical formulations are far from satisfactory, due to the complicated interrelation of parameters such as material properties that cannot be easily considered in an analytical simulation of the process.

In **(Rich,1971a)** the forging phase of the process was studied. Published temperature data on metals were used, as well as experiments performed with plexiglas to study the material flow in metals. The movement of interfacial matter by its instantaneous velocity field was modelled analytically and

studied experimentally in a similar way to (**Rich,1969**). The resulted discrepancies between predictions and experiments, were due to the fact that the rigid-plastic boundary was not flat as modelled. This stems from the uneven heat generation mechanism of rotary friction welding. Unfortunately, the idea of predicting joint integrity by measuring the extrusion of matter at the interface using an interfacial dispersion parameter was not quantified or correlated to process parameters. It was observed qualitatively from a mathematical formulation that for the process to remove oxides, voids and contaminants from the interface, and the joint to be of high strength, the size of plastic zone is more important than the presence of upset. Therefore the existence of upset is not adequate evidence that oxides and contaminants were expelled from the interface as (**Vill,1962**) had suggested.

In modelling the extrusion phase of the process, (**Healy,1976**) considered mild steel tubes to behave as a temperature dependent modified Bingham solid. However the estimation of the thickness of the plasticised layer for different speeds under various axial forces (fig.5 in (**Healy,1976**)), predicted values of the layer which were verified in certain cases. It produced good agreement between experimental values for the 6 kN axial force case and the predicted upper bound for the thickness of the plasticised layer. When it was attempted to verify the equation for the other load cases, there were differences between the experimental values and the theoretical predictions. Further to that, it was predicted that increasing the axial pressure for a given speed it would cause the plastic zone to increase, which contradicts previously observed patterns of friction welding (see section 2.2.2.5.Joining Mechanism in page 13).

Following this work, the frictioning and the extrusion stages of the continuous drive friction welding of steel tubes were also modelled (**Francis,1985**), where the material is assumed to behave as an incompressible Newtonian fluid of large constant viscosity as well as a Bingham solid. Results did provide a qualitative representation of the material flow fields. It was concluded that the thickness of the plastic layer reaches some equilibrium value, which increases and is achieved at shorter times for higher axial shortening speeds. Unfortunately there were no comparisons to experimental data to check the faithfulness with which the model represents the real process, as there were no available data for material properties at various temperatures and strain rates.

More recently (**Midling,1994**), the heat affected zone temperature and the effective strain rate distribution were estimated, as well as its effect on the microstructure of Al-Mg-Si alloys and Al-SiC metal matrix composites. By assuming localised asperity melting at the rubbing interface and a constant coefficient of friction for every stage of the process, an one dimensional temperature model is presented. Agreement is shown between predicted and measured temperature values. However, as specimens get shorter due to material extrusion, the embedded thermocouples will approach the rubbing interface with the recorded temperatures corresponding to points closer to the interface. By allowing for this, the predicted temperatures will be even higher than those presented. As the predicted temperatures are already higher in most examples given in the paper, this correction will increase the deviation from the experimental values even further. Assuming that the velocity components of the plasticised material change in a similar fashion as the deformed shape of the material, strain rates are predicted for the plasticised zone. The predicted strain rates at the rubbing interface are extremely high, compared to those predicted numerically in (**Soucail,1992**), of the order of 1000 s^{-1}, possibly due to the viscous fluid model used and to the assumption that the width of the plasticised zone is constant across the whole rubbing interface and not uneven as (**Sluetz,1968**) records.

2.2.2.8. Finite Element Models Of Rotary Friction Welding

In recent times the finite element method has been used to analyse this process. In (**Sluzalec,1990**) the incremental approach has been utilised to model friction welding of mild steel. Using non-linear material properties and assuming that the friction coefficient varied with temperature, predicted deformations for the upset formed at the interface were close to experimental ones. Deviation from the experimental strain was attributed to non-uniform material properties and to possible specimen misalignment. Temperatures predicted were in agreement with the experiment, despite the fact they were sampled every 4.5 sec, a very slow sampling rate for experiments that lasted 18 seconds. The fact that predicted temperatures did not reach a steady state was not explained, but could be attributed to incomplete data for the friction coefficient at high temperatures or over-estimation of the plastic work produced. It was also stated that the steady state temperature during extrusion

cannot exceed the temperature at which the yield point of the material is equal to the friction pressure employed. This should provide an upper limit for the temperature at which material extrusion appears. The same researcher in **(Sluzalec,1993)** compared analytical and finite element predictions with experimental results. Although a constant heat input was assumed for the analytical model and the friction coefficient was not stated in the finite element work, all models predicted very similar temperature profiles, except for the points closer to the rubbing interface where experimental temperatures had a variation of up to 100°C.

With the aid of a transient thermal model with non-linear material properties, **(Kim,1995)** used an empirical heat input formula to estimate residual stresses and plastic strain in order to explain the failure mode observed in friction welded joints between 304L steels and titanium. A quantitative analysis confirmed integrity tests, but validation of the numerical work with experimental data would have strengthened this model.

More recently the extrusion flow patterns in rotary friction welding of aluminium alloy 6061-T6 were estimated by solving numerically the Navier-Stokes equations **(Bendzsak,1997)**. Assuming steady state conditions and restricting the investigation to the zone of viscous material at the interface, the size of this zone was estimated and the complex flows of the material during extrusion were predicted. These flow patterns indicated that viscous material recirculates towards the edges of the specimens, instead of being extruded into the flash. This results in retaining contaminated material at the weld interface, and therefore weakening the joint. These patterns were observed to an extent in the experiments, and they are the effect of a heat affected zone with an hourglass shape. Due to the friction pressure and rubbing velocity used in the experiments the plastic zone formed is not flat or largest at the edges of the specimens, but is thickest at some point before the edge.

The inertia welding of nickel based super alloy (NK17CDAT) tubes has been modelled **(Moal,1992)** taking into account thermal and mechanical effects in a viscoplastic finite element formulation. Torsion tests were used to identify temperature dependent material properties at different strain rates and the

change of friction coefficient with speed. Although these properties were not provided in the paper, they were used to predict the axial shortening history as well as strain rate and temperature fields. It is notable that the deformation predicted across the rubbing interface was asymmetrical, which could be attributed to the fact that the rubbing velocity is not uniform along the interface of the rotating tube. Unfortunately no comparison with experimental results was provided. Following this work, the same research group **(Soucail,1992)** used the same finite element code to model the welding of Astroloy, a powder metallurgy nickel based superalloy, and in particular to study the evolution of the microstructure. At the centre of the specimen higher strain rates (by a factor of 10) were observed in reality than those predicted, which was attributed to numerical difficulties. As the velocity derivatives were not continuous from one element to another, a smoothing technique was used which under-estimated predicted strains. Strain rates could have also been under-estimated as the rheological law did not include any incipient melting effects. Further away from the centre, predicted strain rates were close to those expected from the experimental microstructure. Temperature gradients predicted were higher than the metallurgical data indicated, possibly due to the two dimensional nature of the model. The time taken for the duration of the friction welding of the finite element model was overestimated as well, possibly due to the inaccurate modelling of the friction law or other material properties. This finite element code was further improved and used in **(Moal,1995)** to simulate the welding of NK17CDAT again. The friction law used in previous work assumed independence of sliding velocity, which was rectified by further experiments. Axial shortening prediction of the process is close to experiments up to where rotation ceases. This over-estimation of axial shortening at the last phase of the process may originate from inaccurate material properties.

Rotary friction welding, being the oldest variant of the friction welding processes, has been studied extensively. Attempts made over the last forty years to understand in detail the mechanisms involved have yet to produce a complete theoretical model for all materials. Questions relating to the effect of process parameters on frictional work or the temperatures

reached at the rubbing interface have been investigated for a limited number of materials.. Although the material combinations that can be friction welded have been mapped, the choice of optimum process parameters is still empirical. During this time the process has been modelled both analytically and numerically. Due to the complexity of the interrelated parameters, mathematical modelling has been less successful than finite element modelling. Material properties, including a quantitative contribution of friction, have been shown to be of importance to all modelling attempts.

2.3. Linear Friction Welding

Linear friction welding is a joining process similar to rotary friction welding, but applicable to non-axisymmetric parts and where accurate workpiece orientation is required. For example, it has been used in aerospace industry applications for the attachment of blades to discs and repair of aero engines (**Nicholas,1992**). Its ability to join dissimilar metals could be used in bimetallic and special applications, as for example in high strength gear teeth welded to low strength hubs.

However, in the frequency range explored so far commercially and experimentally, the amplitude of oscillation needs to be high, and the pressure force exerted also high to generate sufficient heat. This process constraint can cause problems in holding delicate components and ensuring accurate final alignment. This is no surprise, due to the sinusoidal velocity profiles utilised in this process, reaching maximum values at the middle of the stroke. The inertia forces exerted on the reciprocating mechanism can be substantial when metals are joined.

2.3.1. Previous Work

In contrast to rotary friction welding where a considerable amount of work has been published, little information is available in literature about linear friction welding.

2.3.1.1. Plastic Materials

Appreciable amount of information focuses on plastics and their welding parameters. Behaviour of plastics is different to metals as they melt by the frictional work. In (**Stokes,1988a**), the phenomenology of the process is studied for various amorphous thermoplastics such as polycarbonate, polybutylene terephthalate, polyetherinide and modified polyphenylene oxide. If low amplitudes are to be used with these materials high frequency linear friction welding is required. This will be useful in situations where large amplitude vibrations are impossible, like in cavities. Axial shortening due to melting and outflow at interface, was used to describe the phenomenology of

the process. It is proposed that initially the materials do not melt. Following this phase an unsteady extrusion stage develops before steady state extrusion of molten material happens. In its companion paper **(Stokes,1988b)** analytical models were presented for the first three phases of the welding process. Unfortunately, the models developed did not produce accurate predictions of the time necessary for each phase of the process. This may be due to the assumption that material properties were constant with temperature and the models developed were two dimensional. However, they did provide a quantitative estimation of the size of the heat affected zone. Also in **(Stokes,1988c)** application of the same model on experiments with amorphous and semicrystalline thermoplastics indicated that the optimum weld velocity is inversely proportional to the molten film thickness and proportional to temperature, which is expected as the power input is directly related to rubbing velocity. The need for accurate physical properties for the materials modelled was stressed again.

2.3.1.2. Metals

Orbital friction welding produces velocity conditions similar to linear friction welding. Workpieces are spun with the same angular speed in the same sense about their longitudinal axes. These axes are offset by a small distance, resulting in the same relative velocity for points on the interface. In **(Craine,1987)** a model is presented to estimate the effect of the axial offset on the heat input during the initial phase of the orbital process. It is shown that the heat flux per unit area increases for a given process with larger values of the offset. In comparison to linear friction welding where the contact area changes with time, due to oscillation, and the heat input affected in a similar fashion.

Work done with metals **(Nicholas,1987)** in the Welding Institute used a modified orbital welding machine to produce linear motion, covered the low frequency range (25 Hz). It studied various materials such as Ti 6Al 4V, stainless steel and mild steel. At the same time, work done in the University of Bristol **(Garton,1987)** investigated the low frequency (10 Hz) linear friction welding of Ti 6Al 4V by constructing a specially built machine to operate in similar friction pressures and amplitudes of oscillation as TWI's

experiments. Later work (**Simpson,1988**) with the same experimental set up attempted to measure the interface temperature more accurately, pointing to a possible instrumentation error of (**Garton,1987**) where the welding times indicated were incorrect. Further work studied dissimilar material combinations (**Crooks,1990**), for materials such as aluminium, Ti 6Al 4V, mild steel, CP copper and Nimonic 90-S106 alloy steel. In the case of the unweldable combination of Ti 6Al 4V and mild steel an aluminium interlayer was used to achieve welding conditions. To explain the joining process, a mechanism was proposed where atomic forces are responsible, after intimate contact is achieved through plastic deformation. Mixing and diffusion may take place to form a solid solution layer across the interface. Mechanical mixing at the weld interface has also been observed by (**Baeslack,1994**). Using the same experimental set-up as (**Crooks,1990**), the effect of inert atmospheres on the weld quality was examined by (**Furber,1991**). It was found that an argon shield did stop the oxide formation at the interface. However, this would only be beneficial for the early stages of the process, before appreciable plastic deformation and extrusion of hot material appears.

More recently (**Koo,1992a**) Al-Fe-V-Si alloy 8009 was welded at 50 Hz, where it was observed that the less intense heating cycle and smaller material extrusion in linear friction welding, compared to inertia friction welding, causes softening in the heat affected zone. This could be attributed to different temperature profiles generated between the two processes. In the inertia friction welding the maximum temperature is generated away from the centre of the bar as the velocity changes from zero at the centre to maximum at the periphery, while in linear friction welding the maximum temperature occurs in the centre of the interface. It has been demonstrated (**Baeslack,1994**) that in joining Ti-13.5Al-21.5Nb and Ti-6Al-2Sn-4Zr-2Mo-0.1Si titanium aluminides the appreciable deformation, exposure to supertransus temperatures and the quick cooling of the heat affected zone encourages microstructural variations with martensitic products, which increase the hardness in the interface region. Comparing the linear friction welding joint with one produced with diffusion welding, it was shown that the lower temperatures reached during diffusion bonding affected the microstructures less. In the same paper, spot welds of the same materials would need postweld heat

treatment to stabilise the more ductile beta microstructures produced by the very high heat input and rapid cooling rates experienced.

3. Objectives Of The Present Work

Linear friction welding is a relatively new process aimed at extending the current applications for rotary friction welding to non axisymmetric components. However, the two processes differ considerably in the mode of heat input and the stress field imposed on the plasticised layer, and therefore existing rotary friction welding models are not directly applicable to linear friction welding. The more uniform interfacial energy generation present in linear friction welding may account for higher integrity welds. Moreover, much of the research in rotary friction welding is of an empirical nature, which cannot be used to predict weldability and optimum welding parameters for new materials.

Furthermore it is apparent there is scope for investigating linear friction welding of metals using higher frequencies. Very little is known about this area and as it is expected that higher velocities employed will require smaller friction pressures, making it possible to join more sensitive components that cannot be welded at lower frequencies due to the excessive pressures required to weld. However, it is also clear that the friction coefficient may vary with temperature as well as with velocity. This knowledge is critical to the understanding of the process.

Due to the complexity of the linear friction welding machinery, the process has been confined to a niche market, making it imperative to research the process mechanism and explore the effects of the operating parameters.

The main objectives for the present work are, therefore, to explore the upper frequency range in linear friction welding and to start to construct a scientific base to guide industry towards design of effective commercial linear friction welding machines with particular reference to desirable frequencies and amplitudes of oscillation.

In particular the following areas will be investigated :

- the effect of frequency of oscillation for different amplitudes of oscillation to the linear friction welding of Ti 6Al 4V

- establishment of a process model to further the understanding of linear friction welding
- development of an analytical model for phases of the process to assist the interpretation of the experimental data
- development of a finite element model for phases of the process to assist the interpretation of the experimental data
- provide data for frictional properties at temperature and rubbing velocity conditions that can be used in modelling the linear friction welding process
- establishment of optimum process parameters for linear friction welding of Ti 6Al 4V
- establishment of guidelines for designing linear friction welding machines

4. High Frequency Linear Friction Welding Rig

4.1. Specification

From previous work done it is known that no linear friction welding of metals at a frequency of above 50 Hz has been recorded in literature. The very few available linear friction welding machines for metals operate up to about this frequency, while the ones for plastics have a fixed frequency of 120 or 240 Hz **(Stokes,1988a)** and an amplitude of less than 5 mm.

It is clear that current process specification is based on what can be practically achieved, using conventional primary drive systems capable of withstanding the large forces and accelerations involved. Understandably, therefore, there has been no exploration of process parameters beyond the range specified above.

The design of a high frequency linear friction welding rig was based on the experience gained from the first linear friction welding test rig built in the University of Bristol in 1987 **(Garton,1987)**. That rig and its modifications were designed purely for test purposes and was capable of linear friction welding of materials with an interface area of 120 mm^2, employing an alterable friction pressure and forging pressure up to a maximum of 150 MPa. The specimens could oscillate with a variable amplitude of up to 5 mm and a variable frequency of up to 25 Hz (Figure 4).

Having assessed this first test rig the following specifications were formulated for the high frequency linear friction welding rig **(Phillips,1992)** that was built for this project :

1. Amplitude range 0.05 mm - 0.92 mm
2. Frequency range 10 - 1,000 Hz
3. Controllable burn - off setting
4. Quick disengagement of drive system

5. Adjustable friction and forging pressure

6. Chuck system to hold specimens rigidly during welding

7. Machine fatigue life for 10^7 cycles (or 500 welds at 1 kHz)

8. Easy loading and unloading of specimens

9. Minimum hysteresis in fixed and oscillatory chucks

4.2. Design

A number of methods to oscillate the specimens were considered :

One method to achieve this movement could be to use a rotating swash plate to vary the amplitude. This would provide an infinitely variable amplitude within the selected range and transmit the oscillatory force to the specimen. This arrangement produces an almost sinusoidal motion. Amplitude and movement arrest is achieved by returning the rotating disc to its flat position. Although by its symmetry this system is well balanced, it requires high rotational speeds (up to 60,000 revs/min) to attain the specification frequencies.

Another approach could be by a crank rocker mechanism. Amplitude adjustment would be achieved by altering the length of links. This mechanism however suffers from balance problems, as well as from the same drawback as before, high rotational speeds. The bearing hysteresis and bending induced in the joints would cause lost linear displacement, especially in the smaller amplitudes.

A third method would be with a crank slider, where rotational motion is converted into linear motion. Amplitude modification is achieved by altering the length of the crank. This method still needs high rotational speeds, and the need to rapidly disengage the drive system during the forging stage is a major problem due to the high kinetic energy stored.

A different method would be to use a linear motor to oscillate the moving chuck and supply the high forces necessary. However it would be rather difficult to generate the high magnetic field necessary to meet the specifications set.

Another way to achieve the oscillatory motion desired would be with an eccentric push-pull cam. This arrangement cannot be easily balanced, and the rapid disengagement of the drive system is cumbersome.

The oscillatory movement could be produced at the interface with the help of an Oldham coupling. This transmits motion between parallel shafts that are laterally displaced, to produce sinusoidal motion relative to an intermediate element. The disadvantage of this arrangement is the time taken to bring the materials to be welded to rest. The very short time needed (less than 1 second) is difficult to achieve, thus increasing the chance of damaging the joint.

The design objectives set above were capable of producing the 200 mm/s minimum mean velocity as deemed necessary (**Garton,1987**) for welding titanium and produced the first successful high frequency linear friction welder (**Phillips,1992**). Materials used in the design of rig were chosen for their strength, fatigue properties and low inertia.

4.2.1. Selected Oscillatory Drive Method

The arrangement finally selected one where the moving chuck oscillated only in the plane of oscillation, while the other chuck remained stationary (see Figure 7, and Figure 6 for detail). A multiple lobed cam, a cam follower and a return spring are used to convey the rotational motion produced by an AC motor to the chuck. This allows relatively high oscillation frequency at modest cam rotation speeds. The three phase AC motor is speed controlled by an inverter controller which provides the means to alter the frequency of the process. There is an upper limit to the frequency produced dictated by the maximum motor speed.

The cam has a sinusoid wave superimposed on its circumference (Figure 7) to drive the oscillating chuck. This multiple lobed cam allows for moderate shaft speeds and eliminates the need for the step up gearbox necessary in the approaches described above. A number of cams with different number and amplitude of lobes produce the required range of frequencies and amplitudes. This arrangement provides only step changes in amplitude and the multi lobed cams need to be changed for different amplitude tests (Figure 8). However with fixed amplitude cams, variation of the frequency gives control of the

rubbing velocity, which was considered to be an important factor affecting this process.

4.2.2. Other Aspects Of The Design

In order for the oscillating chuck to follow the cam profile a high compression die spring is used. The spring provides sufficient force to overcome the friction at the specimen interface, forces the chuck to follow the contour on the cam and returns the specimens to alignment at the last phase of the process. This has the added advantage of reducing the duty cycle on the motor and the energy stored is used to trigger the stopping phase of the process through a mechanical system of levers.

A principal problem noticed in the previous linear friction welding machine built at the University was hysteresis caused by the bearings in the link drive. In the current design both moving and stationary chucks were required to move orthogonally over a small distance. To provide this displacement long parallel beams were attached to each chuck. These have low stiffness in the plane of motion. The deflection required dictated the length of each beam, shear stresses and buckling were taken into account in determining the beam thickness.

To reduce dependence on external sources of energy, high compression die springs are used to provide the axial pressure for welding. This pressure is to be used in the frictioning and the forging stage of the process. The axial force is achieved by pre-stressing the springs. For the application of the forging force manual operation is chosen for simplicity. This is achieved with an eccentric cam which gives the required force by further compressing the springs.

Once the required upset has been reached on the specimens a toggle latching mechanism (18 in Figure 5, and Figure 9) is triggered to swing back the motor base plate, bringing the cam out of contact with the cam follower. The specimens are brought into alignment through a system of levers. The force used to swing the motor plate and align the specimens is derived from the energy stored in the chuck-following spring (8 in Figure 5).

The forces produced by the oscillating chuck following spring are reacted by a mechanical linkage system which applies a force to the motor base plate through a toggle latch (Figure 9). This arrangement allows for the rapid removal of the driving cam when the desired axial shortening is achieved.

Control of the axial shortening of the specimens is achieved by attaching an arm to the stationary chuck which reacts on the toggle. When the stationary specimen moves towards the oscillating chuck, due to axial shortening the toggle displaces past the mid point when a critical displacement is exceeded, resulting in rapid disengagement of the drive system. An electromagnetic clutch would be effective but was not used as the cam contact must be removed to allow the specimens to stop in the required position.

It was expected that the range of frequencies used would excite one or more of the machines natural harmonics. Vibration damping was considered, as well as, but proved impractical. The design of the linear friction welding rig therefore concentrated on reducing the effects of vibration by stiffening the structure. A guide structure on the top of the oscillating chuck was added, to constrain the forces acting symmetrically in the plane of oscillation.

4.3. Commissioning

Following the design and construction of the high frequency linear friction welding rig in 1992 by Phillips, improvements have been made by the author to enhance the operation of the machine and provide monitoring of the process. In particular, the operation was enhanced by stiffening components and reducing the radiated noise. The operating envelope of the machine was identified for experimental work. In addition to these, the rig was instrumented to provide data on the shear force and axial displacements during operation, as well as to provide an accurate measure of the applied friction and forging pressure.

4.3.1. Improvements

4.3.1.1. Rig Mounting

The rig had been resting on the concrete floor which intensified the noise produced when the rig vibrated in a vertical position. To isolate the rig vibrationally, it was mounted on a concrete block with a cast iron top. This coupling of the rig lowered the natural and resonant frequencies of the system as a whole, reducing in effect the amplitude of vibrations especially at the frequencies at which resonated before. The block weighs approximately one tonne and is decoupled from the floor by rubber machine mounting pads at each corner. Rubber pads are appropriate for resonant frequencies greater than 10 Hz.

4.3.1.2. Rig Stiffening

The rig structure had two steel plates on the top and the bottom, with beams running underneath the bottom plate for further stiffness. This method was used to tie together the components under greatest stress, and prevent large standing waves. Half of the force carrying elements were attached to both of these plates, with the others connected to the bottom plate only, for reasons of accessibility (Figure 10).

After the rig was mounted on the concrete block, the top plate was removed in an effort to reduce the radiated noise and improve access to the machine while running. The rig base plate was stiffened by two transverse beams.

A series of beams were added in replacement of the top plate which was removed. A large beam was designed with its second mode of flexural vibration being greater that 1 kHz. The first mode was not considered as the beam was fixed in its centre. The dimensions of the cross section of the top beam are 112 x 12 mm flange (base) and 100 x 100 mm web (vertical). This top beam (Figure 11) ties the stationary chuck spring location block to the oscillating chuck mounting block providing extra stiffness across the rig. It also has, sited on its underside, two blocks from the original plate, one to hold the friction springs straight and one to hold the static chuck down. In addition, steel plates joined the stationary chuck's parallel beams (1 in Figure 5) to the

linking mechanism (4 in Figure 5), and the linking mechanism block (4 in Figure 5) to the top beam running along the length of the rig (Figure 11). The two toggle blocks were tied to the top beam with a steel plate.

Due to the nature of the operation of the machine and the lightweight construction of it, resonance of structures resting on the base plate affect the operation of the machine as a whole. Dry sand was used to identify the areas of the base plate which vibrated most. As can be seen in Figure 12 and Figure 13 the yellow areas where the sand is concentrated, are the nodes of the complex modes of vibration of the plate. The areas where there is no deposit of sand, are where the maximum amplitude of oscillation occurs. Bolts joining the base plate to the support beams, running underneath the machine, were added. The effect of that action can be seen Figure 14 and Figure 15, where the area under vibration has been reduced dramatically. As a result the operating range of the machine was restricted to below 175 Hz.

The beneficial effect of this strengthening operation was also verified (Figure 16), when an accelerometer was used to record the acceleration experienced by the strengthening beam which runs across the top of the machine, at a place above the oscillating chuck's linear bearings. When the machine operated with the 20 lobe cam, which has an amplitude of oscillation of 0.25 mm, the resonance peaks of 150 Hz and 200 Hz had been reduced, with the operation between 50 and 220 Hz becoming smoother. The same technique indicated that in the region of 250 - 275 Hz strong resonance occurs, which would affect the movement of the moving chuck and alter the expected sinusoidal motion.

Using a laser velocity meter (Figure 17) the behaviour of the beam was observed for the 40 lobe cam (with an amplitude of oscillation of 0.05 mm). A quiet region existed for the 40 lobe cam up to 150 Hz, where the same resonant behaviour as that of the 20 lobe cam was observed. Operation in frequencies above 500 Hz demonstrated as a series of resonant peaks.

4.3.1.3. Other Machine Enhancements

Three cams were produced initially (Table 1). A new single lobe cam was added with an amplitude of 3 mm. This was done to explore the low frequency, high amplitude region that was covered in the previous low frequency linear

friction welding machine built in the University. From the four cams available, experiments were done with the single and the four lobe cam (Figure 18 for operating frequencies and velocities for each cam used).

To further enhance the operation of the oscillating chuck and increase the life of its components, the oscillating chuck was further constrained at four points with the aid of linear bearings, in place of the single rolling bearing. Two were placed above and two below the oscillating chuck, to ensure that it could not move except in the horizontal direction. These linear bearings react to forces normal to the frictioning direction. Both the rollers and the flat areas that it rolls on were hardened to 800 VPN.

The stationary chuck is attached to the rig in a similar way to the oscillating chuck, with the aid of two beams. They are designed to be stiff in the direction parallel to the plane of movement, and provide little resistance to any vertical forces. But these forces can appear due to welding instabilities or machine behaviour. To limit this, without affecting its ability to move towards the oscillating chuck, the stationary chuck was further restricted in the vertical direction. This was achieved by positioning a support block underneath it. The top of this block was covered by a lubricated solid surface (PTFE) to minimise any friction forces that may be appear during welding as the stationary chuck moves towards the oscillating chuck due to axial shortening.

The initial coupling of the motor shaft to the multi-lobe cam shaft was a machined steel tube with a square keyway running the length of it. The inside diameter matched that of the camshaft. To accommodate the slightly smaller motor shaft, an annular insert was fitted inside half of the tube. Two keys fitted at either end and two screws acted on the shaft on the opposite side to the keys. Due to the large torque present, the keys and the keyway were damaged with one key apparently welded in place, and the camshaft was badly fretted.

The coupling between the AC motor shaft and the camshaft was therefore changed. The revised coupling comprises of a split ring over the shaft with annular wedges. The annular wedges are tightened together from each end of

the coupling by cap head bolts running parallel to the shaft. This way stresses are not concentrated in the keyway as before, and the torque is carried by the whole circumference of the shaft. It should be noted that any joint between the two shafts has to be easily removable as the multi-lobe cam needs to be changed for experiments.

The camshaft was also reduced in diameter to match that of the motor shaft.

A flywheel (32 in Figure 5) was added to the rig on the motor shaft, between the motor and the motor coupling. The purpose of this was to provide additional energy during welding with the twenty lobe cam. The additional force was necessary due to changes in the frictional resistance between the workpieces (9 and 30 in Figure 5), when the return spring force was set high.

A split collar specimen holder was made to accommodate smaller size bar specimens. This was made to extend the experimental work by using efficiently the available titanium alloy.

4.3.2. Instrumentation

4.3.2.1. Force Measurement

The parallel steel beams holding the stationary chuck were used to monitor the shear force acting on the frictioning interface (Figure 19) by means of strain gauges. The strain gauge bridge configuration is such as to compensate for temperature changes, zero out bending forces and sum compressive strains in the beams. Each beam has a separate strain gauge bridge, with the signal from each bridge added electronically after amplification (see Figure 20 for calibration chart).

The change in the area of the two supporting beams although provided a means to study the force acting on the frictioning interface, altered the behaviour of the stationary chuck. In effect it weakened the stationary chuck, causing it to vibrate, if friction pressures above a certain limit were used. This movement resulted in reduction of the effective amplitude of oscillation. This effect was pronounced in the case of the multi-lobe cams which is used to explore the higher frequency region above 300 Hz (see section "4.3.1.2.Rig

Stiffening" on page 35). For this reason the single (3 mm) and four lobe (0.92 mm) cam were used.

4.3.2.2. Linear Displacement Measurements

This was achieved with two LVDT transducers. The first was used to record the axial shortening of the specimens during welding (see Figure 21 for calibration chart). It was achieved by registering the movement of the fixed chuck during experiments relative to the stationary chuck restraint (see section "4.3.1.2.Rig Stiffening" on page 35). The other transducer was used to record the initial compression of the frictioning force springs, so as to interpret accurately the initial pressure applied, as well as the forging force employed at the end of the process (see Figure 22 for calibration chart). The axial shortening data provide an accurate history of the friction pressure applied to the specimens. Friction pressure changes during the process as the two specimens shorten due to plastic material extrusion, which in turn causes the frictioning pressure springs to expand and reduce the applied pressure.

5. Material Characterisation

5.1. Introduction

This chapter describes the composition and high temperature behaviour of the titanium alloy used primarily in the linear friction welding work described in this thesis. It also covers the experimental work done to characterise the frictional behaviour of Ti 6Al 4V, among other materials, for conditions that may be encountered in linear friction welding. The objective is to provide the experimental data for the constitutive equations used in the finite element code employed, in chapter 6 on page 55.

5.2. Titanium Alloy Ti 6Al 4V

Titanium and its alloys are noted primarily for outstanding strength-to-weight ratios, elevated temperature properties and corrosion resistance. They also possess good fatigue strength and toughness and in some cases excellent cryogenic properties. Ti 6Al 4V is the most widely used titanium alloy (Table 5). It is used in a variety of applications in the aerospace industry, such as gas turbine disks and blades, or for airframe structural components and other applications requiring strength at temperatures up to about 315°C. Other applications include high-strength prosthetic implants and chemical processing equipment.

5.2.1. Composition And Structure

5.2.1.1. Crystal Structure And Phases

Titanium has a hexagonal close packed crystal structure, called alpha (α), at room temperature. This structure changes to a body centered cubic crystal structure, called beta (β), at 883°C, which is stable up to the melting point of 1660 ± 15°C. Alloying elements favour one or the other structure, and cause the single transus temperature to change to two temperatures, the alpha, below which the alloy is completely alpha, and the beta transus, above which the alloy is completely beta. Between those two, both structures are present.

Alpha alloys can be welded, are non-heat treatable, stable up to 538°C, strong and tough at cryogenic temperatures, more oxidation resistant than beta or alpha-beta alloys and relatively difficult to form. Beta alloys can be heat treated in general, can be welded, stable up to 315°C, strong at higher temperatures for short periods, relatively brittle below -73°C and quite formable at room temperature. Alpha-beta alloys are a compromise between the single-phase alpha and beta alloys. They are heat treatable, stable in some cases up to 538°C, strong , and are more formable than alpha alloys. However, they are less tough than alpha alloys and, for the most part, somewhat more difficult to weld.

Ti 6Al 4V is an $\alpha + \beta$ alloy containing 6% aluminium and 4% vanadium (Figure 23). It has a comparatively high aluminium content which gives it excellent strength and elevated temperature properties. It is considered a "general purpose" titanium alloy. Aluminium stabilises the alpha phase and strengthens this phase by solid solution strengthening. The strengthening effect continuous up to about 538°C. Vanadium is the beta phase stabiliser and supplies more of the ductile beta phase during hot working, and sets the $\alpha + \beta$ / β transus temperature to 995 ± 15°C (**Imi**). At the transus temperature an allotropic transformation occurs from a beta BCC to an alpha HCP phase. Quenching the alloy from the beta stable region, where temperature is above 995°C, leads to the formation of an alpha structure produced by the martensitic transformation of the beta phase. This structure results from the nucleation and growth of the phase along one or several crystallographic planes of the prior beta matrix. Such grains take on a wide platelike appearance called a Widmanstäten structure. The coarseness of acicular alpha is related to cooling rate (**ASM,1972**).

The chemical activity of Ti 6Al 4V alloy increases with temperature. The most easily observed reaction illustrating the temperature effect is oxidation. Like almost all titanium alloys, a surface discoloration appears with air exposure at elevated temperatures. Various degrees of discoloration are detected, with the increasing titanium - oxygen reactivity indicated by stronger colour.

Interstitial elements are relatively small atoms which can assume a position in the interstices of the titanium lattice. The interstitial impurities present in the

Ti 6Al 4V alloy increase the transus temperature, and have an effect on strength. The strengthening effect of these interstitials decreases with temperature. At low temperatures, under severe stress conditions, brittleness may occur.

Ti 6Al 4V is also available in extra low interstitial content (ELI) grades, containing a maximum of 0.13 percent oxygen. It is used in applications which require significant ductility like cryogenic tankage, or resistance to crack in aqueous environments. They are also being used for their higher fracture toughness.

5.2.1.2. Processing

Normally shaped forgings are accomplished with finishing temperature in the alpha-beta region. This method has the advantages that oxidation rates are lower below the beta transus temperature, and the finish forging in the $\alpha + \beta$ condition produces a microstructure of primary equiaxed alpha in a matrix of transformed beta. This type of microstructure has been associated with maximum tensile ductility. Forging above the beta transus temperature allows to use less material at the beginning due to the easier flow of the metal and lowering machining requirements. Also, fracture toughness does improve **(Maykuth,1971)** with the acicular structure. The majority of beta forgings receive some deformation at temperatures below the transus temperature to restore tensile ductility.

Heat treatment procedures can be used to control mechanical properties, but the properties of the heat treated material represent the variables introduced prior to heat treatment. Annealing results in moderately low strength but ductile material, while specialised annealing heat treatments like beta annealing ensues nearly the same strength and ductility as annealing but with improved fracture toughness characteristics. Solution heat treatment with ageing treatment produces improved strength with some sacrifice in ductility and toughness. Beta heat treatments tend to lower strength and ductility but to improve toughness.

5.2.2. Material Properties

In a manner similar to that in most metallic materials, the strength of Ti 6Al 4V tends to decrease with increasing temperature. At temperatures in and above the age-hardening range, time becomes an influential variable. As the times involved in the linear friction welding are less than one-half hour (**Maykuth,1971**), only short time effects are concerned.

Typical physical properties for Ti 6Al 4V, like the coefficient of linear thermal expansion (Figure 24), thermal conductivity (Figure 25), specific heat (Figure 26) and yield stress (Figure 27) were obtained from (**Imi**) and for the dynamic high temperature behaviour (Figure 28) from (**Chaudhury,1992**). In the latter compression experiments were done at strain rates comparable to those found in linear friction welding and at similar temperatures.

5.2.3. High Temperature Dynamic Behaviour

Ti 6Al 4V has been shown to be strain rate sensitive at high strain rates, with no strain history effects on this sensitivity (**Duffy,1979**). All experimental results show a dependency of the stress-strain diagram on the strain rate and the temperature at which the tests were performed.

The temperatures encountered in friction welding of Ti 6Al 4V are in the superplastic range. During superplasticity, necking is delayed during plastic deformation. In areas where necking has begun already, the local reduction in the cross sectional area causes an increase in the local strain rate. Therefore, an increase in stress is required to continue deforming at the reduced cross sectional area. The higher the strain rate sensitivity value, the higher is the local stress which would be required for neck formation. The stress which is required to maintain deformation is mainly dependent on the level of the deformation rate and is independent of the instantaneous strain. Strain rate sensitivity values are derived from the flow stress and the corresponding strain rate

$$m = \frac{d \ln \sigma_f}{d \ln \dot{\varepsilon}} \quad (5.1)$$

where σ_f is the flow stress.

The strain rate sensitivity of metals could arise from the resistance presented by internal obstructions in the material. In most superplastic materials, strain hardening is due to the concurrent grain growth and not to the accumulation of defects. Grain size has the strongest effect on the strain rate sensitivity. As grains become finer, the flow stresses lower, producing higher strain rate sensitivity and longer tensile elongation. Fine grain size as exhibited by high strain rate sensitivity values and low flow stresses is not an adequate condition for large elongations. Grain growth causes accelerated strain localisation.

Characterisation of stress / strain rate behaviour can be made with step strain rate tests, where the strain rate is increased in consecutive steps and the steady (or saturated) flow stress is recorded. Unfortunately, with these kind of tests strain can become a variable along the stress - strain rate curve. Even when load relaxation tests results are used to derive the curves, more complex transient effects might be associated with the load relaxation tests (**Ghosh,1982**) producing erroneous results for applications where strain rates increase with accompanying strain.

In (**Lee,1967**) was the first published data on the superplastic behaviour of titanium and zirconium alloys. From a large number of tests at 800 - 1000°C, they observed a variation in the values of the strain rate sensitivity as a function of temperature. They related the rapid decrease in the strain rate sensitivity value to the transformation from alpha to beta phase. Experimental values of flow stresses were close to those reported by (**Chaudhury,1992**) for the same temperatures and strain rates. As temperature increases above beta transus, strain rate sensitivity decreases. In the beta region the structure coarsens, which is associated with low strain rates, while more refined structures were developed at higher strain rates.

In a recent report, a series of compression tests were performed on Ti 6Al 4V ELI (**Chaudhury,1992**) for temperatures between 800 and 1080°C and strain rates between 0.001 and 25 s^{-1}, which are close to those encountered in linear friction welding of Ti 6Al 4V. From the true stress - true strain flow curves, the strain rate sensitivity of the material is clearly exhibited (Figure 28 and Figure 29). At low strain rates (0.001, 0.01, 0.1 and 1 s^{-1}) and for the isothermal compressions at 800, 850 and 900°C the material strain softens after yielding. As the temperature of the experiment increases to 950, 1000, 1040 and 1080°C behaviour changes to strain hardening after yielding for the same strain rates. At the high strain rate of 25 s^{-1} the material has a small strain hardening region, followed by a plateau and softening after the small peak flow stress, for all temperatures. The strain rate of 5 s^{-1} follows an intermediate behaviour. At temperatures of 800 and 850°C has a true stress - true strain curve similar to the high strain rate tests, but from 900°C and onwards strain hardens as the lower strain rate tests.

Ti 6Al 4V is an α + β alloy with good elevated temperature properties. Its ductility and toughness are influenced by the temperature that it has been exposed, due to phase transformations occurring above the beta transus temperature. The material exhibits strain rate sensitive behaviour for the intermediate strain rates, which are those encountered in linear friction welding. The material properties described in this section have been used in the numerical modelling of the process, as well as to interpret experiments done with Ti 6Al 4V.

5.3. Frictional Behaviour Of Various Materials

As Amonton has stated in his empirical law of sliding friction, the friction force is proportional to the normal load, or if expressed mathematically

$$F_{fr} = \mu \times F_N \qquad (5.2)$$

where F_{fr} is the friction force, μ the coefficient of friction and F_N in the normal force. In most cases the precise value of the coefficient of friction depends strongly on the experimental condition under which it is measured.

Coulomb, also, stated in his third law of friction, that friction force is independent of sliding velocity. It is common experience that the frictional force to commence sliding a material is greater than that to maintain it, and therefore the coefficient of static friction is greater than that of sliding friction. It has been stated in the scientific literature that the coefficient of sliding friction is nearly independent of sliding velocity for a wide range, up until high sliding speeds of the order of tens of metres per second are reached, when the coefficient of friction starts to fall rapidly with velocity (**Bowden,1964**). Similar behaviour is exhibited for temperature changes, where the coefficient of friction is expected to remain constant unless phase transformations appear. In spite of these, other experimenters have found the coefficient of friction to be heavily dependent on temperature (**Sluzalec,1990**). These contradictory indications can be explained by the fact that the precise value of the coefficient of friction depends critically on the experimental conditions under which it is measured.

The aim of these measurements was to investigate the change in the coefficient of friction in loading conditions and material combinations that could be used in the numerical modelling of linear friction welding (Table 2). About 200 tests were conducted using different alloys in interface

temperatures from room temperature up to 900°C, under normal stress conditions of up to 30 MPa and rubbing velocities of 178 mm/s up to 700 mm/s.

5.3.1. Experiments

5.3.1.1. Apparatus

In order to represent the surface conditions of processes where the rubbing areas are larger than pins, tubular specimens were used. The specimens had typical dimensions of 22 mm length and radius (r) of 24 mm. The tubular specimens have thin walls (1 mm), for all points on the interface to experience the same approximate rubbing velocity. A Bridgeport milling machine was used to provide the rotary motion (Figure 30). The experimental apparatus was instrumented so that the interface coefficient of friction was measured indirectly. The stationary cylindrical specimen was placed in a fixture, which in turn rested on a Kistler piezoelectric transducer. Normal force was applied using a spring balance. The load cell was used to directly measure the normal force exerted by the rotating specimen on the stationary specimen, and to measure indirectly the horizontal friction force acting on the specimen. The vertical force applied on the specimen was transferred to the force measuring plate by means of a thrust bearing. The stationary specimen holder was free to rotate, resting on a thrust bearing which was firmly attached to the force transducer. As the bottom stationary specimen came in contact with the rotating specimen at the top, it would try to rotate as well only to be stopped by the pin. The horizontal reaction friction force F_{fr}, which was produced by the friction force on the rotating interface, was transmitted to the plate via a lever (Figure 31). The output from the charge amplifiers of the plate was recorded on a digital storage oscilloscope to be printed off line (Figure 32). Physically, the normal load applied F_N, the force F_{fr} produced by the friction force and the friction coefficient μ can be related by

$$\mu = \frac{F_{fr}}{F_N} \quad (5.3)$$

with R=r/d (Figure 31), where d is the distance of the pin attached to the load cell plate from the centre of rotation, transmitting the friction force experienced by the stationary specimen, and r the radius of the cylindrical specimen.

Alternatively, the coefficient of friction can be related to the stress conditions at the rubbing interface, with

$$\mu=\tau/\sigma_N \quad (5.4)$$

where τ is the shear stress at the rubbing interface, and σ_N is the normal stress at the rubbing interface. As the shear stress is

$$\tau = \frac{F_{fr}}{2\times\pi\times r\times\delta} \quad (5.5)$$

and the normal stress is

$$\sigma_N = \frac{F_N}{2\times\pi\times r\times\delta} \quad (5.6)$$

where δ is the thickness of the specimen walls, then Eqn. (5.4) becomes :

$$\mu = \frac{F_{fr}\times d}{r\times F_N} \quad (5.7)$$

as shown earlier in Eqn.(5.3).

5.3.1.2. Experimental Procedure

Measurements of F_N and F_{fr} were used to determine the coefficient of friction μ experimentally. A thermocouple was used to record the temperature (Figure 33) on the stationary specimen, which was spot welded on the outside face of the specimen at a known distance from the interface. The axial shortening of the specimens was also registered using a lever dial gauge, to compensate for the move of the rubbing interface closer to the thermocouple due to wear. These temperatures were later used to estimate the temperature at the sliding interface, by means of a transient finite element model for each material and interface temperature. Normal force was applied instantaneously on the stationary specimen by lowering the rotating specimen under spring pressure. The manual application of load allowed the applied force to fluctuate by ±15%.

5.3.1.3. Finite Element Model

As the recorded temperature was an indirect measure of the actual rubbing interface temperatures, a non linear finite element model was used to estimate the true temperatures encountered at the interface. The thermal analysis model comprised of a rectangular block of 800 two dimensional elements (Figure 34), where the material properties were temperature dependent. Thermal loads were applied at one face of the block and the transient response to that load was calculated over 100 time steps of 0.1 sec. The transient model incorporated the convective heat loss to the surroundings during the first few seconds after initial contact, from the side faces of the model, using a convection coefficient of 100 W/m^2 °C to represent the flow of air around the specimens, as well as conduction to the bulk of the block, which was initially at 20°C. The numerical simulation enabled the prediction of the true interface temperature, as it produced plots of the recorded temperature against the actual interface temperature for different thermocouple distances from the interface (Figure 35). As the axial shortening was recorded and the time when

the coefficient of friction was estimated, was known, this enabled the prediction of the interface temperature at that time.

5.3.1.4. Measurement Of The Coefficient Of Friction

The measured friction coefficient is valuable in representing the frictional behaviour, but it is difficult to corroborate its dependence on the various physical parameters. This is due to the sensitivity to vibration of these measurements, the fluctuation in the manual application of the normal load as well to other disturbances that occur during the experiments. An additional obstacle is that the recorded frictional force includes the torque necessary to overcome the frictional forces occurring in the transmission assembly, as well as the friction force generated at the rubbing specimens. The recorded coefficient of friction may be, therefore, slightly higher than that experienced by the rubbing materials. Figure 36 to Figure 59 show the experimental relationship between the coefficient of friction and normal stress or interface temperature for various material combinations and rubbing velocities.

In most cases (180 out of 202), each test resulted in a single value for the friction coefficient for a particular stress, interface temperature condition and rubbing velocity. The state represented was that of the steady state, where the friction force reached a plateau (Figure 32). In some experiments, more than one value of the coefficient of friction were calculated at intermediate temperatures during each run.

To verify the applicability of the experimental procedure followed, intermediate values of the friction coefficient where a large normal load was applied, were compared to the predicted values of the coefficient. In the case of Ti 6Al 4V, and stainless steel, a single test of the same material specimens, was taken to high temperatures (~800°C), for each case. The specimens exhibited noticeable extrusion and the rubbing interface became red. During these experiments, it was verified that the results obtained from the individual experiments for individual temperatures correlated with what really happens during rubbing of materials, where the temperature increases from room temperature to high values. The values of the coefficient of friction for intermediate temperatures produced were within 15% of the values expected

by the curves fitted to the experimental data (Table 3). Another tool that was used to validate the experimental results, were graphs relating interface temperature to normal stress and shear stress (Figure 60 and Figure 61). During these experiments plasticity was not observed macroscopically, and therefore the relation between temperature and stress, was linear.

5.3.1.5. Measurement Errors

Temperatures at the rubbing interface were measured indirectly with a thermocouple attached at a known distance from the end of the stationary specimen. As the two specimens rubbed together, wear caused axial shortening reducing the distance of the thermocouple from the interface. Although this was registered at the end of each run and was taken into account when interface temperatures were estimated, intermediate values would make temperature estimation more accurate. The effect of this error will be an underestimation of the interface temperature as the actual distance from the interface would have been bigger than the one recorded. Another source of error concerning temperature measurements, was the method of attaching the thermocouple to the specimen. Spot welding of the thermocouple wire to the stationary specimen allows calculation of the distance of that from the rubbing interface within 0.5 mm.

The measurement of the friction force was performed indirectly and average values were used to that effect, ignoring the initial force fluctuations due to seizing and galling (Figure 32).

5.3.2. Frictional Behaviour

More than two hundred frictional behaviour tests were analysed to determine the general effect of normal stress, interface temperature and rubbing velocity on friction coefficient. All experiments were conducted under normal atmospheric conditions at room temperature, and investigated the coefficient of friction up to temperatures of 900°C, normal stress conditions of up to 30 MPa and rubbing velocity from 178 mm/s up to 700 mm/s. All the experiments were performed under conditions where two equal area surfaces rub together, and can be used in the numerical modelling of such manufacturing processes where friction plays an important role.

All results were tabulated in graphs relating the coefficient of friction to interface temperature or stress, normal to the interface, for a given rubbing velocity (Figure 36 to Figure 59). A significant scatter in the results was observed due to fluctuations in the spring balance used to apply the load. Therefore a least squares line was fitted to the data. In these figures the lines allowing for the fluctuation of the normal load are included, as well as the lines where the standard error is included. The majority of the experimental data are between these limits.

All metal surfaces exhibit very strong adhesion in high vacuum and their coefficient of friction has high values, from 2 to 10. The reason for this behaviour is the strong metallic bonds which form at the interface. The extent of junction growth is limited only by the ductility of the material. When metals slide in air, much lower coefficients of friction are exhibited, similar to the ones observed in these experiments. Due to the presence of oxygen, oxide films form and play an important role in determining the frictional behaviour of metals. These films together with absorbed contaminants effectively isolate the two metal surfaces and inhibit the growth of strong adhesional films. As oxides act as low shear strength films and have low ductility which restricts junction growth, lower coefficient of friction is observed, compared to vacuum.

Results obtained in the frictional behaviour experiments are similar to experimental values reported in literature. In particular (ASM, 1992), the dynamic coefficient of friction of Ti 6Al 4V is reported to be 0.4 and 0.31 in different experimental arrangements. This is not in disagreement with the average room temperature value of 0.43 recorded here. Fluctuation in frictional force recorded (Figure 32) in the experiments indicate that stick-slip behaviour is exhibited, with the calculated friction coefficient being the steady state value for the experiment for each temperature state.

5.3.2.1. Rubbing Velocity

In all materials studied, a weak dependency on velocity appears to exist. The titanium alloy Ti 6Al 4V, mild steel EN 3 and stainless steel EN 58 studied showed the greatest sensitivity to rubbing velocity in the velocity range 178 -

480 mm/s, while the other steel showed the least. Increasing sliding speed has a direct beneficial effect on thermal softening and simultaneously reduces the time available for surface oxidation. These lead to higher junction growth and larger true area of contact, causing the coefficient of friction to increase slightly as witnessed in the experiments.

5.3.2.2. Materials

Every material studied exhibited the same trend in the coefficient of friction in relation to interface temperature or normal stress. If the coefficient of friction decreases with increasing normal stress, it will be inversely proportional to interface temperature also.

In the titanium alloy Ti 6Al 4V examined, the coefficient of friction is almost constant with interface temperature (Figure 36, Figure 37 and Figure 38). This insensitivity to interface temperature conditions, could be attributed to the mild wear regime experienced and the low oxide forming characteristics of the alloy (**Kubaschewski,1962**).

All three steels examined (stainless steel EN 58, mild steel EN 3 and through-hardening steel EN 31) showed similar frictional behaviour with respect to temperature (Figure 42 to Figure 44, Figure 48, Figure 49, Figure 52 and Figure 53). The coefficient of friction changes inversely proportional to temperature. In the case of the austenitic stainless steel EN 58 this effect is more pronounced. The increased power dissipated, indicated by the higher temperatures achieved, caused the friction coefficient to drop from the very high values of 1 to 0.25, possibly due to a reduction of strength of the asperities and the near-surface material. In the other two low alloy steels, the increased temperature resulted in surface oxidation, which produced a layer of oxides with the effect of reduced coefficient of friction. During the experiments with EN 3 and EN 31, when more than one tests were attempted with the same specimens, very low coefficients of friction were observed because of the oxides formed during the first test. To overcome this, the rubbing faces of the specimens were machined after each run to remove any oxides.

The dissimilar material experiment between the titanium alloy and stainless steel (Figure 56 and Figure 57) showed an inversely proportional relationship between coefficient of friction and temperature. Friction values and behaviour of this system fall in between those of each individual material, and some of the temperature sensitivity of stainless steel was exhibited.

The data produced by these experiments could not be characterised in a non-dimensional form, due to the number of variables. To represent the frictional behaviour of each material combination in terms of normal stress and temperature for the rubbing velocity and stress range studied in these experiments, a three dimensional surface was calculated as least squares fit to the experimental points for each material in the form of

$$\mu = A \times \sigma^{B} \times T^{C} \qquad (5.8)$$

where A is a process parameter lumping together external parameters , σ is the stress normal to the plane of movement and T the temperature at the rubbing interface (see Figure 62 for a typical frictional behaviour surface and Table 4 for the coefficients of the materials studied).

An experimental arrangement was devised to measure the coefficient of friction of sliding surfaces under a variety of temperature, normal stress and sliding velocity conditions similar to those found in linear friction welding. Measurements were made for four unlubricated similar couples (Ti, 6Al 4V, En 58, En 3, En 31) and one dissimilar metal combination (Ti 6Al 4V rubbing on En 58). Interface temperatures and normal stress conditions are shown to affect the value of the friction coefficient in the steels studied, while it did not affect the frictional behaviour of the titanium alloy. Rubbing velocity of the rotating surfaces is shown to have an effect on the friction coefficient of all steels, while affecting the titanium alloy studied by increasing its average value for velocities in the range 178-480 mm/s. Data from these experiments were used in the numerical modelling of the process.

6.Modelling Of The Linear Friction Welding Process

6.1. Introduction

This chapter describes the process model established for linear friction welding, and an analytical model to predict temperature rises during the initial phase of the process. The effects of the exothermic reaction of titanium with oxygen during extrusion are also discussed. The heat input of the process is presented as well. In addition to these, an analytical material flow model to predict strain rates during the extrusion phase is presented. Finally, the finite element model developed is described.

6.2. Process Model

The process can be divided into four distinct phases :

6.2.1. Phase I , The Initial Phase

During the initial phase the two materials are brought in contact under pressure. At this stage the two surfaces rest on asperities, and heat is generated from solid friction. Surface contact area is expected to increase throughout this phase. Although the shear force experienced is expected to rise as a consequence of the increase in contact area it remains sensibly constant (as seen in Figure 63 during the first 4.5 seconds, and in Figure 64 for the first 45 seconds). This is thought to be due to the fact that the shear yield stress decreases as the temperature increases, which compensates for the increase in the true contact area. There is no weld penetration at this stage (as can be verified in Figure 63 and Figure 64). Peak temperatures recorded are of the order of 630°C (Figure 65).

During phase I, if the speed at the interface is too low for a given axial force, insufficient heat will be generated. The heat produced must exceed that conducted away from the interface. If not, this will lead to insufficient thermal softening for the actual contact area to reach 100%.

6.2.2. Phase II , The Transition Phase

Following stage I, and provided sufficient heat has been produced for softening to occur, large wear particles begin to be expelled from the interface, and the heat affected zone expands until phase III is reached. From this stage onwards the contact area is considered to be 100%, and the plasticised layer formed between the two materials is no longer able to support the axial load. The shear force begins to increase (see Figure 63 during 4.5 and 5.5 seconds), while axial shortening shows no appreciable changes.

Macroscopically, in certain materials such as Ti 6Al 4V, red hot spots appear at the interface, that extend with time till they cover the whole of the rubbing interface, and are accompanied by an exothermic reaction with oxygen.

6.2.3. Phase III , The Equilibrium Phase

Succeeding stage II, axial shortening begins as a result of the expelled upset (Figure 63). The axial shortening varies approximately linearly with time. In the plasticised layer formed at the interface, the local stress system with the assistance of the oscillatory movement extrudes material from the interface into the flash. Temperatures reached at this stage measured by a thermocouple embedded in the specimen were found to be of the order of 840°C (Figure 65). After careful consideration of the factors which might affect temperature measurements, i.e. high temperature gradient, thermal response and positioning of the junction on the specimen, it would be ill-advised to use thermocouples as the sole method to obtain reliable temperature data from the rubbing interface in linear friction welding.

Instabilities can appear at this stage, due to uneven distribution of temperature. If the temperature increases in one part of the interface, the plasticised layer becomes thicker in that section, and more material is extruded. This can result in rotation of the interface from the original plane. The origin of this irregular behaviour could be attributed to an initial misalignment of the specimens. However, even the smallest difference may shift the area, where the maximum temperature appears on the rubbing interface, from the middle where it should be, in perfectly aligned specimens, to one side of the specimen parallel to movement. This then produces an

uneven distribution of temperature which causes further rotation of the interface. In some cases it can cause weakening of the weld (experiment D2 has low impact strength due to this reason).

Macroscopically, in certain materials such as Ti 6Al 4V, there is an exothermic reaction with oxygen.

In the case of Ti 6Al 4V the extruded material from the two specimens forms a single joined flash, and not separate flashes for each specimen. This indicates that the plastic material at the rubbing interface has joined at this stage.

6.2.4. Phase IV , The Deceleration Phase

When the desired upset is reached the two materials are brought to rest very rapidly (in less than 0.1 second), and forging pressure is applied to consolidate the weld. This last phase is thought of importance in industry, to consolidate the weld, the integrity of which is judged from the flash geometry.

See Figure 66 for a schematic illustration of the flash development during the four phases of the process.

6.3. Analytical Models

6.3.1. Temperature Prediction

6.3.1.1. Parameters Of Heat Flow Model

An analytical model was developed, which may give some insight into the early stages of linear friction welding. In order to retain a certain degree of predictive ability, this model forms a physical framework within which the semi-empirical descriptions of the material behaviour are incorporated. As pointed out by **(Ashby,1992)** there is a well accepted precedent for this approach in literature as an alternative to physical modelling.

As previously described, linear friction welding consists of four distinct phases. The purpose of the analytical model is to try to predict the early stages of the process when the temperature is rising rapidly.

At the beginning of the motion it is proposed that the two specimens are resting on asperities at the interface (Figure 67). The asperities are deforming predominantly in a plastic fashion under the normal load applied, as the contact is between rough metal surfaces. This incipient yield condition means that the area of contact will depend on the applied normal load and the yield stress of the material, with the latter depending on temperature. Thus the shear force will, under certain conditions, remain constant during phase I as temperature will increase due to friction, causing a reduction in yield stress.

6.3.1.2. Heat Flow Model

The specimens are moving in a sinusoidal motion (Figure 68). The shear stress (τ) exerted on the interface will be

$$\tau = \mu \times P_N \quad (6.1)$$

where μ is the coefficient of friction and P_N is the normal pressure. The heat generation rate per cycle per unit interfacial area (q) is

$$q = \tau \times \upsilon \quad (6.2)$$

where τ is the shear stress at the interface and υ is the rubbing velocity. By using Eqn. (6.1), Eqn. (6.2) becomes

$$q = \mu \times P_N \times \upsilon \quad (6.3)$$

The average heat rate can be determined by integrating Eqn. (6.3) over a cycle, or as the oscillatory motion is symmetrically cyclic, integrating four times a quarter of the cycle

$$q_0 = \frac{1}{T}\int_0^T q\,dt = \frac{4}{T}\int_0^{T/4} q\,dt = \frac{4}{T}\int_0^{T/4} \mu \cdot P_N \cdot \upsilon\,dt = \frac{4}{T}\int_0^{T/4} \mu \cdot P_N \cdot \alpha \cdot \omega \cdot \cos(\omega \cdot t)\,dt = \frac{2}{\pi} \cdot \mu \cdot P_N \cdot \alpha \cdot \omega$$

(6.4.)

The heat input to the surface calculated above will result in a temperature increase. This static model is similar to the case of a heat flux input to a solid

(slab) bounded by a pair of parallel planes, one of which is at the rubbing interface (Figure 69). This case of linear heat flow has been solved analytically (**Carslaw,1959**), with the heat flux a prescribed function of time.

The total heat flux is assumed to be a prescribed function of time, as it is related to the increase of true area of contact during initial rubbing. The true contact area is assumed to increase linearly during this phase from zero to the cross sectional area of the specimens at the end of the phase. No heat losses are assumed to the environment, as phase I is very short taking only a few seconds. The temperature θ, for different positions of the workpiece at a distance x from the interface, as a function of time during phase I will be (**Carslaw,1959**)

$$\vartheta = \frac{2^{m+1}\cdot q_0 \cdot \kappa^{1/2}\cdot t^{(m+1)/2}\cdot \Gamma\left(\frac{1}{2}m+1\right)}{K}\sum_{n=0}^{\infty}\left\{ i^{m+1}\,erfc\frac{(2n+1)\cdot L_o - x}{2(\kappa\cdot t)^{1/2}} + i^{m+1}\,erfc\frac{(2n+1)\cdot L_o + x}{2(\kappa\cdot t)^{1/2}}\right\}$$

(6.5)

where κ is the diffusivity, Γ the Euler gamma function, t the time, L_o the length (overhang) of the specimen. The flux input is a prescribed function of time $q_0 t^{1/2m}$, where m = -1,0,1. In this case m=2 as the flux is assumed to change linearly with time as is the true area of contact.

This equation (6.5) predicts that heating time will be inversely proportional to the square of the ratio of the heat generation per unit interfacial area. As a result of that, short heating time requires the use of high specific power during welding, which can be achieved with high rubbing velocities, or small areas of contact, or high frictioning pressures.

6.3.1.3. Temperature Model Validation

Using the modelling capabilities of the Mathcad simulation package, the model described above was used to predict temperature profiles during initial rubbing. Non-linear material properties were used, with the yield stress of Ti

6Al 4V assumed to change linearly with temperature. Other mechanical and physical properties were taken at the average values for the temperature range predicted. The true area of contact was taken to change linearly with time during phase I, as the process model proposed earlier suggests. At the end of this phase, there is 100% contact between the two rubbing surfaces. The friction coefficient was assumed to change with time as in the experiments. Temperatures were predicted in steps of 0.01 seconds using Eqn. (6.5), where the value of the yield stress used to calculate the frictional heat varied in every step according to the previous step's temperature value.

The temperature increase at the position of the embedded thermocouple was calculated and compared to experimental results (Figure 70). The model assumed oscillating specimens at a frequency of 30 Hz with interface area of 60 mm^2 and an amplitude of oscillation of 0.92 mm as in the experiment. From the experimental data the time length of phase I was identified to be 4 seconds approximately, before the axial shortening of the specimens becomes appreciable. During this time the coefficient of friction changed linearly from 0.25 to 0.55. The temperature profile predicted by this one dimensional model is similar in shape to the one observed in the experiment, with the temperature rising rapidly at the beginning and then decreasing its rate of increase and reaching a higher temperature at the end of the phase. The temperature prediction could be improved if a two dimensional model or temperature dependent material properties were used. The importance of the later is shown when temperature independent properties were used in the model.

Both solutions for temperature dependent and temperature independent material property values were calculated. If the dependence of yield stress on temperature is taken into account then the interface temperature predicted is much closer to the experimental data (Table 6 and Figure 70) with the shape of the temperature profile following the experiment.

6.3.1.4. Exothermic Reaction Effects

As the process enters phase III, bright sparks appear at the interface due to reaction of titanium with oxygen in the atmosphere forming titanium oxide. The heat of formation of TiO_2 from titanium is Δh_{25} = -214.1 kcal/mole at

25°C (**Perry,1984**). The increment in heat content (Δh) is the reaction of forming the given substance from its elements, in their standard states. When Δh is negative heat is evolved in the process. As the reaction takes place at much higher temperatures than 25°C the heat of formation can be estimated from (**Perry,1984**):

$$\Delta h_T = \Delta h_{25} + \int_{298}^{T} c\, dT \qquad (6.6)$$

where the heat capacity can be calculated from $c=a_1+a_2T+a_3T^2+a_4T^3$. Using data for Ti 6Al 4V (**Imi**) the temperature dependency of c can be found to have the following coefficients : $a_1=585.8$, $a_2=0.4727$, $a_3= -0.0009$ and $a_4=7E-7$.

As the highest temperatures encountered are at the interface, it is assumed that this exothermic reaction may take place with the hot material that is extruded into the flash every cycle. Therefore, to estimate the rise in temperature due to this reaction the mass of the material that is available every cycle for oxidation should be known. From experimental data on the size of the flash, it can be estimated that the mass of material that can be oxidised will be

mass oxidised=ρ x flash area x thickness of layer consumed during oxidation

(6.7)

where the surface area of the flash can be calculated from the measured average thickness of the flash, the dimensions of the specimens and the length of the flash material extruded every cycle. The length of the flash material extruded every cycle which is added to the existing flash matter can be estimated from the material flow analysis section in chapter 7. Average values for the 3 mm amplitude case are 1 mm for the thickness of flash, 0.3 mm of length is added every cycle to the existing flash in the direction of movement and 0.1 mm of length is added every cycle to the existing flash from the specimen face parallel to movement. Assuming that the thickness of the layer

consumed is 0.01 mm, the temperature rise in the flash material that was just extruded due to the formation of TiO_2 is 8.8°C, if all the titanium around the outer surface of the flash reacted with oxygen.

The temperature increase is similar for both amplitudes of oscillation, and depends on the thickness of the flash and the material consumed. However, this spectacular effect during linear friction welding of Ti 6Al 4V will not be an important contribution to the temperature rise in the flash or the neighbouring specimen.

6.3.2. Process Heat Input Model

Frictional heat input in linear friction welding is not uniform with time as the two specimens move sinusoidally. From Eqn. (6.3) it can be seen that normal pressure P_N will change during every cycle causing the heat input to fluctuate as well. While the normal force remains constant, the area of contact between the two workpieces will change with movement with the normal pressure oscillating in turn. With the velocity changing with time as :

$$\upsilon = \alpha\, \omega \cos(\omega\, t) \quad (6.8)$$

and the normal force being

$$P_N = \frac{F_{fr}}{cross-sectional\ area} = \frac{F_{fr}}{W \times (L - \alpha \sin(\omega t))} \quad (6.9)$$

where F_{fr} is the friction force, W is the width and L the length of the specimen. Then the frictional heat (6.3) generated will be

$$q = \frac{\mu F_{fr} \alpha \omega}{W} \cdot \frac{\cos(\omega t)}{L - \alpha \sin(\omega t)} \quad (6.10)$$

The instantaneous heat input is therefore affected by the second fraction of Eqn. (6.10). Plotting this normalised frictional heat term against time and comparing it with the displacement of the specimens which oscillate at 5 Hz (Figure 71) for two different amplitudes of oscillation (0.5 mm and 5 mm), it can be seen that the larger amplitude of oscillation has the effect of shifting the heat input curve towards the extreme points of oscillation. Maximum heat

input does not happen any longer at the middle point of oscillation but at a point in time before that. This has the added effect of concentrating heat input during the same half of the cycle instead of being symmetrically distributed during every half of the cycle.

6.3.3. Material Flow Model

6.3.3.1. Constitutive Equations

During extrusion in phase III the strain rates encountered by the rubbing material must be influenced by the amplitude and the frequency of oscillation, as well as the size of the heat affected zone formed at the interface. These strain rates will be experienced by material in a narrow zone adjacent to the rubbing interface. They will unavoidably affect yielding of the hot material. If strain rates are high enough to limit the drop in yield stress of the material due to temperature, plasticity will not appear and material extrusion will not take place.

The heat affected zone of the rubbing interface can be divided into the following sections (Figure 72) similarly to (**Midling,1994**)'s model of rotary friction welding :

a) the plastic section at the interface. The strain rate is influenced by the rubbing velocity υ, the axial shortening velocity υ_o and the rate that the material is expelled from the stationary side of the specimens. Material extrusion into the flash is due to the existence of this section.

b) the partially deformed section. The plastic deformation is limited by the axial shortening velocity υ_o and the rate that the material is expelled from the stationary side of the specimens.

It is assumed that at phase III, steady state conditions have been reached, with the rate of axial shortening being effectively constant. It is supposed that the size or the shape of these regions do not change with time. It is also assumed that the elastic section of the specimen supports the sections that have plastically deformed. Another assumption used is that material extrudes continuously, due to the movement of the specimens.

The distribution of strain rate in the section of interest can be calculated from a number of velocity equations, which satisfy the boundary conditions of the system. The cartesian velocity profiles along the interface are assumed to follow the profile of the deformed sections. Material extrusion is assumed to be the combined effect of the friction pressure, which extrudes material from all faces of the specimen, and the oscillatory movement. The latter is assumed to affect the velocity profile in the direction of movement, and does not exist in rotary friction welding (compared to (**Midling,1994**)). The following kinematically admissible velocity equations can be formulated :

$$\upsilon_x = \upsilon_z + \upsilon \cdot \left[1 - \left(\frac{y}{y_{pl}}\right)^{\xi}\right], \quad y \le y_{pl}$$

or (6.11)

$$\upsilon_x = \alpha_x \cdot \upsilon_0 \cdot \frac{x}{L_2} \cdot \left[1 - \left(\frac{y}{h}\right)^{\rho_x}\right] + \upsilon \cdot \left[1 - \left(\frac{y}{y_{pl}}\right)^{\xi}\right]$$

$$\upsilon_y = \upsilon_y(y) \qquad (6.12)$$

$$\upsilon_z = \alpha_x \cdot \upsilon_0 \cdot \frac{z}{W/2} \cdot \left[1 - \left(\frac{y}{h}\right)^{\rho_x}\right], \quad y \le h \qquad (6.13)$$

where z is the direction perpendicular to movement, x the direction of movement and y the axial distance in the heat affected zone. The term ξ is a dimensionless term which characterises the strain rate distribution in the plastic section, ρ_s another dimensionless term characterising the flash shape and α_s a dimensionless term characterising the velocity distribution in the plastic zone.

The equation (6.11) for υ_z suggests that it increases from a minimum value of zero at the border of the undeformed material to a maximum value of $\upsilon_z = \alpha_s \cdot \upsilon_0 \cdot {}^{z}/_{W_2}$ at the rubbing interface. The velocity component in the direction of movement υ_x incorporates two components. The first equals to υ_z and the other is due to the oscillatory movement.

The individual components of strain rate can be evaluated as follows :

$$\dot{\varepsilon}_{xx} = \frac{\partial \upsilon_x}{\partial x} = \frac{\alpha_s \cdot \upsilon_0}{L/2} \cdot \left[1 - \left(\frac{y}{h}\right)^{\rho_s}\right] \tag{6.14}$$

$$\dot{\varepsilon}_{yy} = \frac{\partial \upsilon_y}{\partial y} \tag{6.15}$$

$$\dot{\varepsilon}_{zz} = \frac{\partial \upsilon_z}{\partial z} = \frac{\alpha_s \cdot \upsilon_0}{W/2} \cdot \left[1 - \left(\frac{y}{h}\right)^{\rho_s}\right] \tag{6.16}$$

$$\dot{\varepsilon}_{xy} = \frac{1}{2}\left(\frac{\partial \upsilon_x}{\partial y} + \frac{\partial \upsilon_y}{\partial x}\right) = \frac{1}{2}\left(-\frac{\alpha_s \cdot \rho_s \cdot \upsilon_0 \cdot x}{L/2} \cdot \left(\frac{y}{h}\right)^{\rho_s - 1} - \upsilon \cdot \xi \left(\frac{y}{y_{pl}}\right)^{\xi - 1}\right) \tag{6.17}$$

$$\dot{\varepsilon}_{yz} = \frac{1}{2}\left(\frac{\partial \upsilon_y}{\partial z} + \frac{\partial \upsilon_z}{\partial y}\right) = \frac{1}{2}\left(-\frac{\alpha_s \cdot \upsilon_0 \cdot z \cdot \rho}{W_2} \cdot \left(\frac{y}{h}\right)^{\rho_s - 1}\right) \tag{6.18}$$

$$\dot{\varepsilon}_{xz} = \frac{1}{2}\left(\frac{\partial \upsilon_x}{\partial z} + \frac{\partial \upsilon_z}{\partial x}\right) = 0 \qquad (6.19)$$

From volume constancy :

$$\dot{\varepsilon}_{xx} + \dot{\varepsilon}_{yy} + \dot{\varepsilon}_{zz} = 0 \qquad (6.20)$$

which leads to

$$\dot{\varepsilon}_{yy} = \left(-\frac{2 \cdot \alpha_s \cdot \upsilon_0}{1/W + 1/L} \cdot \left(1 - \left(\frac{y}{h}\right)^{\rho_s}\right)\right) \qquad (6.21)$$

after integration of Eqn.(6.15)

$$\upsilon_y = -2 \cdot \alpha_s \cdot \upsilon_0 \cdot \left(\frac{1}{L} + \frac{1}{W}\right) \cdot \left[y - \frac{h}{\rho_s + 1} \cdot \left(\frac{y}{h}\right)^{\rho_s + 1}\right] + C \qquad (6.22)$$

Factor C in equation (6.22) can be determined as at y=h $\upsilon_y = -\upsilon_0$

$$C = -\upsilon_0 + 2 \cdot \alpha_s \cdot \upsilon_0 \cdot h \cdot \left(\frac{1}{L} + \frac{1}{W}\right) \cdot \left(1 - \frac{1}{\rho_s + 1}\right) \qquad (6.23)$$

$$\text{so } \upsilon_y = -\upsilon_0 + 2\cdot\alpha_s\cdot\upsilon_0\cdot h\cdot\left(\frac{1}{L}+\frac{1}{W}\right)\cdot\left(1-\frac{1}{\rho_s+1}-\frac{y}{h}+\frac{1}{\rho_s+1}\cdot\left(\frac{y}{h}\right)^{\rho_s+1}\right) \qquad (6.24)$$

then α_s can be evaluated from Eqn.(6.24), as $\upsilon_y = 0$ at y=0

$$\alpha_s = \frac{\rho_s+1}{\rho_s}\cdot\frac{1}{2\cdot h\cdot\left(\frac{1}{L}+\frac{1}{W}\right)} \qquad (6.25)$$

substituting back these values, the velocity components become :

$$\upsilon_x = \frac{\upsilon_0}{\rho_s}\cdot\left(\rho_s+\left(\frac{y}{h}\right)^{\rho_s+1}-y\frac{\rho_s+1}{h}\right) \qquad (6.26)$$

$$\upsilon_y = \frac{\rho_s+1}{\rho_s}\cdot\upsilon_0\cdot\frac{z}{W\cdot h\cdot\left(\frac{1}{L}+\frac{1}{W}\right)}\cdot\left[1-\left(\frac{y}{h}\right)^{\rho_s}\right] \qquad (6.27)$$

$$\upsilon_z = \frac{\upsilon_0}{\rho_s}\cdot\left[\rho_s+\left(\frac{y}{h}\right)^{\rho_s+1}-y\cdot\frac{(\rho_s+1)}{h}\right] \qquad (6.28)$$

and the strain rate components are :

$$\dot{\varepsilon}_{xx} = \frac{\rho_s + 1}{\rho_s} \cdot \frac{\upsilon_0}{L \cdot h \cdot \left(\frac{1}{L} + \frac{1}{W}\right)} \cdot \left[1 - \left(\frac{y}{h}\right)^{\rho_s}\right] \qquad (6.29)$$

$$\dot{\varepsilon}_{yy} = \frac{\upsilon_0 \cdot (\rho_s + 1)}{\rho_s} \left[\left(\frac{y}{h}\right)^{\rho_s} - \frac{1}{h}\right] \qquad (6.30)$$

$$\dot{\varepsilon}_{zz} = \frac{\rho_s + 1}{\rho_s} \cdot \frac{\alpha_s \cdot \upsilon_0}{W \cdot h \cdot \left(\frac{1}{L} + \frac{1}{W}\right)} \cdot \left[1 - \left(\frac{y}{h}\right)^{\rho_s}\right] \qquad (6.31)$$

$$\dot{\varepsilon}_{xy} = -\frac{1}{2}\left(\frac{(\rho_s + 1) \cdot \upsilon_0 \cdot x}{L \cdot h \cdot \left(\frac{1}{L} + \frac{1}{W}\right)} \cdot \left(\frac{y}{h}\right)^{\rho_s - 1} + \upsilon \cdot \xi \left(\frac{y}{y_{pl}}\right)^{\xi - 1}\right) \qquad (6.32)$$

$$\dot{\varepsilon}_{yz} = -\frac{(\rho_s + 1) \cdot \upsilon_0 \cdot z}{2 \cdot h \cdot W \cdot \left(\frac{1}{L} + \frac{1}{W}\right)} \left(\frac{y}{h}\right)^{\rho_s - 1} \qquad (6.33)$$

$$\dot{\varepsilon}_{xz} = 0 \qquad (6.34)$$

The dimensionless term ρ_s can be evaluated by measuring the length (ℓ) of the extruded matter at y=0. The flash is generated during the axial shortening time (t_t), which is less than the total welding time. Then ℓ can be calculated by integrating the velocity component in the direction perpendicular to movement υ_z (Eqn.(6.28)) over t_t :

$$l = \int_0^{t_f} \upsilon_z (y=0)\, dt = \frac{\rho_s + 1}{\rho_s} \cdot \frac{\upsilon_0 \cdot z \cdot t_f}{h \cdot W \cdot \left(\frac{1}{L} + \frac{1}{W}\right)} \qquad (6.35)$$

estimating it at the face of the specimen, i.e. $z = \frac{W}{2}$

then Eqn. (6.35)

$$\rho_s = \frac{\upsilon_o \cdot t_f}{2 \cdot h \cdot l \cdot \left(\frac{1}{L} + \frac{1}{W}\right) - \upsilon_o \cdot t_f} \qquad (6.36)$$

6.3.3.2. Strain Rate Predictions

The application of this model to linear friction welding requires the estimation of the dimensionless parameter ξ. This parameter influences the form of the velocity field in the direction of oscillation. Its value can be estimated at the centre of the specimens by the difference of the velocity components :

$$\xi = \frac{\ln\left(1 - \frac{\upsilon_x - \upsilon_z}{\upsilon}\right)}{\ln\left(\frac{y}{y_{pl}}\right)} \qquad (6.37)$$

Using these equations, the main components of strain rate were calculated for two experiments done at 0.92 mm amplitude of oscillation (D12 and D17)) and frequencies of 65 Hz and 100 Hz (see Figure 73 for prediction of strain rates in the xx and zz direction, using parameters from Table 7). The effect of the higher frequency of oscillation is shown in the predicted strain rates in both directions. In the 100 Hz experiment both strain rate components were below 3.5 s^{-1}. These appear as overestimates as at such high strain rates the initial

applied friction pressure of 50.2 MPa would have been inadequate to yield the material at the interface. If the temperature at the rubbing interface is at about 900°C (see process model in this chapter) at these strain rates the shear yield stress is around 100 MPa (**Chaudhury,1994**). But both predictions indicate that the higher strain rates encountered at the interface with increasing frequency of oscillation will require increased friction pressures to achieve yielding conditions and therefore weld (see chapter 8 for experimental verification).

6.4. Numerical Model

Linear friction welding is a complex physical process whose realistic modelling requires a numerical tool with the following features :

- Thermal-mechanical coupling The process can be separated into a mechanical and a thermal problem to be solved in parallel during every time step in the analysis. Work done due to friction and plasticity in the mechanical side of the analysis affect the temperature field. Following data transfer from the mechanical analysis, the updated temperatures are taken into account to calculate strains and stresses. This sequential process takes place for every step in the analysis.

- Material non linearity As early work with simple analytical models has shown, material properties affect considerably the accuracy of the predictions. Temperature dependent material properties are essential in the accurate representation of the process including the use of viscoplastic constitutive laws for the case of Ti 6Al 4V.

- Complex thermal boundary conditions This includes conduction of heat from the rubbing interface to the bulk of the specimens, convection losses to the surrounding air, radiation losses due to the high temperatures reached (of the order of 1000°C) and friction flux as a result of movement between the two specimens.

- Complex mechanical boundary conditions. These involve variation with time of both the surface contact area and the frictional parameters. The surface contact area changes with time due to the sinusoidal movement of

the specimens. The frictional parameters vary with temperature as experiments have shown. In the vast majority of the finite element work reviewed frictional heat input is modelled to follow experimental values. Obviously, this approach limits the ability to use numerical modelling as a predictive tool.

- Error estimation In a non-linear analysis an iterative procedure is used for solution. It is therefore required for both the thermal and mechanical fields to guarantee a sustained accuracy throughout the process by controlling the error due to the residual forces at the end of every iteration..

6.4.1. Finite Element Model

The finite element method has been used in this work. The reader will be able to refer to a number of textbooks, such as **(Owen,1980)** and **(Zienkiewicz,1989)**, for information on this established method. The numerical simulation of the process was undertaken with recourse to Elfen (version 2.6), a proprietary finite element software programme developed by Rockfield Ltd.

Rotary friction welding may be modelled axisymmetrically, therefore creating a much smaller model with reduced computational requirements. The process model of linear friction welding of similar metals can be reduced to half of the original model size. This can be achieved by defining one of the two specimens as rigid, leaving the other object as deformable body. Although frictional heat is generated between deformable and rigid surfaces, temperature rises are effected only on the deformable body reducing the processing time respectively. Due to the long processing times involved (of the order of 15 hours of CPU time on a Silicon Graphics Challenge computer), a two dimensional model can provide an insight into the physics of the problem at reasonable processing times.

The linear friction welding model comprises of two objects, representing the two specimens in the process (Figure 74). A total of 764 isoparametric triangular elements are employed to discretise the two blocks. The top object is set as deformable, while the one at the bottom as rigid in an effort to reduce the problem and shorten the analysis time. Plane stress elements are used in

the mesh, as experiments have shown that there is limited material extrusion from the interface side early in the process. This material extrusion appears not only from the direction of movement, but also from the direction parallel to that. Another benefit of the plane stress elements is that they are not as stiff as the plane strain elements, reducing the numerical difficulties encountered by the finite element programme during the iterative solution.

The bottom object is constrained in the x and y directions along the bottom face of it. The nodes at the top face of the top block are coupled to move together in both degrees of freedom, as they are the nodes where the oscillatory movement and the friction pressure is applied on. The constraint for the thermal model is to set an initial temperature of 20°C for both objects.

The mechanical loads applied are the friction pressure on the top face of the top block, and a prescribed displacement at the corner node of the same face. The top block is displaced in the direction parallel to the long sides of the specimens by an amount equal to the amplitude of oscillation. The displacement changes with time to a sinusoidal function at the required frequency of oscillation. This load is effected from the beginning of the analysis, with the oscillation cycle discretised into 40 steps. The time increment between every step in the analysis are set to correspond to the time steps of the movement. The applied pressure is increased to the required friction pressure in two increments during the first two time steps of the analysis, to assist convergence during the beginning of the analysis.

Loading for the thermal analysis includes convection and radiation losses. A boundary is used to represent heat removal to the environment by convective heat transfer. The rate of heat transfer is dependent upon the thermal properties of the medium, the degree to which flow is being forced past the surface, and the ambient temperature of the environment. All these factors are combined and represented using a single convection coefficient. The direction of the convection is normal to the surface and the coefficient used has a value of 100 W/m^2 °C. The radiation boundary is applied to the rubbing surface, as well as the sides of the specimen, to represent energy lost by black body emission. The only factors which affect the energy transmission are the temperature differential between the surface and the surrounding medium, and

the emissivity of the surface which was set to 0.8, similar to those for metal oxides.

Non-linear mechanical and thermal material properties (**Imi**) are used, whose values depend temperature (as described in chapter 5). The power law viscoplastic option is used in Elfen (**Elfen,1996**) to represent the material flow rule. The viscoplastic flow rate $\dot{\tilde{\varepsilon}}^{vp}$ can be associated to stress conditions in the finite element formulation with :

$$\dot{\tilde{\varepsilon}}^{vp} = \gamma \left[\frac{\tilde{\sigma} - \tilde{\sigma}_y}{\tilde{\sigma}_y} \right]^N \qquad (6.38)$$

From experimental data at the temperatures and strain rates most likely to be encountered in linear friction welding of Ti 6Al 4V (**Chaudhury,1992**) the fluidity parameter γ is set to 2.75E-4 and the exponent N to 4.

Contact between the two sliding surfaces is modelled with a series of contact sets, commonly known as slidelines. The slidelines belonging to the bottom surface are defined as rigid. Rigid surfaces are used where there is no deformation and the object stays in the original position unless it is moved. The top surface which is the one under study is defined as deformable. As the surfaces are in sliding contact the friction law of Coulomb is used. Frictional work is generated only when parts of the contact surfaces are in contact.

For the contact algorithm to simulate the process of friction, special elements are used in slidelines. These elements allow bodies to invade the space occupied by the object they belong to and resist this intrusion according to the value of a normal penalty coefficient. This coefficient is set to the product of the average Young's modulus and the average element length on the surface. To define the mechanical behaviour of the slidelines a number of associated data are necessary, such as the friction coefficient and parameters for the numerical simulation of deformable bodies. For these analyses, data relating the change of the friction coefficient with interface temperature are used as

provided by the frictional behaviour experiments described in the previous chapter (Figure 75).

During the course of the numerical work it was found that convergence problems occurred during oscillation of the objects. They originated in the sharp corners of the deformable object at the top, where the reaction forces introduced locally by the analysis to overcome intrusion of elements by these nodes produced numerical difficulties which often resulted in crashing the analysis. To overcome this, rounded corners were introduced, composed of smaller slideline segments.

The experimental procedure and results used to confirm the accuracy of this numerical model are given in chapter 7. As fully coupled thermo-mechanical adaptivity was not available for the software release used, the model was employed to investigate the process up to where large deformations begin to form.

7. Experimental Results

The experimental work undertaken in this thesis can be separated into five distinct sections:

(i.) An investigation into the frictional behaviour of various materials. The aim is to quantify the parameters that affect the value of the coefficient of friction under conditions similar to those encountered in linear friction welding. The effects of normal pressure, sliding velocity and temperature were explored for a number of materials, including Ti 6Al 4V. Results from this work as described in chapter 5 are used in the numerical work undertaken in chapter 6 of this thesis.

(ii.) An investigation into the effects of frequency and amplitude of oscillation on linear friction welding of Ti 6Al 4V. The influences these two parameters have on reaching the conditions to achieve a weld are analysed.

(iii.) Identification of process parameters which have a significant effect on the weld integrity of linear friction welding of Ti 6Al 4V. Fractional factorial experimental design techniques are also used to estimate the importance of some parameters, as well as their combined effect.

(iv.) Experimental verification of the numerical models developed to study the early stages of the linear friction welding process. The two-dimensional model developed, incorporating the strain-rate dependent behaviour of Ti 6Al 4V at high temperatures as well as its frictional behaviour, enabled to qualitatively study the effects of frequency of oscillation and friction pressure on achieving weldability conditions and to study the conditions under which welds fail to develop. Temperatures and stress conditions recorded from the experiments compare favourably to numerical simulations.

(v.) A preliminary study of linear friction welding of pure lead. Using a pure single phase metal, the conditions under which the process fails were studied and related to the numerical and experimental work with Ti 6Al 4V.

7.1. Experimental Procedure

The experiments were performed at 293 K (room temperature) and prevailing atmospheric conditions. Specimens of all materials were machined to 10 mm (L) by 6 mm (W) dimensions, where the length (L) of the specimen is in the direction of movement. The amplitude of oscillation studied was 0.92 mm and 3 mm, using a four lobe and a single lobe cam respectively. The large amplitude single lobe cam was used to explore the low frequency region at an amplitude of oscillation that had been used previously (**Garton,1987**), with the small amplitude four lobe cam to investigate higher frequencies of oscillation effects, at moderate rubbing velocities. The explored frequency range was from 5 Hz to 119 Hz, for friction pressures ranging from 5.3 MPa to 79.8 MPa.

The following procedure was followed during testing (see chapter 4 for rig details):

1. Ensure return spring is fully released.
2. Latch the toggle mechanism
3. Set the desired axial shortening
4. Insert specimens into chuck, and ensure that they are tightened sufficiently to stop rotation
5. Place tightening beams across the top of the rig and bolt them
6. Tighten return spring to desired force, for it to push the oscillating chuck into contact with the cam at all time.
7. Tighten axial force springs to set desired friction pressure.
8. Run motor up to desired speed. Welding commences.
9. When cam disengages, apply forging force if necessary.

7.1.1. Process Monitoring

The process is monitored by recording the axial displacement of the stationary chuck and the shear force exerted on the rubbing interface. The strain gauge bridge registers the strain induced on the supporting beams of the stationary chuck by the shear force. Due to the construction of the rig, the friction pressure applied changes during operation with material extrusion at the rubbing interface. As the two specimens shorten, the friction pressure springs expand reducing the friction pressure. The axial shortening history provided by an LVDT supplies the data necessary to calculate the changing friction pressure, and estimate the coefficient of friction during the process. The shear force recorded together with the normal force applied to the rubbing specimens characterise the stress condition at the interface.

In Figure 63 shear force and axial displacement history traces are shown. The apparent drift of zero in the shear force trace in Figure 63, is due to incomplete cancellation of bending strains in the stationary chuck beams (item 31 in Figure 5) which was taken into account in calibration.

In Figure 65 a temperature plot from a test done at an oscillating frequency of 10 Hz is shown. The thermocouple junction was initially at 0.7 mm away from the rubbing interface, and the experiment was done with a stepped friction pressure profile to investigate the temperatures reached at the various stages of the process. The peak temperature reached at the beginning corresponds to 630 °C and represents peak temperatures during phase I (as described in chapter 6). The shear force (see Figure 64 remains constant during the first 45 seconds and there is no axial shortening. Following this stage, the friction pressure was increased for extrusion to occur (as described for phase III conditions in chapter 6) and the peak temperature recorded was 840°C. This was achieved when the thermocouple reached the interface, after some material was extruded from the sides. However, it must be noted that thermocouple measurements can give underestimates of the actual conditions due to the limited control over the themal inertia, the response time and the positioning of the junction in the specimen

A specific power input parameter (w) is used to characterise the process parameters employed for each experiment :

$$w = \frac{\alpha \times f \times P_{fr}}{2 \times \pi \times cross-sectional\ area} \quad (7.1)$$

where the amplitude of oscillation is measured in millimetres, the frequency of oscillation in Hertz and the friction pressure in MPa, and the units of w are kW/mm^2.

Alternatively, the RMS *heat input* at the rubbing interface can be estimated from the apparent friction coefficient calculated in the following section

$$Heat\ input = \mu \times P_{fr} \times \alpha \times 2 \times \pi \times f/\sqrt{2} \quad (7.2)$$

As the friction coefficient changes during the process due to temperature and interface conditions, in the heat input calculations the value towards the end of phase I is used. This represents the heat input conditions just before entering the extrusion phase.

7.2. Stress Conditions

7.2.1. Coefficient Of Friction

Friction welding joins materials by extruding plastic material at the rubbing interface. Hence, stress conditions will control the onset of plasticity and the subsequent flash formation.

Shear stress (Figure 64) changes as the rubbing specimens go through the different phases of the process. The apparent coefficient of friction can be used to describe the stress conditions at the interface, as it is the ratio of the

shear force at the interface to the normal force applied (Figure 76). As the process progresses into phases II and III the apparent coefficient of friction is influenced by the frictional behaviour of the material for the temperature prevailing at the rubbing interface. It is also affected by the presence of extruding plastic material, as well as the existence of a zone of material which is plastically deforming during movement before being extruded. The extent of the plastic zone and the plastic work done is responsible for the very large values of friction coefficient recorded, which can be up to 5.4 (experiment A16).

7.3. Material Flow

7.3.1. Mass Flow

Weld integrity must be related to the extrusion process, the material flow during phase III is closely investigated. Flash of welded specimens was removed from all sides using an electric discharge machine (EDM). This method of material removal was chosen to minimise the loss of deformed matter due to machining. Another benefit of using operations like electromachining is that neutral surfaces result, with zero residual stresses. The mass lost was limited to the width of the copper electrode which was 0.15 mm in this case.

7.3.2. Velocity Field

As the process reaches phase III, hot plastic material extrudes from all sides of the rubbing specimens. The velocity field in the plastic zone can be investigated from the speed that the two specimens approach each other during extrusion, and from the expulsion rate of plastic material into the flash.

The axial shortening history plots provide the information necessary to calculate the *penetration rate*, which is the rate at which the specimens approach each other. Although there is some shortening during transient phase II, the penetration rate represents the average rate of movement of each specimen in the direction perpendicular to movement during extrusion. Each specimen usually looses about 0.025 mm during phase I and II before entering the extrusion stage.

Expulsion rates have units of s^{-1} and can be estimated from :

$$Expulsion\ rate = \frac{mass\ flow\ velocity_{direction\ of\ movement} - mass\ flow\ velocity_{side}}{length\ of\ specimen} \quad (7.3)$$

where $mass\ flow\ velocity = \frac{mass\ flow}{density \times flash\ width \times flash\ thickness}$, with mass flow as estimated in the previous section. It is assumed that material is extruded uniformly from the whole face of the specimens, and therefore the flash width is equal to the length of the face of the specimen from which material extrudes. In practice, flash width is smaller than the width of the face. Flash thickness is the average thickness of the flash, assuming a uniform thickness of the extruded material. The expulsion rate of the plastic material is related to the strain rate that the flash material is exposed to, but is not the strain rate at the rubbing interface which influences the yielding of the material and its subsequent plastic deformation.

7.4. Parametric Investigation

The linear friction welding process is controlled by a number of parameters such as the frequency of oscillation, the amplitude of oscillation and friction pressure. These parameters directly affect the energy input into the process. Therefore, a joint may be produced depending on the values of the parameters used, with its weld strength affected by these as well as the forging force applied at the end of the process.

Using the Taguchi method of designing fractional factorial experiments, the effects of these parameters were explored using two orthogonal L_4 arrays. The effect of the individual parameters is studied, as well as the combined effect that may have on the strength of the weld. The L_4 array is used in these designed experiments where two factors are changed to two levels each. Although this design does not reduce the number of experiments performed, it should identify any statistically significant factors and distinguish any

combined effect of them on the process. Analysis of the results indicates the effect of every factor on the parameter used for assessment and the effect of the combined interaction of the two factors as well. All experiments were repeated as it is common practice for justification of results. Once experiments have been completed, results are analysed by calculating the signal-to-noise (S/N) ratio for each factor and each level in these experiments. This ratio is the reciprocal of the variance of the measurement error. It is maximal for the combination of parameter levels that has the minimum error variance. Calculating the average of S/N value for each factor and plotting them for each level reveals the effect of the factor on the variable used to assess these experiments.

Joints produced were assessed using the Charpy impact test. The welded specimens were tested on an Avery impact test machine. They were tested unnotched, as the stress concentration effect of the notch was effected by the heat affected zone of the joint.

7.4.1. Effect Of Frequency Of Oscillation And Friction Pressure

At a constant amplitude of oscillation of 0.92 mm, eight linear friction welds of Ti 6Al 4V were produced at a frequency of oscillation of 50 and 100 Hz, and at two friction pressures of 32 and 39 MPa (Table 11). As the mechanism to apply the friction pressure produced a varying pressure during the process, the friction pressure value used was the one achieved at the end of the process, as it is more representative of the conditions that exist at the end of the process and could govern the impact strength of the joint. The initial friction pressures applied were higher, by such an amount as to take into account the reduction in frictional force due to axial shortening that would be produced during the subsequent run.

Analysing the results (Table 13) showed that the parameters studied in this experiment, i.e. frequency of oscillation and friction pressure, were not statistically significant, as their variance ratio was below 2. As expected, the combined effect does not affect the weld integrity as well. Increasing the friction pressure produced no statistically stronger welds. It should be noted that the range of the friction pressures used in this set of designed

experiments was limited by the operational characteristics of the rig. A large number of experimentals perfomed later, where the full allowable range of friction pressure was used, showed the significant effect of friction pressure (see next chapter for details).

7.4.2. Effect Of Specific Power Input Parameter And Forging Pressure

Power input, as described by the specific power input parameter, and the forging pressure applied at the end of process were examined using the same orthogonal array as before, at an amplitude of oscillation of 3 mm. The power input parameter was changed by altering the friction pressure, and the forging pressure was investigated at two levels, one the same as the final friction pressure and the other at 80 MPa (Table 12). The low level of forging force, was effected by not applying an additional further pressure at the end of the process, but leaving the welded specimens in the chucks under the friction pressure.

As it can be seen (see Table 14) all three factors are not significant, the specific power input parameter, the forging pressure as well the combined interaction between the two parameters as their variance is below 2. It should be noted that the range of the friction pressures used was limited by the operational characteristics of the rig and the design of experiment procedure. As stated earlier, experimental results where the full allowable range of friction pressure was used showed the significant effect of friction pressure (see next chapter for details).

7.5. Metallography

Welded specimens were sectioned, polished to 1 μm finish and etched using solutions of hydrofluoric acid at various concentrations (2% up to 10%) to reveal the microstructure at the weld interface. The microstructure in the bulk of the material was revealed as expected (Figure 77). The area at the weld interface was not attacked by the etchant sufficiently to reveal in detail the grain structure, when studied under the light microscope. This has been observed in friction welds of Ti 6Al 4V before (**Gillband,1997**). When examined under the scanning electron microscope (SEM) the etched specimens showed a very deformed structure (Figure 78) at the interface area, which

under the local stress conditions followed the flow lines of the extruded material. The interface temperatures must have exceeded the beta transus, as there was evidence of acicular alpha. This transformed beta structure is produced on quenching the hot material from temperatures above the transformation from alpha to beta temperature. However, the temperature reached at the rubbing interface cannot be concluded to any degree of certainty from this observations.

In the welds studied there was no indication of incomplete adhesion between the specimens, although inclusions were observed.

7.6. Fractography

The fracture surfaces of three specimens that were impact tested were studied under the scanning electron microscope. Two welds were achieved at high frequencies of oscillation (Figure 79 and Figure 81) and one at a lower frequency (Figure 82). Two of them belonged to low impact strength welds (Figure 79 and Figure 82), the other (Figure 81) to a high impact strength joint.

All fractured surfaces were characterised by essentially 100% dimpled rupture. This is an indication of a ductile overload fracture of the welds. On a macroscopic level the fracture area was flat and fibrous in appearance. When overload is the principal cause of fracture, fracture is achieved by microvoid coalescence. The microvoids nucleate at regions of localised strain discontinuities, such as those associated with particles, inclusions, grain boundaries and dislocation pile-ups. In this case, they originated from equiaxed α phase that ruptured in ductile shear. As the strain in the material increases, the microvoids grow, coalesce, and eventually form a continuous fracture surface. The uplike depressions formed are a direct result of microvoid coalescence, and they are called dimples. The size of the dimples is governed by the number and distribution of microvoids that are nucleated. The shape of them depends on the state of stress existing when the microvoids formed and coalesced. If there was tensile load applied they are equiaxed, while in shear they are elongated. In these experiments there is variety of dimple shapes and orientations. This is due to the fact that local fracture

planes often deviate from the macroscopic plane and fracture is the result of the combined effects of tensile and shear stress, which generally exhibits a variety of dimples.

Few inclusions are present, and there are small dimples present both at the edges of and within the large dimples (Figure 80).

7.7. Hardness Across Weld Interface

The Vickers microhardness was obtained across the weld zone and the extruded flash using a load of 105 grams. Three welds were sectioned, polished and tested. The sectioned specimens represented the frequency range studied, at 25 Hz, 41 Hz and at 100 Hz. An increase in hardness is observed in all welds in the area adjacent to the interface (Figure 83) for the same amplitude of oscillation. The lower frequency weld has a larger affected zone of about 1000 μm, while the joint of 100 Hz had a smaller zone of 800 μm. A longer process time is the reason behind this difference in the extent of the hard zones.

The hardness reached at the interface is similar to that of the material extruded in the flash. In (Figure 84) the microhardness at various points across the weld interface was recorded to demonstrate that the temperature reached across the interface of a successful weld must be the same, well up to the extruded material in the flash. The hardness profile at the edge of the specimen shows that the thickness of the harder zone is slightly smaller at the edges, by 50-100 μm, as the hardness profile reduces to the parent material values earlier than in the middle line (line 1 and 2 in Figure 84). This could be due to smaller temperatures reached at the edges of the specimen, as a result of conduction losses and the intermittent heat input from the sinusoidal movement of the specimens.

The increase in microhardness in the heat affected zone did not exceed 30% indicating that hard phases did not form to a large extent during the process, although temperatures at the interface did exceed the beta transus limit. This could be due to the very rapid cooling times that the heat affected zone was subjected to from the quenching effect of the bulk of the specimen. As stated

earlier maximum temperatures reached cannot be concluded from the metallurgical observations.

7.8. Weld Strength Assessment

A successful weld is defined as one in which a metallurgical bond exists between the workpieces. Impact testing was considered the appropriate testing method to characterise weld integrity. Tensile testing does not distinguish between strong and weak welds (**Weiss,1965**), whereas impact testing does provide such a distinction. The reason for this may lie in the small heat affected zone of the welds, where brittle phases are responsible for high tensile strengths. The thin heat affected zone at the interface creates a triaxial state of stress analogous to brazing, where joints demonstrate high tensile strengths even though the filler metal is soft.

Welded specimens were tested on a Charpy impact test machine at room temperature. The joints were not notched, as the weld line introduced a stress concentration effect similar to a notch. All failures were found to occur at the interface. The average parent material impact strength for a notched specimen, of the same dimensions as the original specimens, was found to be 17750 mJ.

7.9. Pure Lead Experiments

A series of test were done at the low frequency end of the operating capabilities of the machine using pure lead (99%) (see Table 15 for process parameters).

These tests were conducted while a series of modifications were performed on the machine, as lead is an example of a material whose phase changes other than solidus-liquidus would not be expected.

Visual examination of the welds showed no unusual extrusion features (Figure 85) Although plastically deformed at the interface, there were no fin type extrusion patterns as observed in titanium specimens. Most of lead welds were weak, as they broke by application of manual force.

An interesting feature observed during welding pure lead was the expulsion of small spheres from the interface. They originate from local hot spots on the

rubbing surface, where material may be melting locally. If there is any liquid present at near-solidus temperatures it would be so weak that it will be extruded prior to onset of melting, possibly in the form of globules. This effect could lead to a reduction in frictional energy from the lubrication effect of the molten material. Another explanation for the existence of the small spheres could be that they are wear particles due to ploughing. The wear particles gouge a groove in the rubbing surfaces (Figure 86) and grow in time as material is transferred from the specimens to them.

Similar behaviour of restricted yielding at hot spots on the interface has been observed in the experiments with Ti 6Al 4V (Figure 119), and the finite element simulations for the titanium alloy (Figure 86).

8. Discussion

8.1. Frequency And Amplitude Of Oscillation Effects

8.1.1. Weldability

In the frequency range explored so far experimentally the power input to achieve welding conditions requires the amplitude of oscillation to be high (2 - 3 mm), while there is no evidence that these parameters are optimal. It has been shown (**Garton,1987**) that a critical heat flux is required to successfully weld Ti 6Al 4V. This heat flux is proportional to the axial load, as well as the amplitude and frequency of oscillation. It follows that an increase in frequency might allow the axial forces to be reduced, making it possible to weld relatively delicate components like turbine blades, successfully without buckling. However the inertial forces increase as the square of the frequency, which means that close attention to the holding method would be needed. Conversely if the amplitude of oscillation is reduced, the frequency would necessarily need to increase proportionally for the same axial load, leading to similar conclusions. This could however be a useful strategy for materials prone to oxidation, as it would reduce the overlap interface area exposed to the atmosphere.

The power input to the rubbing surfaces is expected to be a function of the amplitude of oscillation, the frequency of oscillation, the pressure applied on the rubbing specimens to generate frictional heat and the coefficient of friction between the two rubbing specimens. The coefficient of friction is affected by temperature, normal stress and the rubbing velocity at the interface (see chapter 5), and therefore it does change during the process.

For the 85 tests performed with Ti 6Al 4V with oscillating frequencies up to 119 Hz (see Table 8 to Table 10 for process parameters), the minimum specific power input parameter to reach welding conditions and achieve a joint was found to increase with frequency as shown in Figure 88 and Figure 89, where the boundary conditions for adhesion are shown. The friction pressure used to calculate the specific power input parameter corresponded to the pr+8Xessure conditions at the end of each experiment.

8.1.2. Strain Rate Sensitivity Effects

This effect can be attributed to the strain rate sensitivity of the material. The strain rate sensitivity of this alloy has been documented in (**Chaudhury,1992**) at high temperatures and at strain rates between 0.001 and 25 s^{-1}, where the compressive yield stress increases from 10 MPa during static loading to 255 MPa at 850°C for a strain rate of 5 s^{-1}. The maximum theoretical strain rate that the hot material could experience in linear friction welding would be of that order.

As the material heats up to high temperatures due to friction, the yield stress of the material at the interface drops below the effective stress at the rubbing interface. This results in plastic deformation and subsequently this material is extruded under the combined action of hydrostatic pressure and oscillatory movement. The effect of the strain rate sensitive behaviour will be that higher friction pressures will need to be applied for yielding to occur at the same interface temperature as before. Alternatively, higher interface temperatures will have to be attained to compensate for the increase in yield stress.

As the two specimens oscillate in a sinusoidal manner, the maximum strain encountered at the rubbing interface, assuming no slippage, will be during the extreme point of oscillation where the distance from the middle point will equal the amplitude of oscillation. The maximum deformation that the material would be exposed to will equal the distance travelled from the opposite extreme point of oscillation, and will be two amplitudes of oscillation. This deformation occurs in half a cycle, and the theoretical strain rate can be calculated from :

$$\dot{\varepsilon} = \frac{\partial \varepsilon}{\partial t} = \frac{2\alpha / L}{2 / f} \qquad (8.1)$$

where L is the length of the specimen in the direction of movement, f is the frequency and α is the amplitude of oscillation.

If this material did not exhibit strain rate sensitivity, the minimum power required to achieve welding conditions could remain constant. Assuming that the specific power input parameter is the same for every experiment at the same amplitude of oscillation, the minimum friction pressure required to produce welding conditions can be estimated for various frequencies. Hence, the weldability line can be redrawn to show the strain rate effect (Figure 90 and Figure 91) on the minimum friction pressure necessary.

8.2. Stress Conditions

8.2.1. Coefficient Of Friction

8.2.1.1. Initial Friction Conditions

The average value of the coefficient of friction during initial rubbing is 0.44, which is very similar to 0.43 observed in the frictional behaviour experiments at room temperature. The change in the coefficient of friction during initial rubbing at phase I is influenced by velocity in a different way for each amplitude of oscillation (Figure 92). For the large amplitude tests the friction coefficient is inversely proportional to velocity, as observed in the frictional behaviour experiments (chapter 5). The average value for the coefficient of friction for the large amplitude test is 0.56, while for the small amplitude experiments is 0.29. This, together with the fact that there appears to be no dependency of the friction coefficient during the lower amplitude tests on velocity, indicates a different friction mechanism operating in the 0.92 mm amplitude experiments. This may be due to area effects, that arise from the small amplitude of oscillation. As the distance travelled in every cycle is very small compared to the overall length of the specimen, conditions similar to fretting may be responsible for the low coefficient of friction present. Although the velocities present are higher than those encountered in fretting, the effect could be similar. Wear debris is not expelled from the rubbing interface at the rate that is generated due to the small amplitude of oscillation. Hence, lower coefficients of friction are encountered due to the mild lubricating effect of the wear particles remaining on the interface for some time before expelled. This effect of the amplitude of oscillation has been observed in **(Garton,1987)** as well.

In addition to the above, the friction coefficient during the initial rubbing of phase I showed to be insensitive to normal stress (Figure 93) for both amplitudes of oscillation. As these represent transient values during the first second of the process, they cannot be compared to the frictional behaviour experiments which achieved steady state conditions.

Despite the range of the friction coefficient values at the beginning of the process, the value reached at the end of phase I is not related to the friction coefficient at the beginning of the process (Figure 94). The end of the first phase is macroscopically characterised by the appearance of hot spots on the interface which extend to cover the whole cross-sectional area. The apparent friction coefficient should not be related to the initial value of it, but to the pre-extrusion condition that exists at this stage.

8.2.1.2. Extrusion phases

The state of the rubbing interface at the end of phase I, as characterised by the friction coefficient, correlates to the apparent friction coefficient at the end of the process (Figure 95). This indicates that the extent of plasticity at the interface at the phase prior to extrusion influences in a positive way the extent of the plastic zone later. At the small amplitude experiments a relatively small plastic zone begins to form at the end of phase I, which is associated with small plastic zones at the later phases. In the large amplitude tests, the heat affected zone and material extrusion develops to a reasonable size during the process as the friction coefficient indicates. In both cases, there is a relationship between the extent of the plastic zone at the end of process, and the pre-extrusion conditions, evidence that linear friction welding is a self regulating process.

As the final friction pressure decreases the apparent friction coefficient at the end of the process reaches higher values (Figure 96), as the heat affected zone becomes larger due to the lower normal stress. This has been observed in rotary friction welding experiments (see chapter 2) where larger friction pressures create smaller heat affected zones. In linear friction welding it is more pronounced in the large amplitude experiments, where the size of the

heat affected zone is larger than in the small amplitude experiments and the friction coefficient reaches higher values.

The extrusion phase of linear friction welding is a steady state stage. As such, the stress state should remain approximately constant and the apparent friction coefficient invariable. In the experimental work performed it actually increased in most successful experiments. This is the effect of decreasing friction pressure during phase III which subsequently increased the size of the heat affected zone.

8.2.2. Power Input During Phase I

The shear force history can also provide an estimate of the work done during the process. The initial specific power input parameter is proportional to the work rate during phase I of the process (Figure 97) as expected. In the case of the high amplitude tests higher work rates are achieved for the same specific power input conditions due to the higher friction coefficients encountered.

Heat input at the end of phase I depends on process parameters. While it is not influenced by the frequency of oscillation (Figure 98), it is affected positively by increasing friction pressure. This is more pronounced for the large amplitude case than for the small amplitude experiments, due to the different size of heat affected zones reached at the end of this phase (Figure 99). The heat affected zone created is much smaller in the small amplitude case.

8.3. Forging Pressure

In the majority of cases, the forging force applied at the end of the process cycle did not exceed the frictional force applied during the process. In the cases where it did exceed this (experiments A1, A2, A3, A7, A11, A12, and A13 in Table 8), sound joints were produced, although the specific power input parameter was below the lower limit required to weld (Figure 88).

8.4. Material Flow

8.4.1. Mass Flow

As expected, axial shortening is directly related to the total mass expelled into the flash (Figure 100), as the volume of the material extruded into the flash and the volume lost to wear during phase I must equal the volume of the material displaced from every specimen during the process.

The mass expelled per cycle of oscillation, from the direction of movement, was found to be unaffected by frequency of oscillation (Figure 101), but was inversely proportional to the final friction pressure applied (Figure 102). This holds true for both amplitudes of oscillation used in these experiments. The amount of the material extruded in every cycle is not dependent on how often this extrusion takes place, but on the local stress conditions. These are related to the extent of the plastic zone present at the rubbing interface. By increasing the friction pressure applied at the interface, the width of the heat affected zone varies inversely extruding smaller quantities of plastic material during every cycle. Similar behaviour has been observed in rotary friction welding (see chapter 2) where large friction pressures where associated with small heat affected zones.

Similarly, the power input to the interface during the extrusion phase, as described by the final specific power input parameter, affects the mass expelled per cycle in a more pronounced way for the large amplitude tests (Figure 103). As there are no important rubbing velocity effects (Figure 104) or frequency effects on the mass expelled per cycle, friction pressure must influence the amount of mass expelled per cycle and the associated plastic zone from where it is expelled from.

The apparent friction coefficient at the end of the process may be more influenced by the amount of plastic work done in the plasticised material zone and less by the size of it, for values up to 2 (Figure 105). The lower amplitude tests have a very confined plastic zone, as the mass expelled per cycle shows, but the plastic work done has a wider range as indicated by the friction coefficient at the end of the process. In the large amplitude tests where larger

plastic zones are created, with the associated increase in mass flow, the friction coefficient increases to values over 2.5.

The stress and heat input conditions prior to phase III influence the development of the plastic zone and consequently the mass expelled per cycle. Large values for the friction coefficient at the end of phase I indicate the presence of appreciable plasticity just before large scale extrusion occurs in phase III. As a consequence, friction coefficient is related to the mass expelled per cycle during the extrusion phase of the process (Figure 106), indicating that the appropriate conditions have been reached for the creation of large plastic zones during subsequent phases, where large masses will be extruded every cycle. These effects are negligible for the small amplitude tests where the heat affected zone created is small.

In addition to this, the beneficial effect of the heat input to the surface at the end of phase I on the plastic mass expelled during phase III is shown in Figure 107. Higher heat inputs create larger plastic zones in later phases and expel larger amount of mass in every cycle of oscillation.

8.4.2. Velocity Field

8.4.2.1. Expulsion Rates

The strain rate that the extruded matter is exposed to is affected by the rubbing velocity (Figure 108) and not by the average friction pressure (Figure 109), for both amplitudes of oscillation.

In the case of the small amplitude experiments frequency is the influential parameter (Figure 110), possibly due to the restricted size of the plastic zone and the small oscillatory movement. In the case of large amplitude frequency does not influence the expulsion rate, indicating that amplitude affects strongly the expulsion rate for the rubbing velocity to have an effect on expulsion rates. This hypothesis is confirmed by the relationship between the rate of mass flow and expulsion rate (Figure 111). As the mass expelled per cycle is affected by the amplitude of oscillation similar relationship should exist for the expulsion rate as well. This corroborates the importance of the

amplitude of oscillation for the strain rates that the flash material has been exposed to.

The expulsion rate is not related to the local stress conditions and the plastic work done as the parameters are to be associated to the apparent friction coefficient at the end of the process (Figure 112), being influenced by the amplitude of oscillation and not by the plastic work, as demonstrated by the apparent friction coefficient.

8.4.2.2. Penetration Rate

Penetration rate is proportional to the expulsion rate (Figure 115) for volume constancy reasons, and shows similar relationship to rubbing velocity (Figure 113) as expulsion rate does.

As more power is input to the process by using a higher average specific power input parameter, the penetration rate (Figure 114) is affected respectively. This relationship reaches a plateau for values above 3000, after which higher values of friction pressure or frequency produce the same penetration rate for the small amplitude test. Unfortunately, no experiments were done at such high value of power input with the large amplitude cam. This could be attributed to the heat affected zone reaching a limiting size, without extending any further into the bulk of the specimen with high power input.

8.4.3. Material Extrusion Patterns

A successful weld is defined as one having some degree of permanent adhesion. All successful welds demonstrated appreciable flash from both sides of the joint (Figure 116). Flash length is larger in the direction of movement, where a series of large ridges appear (Figure 117). The ridge pattern indicates that they are directly related to the oscillatory movement of the specimens.

Extruded matter from the non-moving sides of the specimen which are parallel to the direction of movement also show some evidence of ridges. As there was no movement of the specimens in that direction, it may be concluded that axial shortening proceeds in a step-wise fashion. Evidence that material is extruded

in a pump-like mode instead of a continued fashion, can also be found in the axial displacement traces. If the axial shortening due to extrusion is removed from the trace, by subtracting the moving average per cycle from the axial displacement signal, the movement of the stationary chuck in the direction perpendicular to movement is established (Figure 118). Compared against the sinusoidal movement of the specimen it can be shown that at the extreme points of oscillation, where the chuck is furthest away from the middle point, the chuck is at a neutral point. As the chuck returns back to the middle point of oscillation where the two specimens are aligned, the chuck moves towards the other specimen to extract plastic material, and then extruding returns to a neutral point at the other extreme position. Another evidence of an interrupted extrusion can be seen in the scanning electron microscope picture of a single ridge (Figure 87), where a groove appears at the peak of the ridge. This notch must be associated with the time in the cycle where the specimens are aligned (see kink in middle of oscillation in Figure 118).

Experiments where the power input was below the minimum required showed limited plastic deformation, with very little material extrusion, if any at all. On these occasions, the process did not progress beyond phase II. Material was extruded from the middle of the interface in the form of rolled strands (Figure 119) indicating insufficient power input to reach the plastic stage throughout the interface. This limited extrusion is believed to be caused by extrusion from a central hot zone at the interface (see Figure 120 as predicted by the finite element analysis), through relatively cool boundary material. The hot material is extruded from the sides parallel to movement as they represent the closest path from the centre of the specimens. Similar behaviour has been observed in the rotary friction welding of copper components **(Aws,1989)** and could not be attributed to any causes. Also some tests with pure lead indicated that local melting may be possible if the extrusion process is impeded by solid regions at the interface (Figure 86).

This suggests that the flash morphosis (i.e. evidence of systematic ridges) is an indication that the correct plasticised interface conditions for integral welds has been achieved. As stated previously, linear friction welding is a self regulating process, where the succession of each stage is governed by the

initial conditions. If minimum starting conditions are not achieved, the progress through subsequent phases is not observed.

In well formed extruded shapes, the flash was connected around the corners of the specimen, indicating that the area of the interface material that had become plastic during the process was uniform and undivided. In this case the true area of the weld is equal to the cross-sectional area of the specimens. In the cases where the flash was not as well formed, the extruded matter was not connected around the corners. In such cases the true area of the weld was found to be less than the cross-sectional area of the specimens.

8.5. Weld Strength Assessment

The impact strength of the welds did not appear to correlate with the rubbing velocity (Figure 121). The latter seems to be at variance with (**Garton,1987**), where despite scattering of the impact strength results it was reported that there was a limit on the beneficial effect of velocity on the impact strength at 200 mm/s.

Increase in friction pressure appears to have a small negative effect on weld integrity as measured by the Charpy impact test (Figure 122), and this relationship holds for both amplitudes of oscillation. However, the increased mass expelled per cycle of operation appears to have a beneficial effect for the large amplitude experiments (Figure 123). Larger plastic zones were created at the rubbing interface, as evident by the larger mass expelled per cycle values, which in turn produced high impact strength values. For the smaller amplitude of oscillation, this does not hold true. The material expelled per cycle did not change appreciably over a wide range of process parameters and the plastic zone created was confined to a small region.

Similarly axial shortening does influence impact strength of the welds (Figure 124). Large axial shortenings produced with large amplitudes of oscillation are associated with large mass flow rates (section 7.3.1.Mass Flow) which are the effect of extended heat affected zones, all leading to good impact strengths. For small amplitudes of oscillation a different mechanism exists, where the very small heat affected zone does not produce the same effect, but possibly creates strong joints by its small size and stress concentration.

In order to create favourable conditions for large heat affected zones, sufficient heat has to be input at the end of the initial phase I, as (Figure 125) shows. During the 3 mm amplitude of oscillation experiments large heat inputs during phase I prepared large heat affected zones and consequently produced high impact strength welds. In the small amplitude of oscillation large heat affected zones are not created, and similarly the effect of the work input rate is less important.

The change of the apparent friction coefficient, as estimated from the shear and friction force histories, provides a measure of the extent of the plastic zone and the plastic work done during phase III. For experiments where the apparent coefficient of friction was steady or increasing during the extrusion phase of the process, i.e. its trend was not negative (Figure 126) average to good impact strength welds were achieved. Poor strengths were obtained in the case where the coefficient of friction reached a peak and then decreased during phase III, indicating a diminishing plastic zone. From (Figure 127) it can be seen that the value of the apparent friction coefficient at the end of the experiment does affect the quality of the weld. In order to achieve strong joints a favourable stress condition needs to exist, as illustrated by the high friction coefficient values which are related to favourable plasticity conditions with large plastic zones.

8.6. Experimental Verification Of Numerical Model

In order to verify the accuracy of the finite element model developed in chapter 6 two parameters require to be identified :

a) the temperature at a known position

b) the shear stress conditions

The temperature was recorded using a chromel-alumel thermocouple embedded in a blind hole in the stationary specimen. The length of the hole was set to a predetermined depth. The thermocouple wire was attached to the hole using a combination of a high strength low temperature adhesive for the part of the wire away from the interface, and a high temperature adhesive able to withstand 1000 °C for the part of the hole closer to the hot interface.

8.6.1. Temperature And Stress Conditions

The process parameters for experiment D1 (see Table 10 for process parameters) were used to verify the finite element model developed, as well as the frictional behaviour assumptions employed. The coefficient of friction was assumed to change according to the phenomenological model produced in chapter 5, for a sliding velocity of 200 mm/s, which was closer to the 178 mm/s of this experiment. As can be seen (Figure 128) the temperature prediction of the finite element model is close to the one recorded up to 4 seconds into the process, where they start to deviate. The recorded temperature in the experiment does reach a plateau, before declining. The reason for this lies in the difficult metalworking conditions present at the rubbing interface. During the first seconds of the process material is removed from the interface due to wear, and frictional heat raises the temperature at the interface. As material yields locally it is extruded from the sides of the specimen, or moves into the hole where the thermocouple is situated. This causes the thermocouple to move away from the interface, where it registers lower temperatures at an unknown distance from the rubbing interface if not damaged.

The temperature plot of the model early in the process (Figure 129) shows the temperature rising across the interface in a relatively uniform manner. Note that the object at the bottom has not been affected by the process with its temperature having remained constant. It was set as a rigid object, in an effort to reduce the long computational times.

The finite element model prediction for a node in the middle of the rubbing interface (Figure 130) predicts that the temperature will not rise above 900°C, and that it will remain steady around that temperature. Although data from thermocouples corroborate the fact that temperatures at the interface should not have exceeded the beta transus temperature of 995°C, metallurgical observations indicated the opposite as acicular alpha was identified in the weld interface. As previously stated thermocouple measurements can give underestimates of the actual conditions due to the limited control over the themal inertia, the response time and the positioning of the junction in the specimen.

The finite element model predicted a shear force of 1500 N at 5 seconds into the process, while at the same time the average experimental value was 1425 N, a difference of 5 %.

Due to adaptivity problems the model was not developed beyond this point into the extrusion phase of the process.

8.6.2. Weldability conditions

By altering the friction pressure and using the two amplitudes of oscillation available in the rig, the high frequency region was explored numerically to identify the conditions that prevail at the end of phase I prior to transient phase II. As linear friction welding is a self-regulating process if the appropriate conditions are reached, welding will continue into phase III, where large scale plasticity is present and material extrudes from all sides of the interface.

From the finite element simulations, two patterns emerged that can be associated with welding conditions at the end of phase I. The first, is the one that is favourable to linear friction welding. After sufficient frictional heating the interface is heated in a relatively uniform way creating a region of yielded material across the whole of the rubbing interface (Figure 131). This material can then be extruded and as more material yields flash is formed. The second pattern that was shown in the finite element analyses, was one of insufficient heating where the area that had yielded was concentrated in the middle of the interface (Figure 120). This material pattern never progressed into the favourable pattern even after very long processing times. This restricted yielding can explain the extrusion of hot material from hot spots at the interface in the form of strands (Figure 119). During the experiments, when the power input was not adequate, extruded material would appear from the interface and would usually originate from the middle of the specimens. These hot spots are located in the middle of the specimens where the heat losses to the environment are minimum and frictional heat is generated continuously during movement.

Using the criterion of the extent and shape of the yielded material at the interface a weldability line was predicted (Figure 132) for various frequencies

of oscillation, similarly to the one obtained from the experimental work (Figure 89). It demonstrates in a quantitative manner the same strain rate effects observed in the experiments. The discrepancy in the specific power input parameter between the experimental values and the numerical predictions could be the result of the two dimensional model used in the analyses. Another factor that may have limited a quantitative agreement, may originate from the frictional behaviour data available. Although they were estimated from conditions similar to the ones observed in linear friction welding, the low amplitude of oscillation experiments showed a lower coefficient of friction than the one predicted by the frictional behaviour experiments.

8.7. Linear Friction Welding Process

Linear friction welding is a self regulating process, where certain stress conditions at the interface and the region adjacent to it have to be reached for the process to undergo its various phases. There is a power input limit, below which welding is not possible.

If operating below this limit either by using a smaller amplitude of oscillation, or rubbing at a lower frequency of oscillation or applying a smaller friction pressure than necessary, the specimens will never reach such conditions which will produce well defined flash and subsequently join to form sound welds. Local hot spots appear at the interface during phase I, from where hot material is extruded. These plasticised areas never extend to cover the whole of the rubbing interface. The result is to extrude material from all sides of the specimen, originating in these areas only. Similar behaviour is observed in pure lead, where a multitude of these hot spots creates and extrudes to the environment small balls of lead. Titanium creates long strands which get extruded from the sides parallel to movement.

This localised yielding in the middle of the specimens was reproduced in the finite element model of the process, confirming the hypothesis that insufficient power input at the first phase of the process produces contained plasticity at the interface. Depending on the material this plastic matter could

be extruded in the form of strands in the case of Ti 6Al 4V, or as small balls in the case of dry-bearing pure lead.

Where the power input is higher than the minimum required a region of plastic material develops at the interface extending to the whole of the interface. From this plasticised area material is extruded to form the flash, which is formed in steps. Extrusion occurs in the middle point of oscillation, where the rubbing velocity is at its highest value and therefore the heat produced maximum. This increases the temperature instantaneously causing more material to yield. This mode of yielding was indicated by macroscopic examination of the flash. The flash does not have a uniform thickness but appears in the form of ridges. In addition to this, the movement of the specimen normally to the plane of movement provided evidence of an oscillatory extrusion movement. At the middle point of oscillation, the specimens would appear to oscillate to extrude plastic material. Examination of the flash with a scanning electron microscope showed a groove at the top of every ridge of flash material, as the pumping was not continuous at that point in time during the cycle. The effect of this action is that material yields and extrudes in pulses, therefore confining the heat affected zone close to the interface.

As Ti 6Al 4V is strain rate sensitive, the power input to reach welding conditions and produce joints increases with frequency of oscillation for a given amplitude in linear friction welding. The increased power requirements observed in the experiments indicate a linear relationship with frequency. If delicate components are to be welded, for which smaller friction pressures may be necessary, the frequency of oscillation should be increased for the power input to remain constant. As the strain rate sensitivity of the titanium alloy would actually require increasing the friction pressure, this could be avoided by using longer contact lengths. The effect would be to compensate for the increase in strain rates due to frequency, and keep the strain rates constant.

It is customary in industry to apply a forging force at the end of the process to consolidate the weld. Using statistical tools it was shown to have an insignificant effect on the impact strength of welds, if the process was

concluded under power conditions above the minimum required. Forging proved useful in cases where power input is below the minimum required. In theses cases material extrusion is not as extended or well formed as in higher power cases, but forging at the end of the process did help to produce a sound joint. This may indicate that although metallurgically clean surfaces have been created at the interface by extrusion of material, an additional pressure needs to consolidate the weld.

The effect of process parameters such as friction pressure, frequency of oscillation and specific power input were found to be statistically insignificant when welding above the power limit. For all of them, this was confirmed in the course of experimental work, with the exception of friction pressure. As friction pressures have a significant effect on a weld, it must be that the friction pressure range used in the fractional factorial experiments was not wide enough to produce a statistically significant effect. Due to the strain rate sensitivity of the material and machine specifications, this hypothesis was not able to be confirmed through statistical methods, but was verified by the experimental work.

The extent of the heat affected zone appeared to influence the impact strength of the joints for the large amplitude of oscillation tests. The size of the zone was inferred from large axial shortenings and the mass expelled per cycle of operation, among other data. Large zones were associated with high impact strengths, close or equal to that of the parent material. In the small amplitude of oscillation experiments this effect was not observed as the heat affected zone size, as inferred by the mass expelled per cycle and the apparent friction coefficient, never became large. High impact strengths in those experiments must be the result of very confined heat affected zones. Very small amplitudes of oscillation, when compared to the overall length of the specimens, produce frictional conditions similar to fretting. This results in wear debris not being expelled readily from the interface and producing low coefficient of friction conditions during the initial rubbing. The consequence of that is lower heat input during the first phase and the subsequent creation of smaller heat affected zones.

The stress state at the rubbing interface as inferred by the apparent friction coefficient between the two rubbing specimens, did provide an indication of the success of the process. Increasing friction coefficients were associated with successful operations and strong welds. Higher values of this coefficient are created by large heat affected zones and extensive plastic work done at that zone. Therefore, recording the forces at the interface could provide an on-line monitoring tool for linear friction welding.

9. Conclusions And Recommendations For Future Work

9.1. Conclusions

9.1.1. Linear Friction Welding of Ti 6Al 4V

The main objective of this research work was to investigate the effect of frequency of oscillation for two different amplitudes of oscillation to the linear friction welding of Ti 6Al 4V.

Linear friction welding is a self regulating process, where certain stress conditions at the interface and the region adjacent to it have to be reached for the process to undergo its various phases. The minimum power required to achieve welding conditions with this material increases with frequency of oscillation due to strain rate effects. As the relationship between power required and frequency is linear, higher frequencies would require lower friction pressures to achieve the slightly higher power requirements, provided intermediate amplitudes of oscillation are used.

The rubbing interface changes from a sliding friction condition to a phase where a zone of plastic material develops at the interface and extrudes due to the stress state and oscillatory movement. Temperatures at the interface, as indicated by metallurgical observations, do exceed the beta transus temperature of the material.

Applying a forging force at the end of the process cycle can improve weld integrity, especially when the power input is lower than that required to achieve satisfactory welding conditions. Otherwise, it was found not to have a statistically significant effect on weld impact strength.

Interface alignment in linear friction welding can be unstable. This effect can be triggered by a small initial misalignment of the specimens, or by asymmetric heat distribution at any time during the process.

The existence of a well formed flash is an indication of good welding conditions which have produced appreciable plastic deformation and strong welds.

Material is extruded in a discontinuous way during the extrusion phase of the process. It is expelled into the flash when the oscillating specimens are aligned, at this point heat generation is at its maximum.

The finite element model developed to study the process and the conditions necessary to reach welding conditions, revealed that if insufficient power input is provided to the interface, a pocket of plastic material develops at the centre of the specimens which never extends to cover the whole cross-sectional area. Experiments have shown that matter extrudes from the hot centre in the form of strands.

The size of the heat affected zone is inversely proportional to the friction pressure applied, affecting the impact strength of the weld. Smaller friction pressures or lower frequencies with larger amplitudes of oscillation, produce large heat affected zones and high impact strength joints.

Contrary to previously reported observations, there is no strong correlation between rubbing velocity and weld integrity.

Very small amplitudes of oscillation have an effect on the size of the heat affected zone, the mass expelled into the flash and consequently to the weld impact strength.

The friction coefficient between the oscillating specimens is influenced by different conditions during the process. During phases I and II indicates the extend of the preparation of the surfaces and the appearance of localised yielding. During extrusion phase III it represents the size the heat affected zone and the amount of plastic work done due to movement. The mass expelled per cycle is directly related to the size of the heat affected zone and is a good guide to for sound welds.

The analytical model developed for the early stage of the process indicates that full true contact is achieved at the end of the first phase, contact being close to linear with time. Temperature profiles predicted by the model were similar to experimental data.

A heat input model developed showed that the amplitude of oscillation affects the cyclic profile of the frictional heat input. Large amplitudes of oscillation,

when compared to the length of the specimen, will produce asymmetrical frictional heat during every cycle of oscillation.

The semi-empirical material flow model developed predicted strain rate conditions that are higher that the experiment, as the experimental values of the required friction pressure show. It also revealed that the zone that experiences high strain rates covers most of the plasticised zone at the interface, and is not confined to the interface.

Finite element modelling was proven feasible. It can produce reasonable agreement between experiments and numerical results in temperatures and shear stress during the initial phases of the process. Further work should be able to produce agreement with axial shortening as well if adaptivity is available.

Frictional material properties used in finite element modelling were obtained from rotary friction welding experiments under conditions similar to linear friction welding. Differences between the values obtained in these and those observed in the linear friction welding experiments stress the need for obtaining frictional data in the same normal stress and interface temperature conditions as the experiments the model is representing.

Material properties, and especially relating to frictional behaviour, have to be drawn experimentally done under conditions similar to the process under study, if they are to be used in numerical simulations.

9.1.2. Linear Friction Welding Machine Design

Alternative linear friction welding machine designs have been explored previously at the University of Bristol. The following specifications are necessary for the design of any friction welding machine :

- Optimum velocity for the material to be welded depending on the strain rate sensitivity of the material. Intermediate amplitudes of oscillation and high frequencies of oscillation provide the benefit of using lower friction pressures and welding delicate objects.

- Controllable burn-off setting. This would control the size of the heat affected zone developed during extrusion and influence the impact strength of the weld.
- Rapid disengagement of drive system to leave the weld intact.
- Adjustable friction and forging pressure. The ability to control friction pressure during operation would allow the regulation of the heat affected zone developed.
- Chuck system to hold specimens rigidly during welding. Accurate initial alignment is very important to reduce interface instabilities.
- Easy loading and unloading of specimens for short turn-over times.
- Accurate final positioning of specimens.
- Minimum hysteresis in fixed and oscillatory chuck to ensure that the workpieces follow the prescribed path.
- Minimum mass for oscillatory chuck parts to reduce inertia forces and reduce vibrations.
- Multiple lobed cams to induce high frequency oscillations at low rotational speeds.
- The reduction of the effects of vibration is crucial to successful welds, and this should achieved through stiffening the structure.
- In-built monitoring of forces for quality control, as they can provide an assessment of the quality of the weld.
- Due to operation of the machine intense noise is produced, requiring adequate noise protection in any commercial machine built.

9.2. Recommendations for future work

As existing numerical work showed the applicability of the method, the current model could be extended to a three dimensional model of linear friction welding. The use of an adaptive programme will allow the reliable simulation of the process when large plastic deformations occur. These efforts would help to predict conditions of weldability.

If the process is to expand its applicability to other materials it will be necessary to investigate the effects of the amplitude of oscillation and frequency on welding of other materials, including dissimilar material combinations.

Investigate the effect of a variable pressure cycle where the friction pressure decreases during the extrusion phase of the process, with the aim to enlarge the heat affected zone and create sound joints. Another benefit of this approach could be the reduction of the shear forces at the interface thereby reducing the forces on the mechanisms of the linear friction machine.

Explore the effect of intermediate amplitudes of oscillation, between 1 and 3 mm, where the strain rate effects would be lower than the large amplitude experiments without the impediment of low friction coefficients of the small amplitudes of oscillation.

Investigate the interface alignment problems, where due to instabilities in the frictional heat generated at the rubbing interface skews the interface. This effect may be related to the aspect ratio of the interface and warrants further investigation.

References

(Ashby,1992) Ashby, M.F., "Physical modelling of material problems", Materials Science and Technology, vol.8,1992, pp.102-111.

(Asm,1972) "Microstructure of titanium and titanium alloys", ASM Metals Handbook, vol.7, 1972.

(Asm,1992) "Friction, lubrication and wear technology", ASM handbook, vol.18, 1992.

(Aws,1989) "Recommended practice for friction welding", American Welding Society, American National Standard ANSI/AWS C6.1-89, 1989.

(Baeslack,1994) Baeslack, W.A., Broderick, T.F., Juhas, M., Fraser, H.L., "Characterization of solid-phase welds between Ti-6Al-2Sn-4Zr-2Mo-0.1Si and Ti-13.5Al-21.5Nb titanium aluminides", Materials Characterization, no.33, 1994, pp.357-367.

(Bendzsak,1997) Bendzsak, G.J., North, T.H., Li, Z., "Numerical model for steady-state flow in friction welding", Acta Materialia, vol.45, no.4, 1997, pp.1735-1745.

(Benn,1995) Benn, B., "Les techniques d'assemblage et les perspectives d'avenir dans la construction des moteurs d'avions", Nouvelle Revue D'Aeronautique Et D'Astronautique, no.3, 1995

(Bowden,1964) Bowden, F.P., Tabor, D., "The friction and lubrication of solids", Oxford University Press, 1964.

(Carslaw,1959) Carslaw, H.S., Jaeger, J.C., "The conduction of heat in solids", Oxford University Press, 1959.

(Chaudhury,1992) Chaudhury., P., Zhao, D., "Atlas of formability : Ti 6Al 4V ELI", National Center for Excellence in Metalworking Technology, 1992.

(Cheng,1963) Cheng, C.J., "Transient temperature distribution during friction welding of two dissimilar materials in tubular form", Welding Journal, vol.41, no.5, 1963, pp.233-240.

(Cola,1992) Cola, M.J., Baeslack, W.A., Altshuller, B., Sjostrom, T., "Inertia friction welding of a particulate reinforced aluminum matrix composite", 3rd International SAMPE Metals Conference, October 1992, pp.424-438.

(Craine,1987) Craine, R.E., Francis, A., "Frictional heat generated in the early stages of an orbital friction welding process", Wear, vol.114, 1987, pp.355-365.

(Crooks,1990) Crooks, D.A., "Linear friction welding of dissimilar metals", M.Eng. thesis, University of Bristol, 1990.

(Duffin,1973) Duffin, F.D., Bahrani, A.S., "Frictional behaviour of mild steel in friction welding", Wear, Vol.26, 1973, pp.53-74.

(Duffin,1976) Duffin, F.D., Bahrani, A.S., "The mechanics of friction welding mild steel", Metal Construction, June 1976, pp.267-271.

(Duffy,1979) Duffy, J., "Testing techniques and material behaviour at high rates of strain", Mechanical Properties At High Rates Of Strain, Institute of Physics Conference Series No.47, 1979, pp.1-15.

(Elfen,1996) Elfen User Manual ver.2.6, Rockfield Software Ltd.,August 1996.

(Ellis,1974) Ellis, C.R.G., Nicholas, E.D., "A quality monitor for friction welding", Advances In Welding Processes, Proceedings of the 3rd International Conference, 7-9 May 1974, pp.14-20.

(Francis,1985) Francis, A., Craine, R.E., "On a model for frictioning stage in friction welding of thin tubes", International Journal of Heat and Mass Transfer, vol.28, no.9, 1985, pp.1747-1755.

(Fritz,1974) Fritz, J., Staudinger, H., "Microstructural investigations on friction welded joints between heat treatable and high speed tool steel - A comparison between flash butt welding and friction welding techniques including some practical investigations", Praktische Metallographie, vol.11, 1974, pp.197-210.

(Furber,1991) Furber, W.J.H., "An investigation into linear friction welding of steel tubes in an inert atmosphere", B.Eng. thesis, University of Bristol, 1991.

(Garton,1987) Garton, J.H.L., "Investigation into linear friction welding of blisks", B.Eng. thesis, University of Bristol, 1987.

(Gel'man,1959) Gel'man, A.S., Sander, M.P., "Power and heating in the friction welding of thick-walled steel tubes", Welding Production, October 1959, pp.53-61.

(Gel'man,1965) Gel'man, A.S., "The nature of friction welding", Avt Svarka, no.3, 1965, pp.5-10.

(Ghosh,1982) Ghosh, A.K., Hamilton, C.H., "Influences of material parameters and microstructure on superplastic forming", Metallurgical Transactions A, vol.13A, May 1982, pp.733-743.

(Gillband,1997) Gillband, P., Private communication, Rolls-Royce, Bristol, 1997.

(Golego,1965) Golego, N.L. , "Formation of joints between metals in a high vacuum", Avt Svarka, no.3, 1965, pp.18-20.

(Greek,1997) Greek, D., "Steel rewrites the rules", Professional Engineering, vol.10, no.13, 1997, pp.19-20.

(Hasui,1968) Hasui, A., Fukushima, S., Kinugawa, J., "Experimental studies on friction welding phenomena", Transactions of National Research Institute for Metals, vol.10, no.4, 1968, pp.207-225.

(Hazlett,1962) Hazlett, T.H., "Properties of friction welded plain carbon and low alloy steels", vol.41, no.2, Feb 1962, pp.46s-52s.

(Hazlett,1967) Hazlett, T.H., "Fundamentals of friction welding", Metals Engineering Quarterly, American Society for Metals, February 1967, pp.1-7.

(Healy,1976) Healy, J.J., McMullan, D.J., Bahrani, A.S., "Analysis of frictional phenomena in friction welding of mild steel", Wear, vol.37, 1976, pp.265-278.

(Hill,1950) Hill, R., "The mathematical theory of plasticity - theory of autofrettage process", Oxford University Press, Oxford Engineering Science Seris, UK.

(Hodge,1964) Hodge, E., "Friction joining", Battelle Technical Reviews, vol.14, 1964, pp.10-13.

(Hollander,1962) Hollander, M., "Developments in friction welding", Metals Engineering Quarterly, May 1962, pp.14-24.

(Hollander,1963) Hollander, M., Cheng, C.J., Wyman, J.C., "Friction welding parameter analysis", Welding Research Supplement, November 1963, pp.495-501.

(Imi) Titanium alloy IMI 318 data booklet, IMI Titanium Ltd.

(Jones,1965) Jones, P.J., "Practical applications of friction welding", Welding and Metal Fabrication, vol.33, 1965, pp.377-382.

(Kim,1995) Kim, Y.C., Fuji, A., North, T.H., "Residual stress and plastic strain in AISI 304L stainless steel / titanium friction welds", Materials Science and Technology, vol.11, April 1995, pp.383-388.

(Klopstock,1941) Klopstock, H., Neelands, A.R., "An improved method of joining or welding materials", U.K. patent no. 572,789, 1941.

(Kobayashi,1989) Kobayashi, A., Iwase, K., Tadauchi, K., Sakurai, T., "Study on the amount of upset of friction welding", JSME International Journal, series I, vol.32, no.3, 1989, pp.385-390.

(Koo,1992a) Koo, H.H., Baeslack, W.A., "Structure, properties and fracture of linear friction welded Al-Fe-V-Si alloy 8009", Materials Characterization, vol.28, 1992, pp.157-164.

(Koo,1992b) Koo, H.H., Sampath, K., Baeslack, W.A., "Characterization of inertia-friction welds between a rapidly-solidified Al-Fe-Mo-V alloy and IM 2024-T351", Journal of Materials Science, vol.27, 1992, pp.3266-3280.

(Kubaschewski,1962) Kubaschewski, O., Hopkins, B.E., "Oxidation of metals and alloys", Butterworths, 1962.

(Lebedev,1986) Lebedev, V.K., Litvin, L.V., Dyshlenko, A.T., Chernenko, I.A., "Determining the friction moment during inertia welding from the angular acceleration", Automatic welding , vol.39, no.8, 1986, pp.31-33.

(Lee,1967) Lee, D., Backofen, W.A., "Superplasticity in some titanium and zirconium alloys", Transactions Of The Metallurgical Society Of AIME, vol.239, July 1967, pp.1034-1040.

(Martens,1971) Martens, C.H., "Apparatus for welding by translational friction", US.Patent 3,771,706, 1973.

(Maykuth,1971) Maykuth, D.J., "Ti-base alloys : Ti 6Al 4V Processes and properties handbook", DMIC Publication , January 1971.

(Midling,1994) Midling, O.T., Grong, O., "A process model for friction welding of Al-Mg-Si alloys and Al-SiC metal matrix composite - I. HAZ temperature and strain rate distribution", Acta metallurgica materialia, vol.42, no.5, 1994, pp.1595-1609.

(Moal,1992) Moal, A., Massoni, E., Chenot, J-L., "A finite element modelling for the inertia welding process" , Proceedings of International Conference on Computational Plasticity, Barcelona 1992, Pinebridge Press, Swansea, 1992, pp.289-300.

(Moal,1995) Moal, A., Massoni, "Finite element simulation of the inertia welding of two similar parts", Engineering Computations, vol.12, no.6, 1995, pp.497-512.

(MTI,1993) "Friction welding", Manufacturing Technology Inc, 1993.

(Nicholas,1987) Nicholas, E.D., "Friction welding non-circular sections with linear motion - a preliminary study", The Welding Institute, 1987.

(Nicholas,1992) Nicholas, E.D., "Friction surfacing and linear friction welding", 3rd International SAMPE Metals Conference, October 1992. pp.450-463.

(Oh,1995) Oh, S.K., Oh, J.H., Jeon, T.E. and Oh,.S.W., "Development of real-time quality evaluation of friction welding by acoustic emission:Report 1", 5th International Offshore and Polar Engineering Conference, The Hague, 1995, pp.163-168.

(Oh,1996) Oh, S.K., Oh, J.H. and Chang, H.K., "Development of real-time quality evaluation of friction welding by acoustic emission: 2nd . Effects of welding parameters on weld strength and AE", 6th International Offshore and Polar Engineering Conference, Los Angeles, 1996, pp.177-184.

(Owen,1980) Owen, D.R.J., Hinton, E., "Finite element in plasticity : theory and practice", Pinebridge Press, Swansea, 1980.

(Perry,1984) Perry, R.H., Green, D. "Perry's chemical engineer's handbook", Mc-Graw Hill Book Company, 1984.

(Phillips,1992) Phillips, N.A., "High Frequency Linear Friction Welding Rig", B.Eng. thesis, University of Bristol, 1992.

(Rabinowicz,1971) Rabinowicz, E., "The determination of the compatibility of metals through static friction tests", A.S.L.E. Transactions, vol.14, no.3, 1971, pp.198-205.

(Rich,1969) Rich, T.P. , "An exploratory study of friction welding", PhD thesis, Lehigh University, Pennsylvania, 1969.

(Rich,1971a) Rich, T., Roberts, R., "The forge phase of friction welding", Welding Journal - Welding Research Supplement, vol.50, 1971, pp.137-145.

(Rich,1971b) Rich, T., Roberts, R., "Thermal analysis for basic friction welding", Metal Construction - British Welding Journal, vol.3, 1971, pp.93-98.

(Ritter,1973) Ritter, K., Ritter, J., Ritter, G., Hans, G., "Apparatus for manufacturing welded wire mesh by friction welding", U.S. patent 3,734,383, 1973.

(Roberts,1988) Roberts, D.A., Daines, J.W., "Friction welder mechanism", U.S. patent 4,858,815, 1989.

(Rykalin,1959) Rykalin, N.N., Pugin, A.I., Vasil'eva, V.A., "The heating and cooling of rods butt welded by the friction process", Welding Production, October 1959, pp.42-52.

(Sassani,1988) Sassani, F., Neelam, J.R., "Friction welding of incompatible materials", Welding Journal, vol.67, no.11, 1988, pp.264-270.

(Searle,1972) Searle, J.G., "Improvements relating to methods of and apparatus for friction welding", U.K. patent no. 1,293,532, 1972.

(Searle,1975) Searle, J.G., Hunt, D.J., "Friction welding apparatus", U.K. patent no. 1,385,471, 1975.

(Searle,1989) Searle, J.G., "Friction welding" , EPO patent no.0360512, 1989.

(Seregin,1986) Seregin, A.S., "Selection of rational duration of the stationary stage of friction welding of metals without artificial deceleration", Welding Production, vol.33, October 1986, pp.5-7.

(Simpson,1988) Simpson, P.B.M., "Amplitude control of a linear friction welding machine", B.Eng thesis, University of Bristol, June 1988.

(Sluetz,1968) Sluetz, E.Z., Oberle, T.L. , Brosheer, B.C., "Inertia welding", American Machinist Special Report no.621, October 1968

(Sluzalec,1990) Sluzalec, A., "Thermal effects in friction welding", International Journal of Mechanical Sciences, vol.32, no.6, 1990, pp.467-478.

(Sluzalec,1993) Sluzalec, A., Sluzalec, A., "Solutions of thermal problems in friction welding - comparartive study", International Journal of Heat and Mass Transfer, vol.36, no.6, 1993, pp.1583-1587.

(Smith,1992) Smith, M.H., "The effects of aluminium oxide on inertial welding of aluminium in space applications", M.S. thesis, Massachusetts Institute of Technology, 1992.

(Soucail,1992) Soucail, M., Moal, A., Naze, L., Massoni, E., Levaillant, C., Bienvenu, Y., "Microstructural study and numerical simulation of inertia friction welding of astroloy", Superalloys 1992, The Minerals,Metals & Materials Society, 1992, pp.847-856.

(Squires,1966) Squires,I.F., "Temperature and mechanical charecteristics of friction welding mild steel", British Welding Journal, November 1966, pp.652-657.

(Stokes,1988a) Stokes, V.K., "Vibration welding of thermoplastics. Part I : Phenomenology of the welding process", Polymer Engineering and Science, vol.28, no.11, 1988, pp.718-727.

(Stokes,1988b) Stokes, V.K., "Vibration welding of thermoplastics. Part II : Analysis of the welding process", Polymer Engineering and Science, vol.28, no.11, 1988, pp.728-739.

(Stokes,1988c) Stokes, V.K., "Analysis of the friction (spin)-welding process for thermoplastics", Journal of Materials Science, vol.23, 1988, pp.2772-2785.

(Summo,1977) Summo, A.M., "Method of joining non-fusible workpieces using frictional energy", U.S. patent 4,058,421, 1977.

(Taguchi,1986) Taguchi, G., "Introduction to quality engineering", Asian Productivity Organisation, Tokyo, 1986.

(Vavilov,1965) Vavilov, A.F, "The friction welding of tools", Avt.Svarka, vol.3, 1965, pp.51-53.

(Vavilov,1968) Vavilov, A.F., Voinov, V.P., "Friction welding", translated from Russian, British Welding Research Association, 1968.

(Vill,1962) Vill, V.I., "Friction welding of metals", translated from Russian, American Welding Society, 1962.

(Weiss,1965) Weiss, H.D., "Study of friction welding parameters in the joining of dissimilar materials", M.Sc. Thesis, University of California, Berkeley, 1965.

(Zhu,1988) Zhu, S.H., Stoltzfus, J.M., Benz, F.J., Yuen, W.W., "Modelling and data analysis of the NASA-WSTF frictional heating apparatus : Effects of test parameters on friction coefficient", Flammability and sensitivity of materials in oxygen-enriched atmospheres, American Society for Testing and Materials, 1988, pp. 172-187.

(Zienkiewicz,1991) Zienkiewicz, O.C., Taylor, R.L., "The finite element method", McGraw-Hill Book Co, 1991.

Tables

No of lobes	Amplitude of oscillation (mm)
40	0.05
20	0.25
4	1.5
1	3

Table 1 : Sinusoidal Cam

	Rubbing Velocity		
Material	**178 mm/s**	**480 mm/s**	**700 mm/s**
Ti 6Al 4V	✓	✓	✓
En 58	✓	✓	✓
En 3	✓	✓	
En 31	✓	✓	
Ti 6Al 4V / En 58	✓	✓	

Table 2 : Frictional behaviour experiments

Velocity (mm/s)	Temperature (°C)	μ_{exp}	μ_{model}	Error (%)
176	217	0.65	0.69	6
"	185	0.68	0.75	9
304	640	0.51	0.59	14
"	385	0.23	0.77	70
"	640	0.33	0.59	44

Table 3 : Additional frictional behaviour experiments with stainless steel

Material	A	B	C
Ti 6Al 4V	0.3281	0.126	– 0.1934
En 58	4.7661	– 0.2295	– 0.4449
En 3	0.4582	– 0.0666	0.0391
En 31	0.421	– 0.0473	– 0.0361
Ti 6Al 4V / En 58	0.9123	– 0.0232	– 0.1661

Table 4 : Coefficient of friction model parameters

Element	%
Al	5.5 - 6.75
V	3.5 - 4.5
Fe	0.30 max
H_2	0.0125 max

Table 5 : Ti 6Al 4V (IMI 318) Chemical composition (IMI)

Temperature (°C)	
522.1	Temperature-dependent material properties
1480.3	Temperature-independent material properties

Table 6 . Temperature Predicted By The Analytical Model At The End Of Phase I For Different Material Laws

	υ_0 (mm/s)	h (mm)	ℓ (mm)	ρ_s	ξ	$\upsilon_{(RMS)}$	y_{pl}
D12	3.059	1	7.29	5.67	0.055	265	0.4
D17	4.448	1	8	5.02	0.0035	408	0.28

Table 7 . Input Data In Material Flow Model (Ti 6Al 4V - α : 0.92 mm - f : 65 HZ (exp.D12) and f : 100 Hz (exp.D17))

No	Frequency	Friction Pressure		Forging	Axial	Impact	Mass expelled	Heat input	Work Rate	Friction	Friction	Friction	Extrusion	Penetration
		Initial	Final	Pressure	Shortening	Strength	per cycle	phase I - RMS		Coefficient	Coefficient	Coefficient	Rate	Rate
	(Hz)	(MPa)	(MPa)	(MPa)	(mm)	(mJ)	(mg)	(kW/m^2)	(J/sec)	Initial	phase I	phase III	(1/s)	(mm/s)
A1	10	44.0	24.8	80	3.71	2283	1.70	5869	217	0.70	1.00	1.60	0.11	0.79
A2	10	41.9	25.3	80	3.20	11413	2.24	8375	206	0.68	1.50	3.50	0.15	0.86
A3	10	45.7	27.4	84	3.53	8876	3.20	12184	227	0.60	2.00	3.20	0.26	1.14
A4	10	42.5	34.9		1.46			5893	149	0.58	1.04	1.20		0.54
A5	10	62.5	52.7		1.89	8242	1.30	9168	268	0.66	1.10		0.19	1.26
A6	10	62.5	53.2		1.80			6667	271	0.72	0.80			1.80
A7	12	42.9	19.0	80	4.60			5147	221	0.60	0.75	4.00		1.84
A8	12	61.8												
A9	15	36.3	21.2		2.92	8876	1.82	11622	333	0.62	1.60	3.30	0.15	1.54
A10	18	23.2	18.4		0.92			7798	255	0.60	1.40	2.40		0.92
A11	19	40.9	14.2	22	5.16	22825	4.56	15554	429	0.50	1.50	4.70	0.56	3.04
A12	19	36.7	14.2	22	4.32	7608	3.88	14854	388	0.48	1.60	4.20	0.80	3.20
A13	19	40.9	14.9	80	5.00	20289	4.74	17080	444	0.53	1.65	4.50	0.30	2.78
A14	19	48.1	16.8	80	6.04	18387	5.21	18883	491	0.54	1.55	4.20	0.71	3.02
A15	19	41.0	19.2		4.20	12681	2.16	14543	157	0.52	1.40	3.80	0.20	
A16	20	42.1	10.8	80	6.04	15217	4.61	20223	353	0.56	1.80	5.40	0.52	2.88
A17	20	41.0	15.4		4.93	13315	4.69	16388	375	0.44	1.50	4.00	0.63	2.90
A18	20	36.8	15.8		4.05	8250	2.60	12353	342	0.50	1.26	3.40	0.35	1.90
A19	20	44.7	16.5		5.44	14583	4.87	19657	427	0.50	1.65	4.10	0.70	2.94
A20	20	40.7	17.7	80	4.44	11413	4.09	17356	369	0.48	1.60	3.90	0.58	2.77
A21	20	43.7	18.8		4.80	13323	3.60	16298	372	0.46	1.40	3.80	0.49	2.30
A22	20	42.5	19.1		4.50	11413	4.41	18116	407	0.56	1.60	3.70	0.72	3.33
A23	20	51.2	20.9		5.84	12681	3.78	20470	455	0 48	1.50	3.30	0.57	2.65
A24	20	50.2	21.2	43	5.59	17753	2.93	20063	461	0.58	1.50	3.30	0.04	1.89

Table 8 : Successful linear friction welds of Ti 6Al 4V (amplitude of oscillation : 3 mm)

No	Amplitude of oscillation (mm)	Frequency (Hz)	Friction Pressure Initial (MPa)	Friction Pressure Final (MPa)	Forging Pressure (MPa)
B 1	3	5	79.8		
B 2	3	5	72.9		
B 3	3	6	61.4		22
B 4	3	10	32.9	13.2	
B 5	3	10	41.9	18.0	
B 6	3	10	42.5	28.1	
B 7	3	10	70.0		
B 8	3	10	70.0		
B 9	3	10	70.0		
B 10	3	10	70.0		
B 11	3	16	34.1	11.7	
B 12	3	17	29.3	15.0	
B 13	3	19	40.7	7.5	6
B 14	3	19	42.5	10.6	6
B 15	3	20	23.2	10.8	
B 16	3	25	14.0	7.2	
B 17	3	25	32.8	8.7	
B 18	3	25	25.9	9.1	
C 1	0.92	14	72.8	66.6	
C 2	0.92	29	45.7	33.3	
C 3	0.92	40	34.5	21.1	
C 4	0.92	45	49.1	29.4	
C 5	0.92	50	20.5	10.6	
C 6	0.92	50	15.0		
C 7	0.92	54	32.7		
C 8	0.92	54	25.4		
C 9	0.92	55	32.7		
C 10	0.92	60	44.1	26.0	
C 11	0.92	62	43.6		
C 12	0.92	62	43.6		
C 13	0.92	69	38.3	19.3	
C 14	0.92	69	25.7	20.1	
C 15	0.92	79	23.9	18.9	
C 16	0.92	84	9.0		
C 17	0.92	89	44.9	16.9	
C 18	0.92	92	19.1	7.4	
C 19	0.92	98	30.2	4.2	
C 20	0.92	99	23.9	10.9	
C 21	0.92	100	37.8	5.6	
C 22	0.92	100	22.1	15 9	
C 23	0.92	101	19.1	14.2	

Table 9 : Linear friction welds of TI 6AI 4V showing no permanent adhesion

No	Frequency (Hz)	Friction Pressure Initial (MPa)	Friction Pressure Final (MPa)	Axial Shortening (mm)	Impact Strength (mJ)	Mass expelled per cycle (mg)	Heat input phase I - RMS (kW/m^2)	Work Rate (J/sec)	Friction Coefficient Initial	Friction Coefficient phase I	Friction Coefficient phase III	Extrusion Rate (1/s)	Penetration Rate (mm/s)
D 1	30	58.1	37.6	2.60	15217	0.35	2851	104	0.18	0.40	1.20	0.11	0.90
D 2	38	64.3	39.9	4.70	6340	1.00	5993	250	0.40	0.60	1.35	0.17	1.27
D 3	41	76.8				0.53							
D 4	41	69.9				0.70						0.20	
D 5	48	43.6	31.7	2.30		0.56	4619	125	0.44	0.54	0.40	0.05	1.29
D 6	49	44.6	30.9	2.65	2536	0.77	7862	209	0.30	0.88	3.20		0.62
D 7	50	52.4	32.3	3.87	10271	0.76	8025	255	0.30	0.75	1.25	0.04	1.95
D 8	50	48.8	32.7	3.10	14710	0.85	7474	190	0.25	0.75	1.05	0.49	1.82
D 9	50	55.3	39.4	3.07	12807	0.61	8476	218	0.30	0.75	1.00	0.35	2.56
D 10	50	57.8	39.9	3.46	6467	0.76	8860	1116	0.30	0.75	0.80	0.33	1.82
D 11	62	50.9			17753		5930	215	0.36	0.46			
D 12	65	52.9	25.9	5.20	12681	1.39	8427	292	0.26	0.60	1.20	0.32	2.26
D 13	79	46.9	25.6	4.10			7567	300	0.42	0.50	1.40		3.42
D 14	89	49.4	22.9	5.10	14444	0.96	7182	262	0.20	0.40	1.00	0.80	3.29
D 15	100	43.1	24.8	3.54			5288	160	0.15	0.30	0.60		4.72
D 16	100	50.5	31.1	3.74	7735	0.77	6197	167	0.35	0.30	0.45		4.66
D 17	100	50.2	34.8	2.98	17246	0.71	5747	162	0.26	0.28	0.75	0.95	4.45
D 18	100	57.7	39.6	3.50	9003	0.72	6607	183	0.25	0.28	0.32	0.92	4.61
D 19	100	56.5	39.7	3.24	8369	0.66	5773		0.30	0.25	0.40		4.63
D 20	119	49.4	34.5	2.87			4326		0.10	0.18	0.30		4.35

Table 10 : Successful linear friction welds of Ti 6Al 4V (amplitude of oscillation : 0.92 mm)

	No	f (Hz)	Final P_{fr} (MPa)	S/N Value (db)
1	D6,D7	50	32	8.15
2	D8,D9	50	39	7.82
3	D14,D15	100	32	8.00
4	D16,D17	100	39	7.88

Table 11 : Experimental Design Used To Investigate The Parameters Of Frequency Of Oscillation And Friction Pressure (α : 0.92 mm)

	No	Power Input Parameter	Forging Pressure (MPa)	S/N Value (db)
1	A17,A9	939	0	8.04
2	A14,A18	951	80	8.05
3	A22,A15	1122	0	8.16
4	A20,A21	1092	80	8.18

Table 12 : Experimental Design Used To Investigate The Parameters Of Power Input Parameter And Forging Pressure (α : 3 mm)

	Degrees Of Freedom	Sum Of Squares	Variance
(A) Frequency Of Oscillation	1	0.0026	0.0026
(B) Friction Pressure	1	0.051	0.051
(A)X(B) Interaction	1	0.011	0.011

Table 13 : Analysis Of Variance Of S/N Data Showing Significance Of Frequency Of Oscillation And Friction Pressure On The Impact Strength Of Linear Friction Welds Of Ti 6Al 4V

	Degrees Of Freedom	Sum Of Squares	Variance
(A) Power Input Parameter	1	0.015	0.015
(B) Forging Pressure	1	3E-4	3E-4
(A)X(B) Interaction	1	1E-6	1E-6

Table 14 : Analysis Of Variance Of S/N Data Showing Significance Of Power Input Parameter And Forging Pressure On The Impact Strength Of Linear Friction Welds Of Ti 6Al 4V

No	Adhesion	Frequency	Friction Pressure		Axial Shortening	Forging Pressure
			Initial	Final		
		(Hz)	(MPa)	(MPa)	(mm)	(MPa)
L1	Yes	5	14.5			22
L2	Yes	5	18.2			22
L3	Yes	8	19.2			22
L4	Yes	17	14.5	12.8	0.4	
L5	No	5	10			
L6	No	10	5.3			22

Table 15 . Linear Friction Welds Of Lead (a : 3 mm)

Appendix A: Experimental Design And Analysis

A.1.Planning Of Experiments

An experiment can be considered as a process seeking to answer one or more carefully formulated questions. It should have carefully described goals. These goals should be used to choose the appropriate factors and their range, the relevant procedure and the knowledge of to what the results are connected. The factors studied should not be covered by other variables, with the chosen experimental sequence removing the effects of the uncontrolled variables. Replication of the experiments will help to randomise the results taken, to limit bias from the experiments. While replication ensures a measure of precision, randomisation provides validity of the measure of precision.

A common experimental pattern is the so-called factorial design, in which several factors are controlled and their effects are investigated at two or more levels. If two levels of each factor are studied, the experimental pattern requires performing experiments at each of the 2^n possible combinations. Design of experiments describes a methodology by which the efficiency of the acquisition of scientific information by experiments is increased. This is usually achieved from a minimum number of experiments. This appendix looks at the requirements of experimental designs and applies a fractional factorial method to the investigation outlined in chapter 7.

An experiment planning method must be able to cover the following :

(a)The degree of disturbance, the influence of various uncontrollable experimental conditions and unknown causes on experimental data can be controlled by randomising the experimental pattern.

(b)The estimated effect of a factor can differ from its true value by random variation only. A measure of this is achieved by repeating an experiment.

(c)The effect of a number of factors on a process can be studied by altering each factor in sequence, and therefore performing a full factorial experiment. This technique produces the maximum amount of information, at the expense of time and resources. Conclusions drawn from such experiments depend on the state of every single factor. The use of orthogonal arrays enables us to simultaneously experiment on many factors.

(d)Enable the use of the analysis of variance as a method of quantitatively evaluating, from the output data, the magnitude of the effects of various types of input causes. The application of signal-to-noise (S/N) ratio to dynamic characteristics are used in the design of experiments.

In the parametric design of the experimental section the fractional factorial method as described by **(Taguchi,1986)** is used to assess the effect of a number of factors on the impact strength of joints produced with linear friction welding. The design of experiments method enables the study of the combined effect of them on the process, known as interactive effects. If the full factorial experiment method was used 2^2 or 4 experiments plus replications would be required. The fractional factorial experimental design enables the reduction of the number of experiments and the study of the combined effect of individual factors. The combined effect of the individual factors has to be less material than that of the main factors. Therefore, some understanding of the influence of both the main factors and the interactive factors is required for aliasing to be carried out. To avoid invalid results, the interactive effect should not be connected with less significant main effects.

In designing a fractional factorial experiment care must be given so that all factors have an undeviating weight on other factors, at all levels that the may take. **(Taguchi,1986)** has developed a simple method to study the effect of factors, both main and interactive, using orthogonal arrays. In these arrays, each factor is equally influenced by the effects of the factors under study.

In (Taguchi,1986) a number of orthogonal arrays are given for different experiments, and a L_4 array is shown in Figure 133. The first row indicates the number of factors which will be tested, which is 3 in this case. The first column shows the number of experiments that must be completed for the fractional factorial experiment, in this case being four. The other columns underneath show the levels of each factor. In the first experiment of this array all factors are set to level 1, and similarly for the other rows.

Each factor in an orthogonal array has a degree of freedom associated with it, which prescribe the orthogonal array selected. The degree of freedom of each factor is equal to the levels that it takes minus one. For an interaction factor, the degree of freedom is equal to the product of the degrees of freedom of the factors that compose it.

The sum of the degrees of freedom of each individual factor studied must be equal, at the most, to the degree of freedom of the orthogonal array. The degree of freedom of the array is equal to the number of experiments performed minus one.

To study the interaction between factors, the orthogonal array can be used to include this interaction as a separate factor. The number of factors under investigation will have to be reduced, so as to retain the correct number of degrees of freedom. A linear graph (Figure 133) is used to maintain the orthogonality in the array. It corresponds to columns in the orthogonal array, and on each line the factors investigated for association are shown. For example in Figure 133 column 3 is reserved for the interaction between factors 1 and 2.

A.2.Analysis Of Designed Experiments

Once experiments have been completed, results are analysed by calculating the signal-to-noise (S/N) ratio for each factor and each level in these experiments. This ratio is the reciprocal of the variance of the measurement error. It is maximal for the combination of parameter levels that has the minimum error variance. Calculating the average of S/N value for each factor and plotting

them for each level reveals the effect of the factor on the variable used to assess these experiments. In addition, analysis of variance (ANOVA) techniques can be used to study the fractional factorial experiments and identify the significance of each factor.

The variable used to assess the linear friction welding experiments in this investigation was the impact strength of the produced joint using a Charpy impact test. The objective of this work was to create joints which would have high value of impact strength.

A measure of experimental error is necessary to estimate the significance of the results. In large factorial experiments estimates of higher order interactions can be obtained. These estimates are actually estimates of experimental error, as it is assumed that higher order interactions are physically impossible. In small factorial designs, as in the one used here, there are no estimates of higher order interactions, and the estimate is based on past experience.

Figures

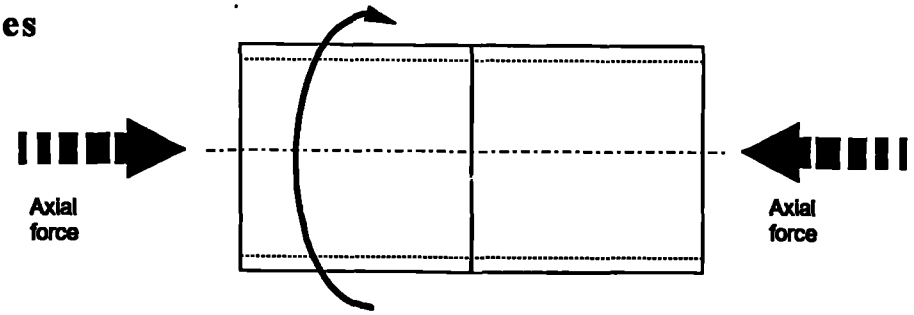

Rotary

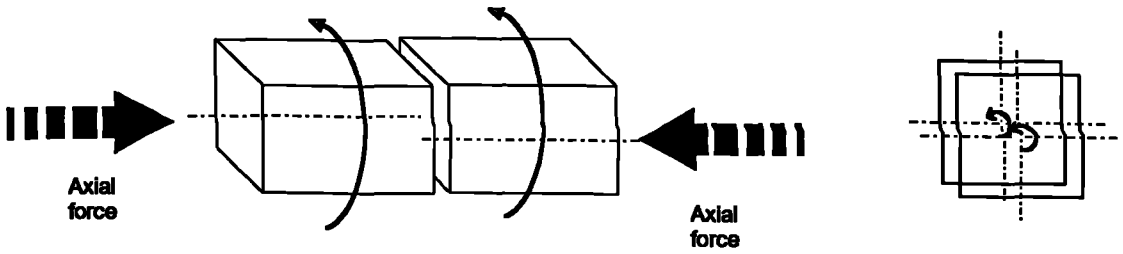

Orbital

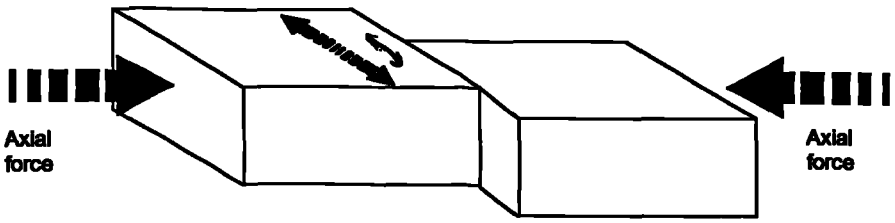

Linear

Figure 1 . Types of Friction Welding

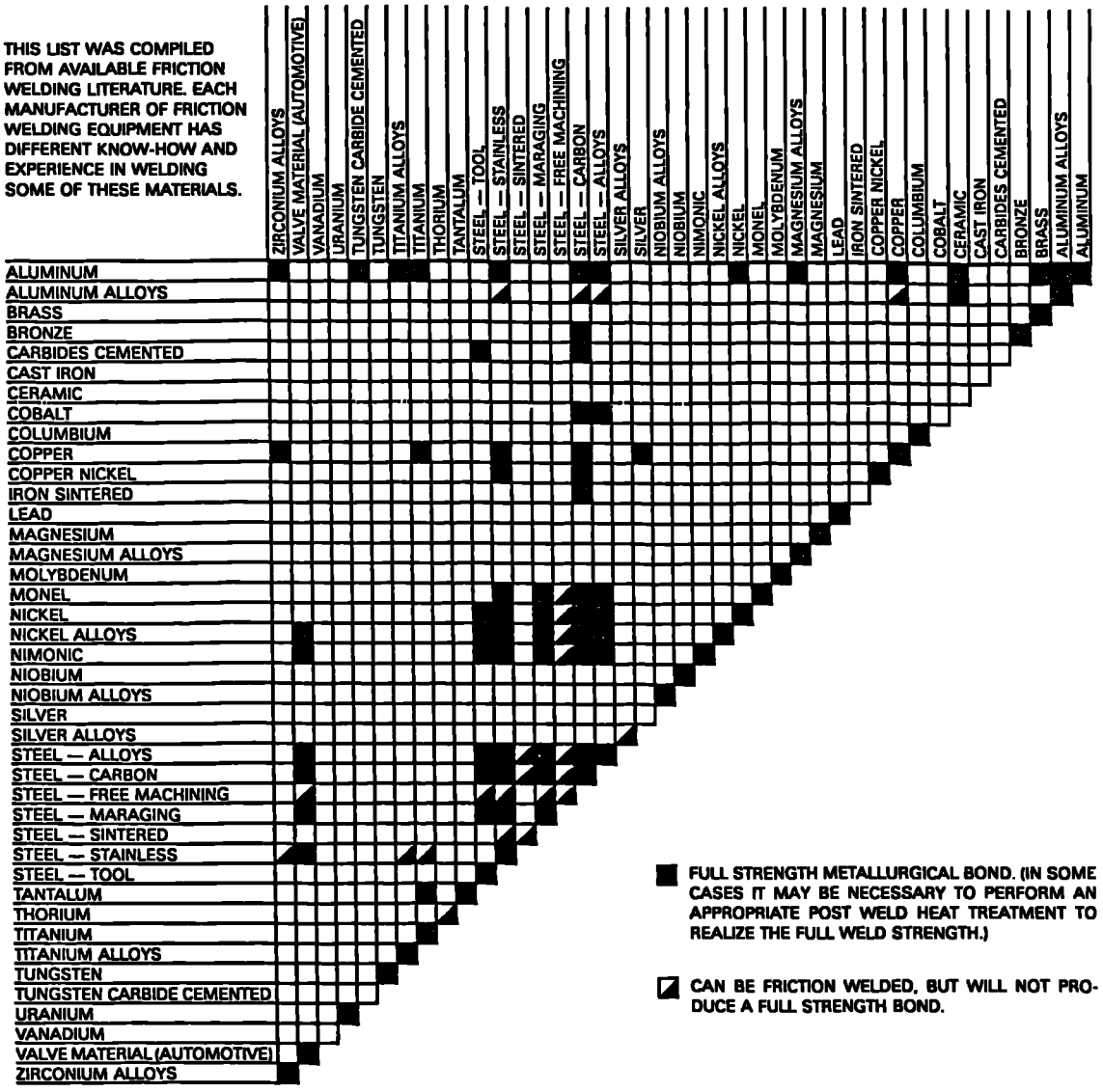

Figure 2 . Material Combinations Weldable by Friction Welding (Aws, 1989)

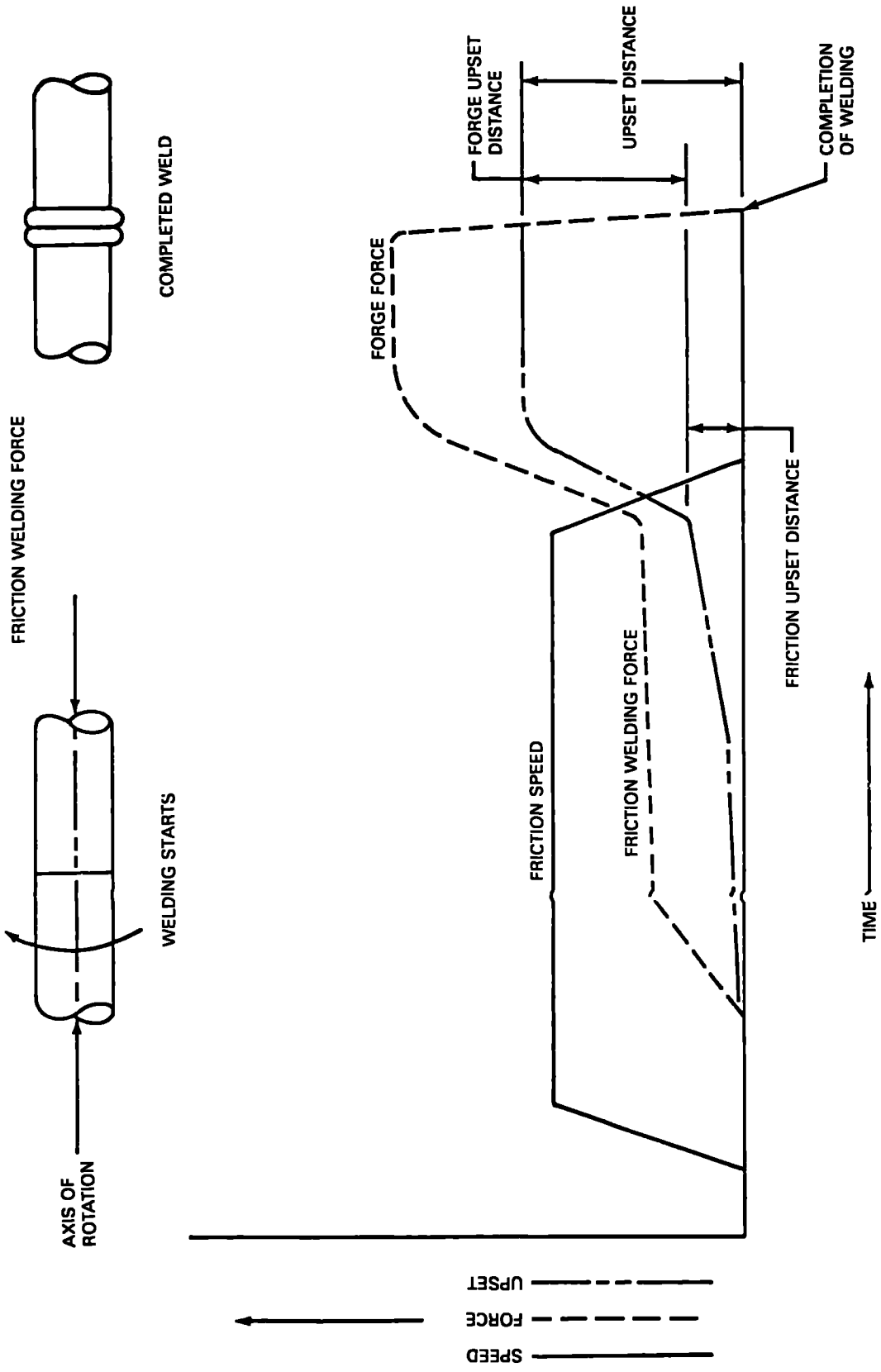

Figure 3 . Idealised Traces Of Variations With Time Of Speed, Force And Axial Shortening During Continuous Rotary Friction Welding (Aws,1989)

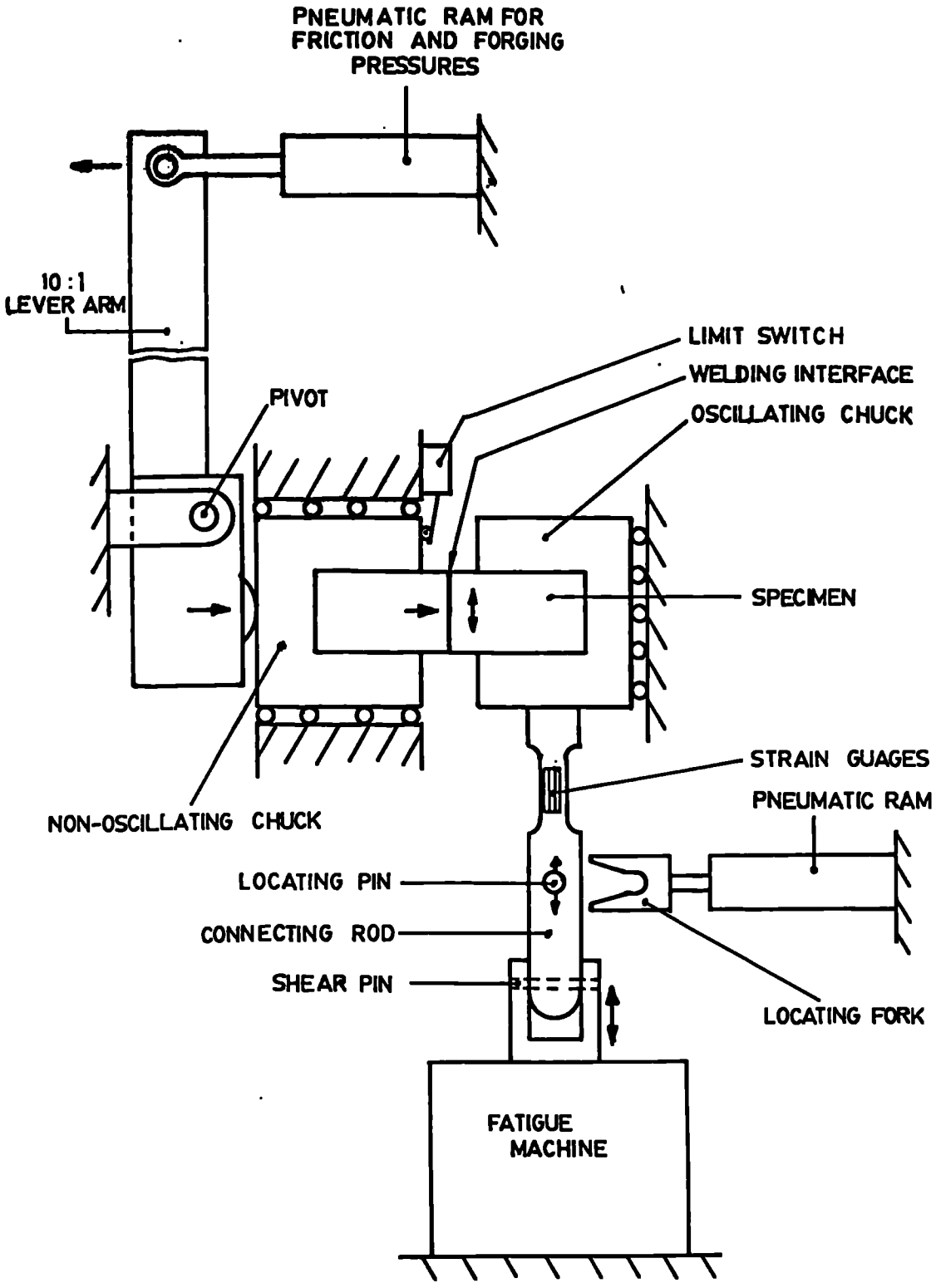

Figure 4 . Schematic General Assembly Of First Linear Friction Welding Rig (Garton,1987)

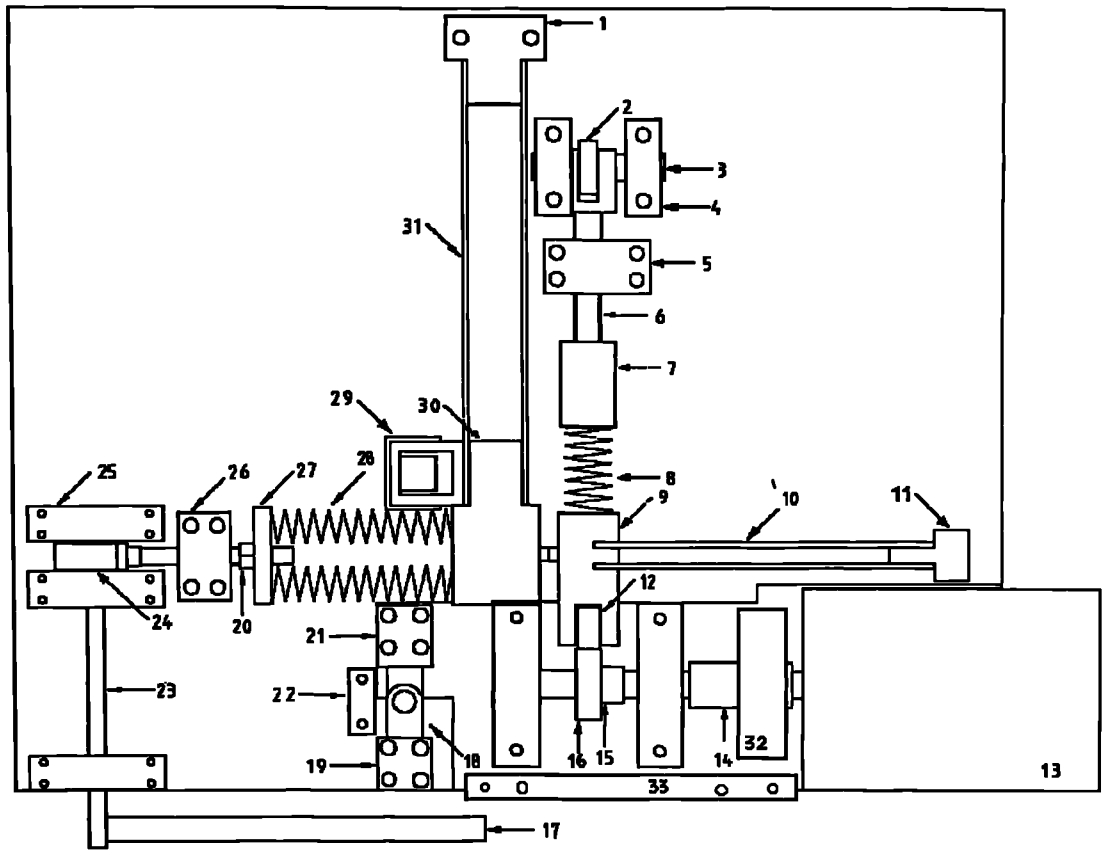

1.	Fixed chuck support block	17.	Forging force application arm
2.	Positioning mechanism link	18.	Toggle
3.	Pivot shaft	19.	Toggle block
4.	Pivot support blocks	20.	Axial spring adjuster and slider
5.	Return spring slider block	21.	Toggle block
6.	Return spring tensioner and slider	22.	Toggle restraint
7.	Return spring locator	23.	Forging applicator cam shaft
8.	Return spring	24.	Forging force cam
9.	Oscillating chuck	25.	Cam plummer blocks
10	Oscillating chuck parallel beams	26.	Axial springs slider
11.	Oscillating chuck support block	27.	Axial springs guide
12.	Cam follower	28.	Axial springs
13.	Motor	29.	Fixed chuck restraining mechanism
14.	Shaft coupling	30.	Fixed chuck
15.	Lobed cam shaft	31.	Fixed chuck parallel beams
		32.	Flywheel
16.	Lobed cam		
		33.	Motor plate stiffening

Figure 5 . High Frequency Linear Friction Welding Rig (Dimensions : 885 by 1000 mm)

A Parallel Bears
B Static Chuck
C Friction / Forge Springs
D Clamp
E Can Follower
F Oscillating Chuck
G Parallel Beans
H Following Spring
I Specimens

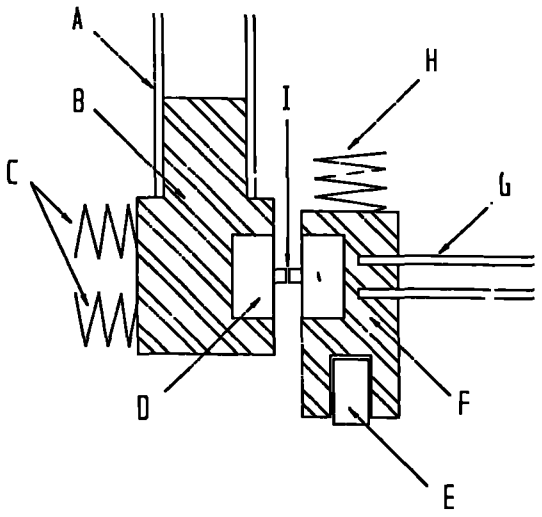

ENLARGEMENT OF CHUCK REGION

Figure 6 . Detail Of Chuck Region

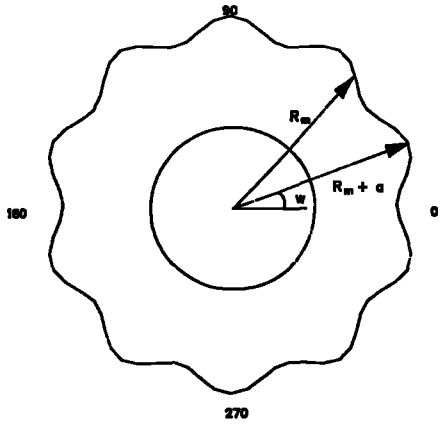

Profile equation :–

$$r = R_m + a \sin (nw)$$

r = cam profile
R_m = mean radius of the cam
n = no. of lobes
w = angle
a = amplitude of sine wave

Figure 7 . Sketch Of The Sinusoidal Cam And Profile Generating Equation

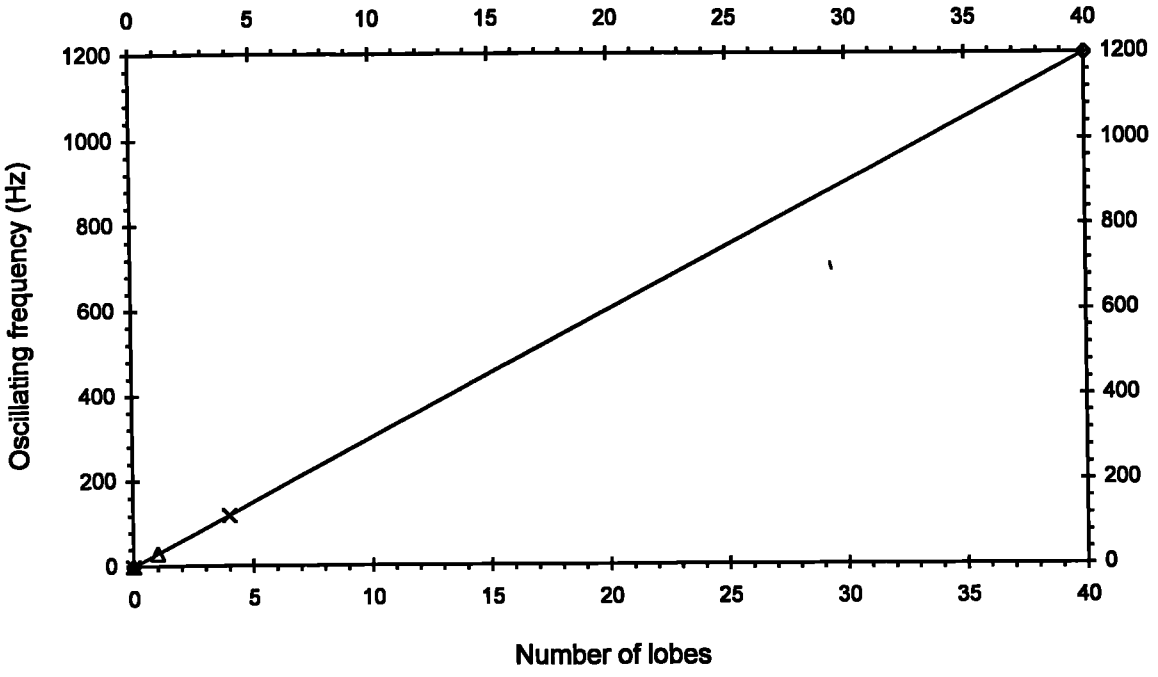

Figure 8 . Range Of Frequencies Attainable With the Cams Provided

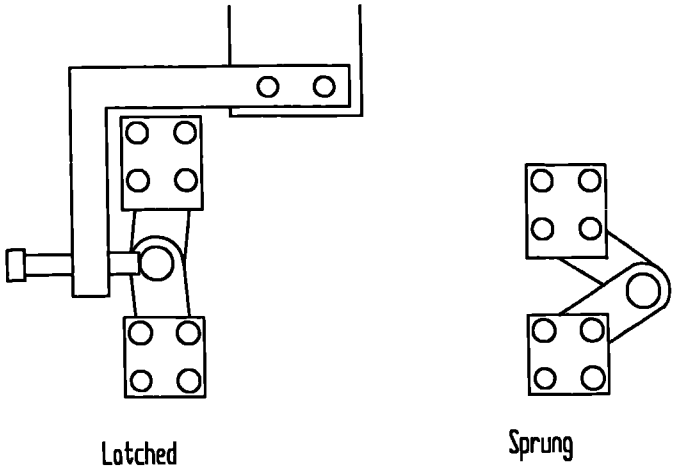

Figure 9 . Toggle

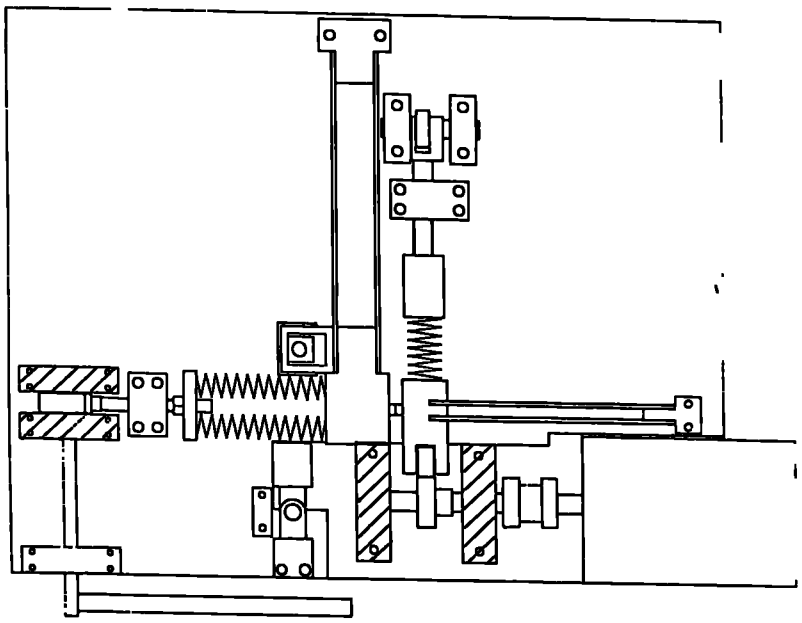

Figure 10 . Components Attached Solely to Base Plate

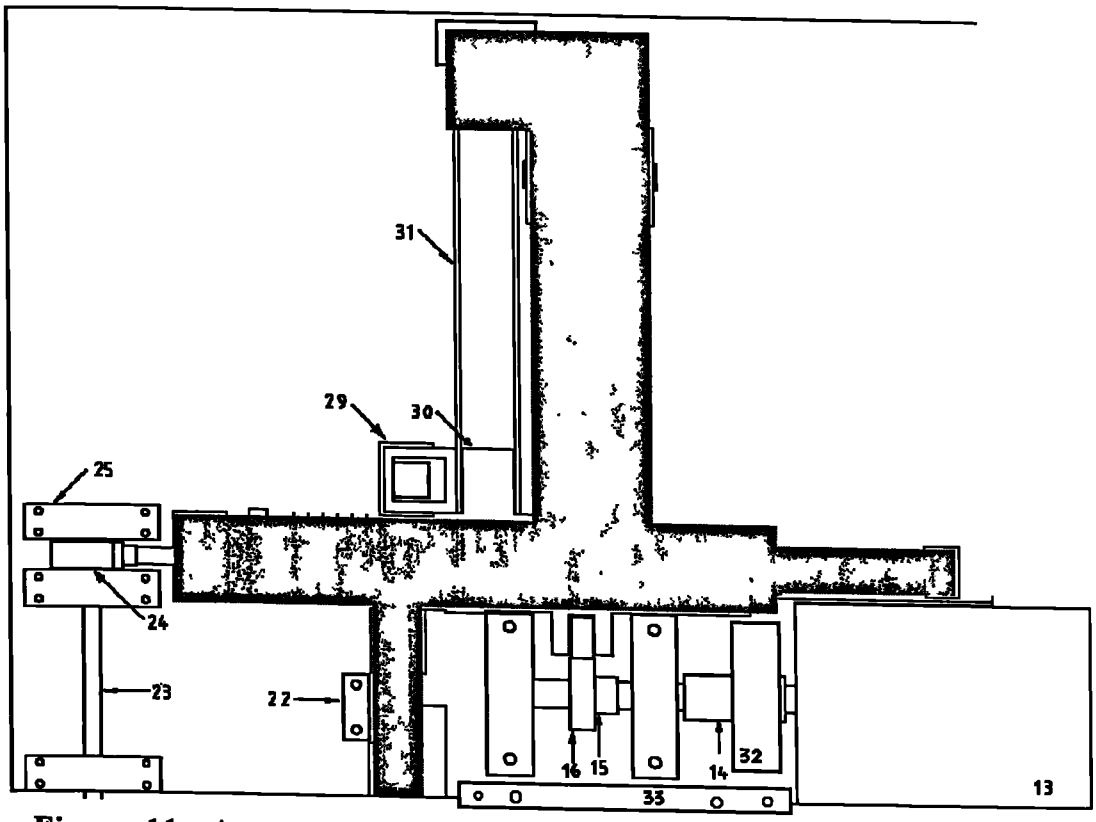

Figure 11 . Areas of the Rig Stiffened With Steel Beams

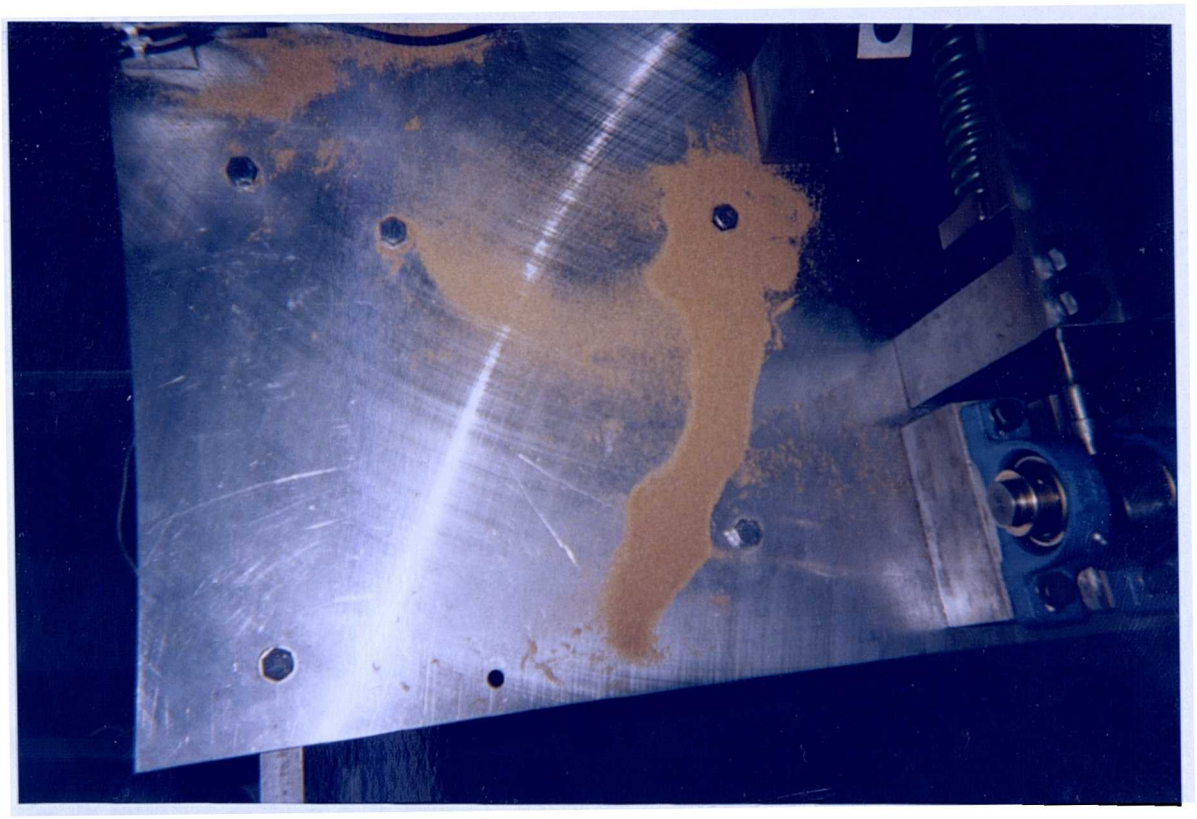

Figure 12 . LFW Machine Plate - Vibration Patterns (Right Side - Before Strengthening)

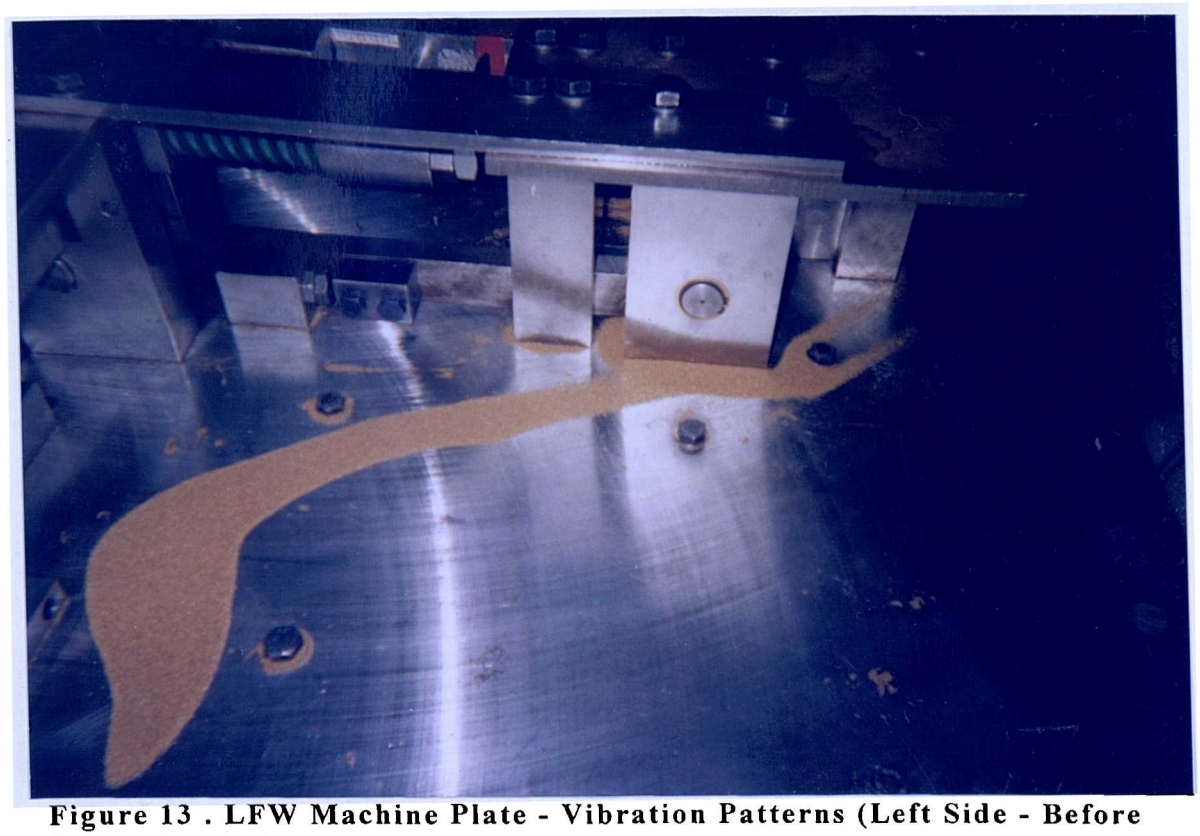

Figure 13 . LFW Machine Plate - Vibration Patterns (Left Side - Before Strengthening)

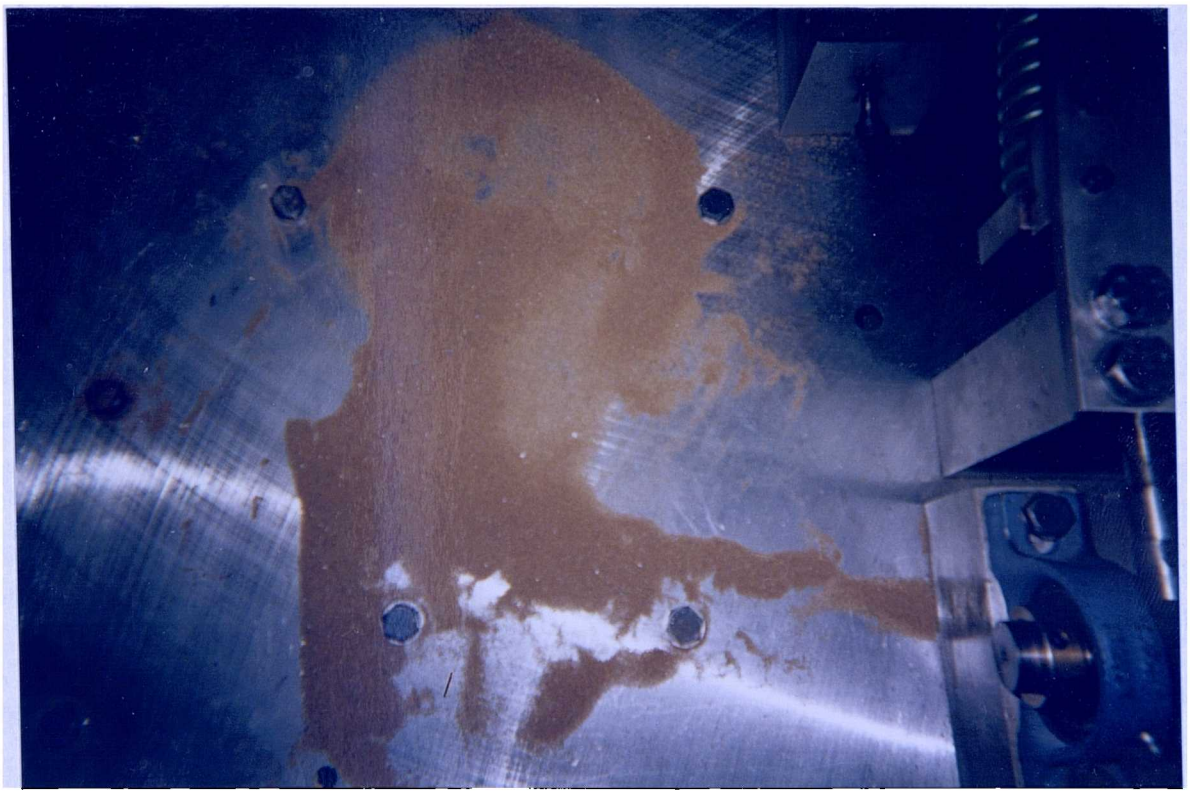

Figure 14 . LFW Machine Plate - Vibration Patterns (Right Side - After Strengthening)

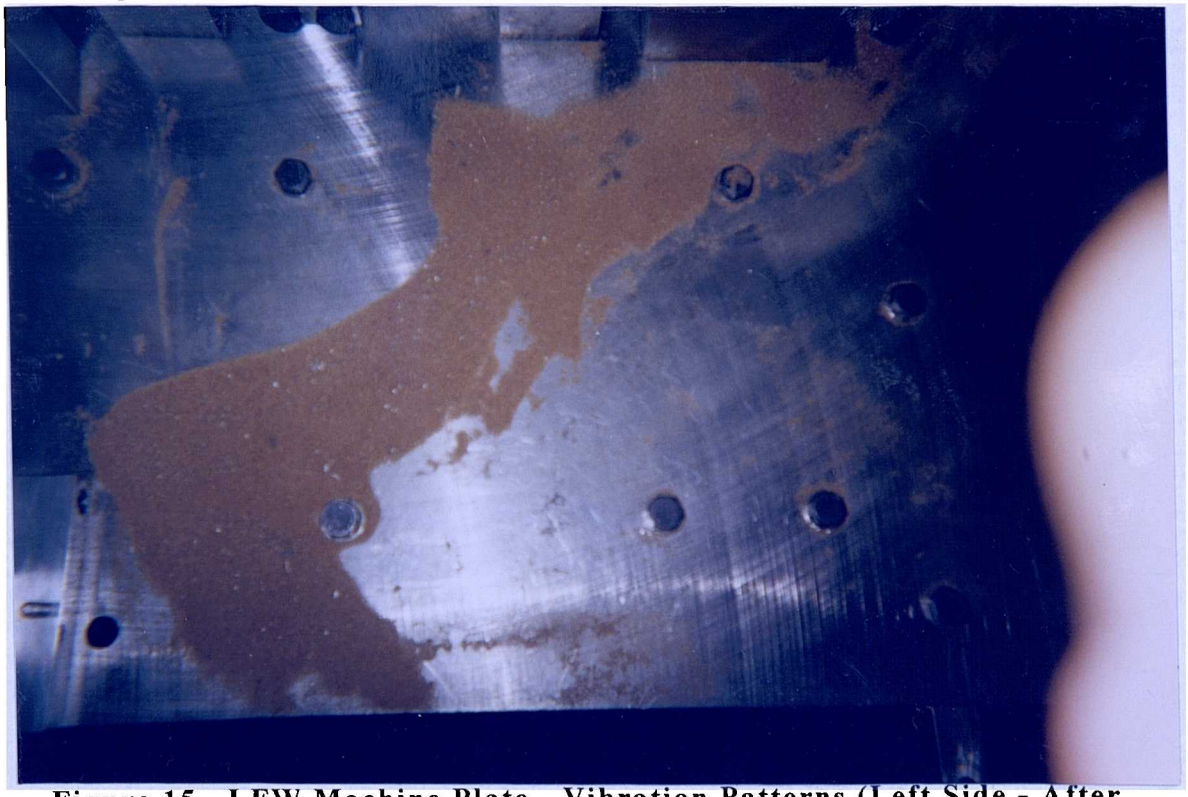

Figure 15 . LFW Machine Plate - Vibration Patterns (Left Side - After Strengthening)

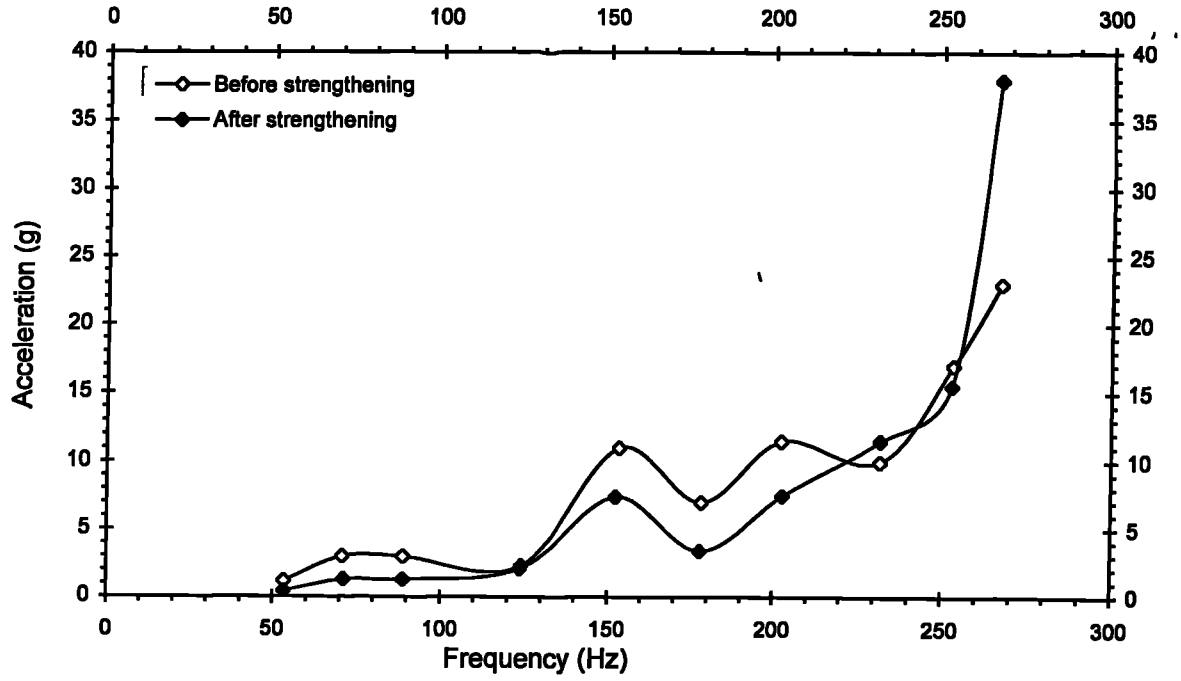

Figure 16 . Vibration Analysis of LFW Machine (Beam on Top of Moving Chuck - 20 Lobe Cam α : 0.25 mm)

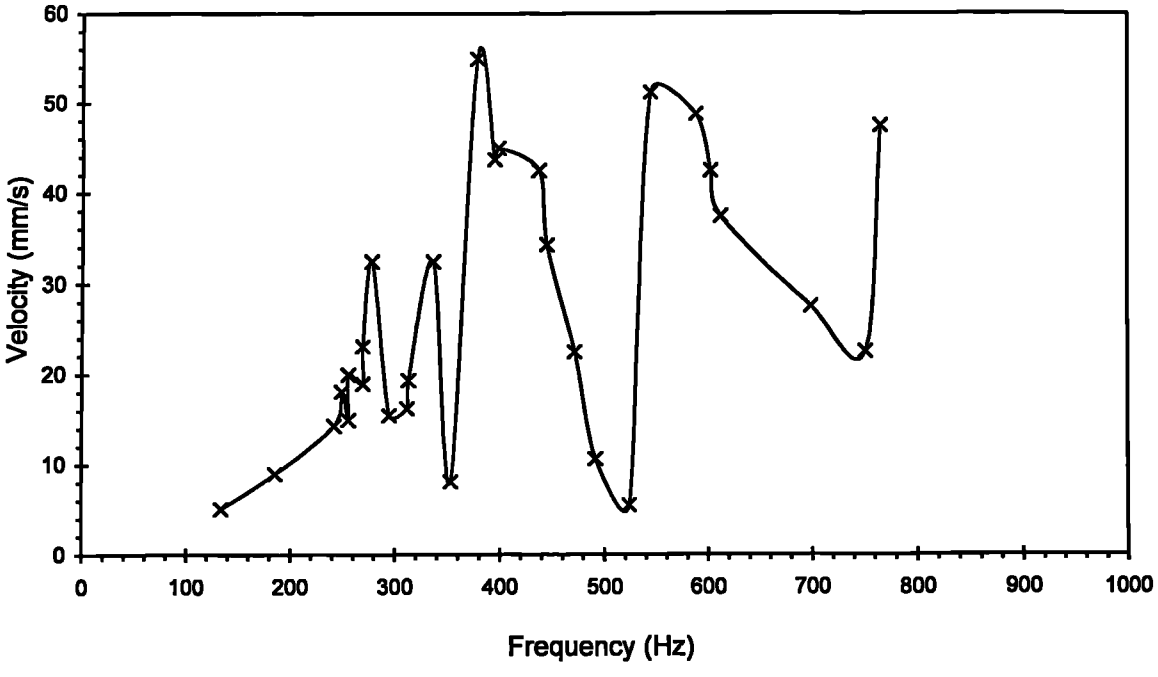

Figure 17 . Vibration Analysis of LFW Machine (Chuck - 40 Lobe Cam - α : 0.05 mm)

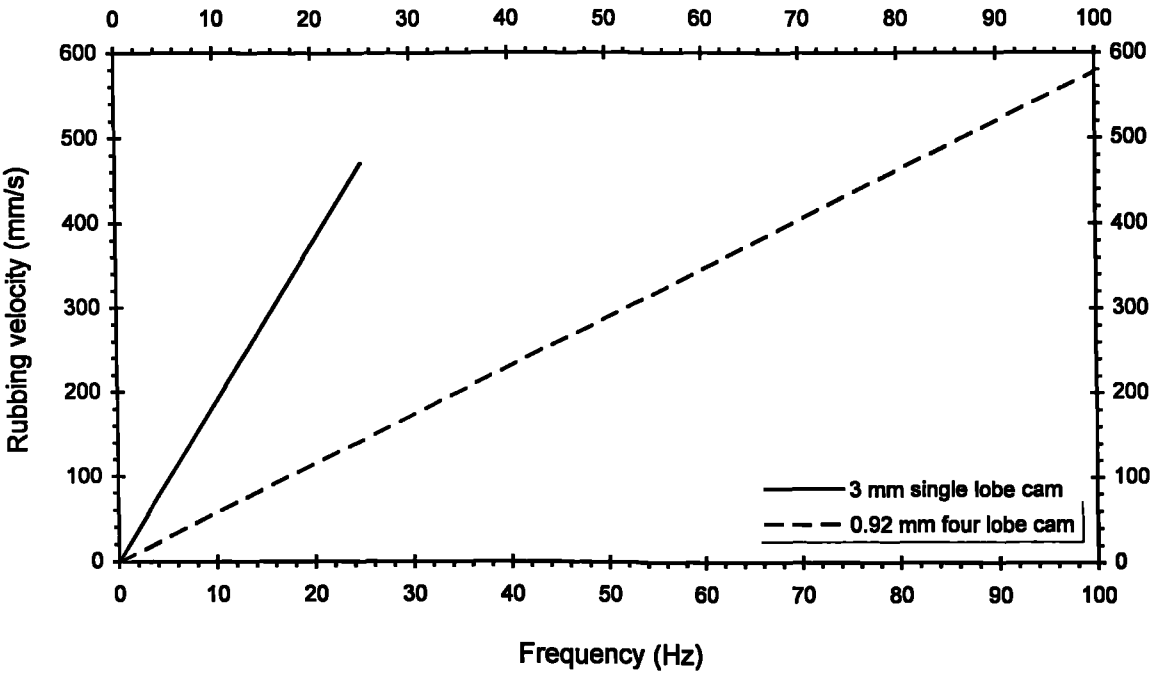

Figure 18 . Operating Frequencies And Rubbing Velocities For The Amplitudes Of Oscillation Used

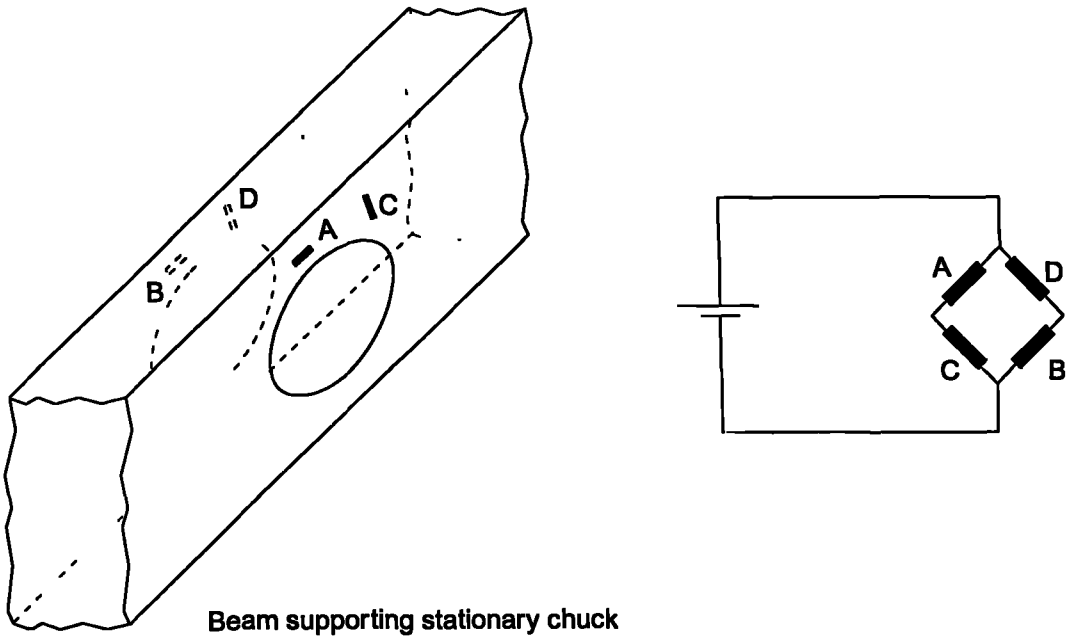

Figure 19 . Shear Force Measurement Instrumentation

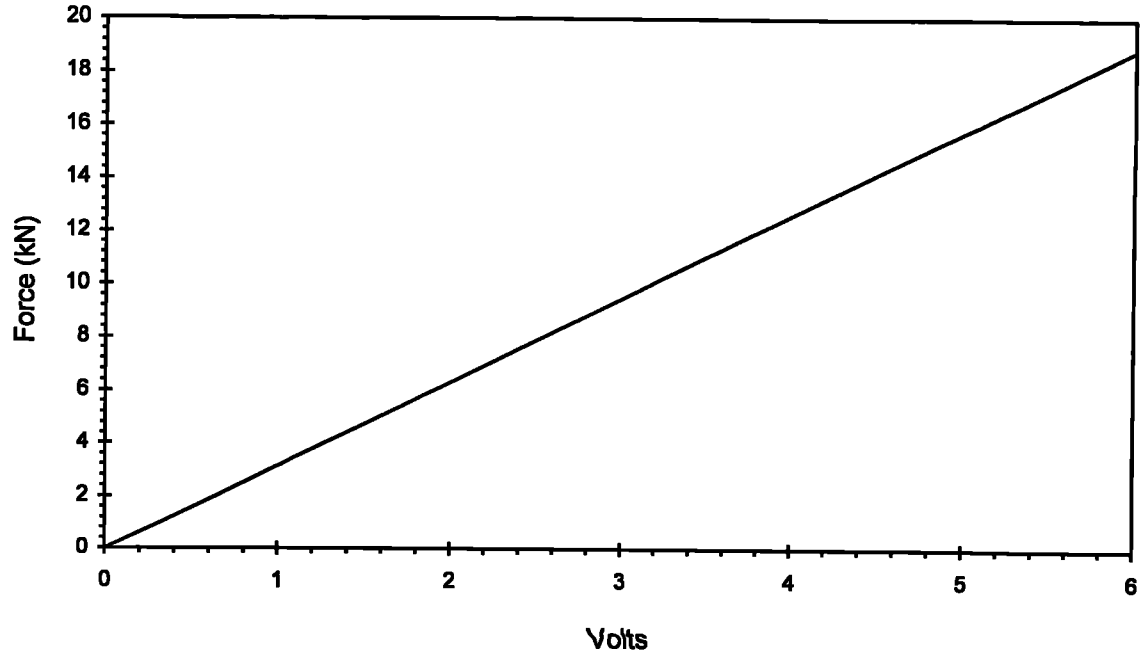

Figure 20 . Calibration Of Strain Gauge Bridge

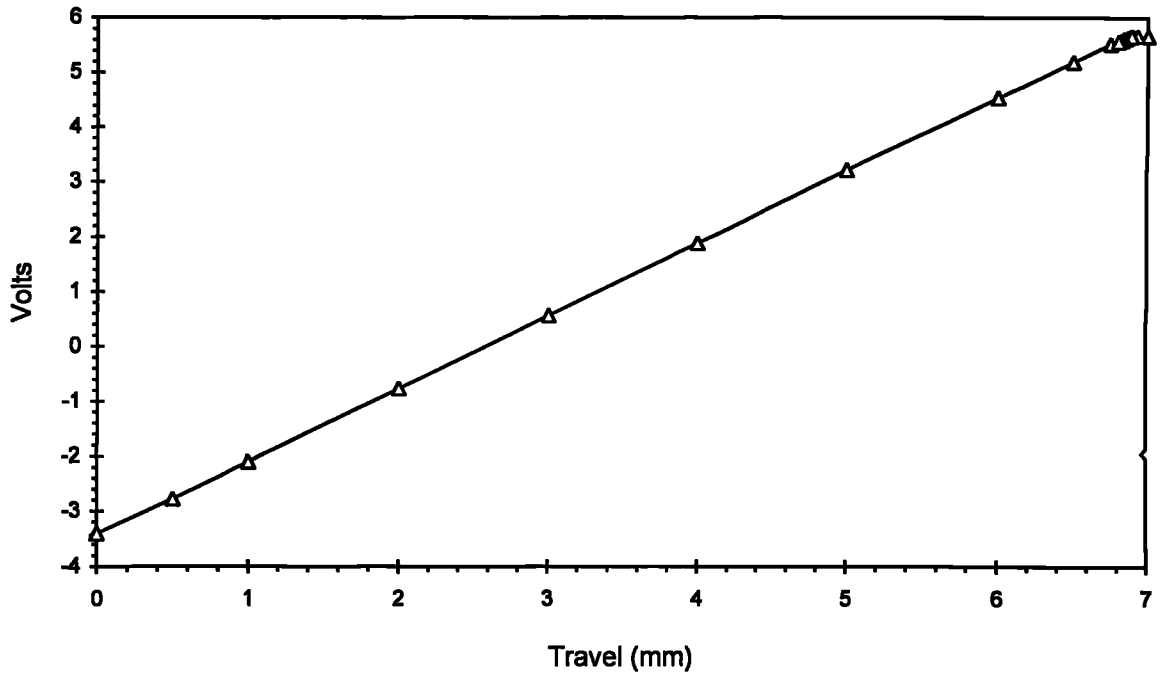

Figure 21 . Calibration Of Short LVDT (To Measure Axial Displacement)

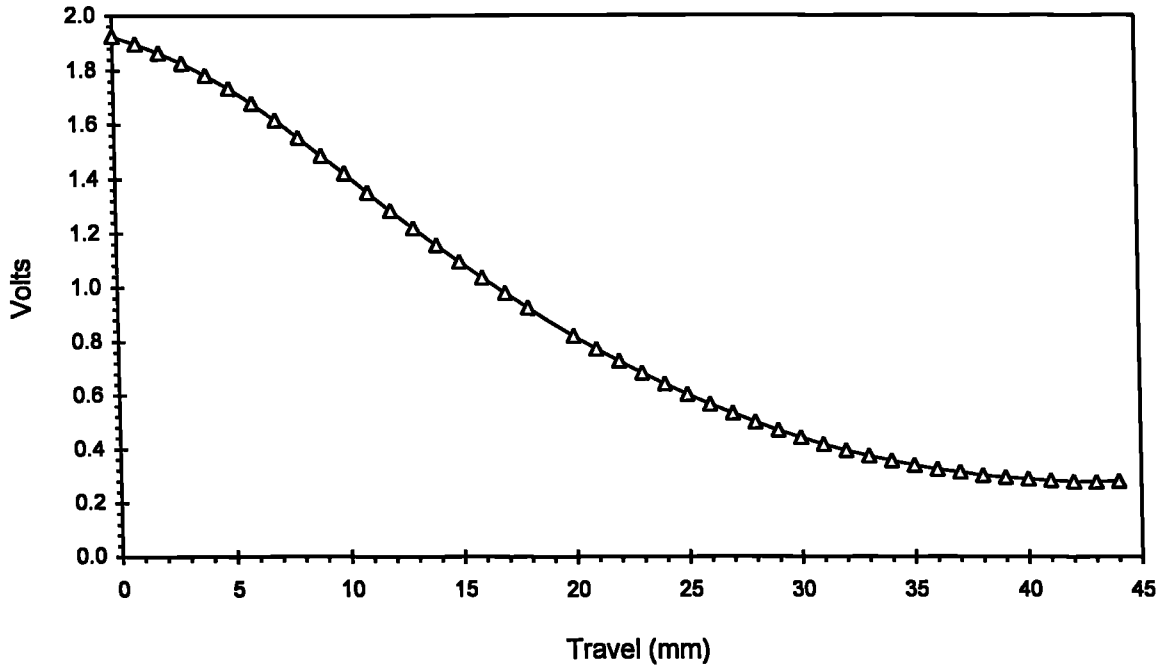

Figure 22 . Calibration Of Long LVDT (To Measure Frictional Force Spring Compression)

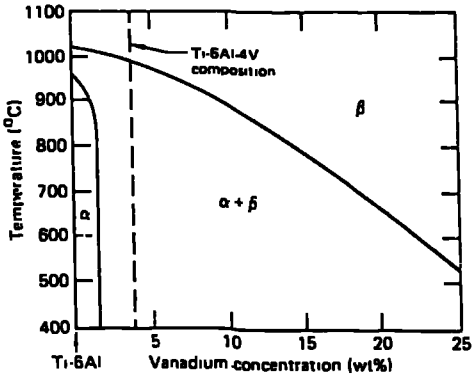

Figure 23 . Ternary Diagram of Ti 6Al 4V

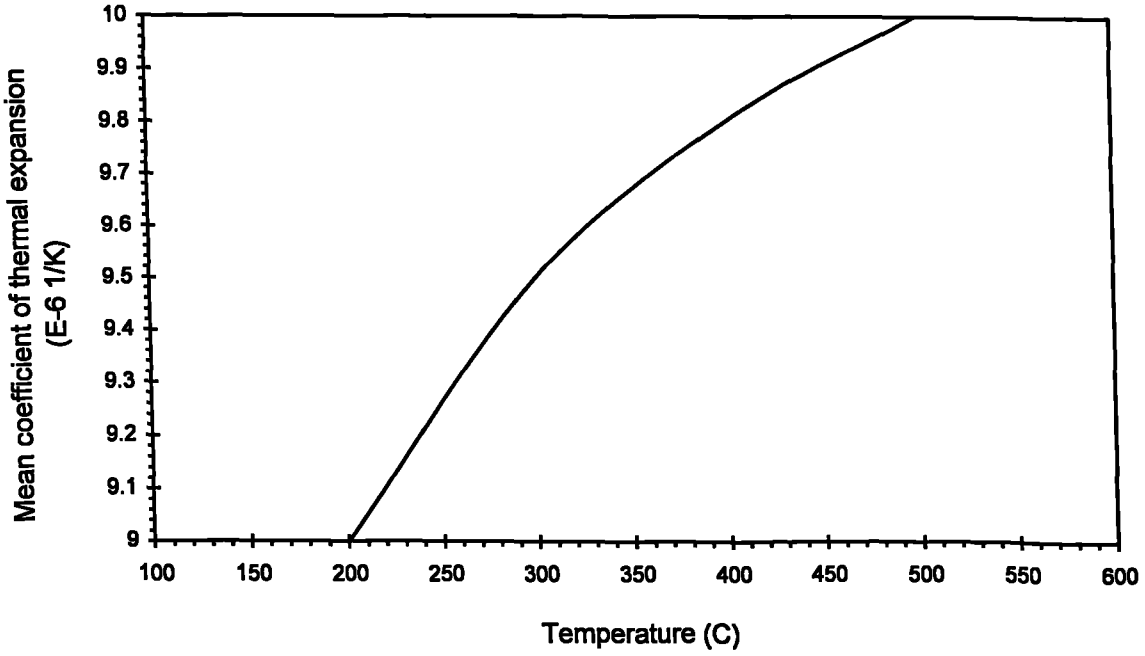

Figure 24 . Effect Of Temperature On Linear Thermal Expansion Of Ti 6Al 4V (Imi)

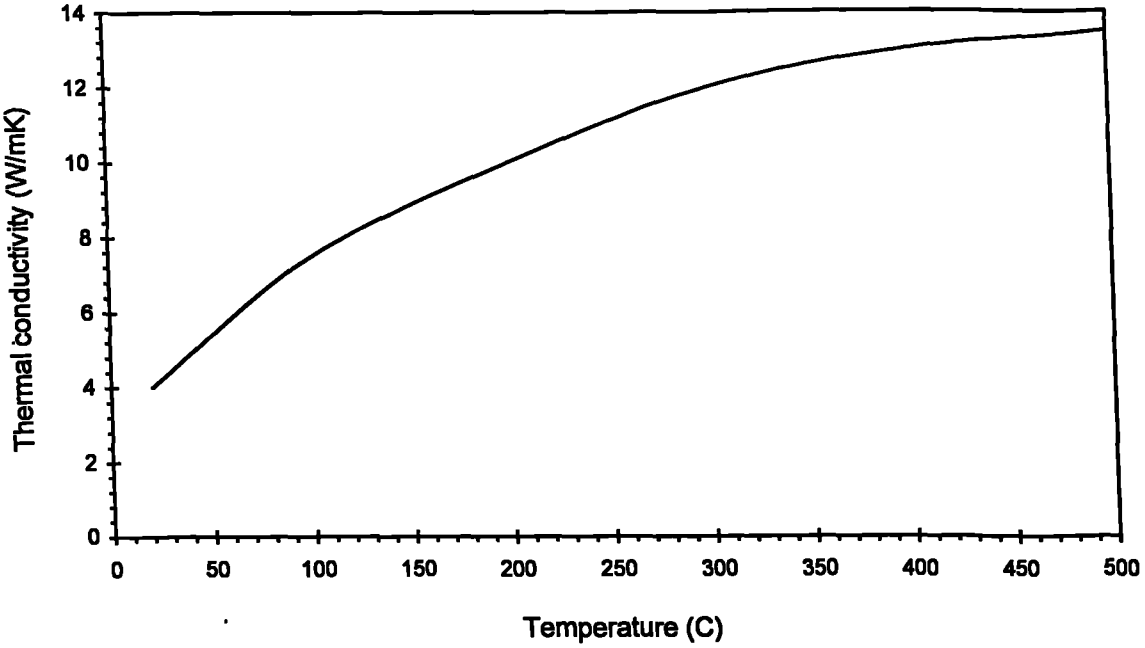

Figure 25 . Effect Of Temperature On Thermal Conductivity Of Ti 6Al 4V (Imi)

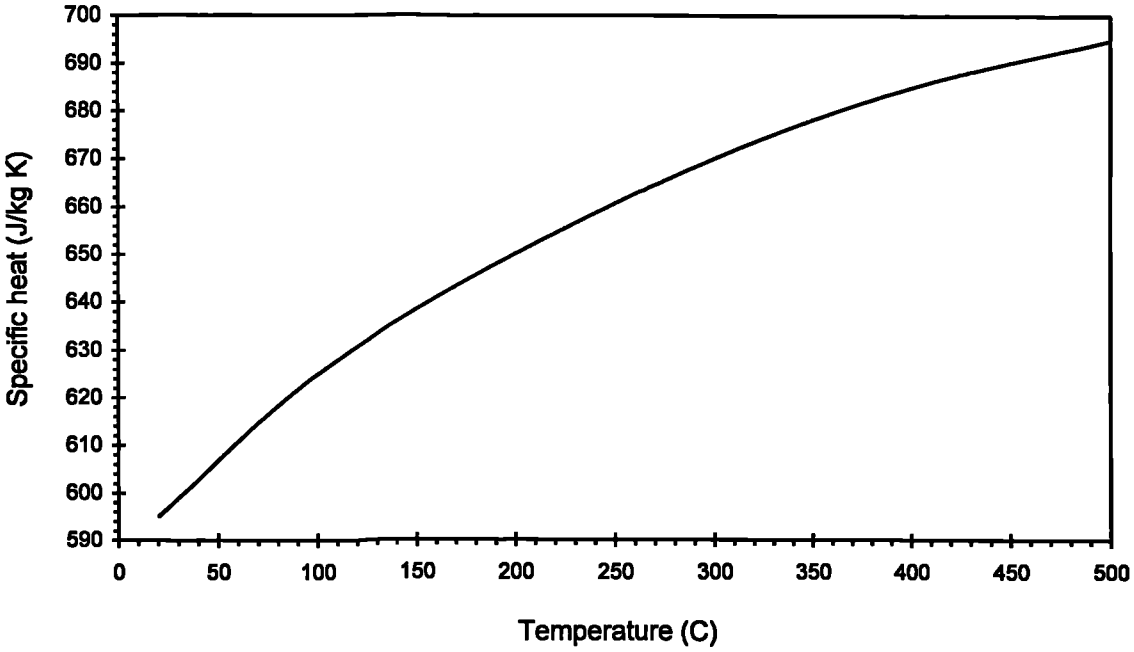

Figure 26 . Effect Of Temperature On Specific Heat Of Ti 6Al 4V (Imi)

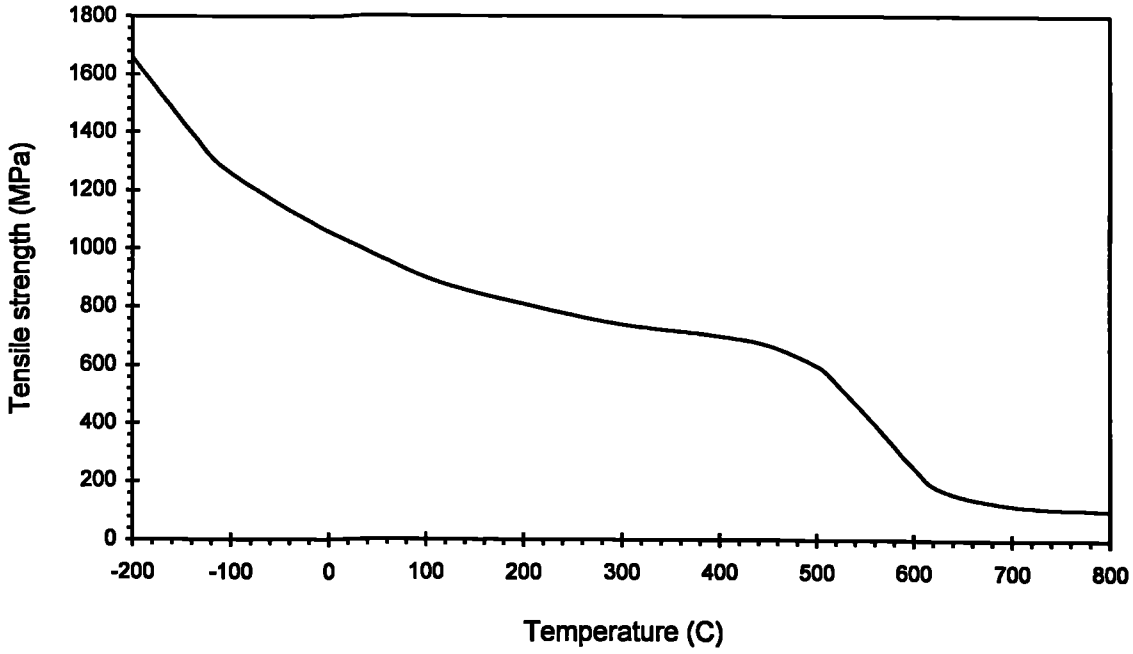

Figure 27 . Effect Of Temperature On Tensile Strength Of Ti 6Al 4V For Static Conditions (Imi)

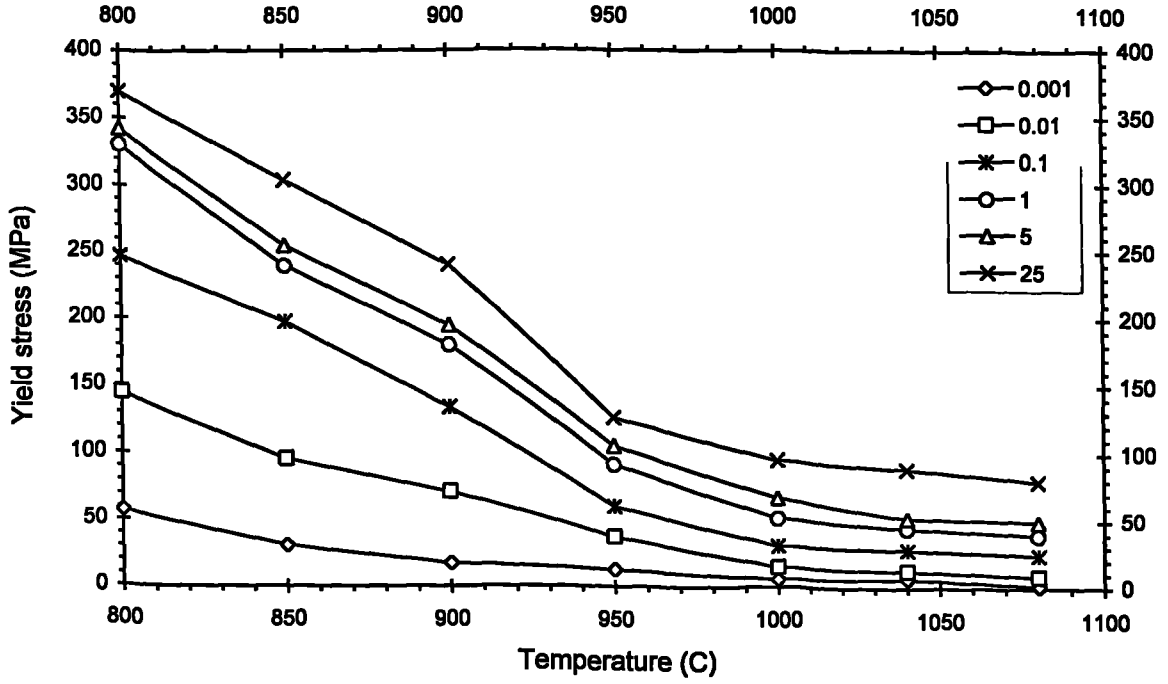

Figure 28 . Effect Of Temperature On Yield Stress Of Ti 6Al 4V For Different Strain Rates (Chaudhury,1992)

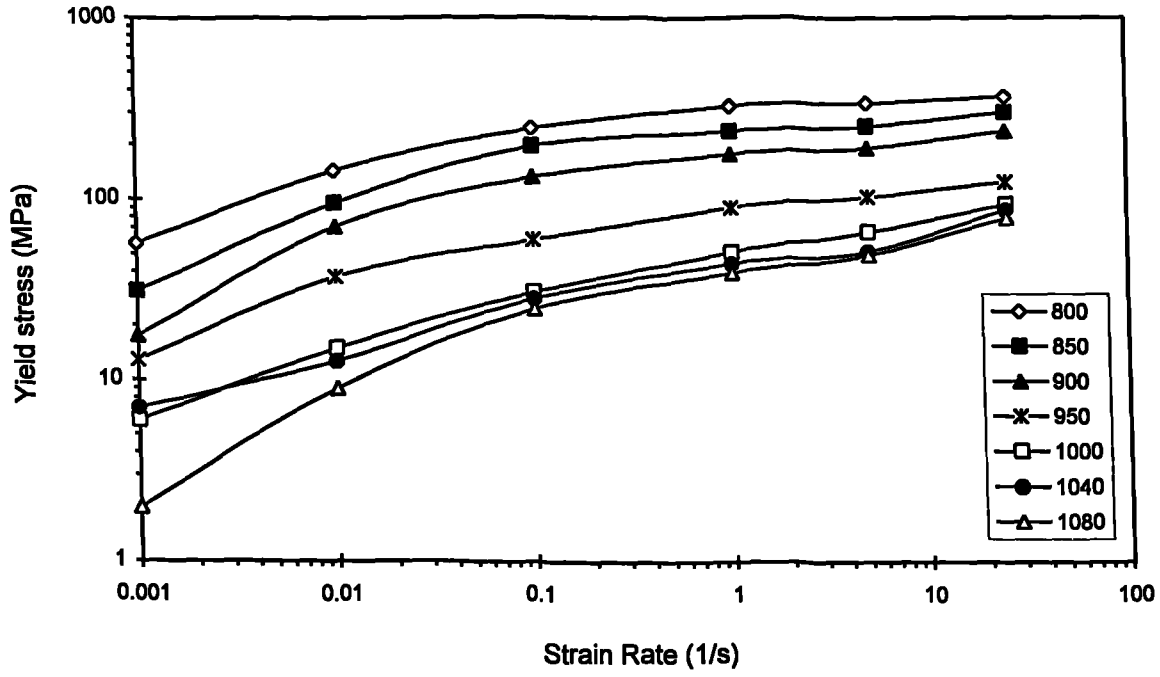

Figure 29 . Effect Of Strain Rate On Yield Stress Of Ti 6Al 4V For Different Temperatures (Chaudhury,1992)

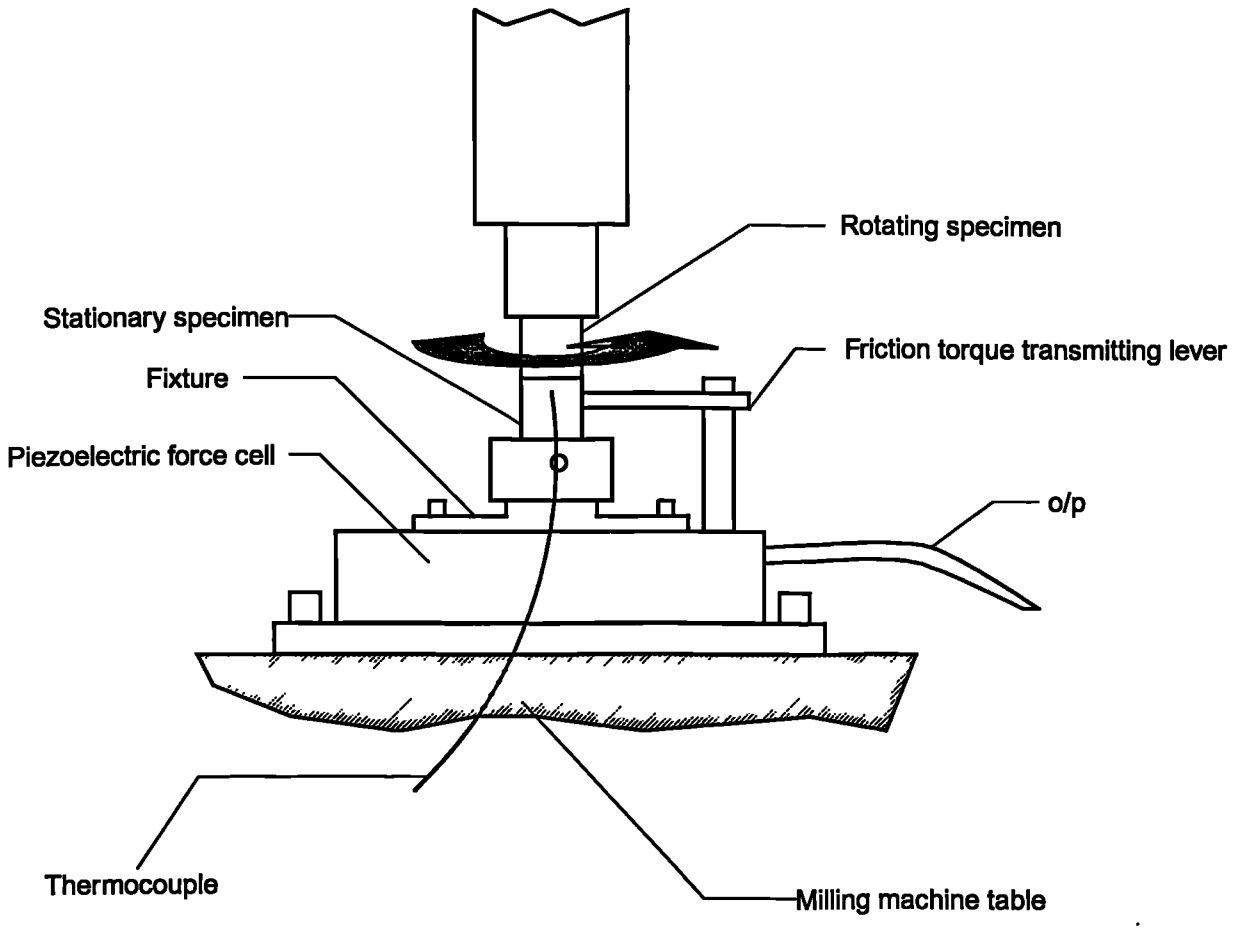

Figure 30 . Frictional Behaviour Experimental Arrangement

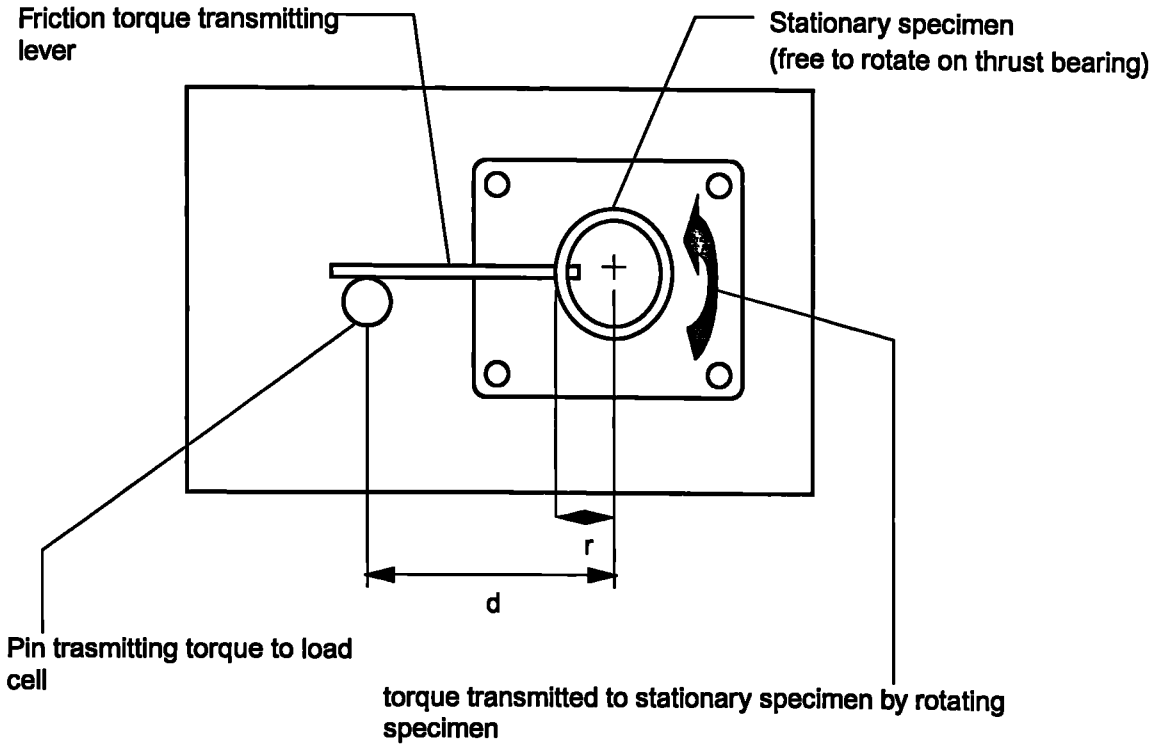

Figure 31 . Schematic View Of Friction Torque Measurements

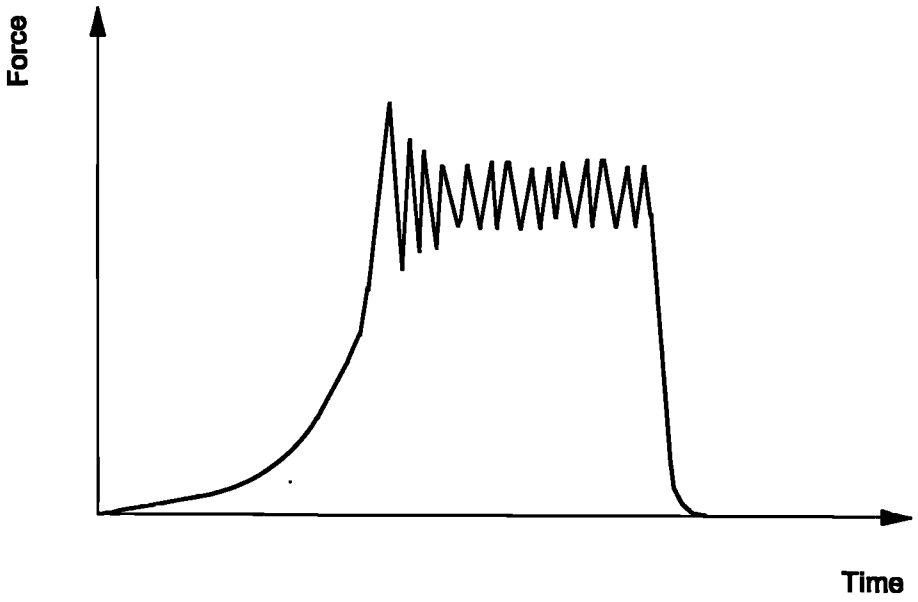

Figure 32 . Typical Force Trace

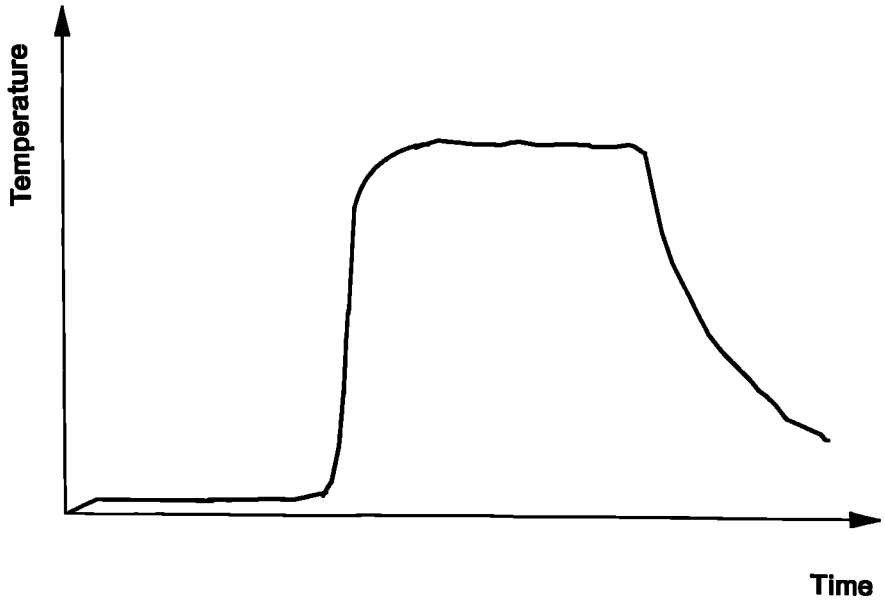

Figure 33 . Typical Temperature History

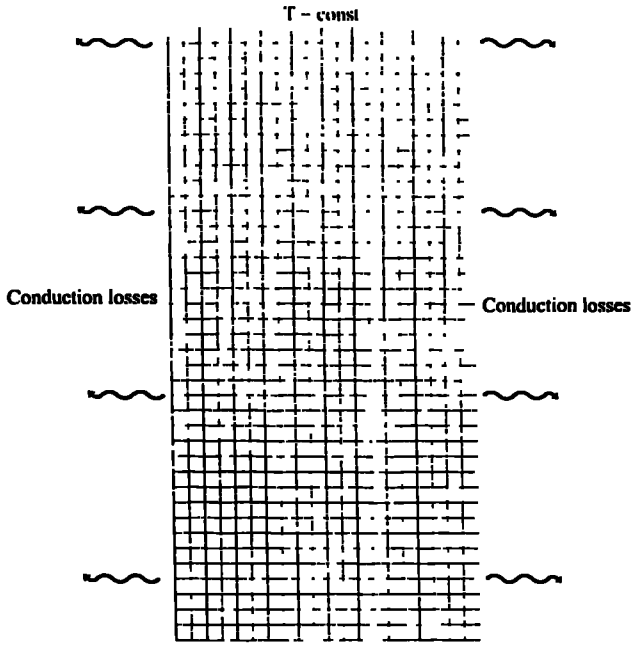

Figure 34 . Finite Element Mesh

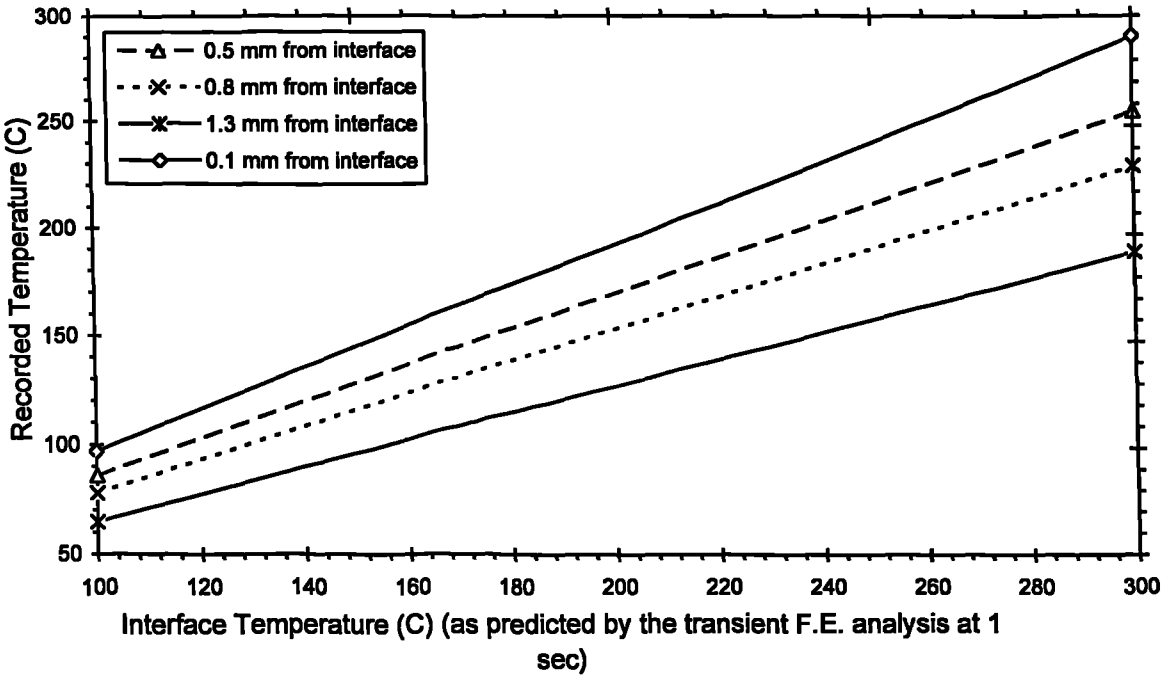

Figure 35 . Association Of Recorded Temperature To Interface Temperature For Different Thermocouple Distances From The Rubbing Interface

Key to Figure 36 to Figure 59 :

A: Least squares line fitted to experimental data

B : Range in which points can be expected to be found due to manual application of normal force. Force is considered to fluctuate at ± 15%.

C : Line B including standard error (S.E.) (for clarity the +15%-S.E. and the -15%+S.E. have not been included)

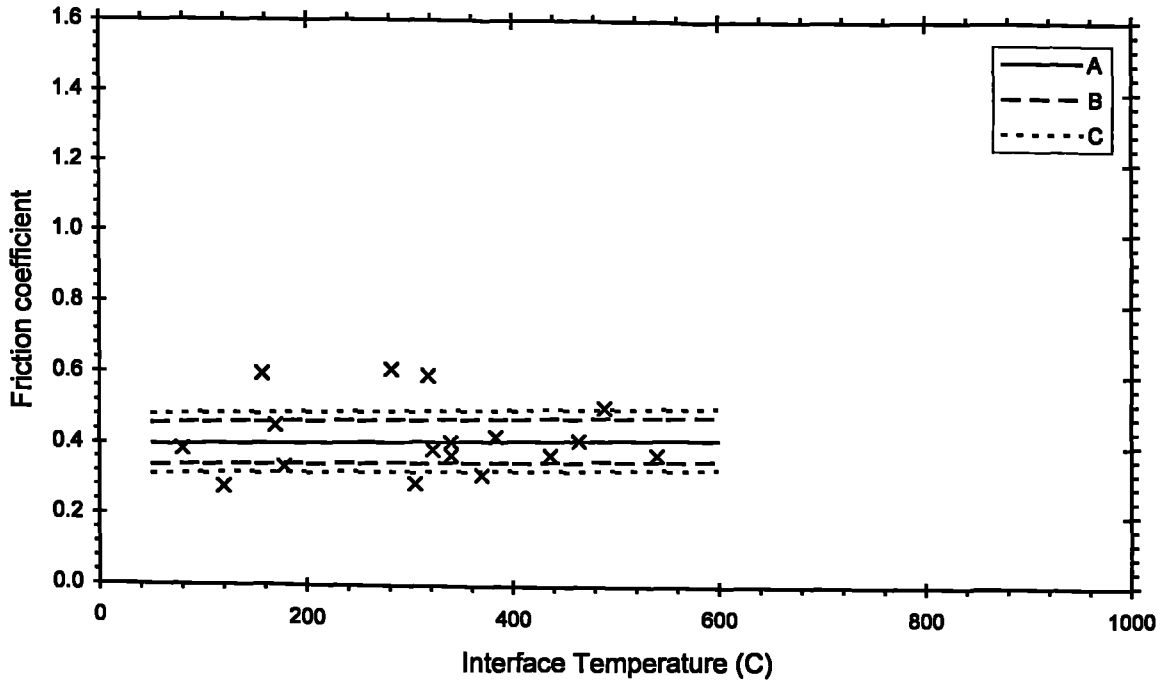

Figure 36 . Change Of The Coeff. Of Friction With Temperature (Ti 6Al 4V 178 mm/s Rubbing Velocity)

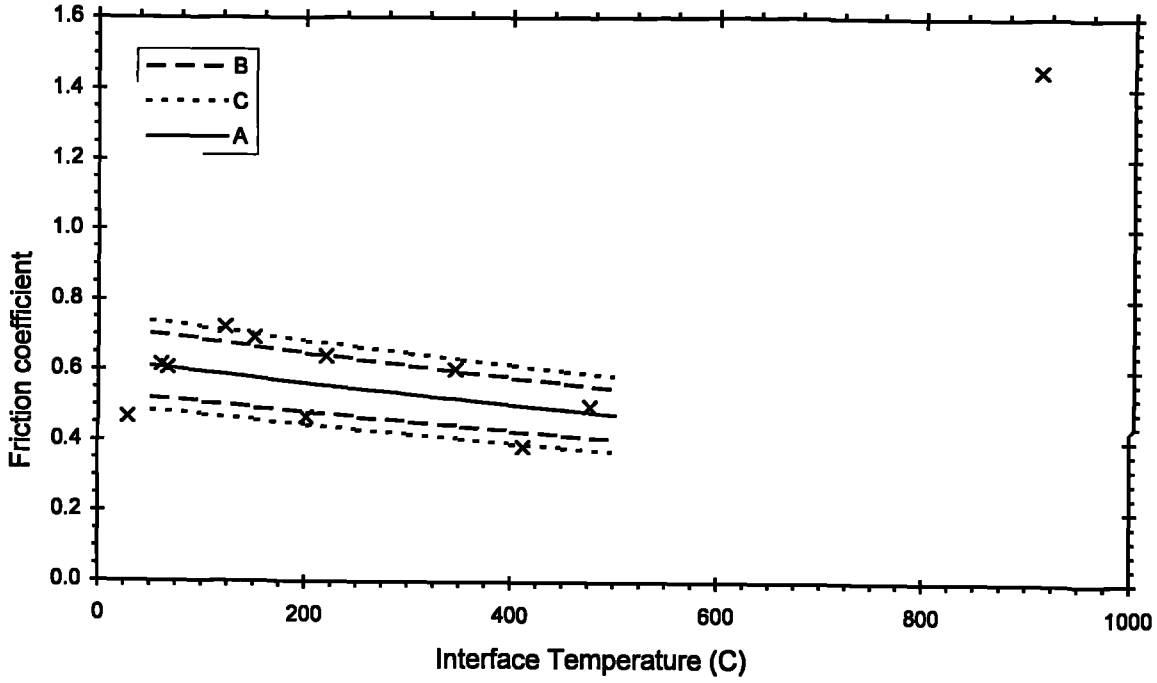

Figure 37 . Change Of The Coeff. Of Friction With Temperature (Ti 6Al 4V 480 mm/s Rubbing Velocity)

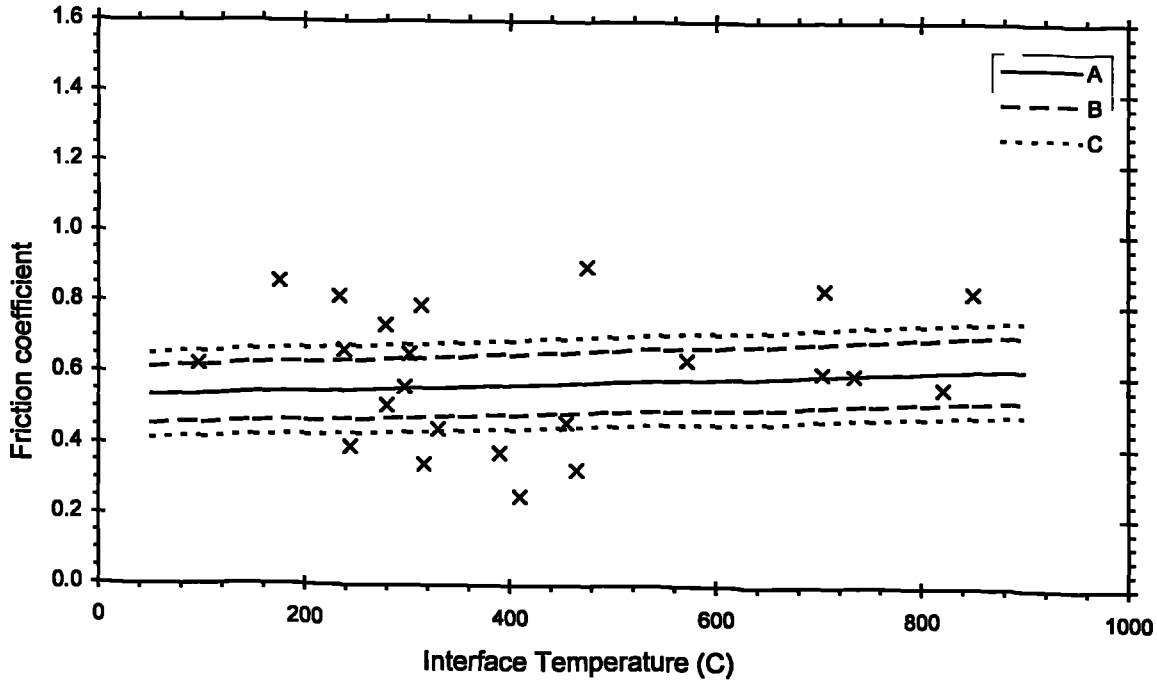

Figure 38 . Change Of The Coeff. Of Friction With Temperature (Ti 6Al 4V 700 mm/s Rubbing Velocity)

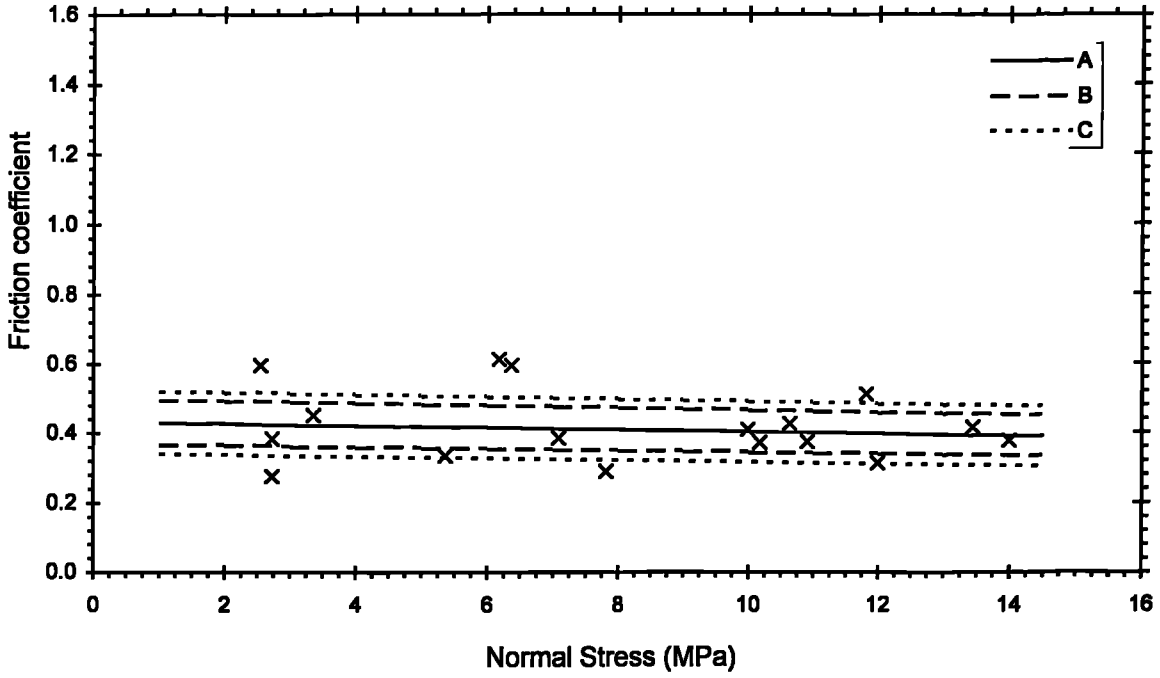

Figure 39 . Change Of The Coeff. Of Friction With Normal Stress (Ti 6Al 4V - 178 mm/s Rubbing Velocity)

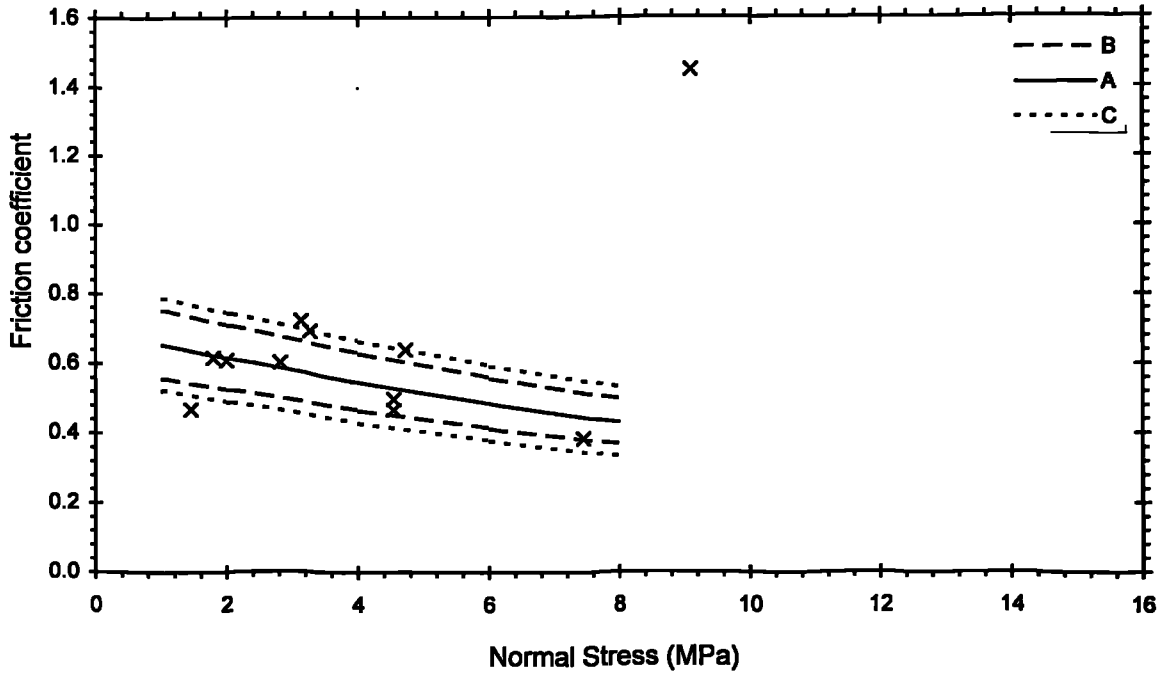

Figure 40 . Change Of The Coeff. Of Friction With Normal Stress (Ti 6Al 4V - 480 mm/s Rubbing Velocity)

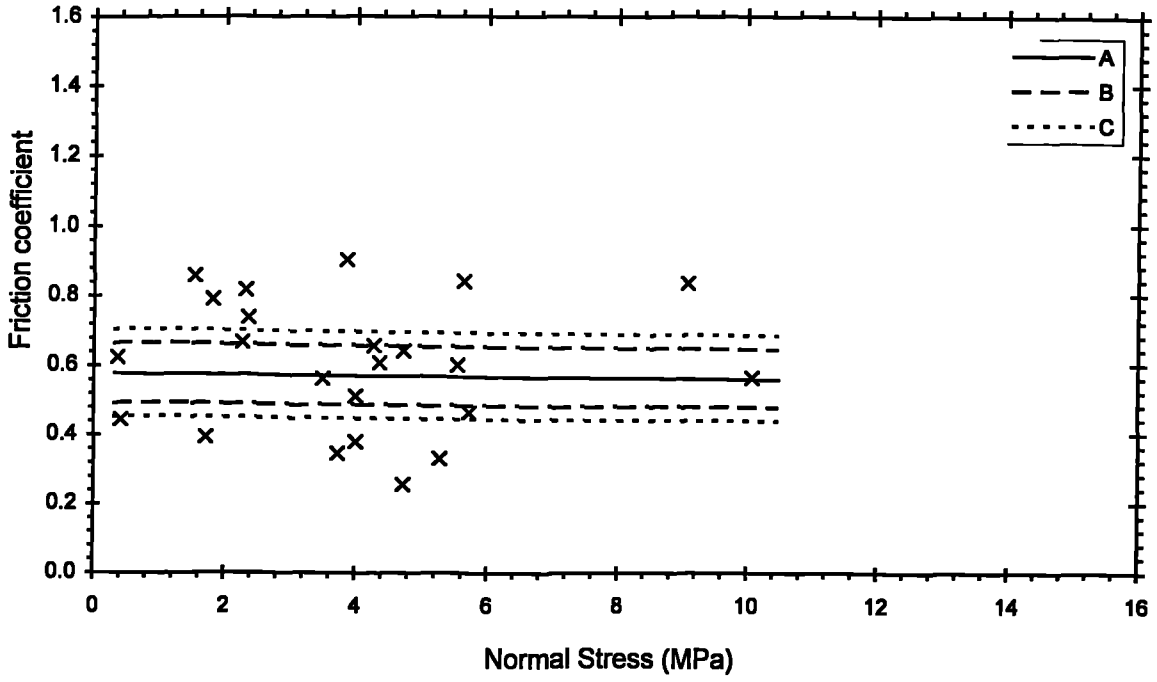

Figure 41 . Change Of The Coeff. Of Friction With Normal Stress (Ti 6Al 4V - 700 mm/s Rubbing Velocity)

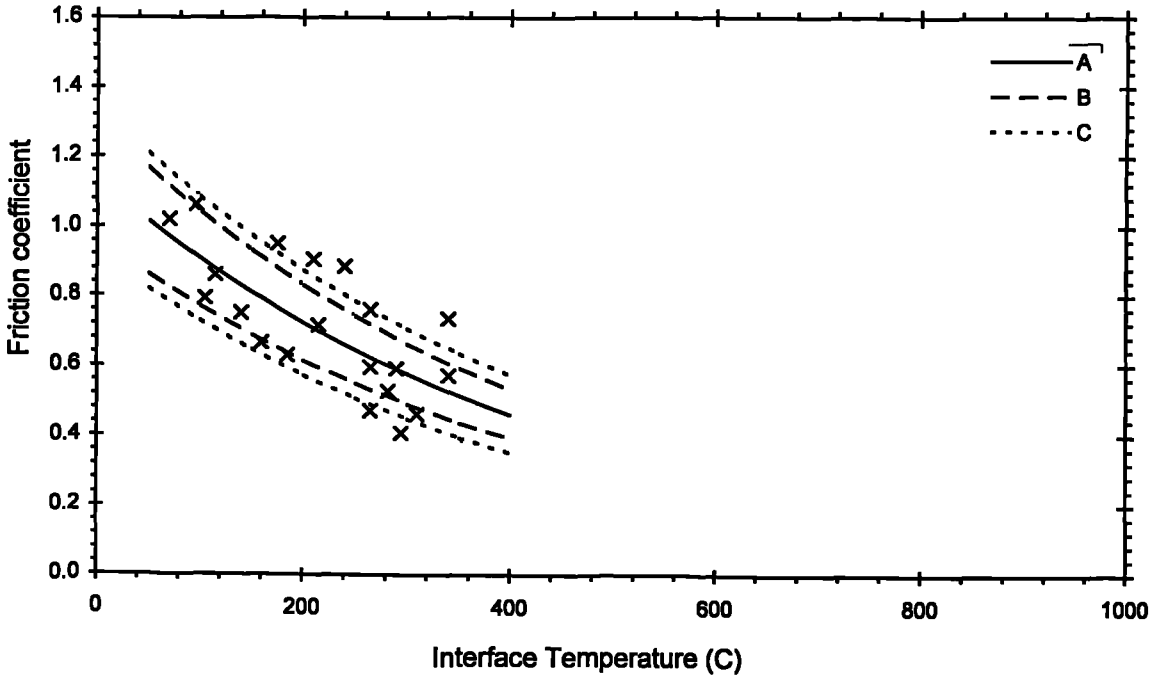

Figure 42 . Change Of The Coeff. Of Friction With Temperature (En 58 Stainless Steel - 178 mm/s Rubbing Velocity)

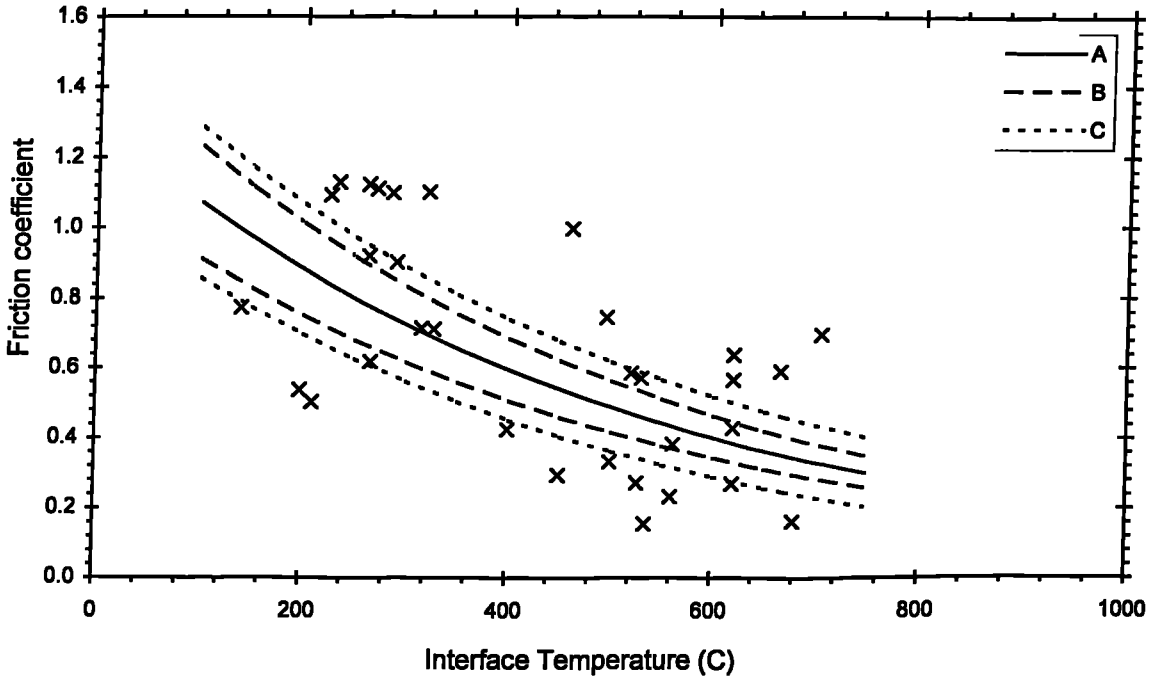

Figure 43 . Change Of The Coeff. Of Friction With Temperature (En 58 Stainless Steel - 480 mm/s Rubbing Velocity)

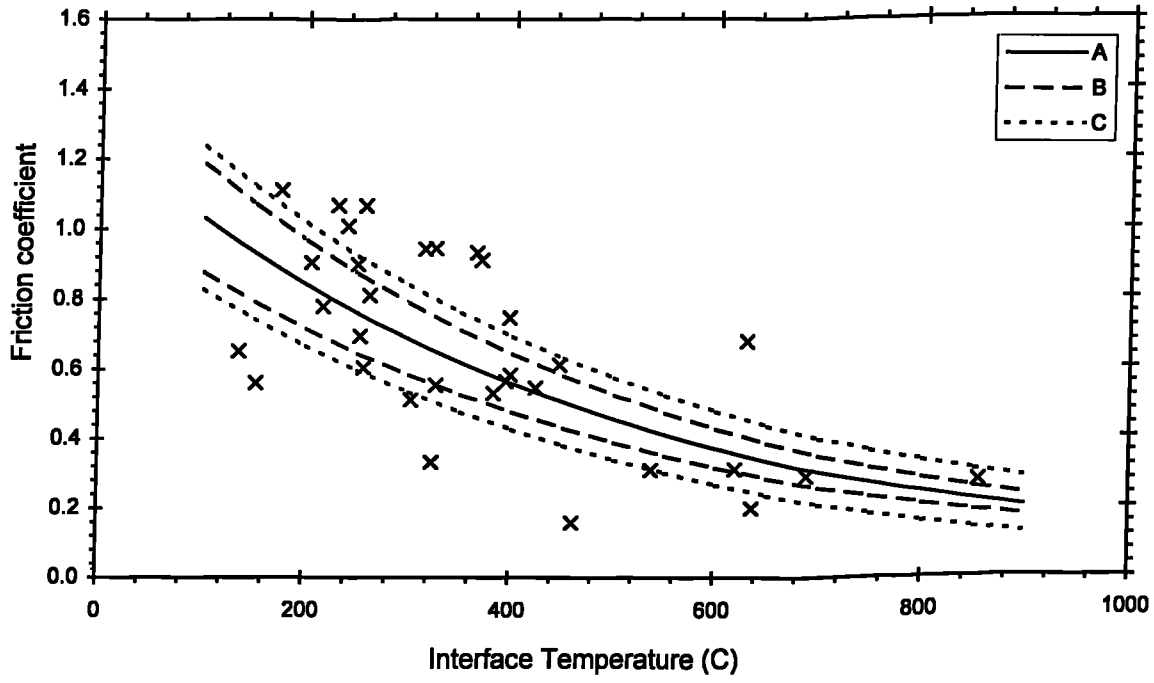

Figure 44 . Change Of The Coeff. Of Friction With Temperature (En 58 Stainless Steel - 700 mm/s Rubbing Velocity)

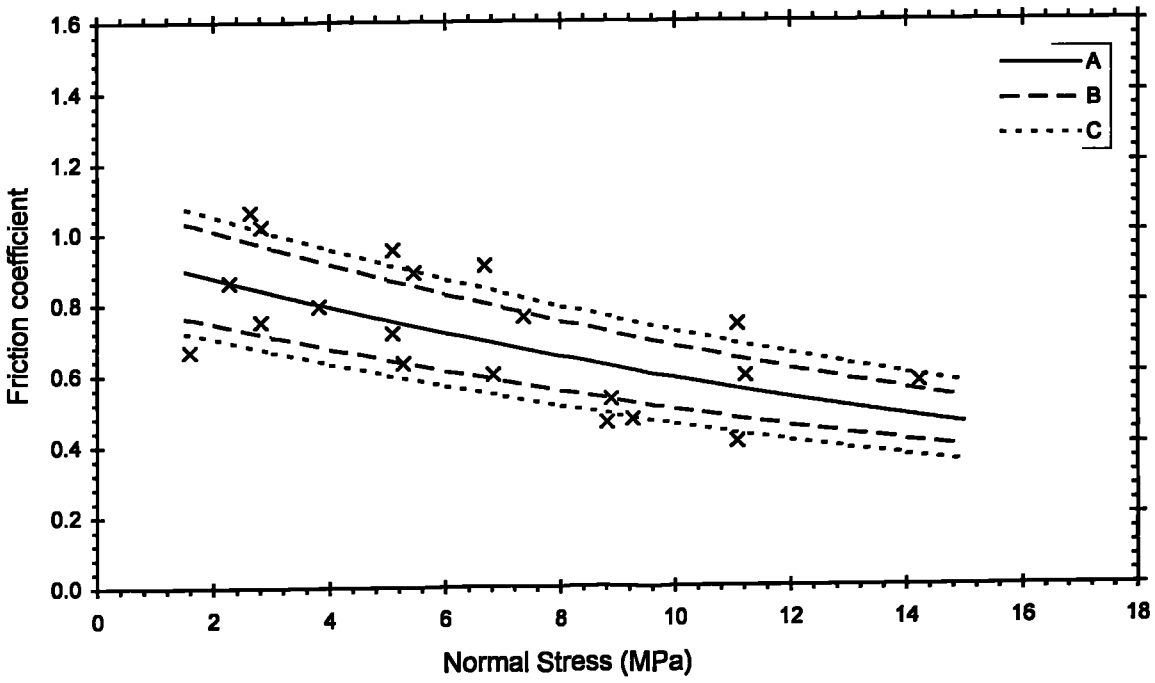

Figure 45 . Change Of The Coeff. Of Friction With Normal Stress (En 58 Stainless Steel - 178 mm/s Rubbing Velocity)

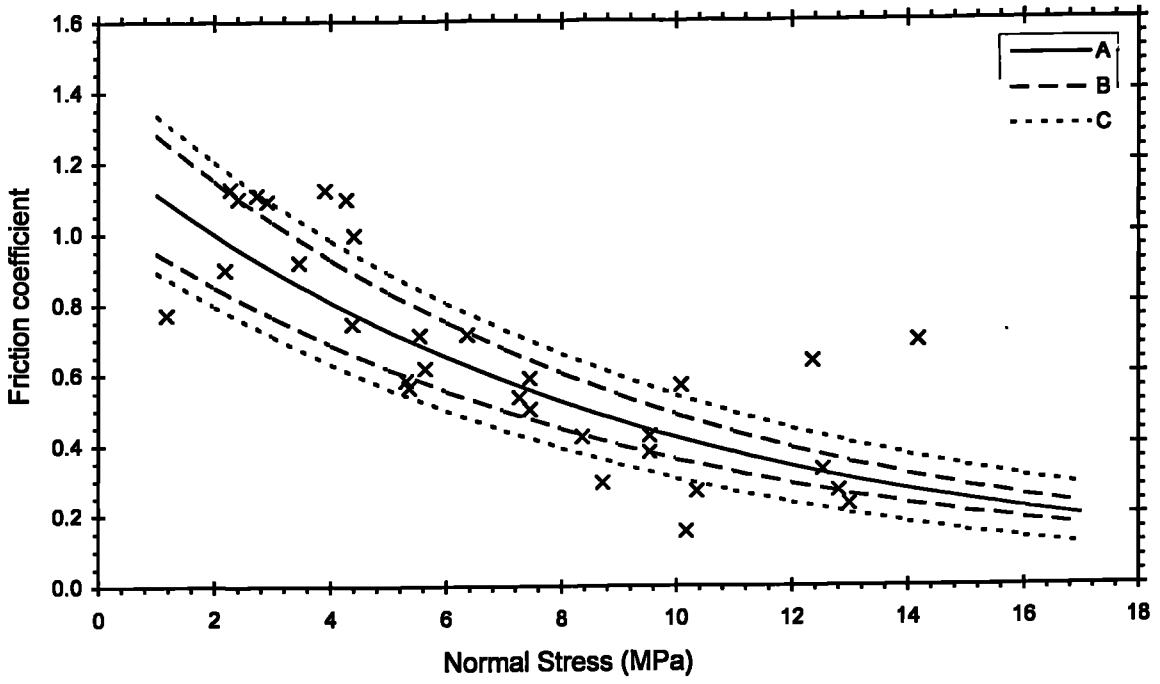

Figure 46 . Change Of The Coeff. Of Friction With Normal Stress (En 58 Stainless Steel - 480 mm/s Rubbing Velocity)

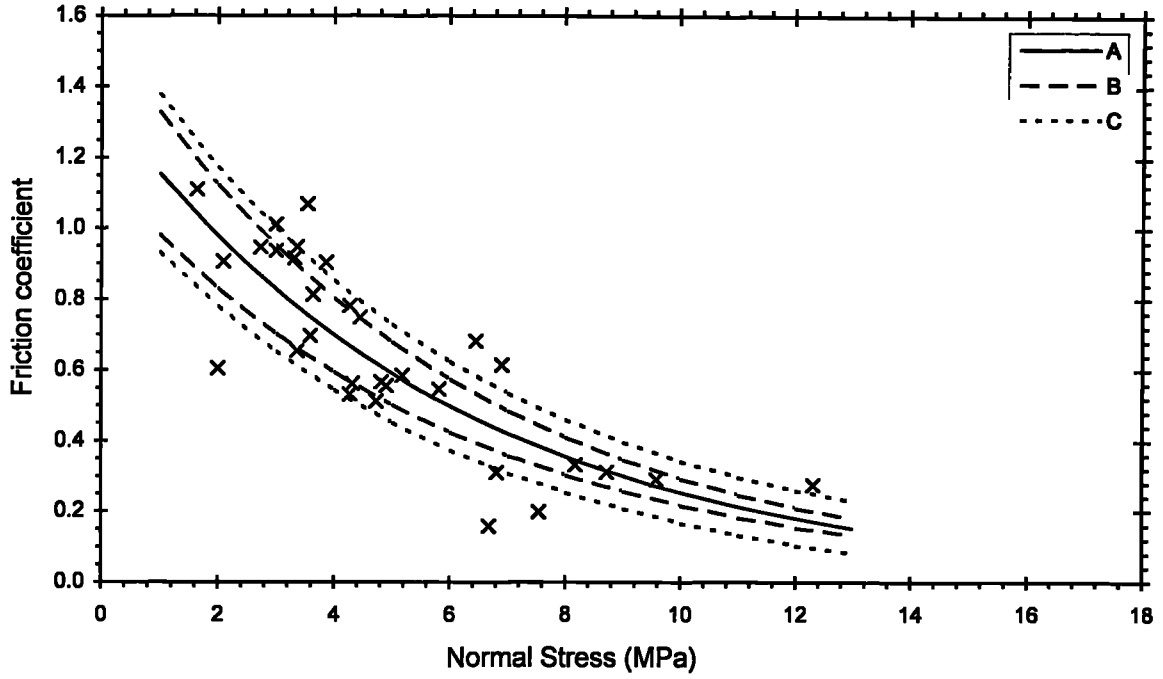

Figure 47 . Change Of The Coeff. Of Friction With Normal Stress (En 58 Stainless Steel - 700 mm/s Rubbing Velocity)

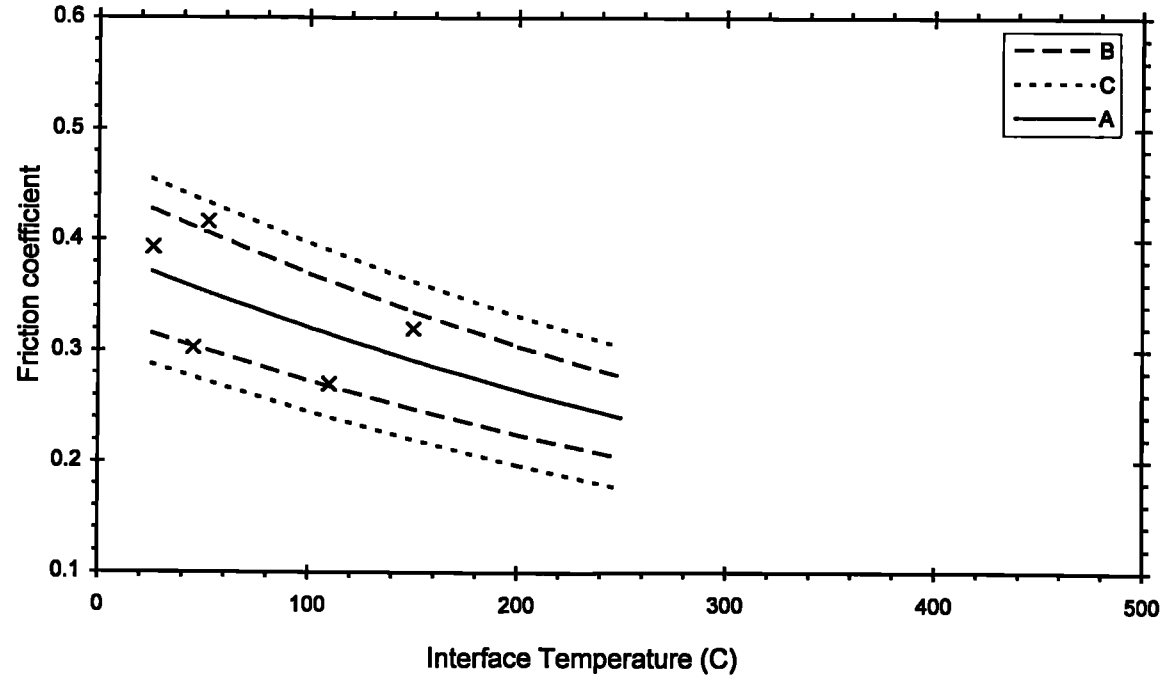

Figure 48 . Change Of The Coeff. Of Friction With Temperature (En 3 Mild Steel - 178 mm/s Rubbing Velocity)

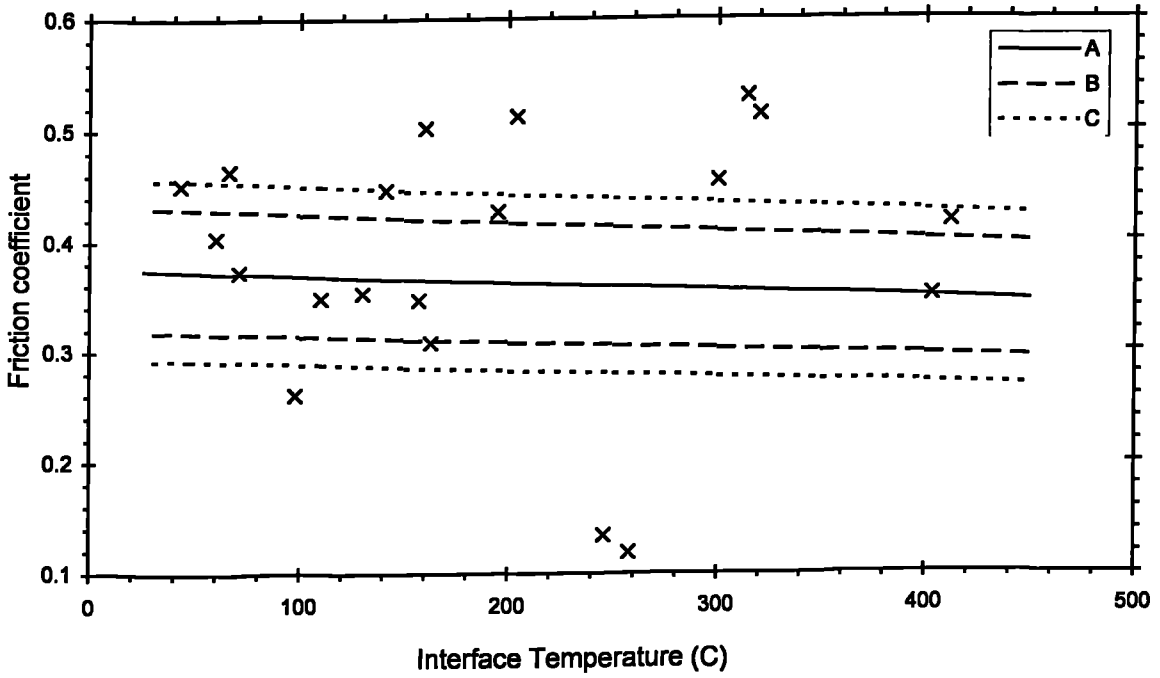

Figure 49 . Change Of The Coeff. Of Friction With Temperature (En 3 Mild Steel - 480 mm/s Rubbing Velocity)

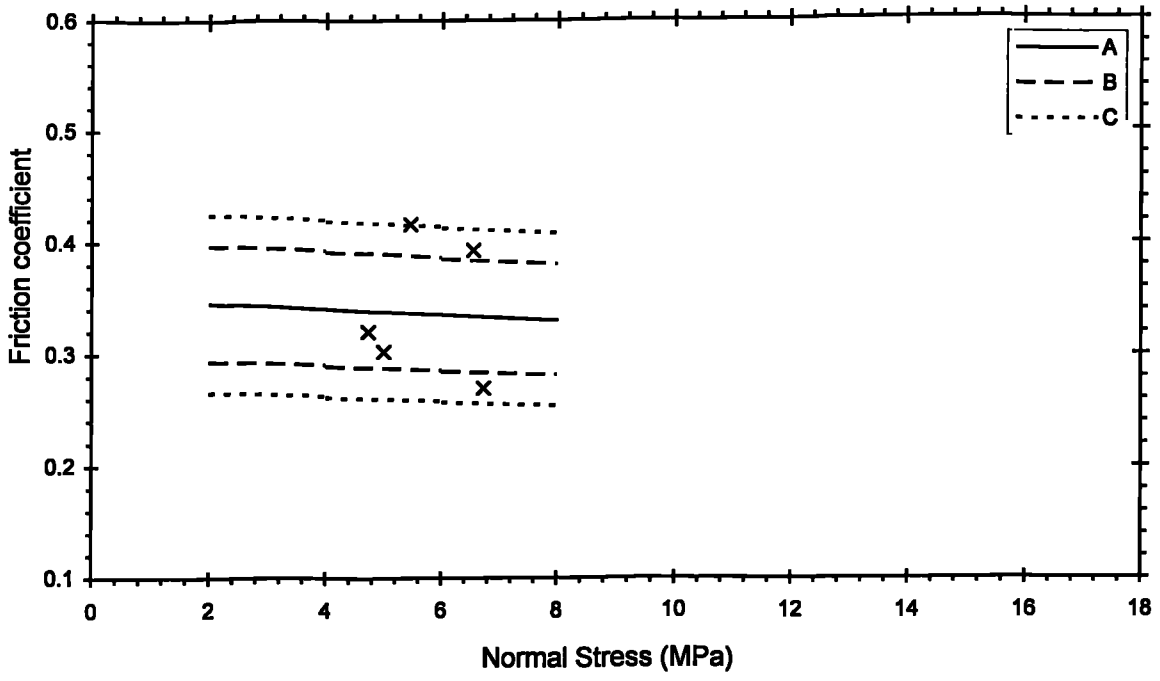

Figure 50 . Change Of The Coeff. Of Friction With Normal Stress (En 3 Mild Steel - 178 mm/s Rubbing Velocity)

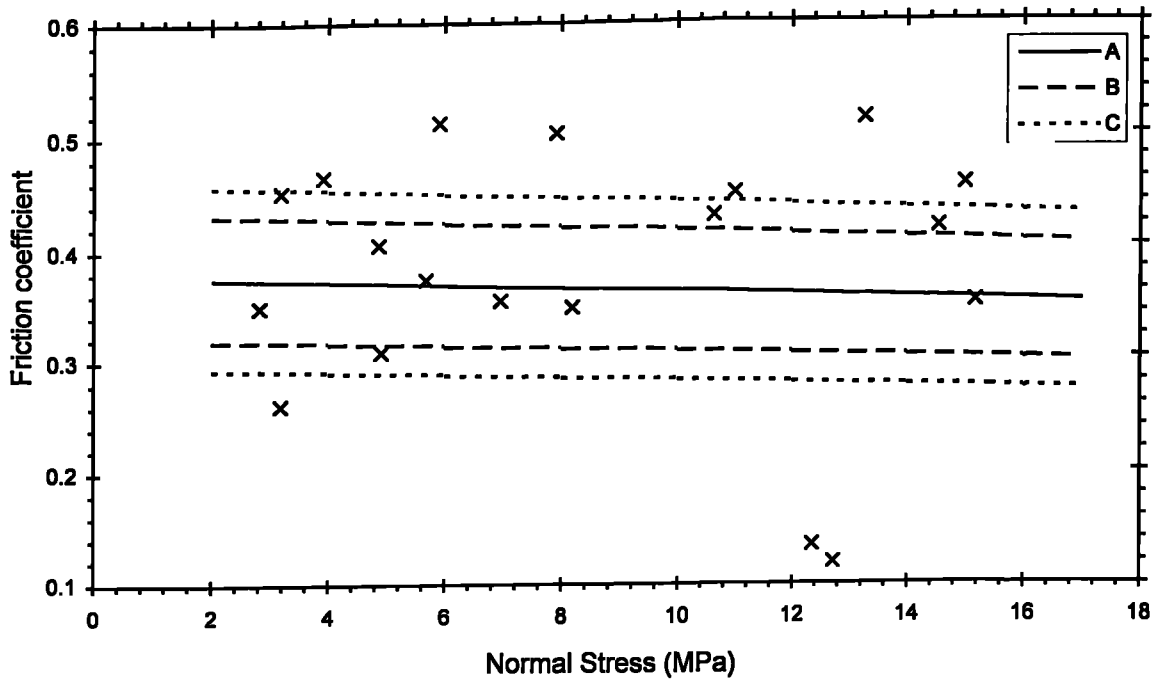

Figure 51 . Change Of The Coeff. Of Friction With Normal Stress (En 3 Mild Steel - 480 mm/s Rubbing Velocity)

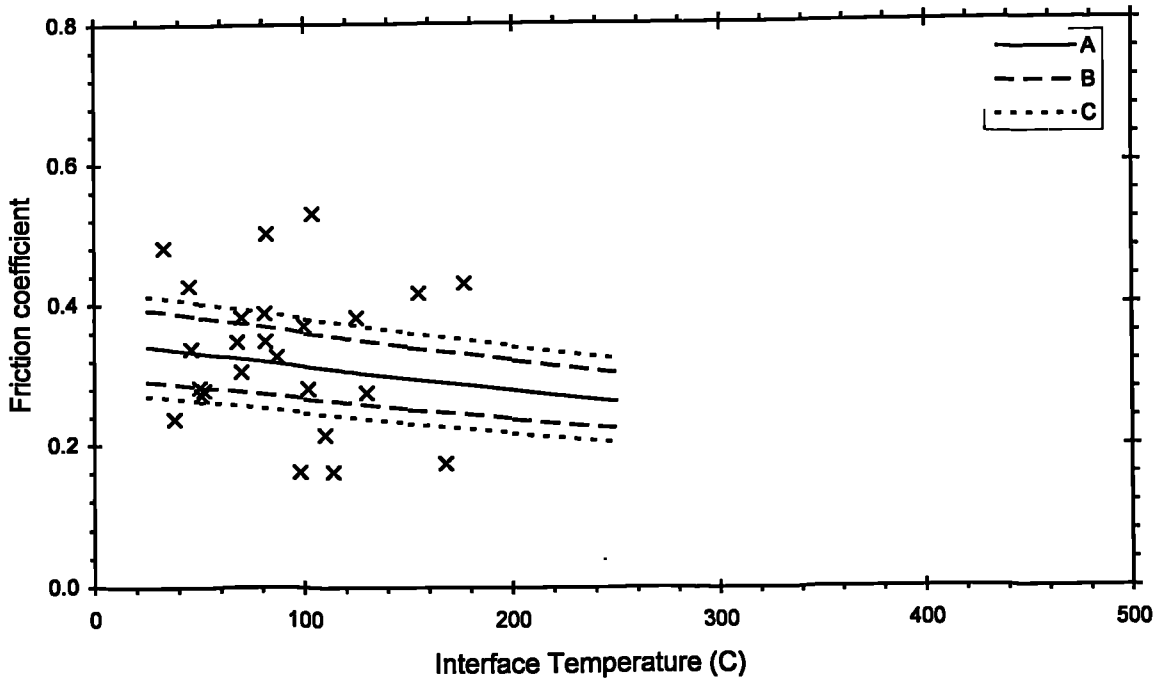

Figure 52 . Change Of The Coeff. Of Friction With Temperature (En 31 - 178 mm/s Rubbing Velocity)

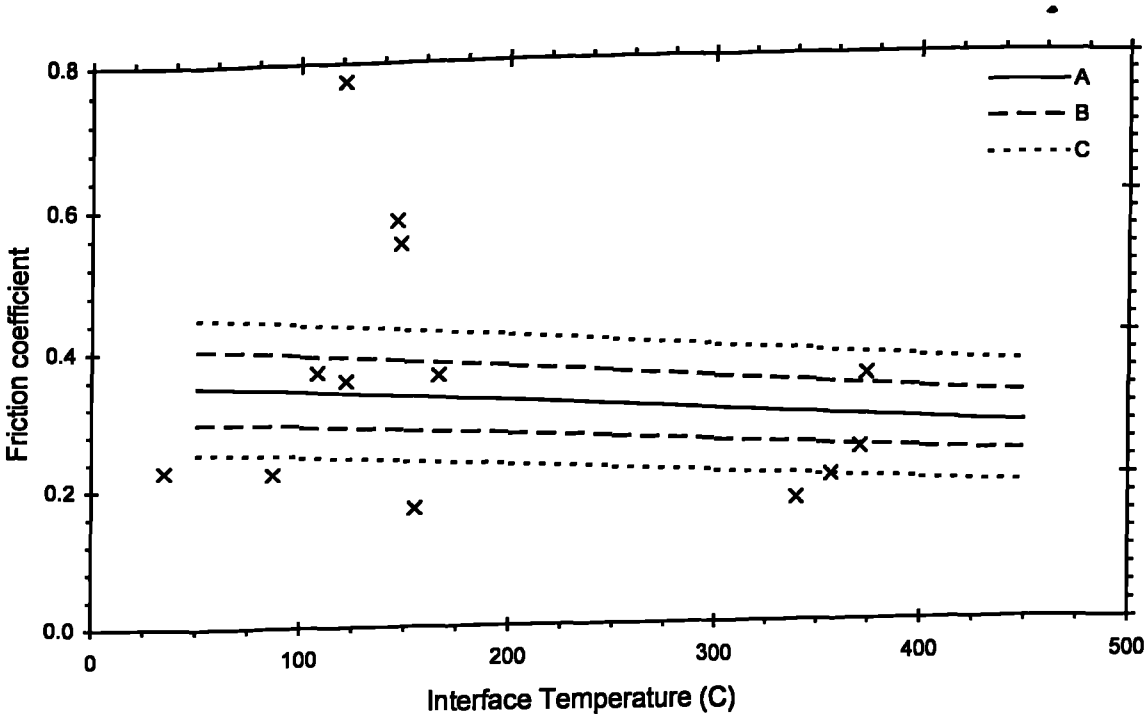

Figure 53 . Change Of The Coeff. Of Friction With Temperature (En 31 - 480 mm/s Rubbing Velocity)

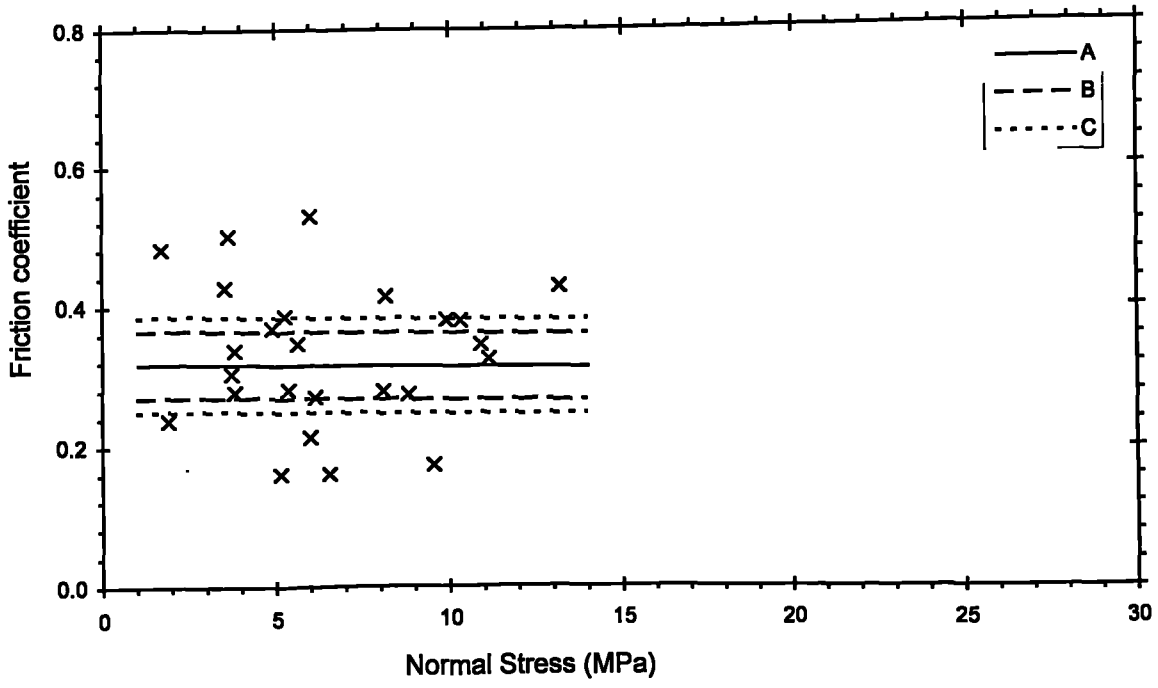

Figure 54 . Change Of The Coeff. Of Friction With Normal Stress (En 31 - 178 mm/s Rubbing Velocity)

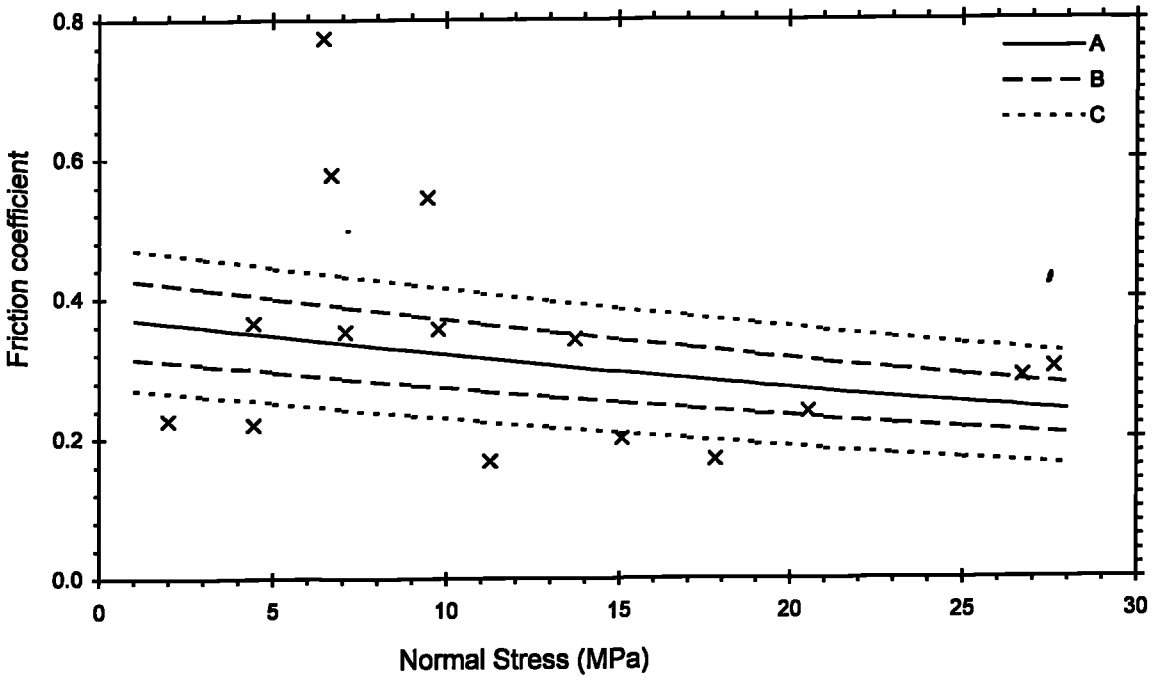

Figure 55 . Change Of The Coeff. Of Friction With Normal Stress (En 31 - 480 mm/s Rubbing Velocity)

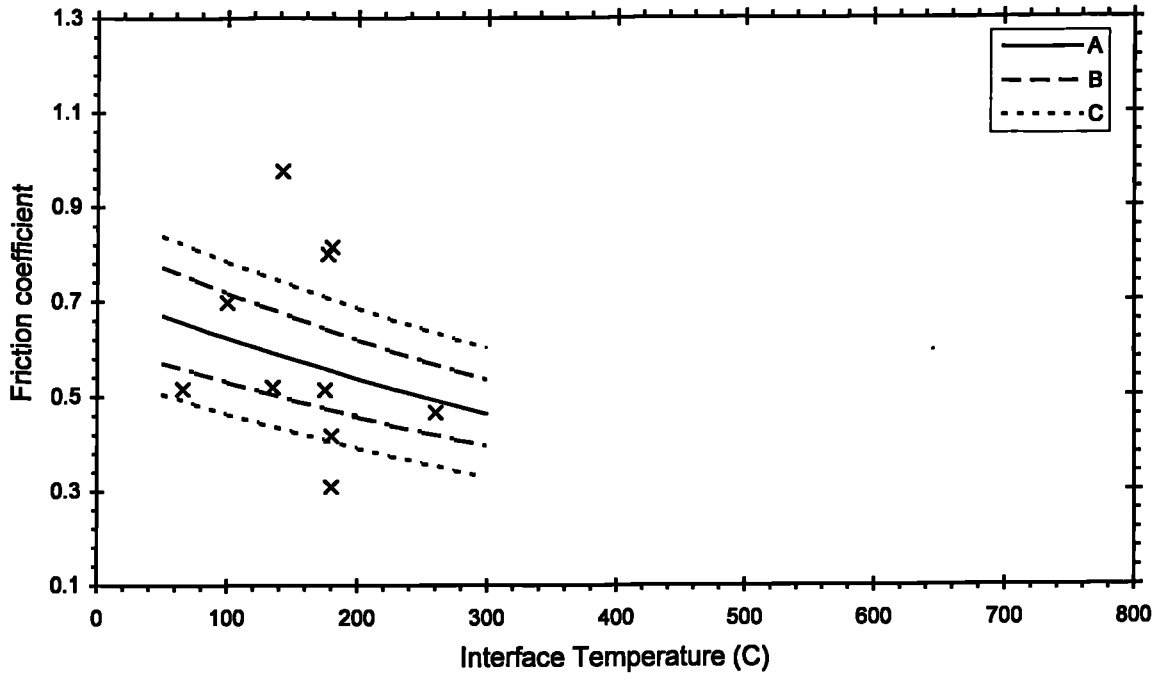

Figure 56 . Change Of The Coeff. Of Friction With Temperature (Ti 6Al 4V /En 58 - 178 mm/s Rubbing Velocity)

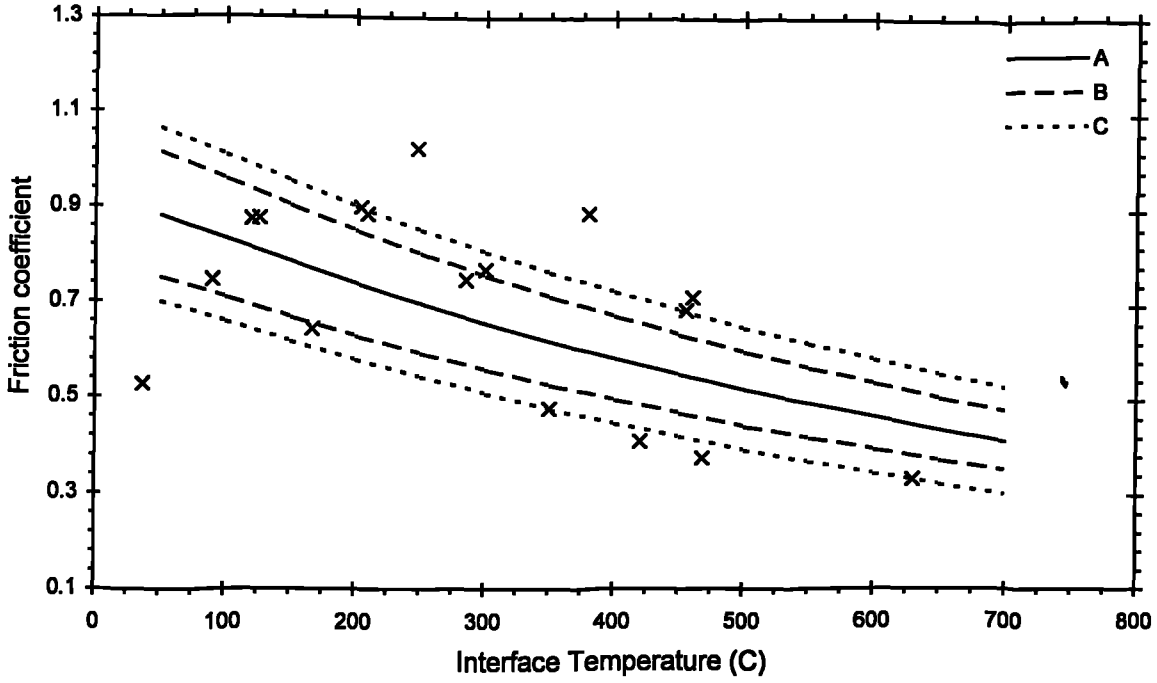

Figure 57 . Change Of The Coeff. Of Friction With Temperature (Ti 6Al 4V /En 58 - 480 mm/s Rubbing Velocity)

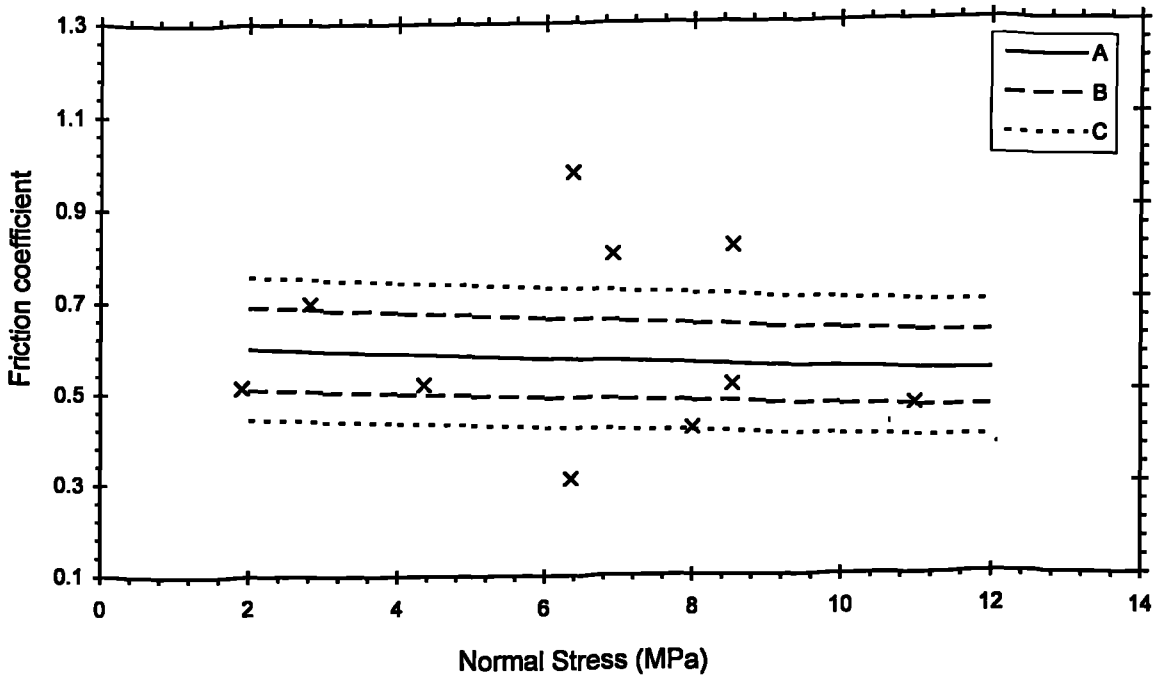

Figure 58 . Change Of The Coeff. Of Friction With Normal Stress (Ti 6Al 4V / En 58 - 178 mm/s Rubbing Velocity)

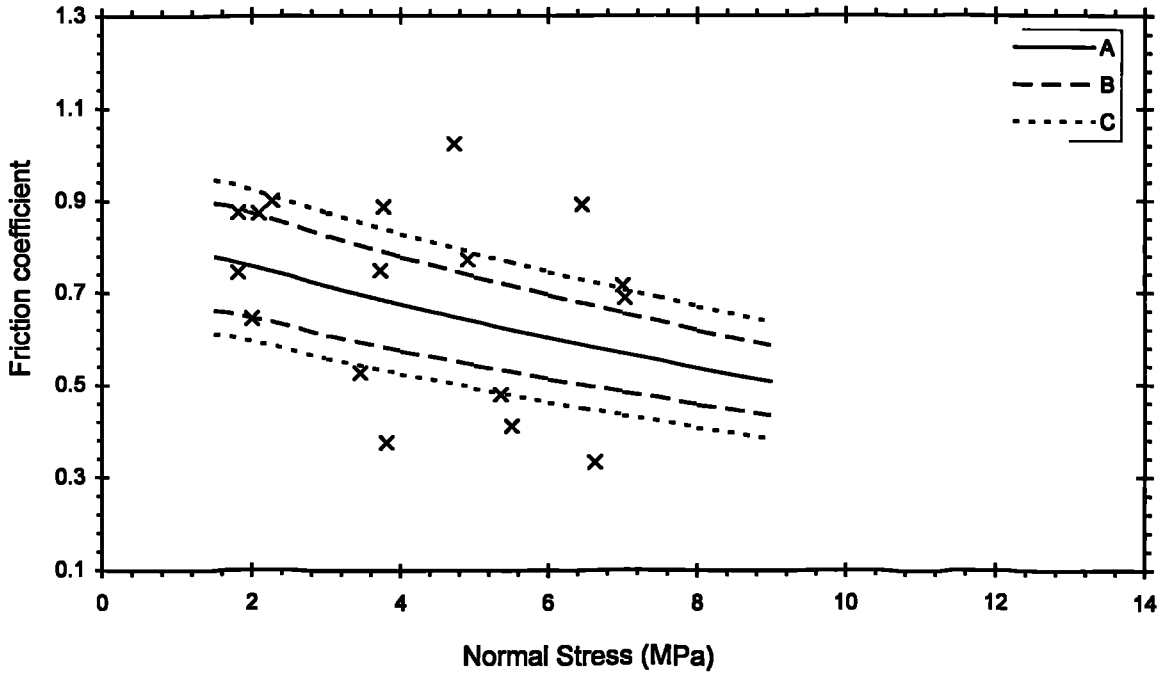

Figure 59 . Change Of The Coeff. Of Friction With Normal Stress (Ti 6Al 4V / En 58 - 480 mm/s Rubbing Velocity)

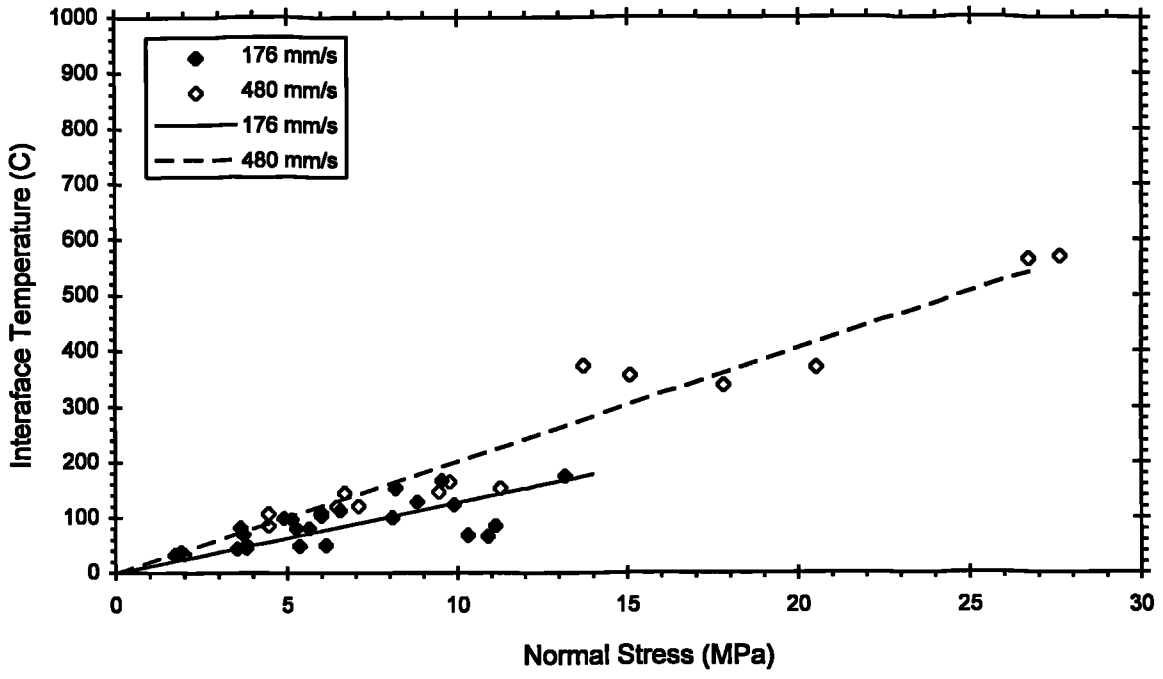

Figure 60 . Temperature At Interface Against Normal Stress For Different Velocities - EN 31

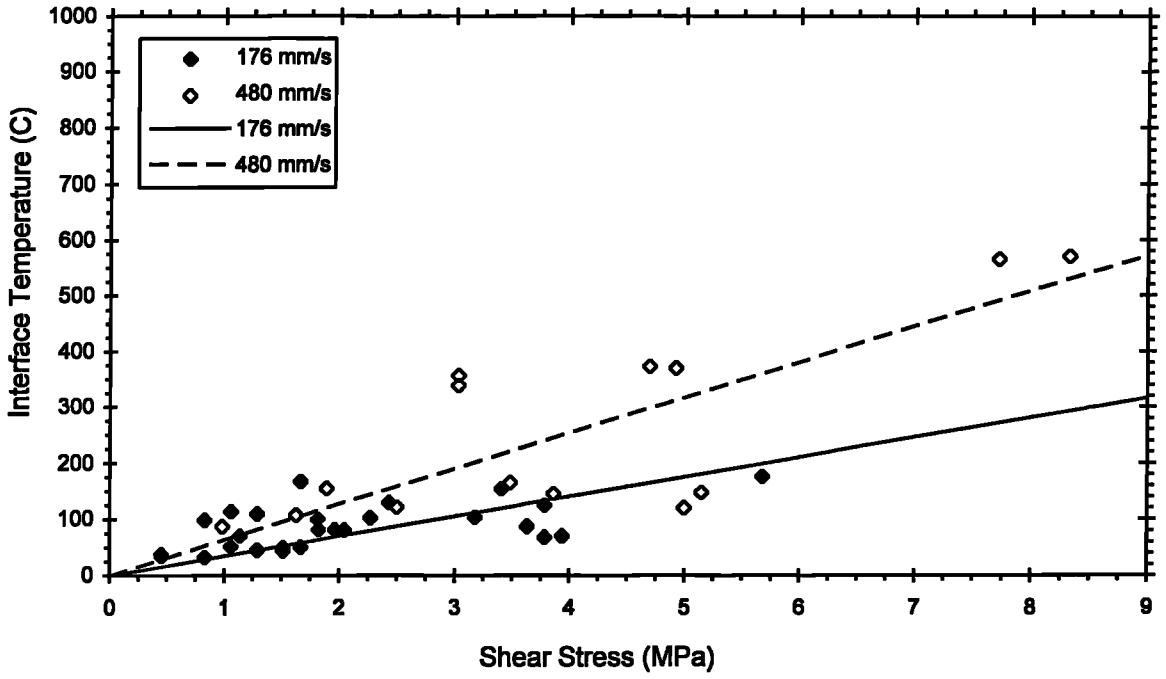

Figure 61 . Temperature At Interface Against Shear Stress For Different Velocities - EN 31

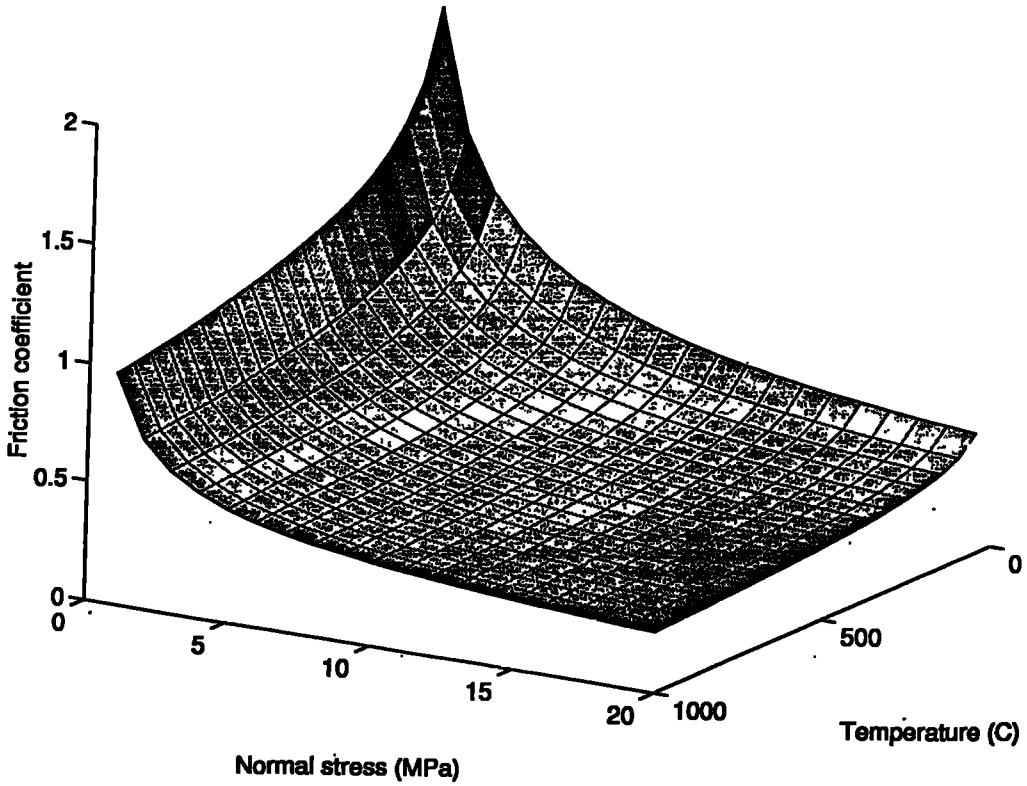

Figure 62 . Friction Coefficient Model (En 58 Stainless Steel) (μ=4.7661 x $\sigma^{-0.2995}$ x $T^{-0.4449}$)

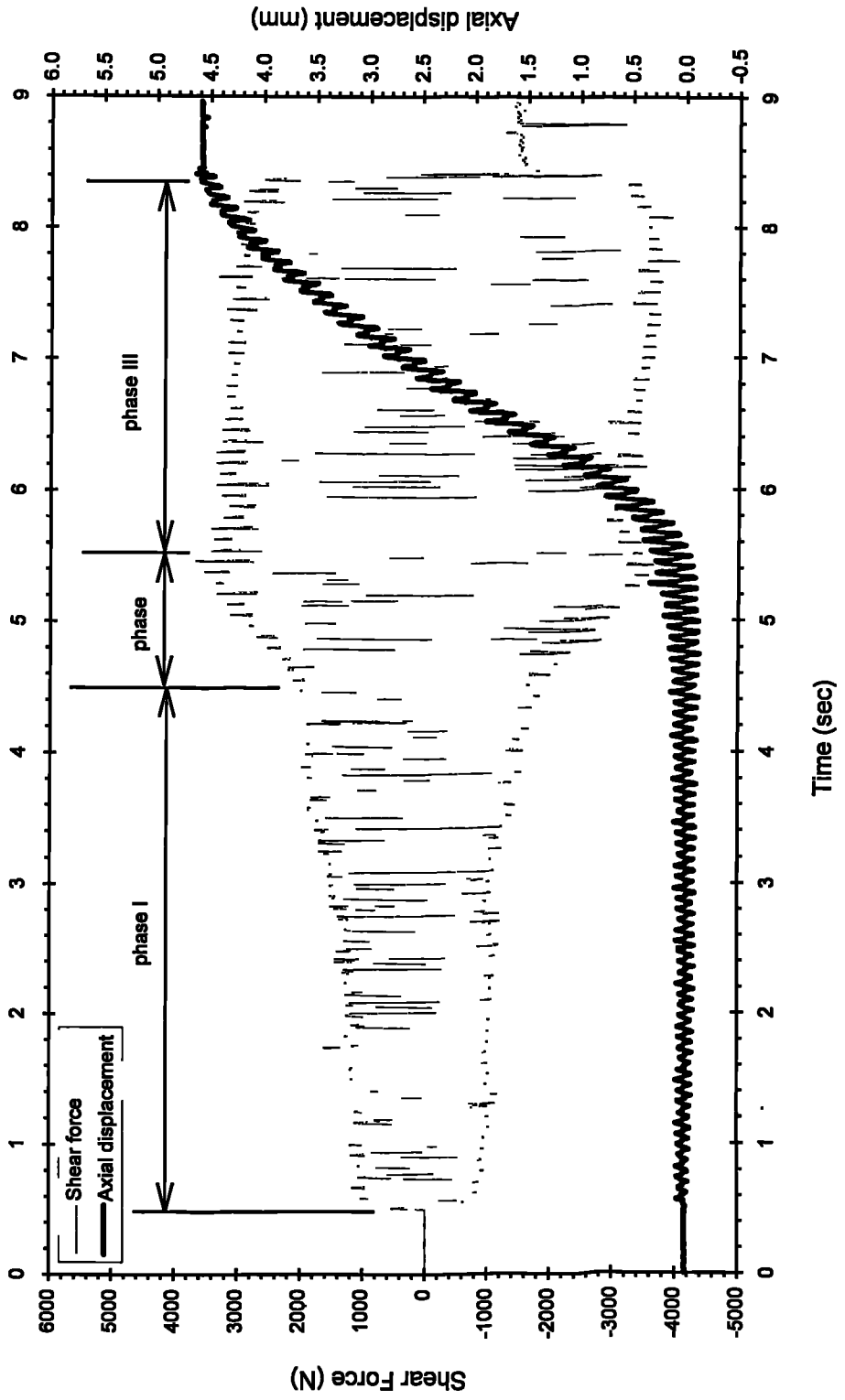

Figure 63 . Shear Force And Axial Displacement History

(Ti 6Al 4V - α : 3 mm , f : 12 Hz , P_{fr} : 42.9 MPa - experiment A7)

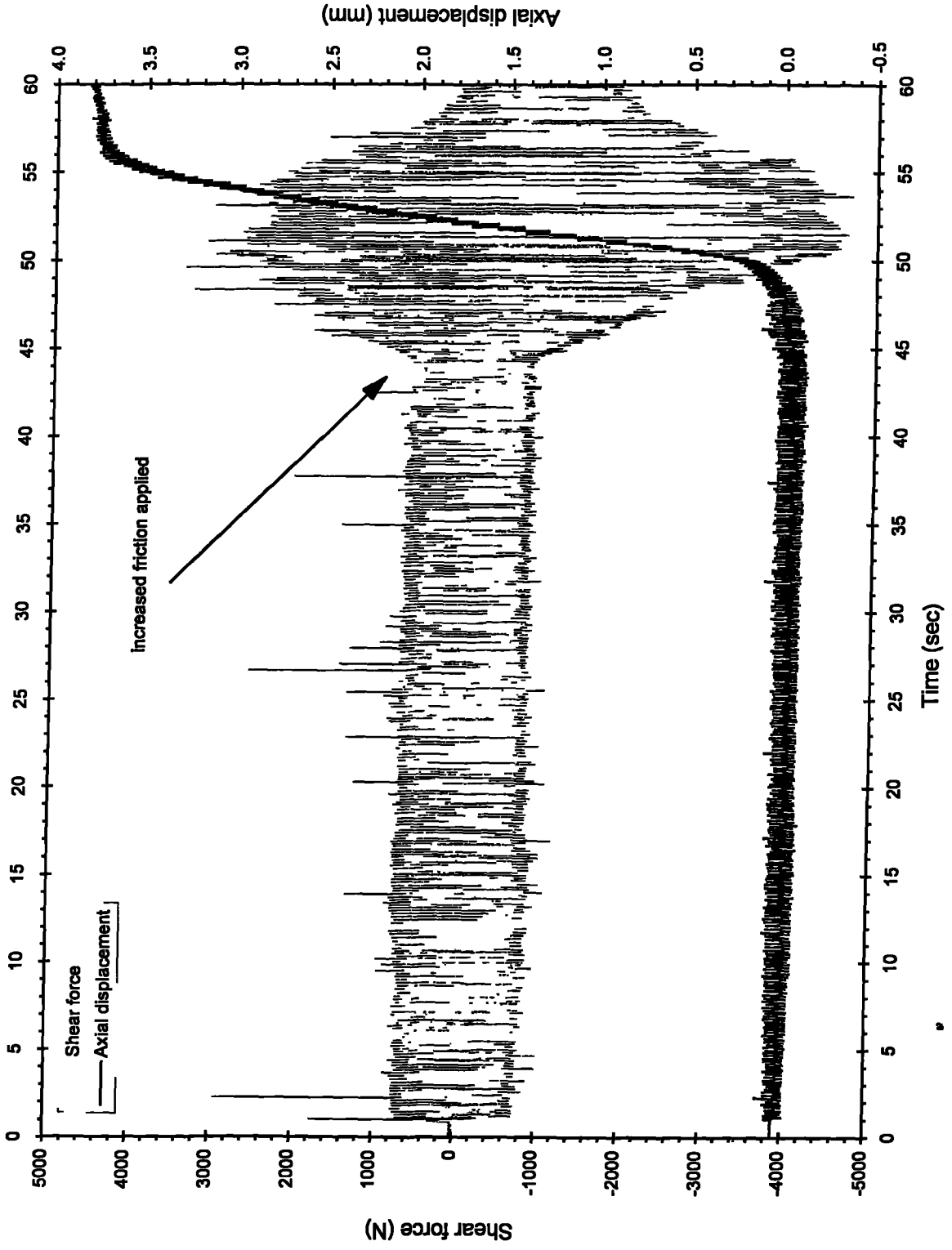

Figure 64 . Shear Force And Displacement History

(Ti 6Al 4V - α : 3 mm , f : 10 Hz , P_{fr} : 32.9 MPa - experiment B4)

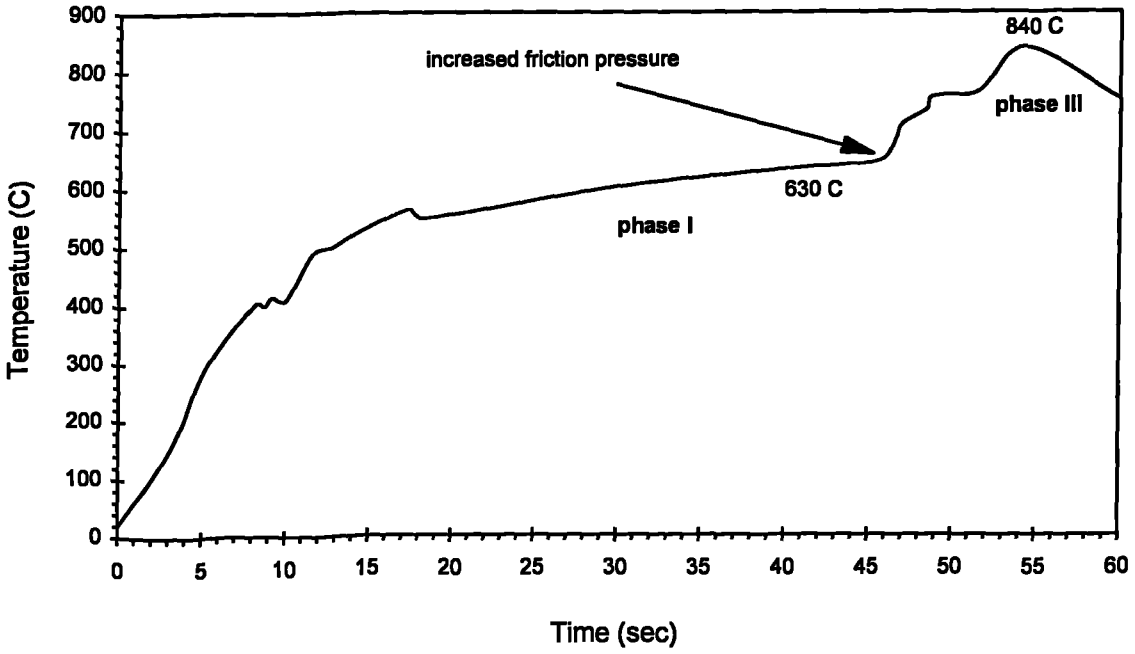

Figure 65 . Temperature Plot (experiment B4)

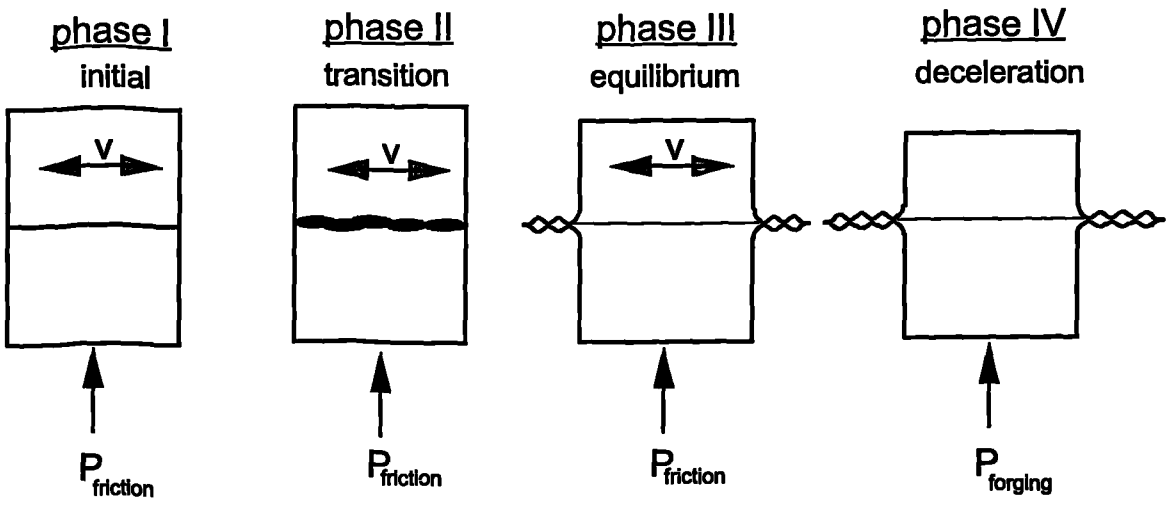

Figure 66 . Formation Of Flash During Process

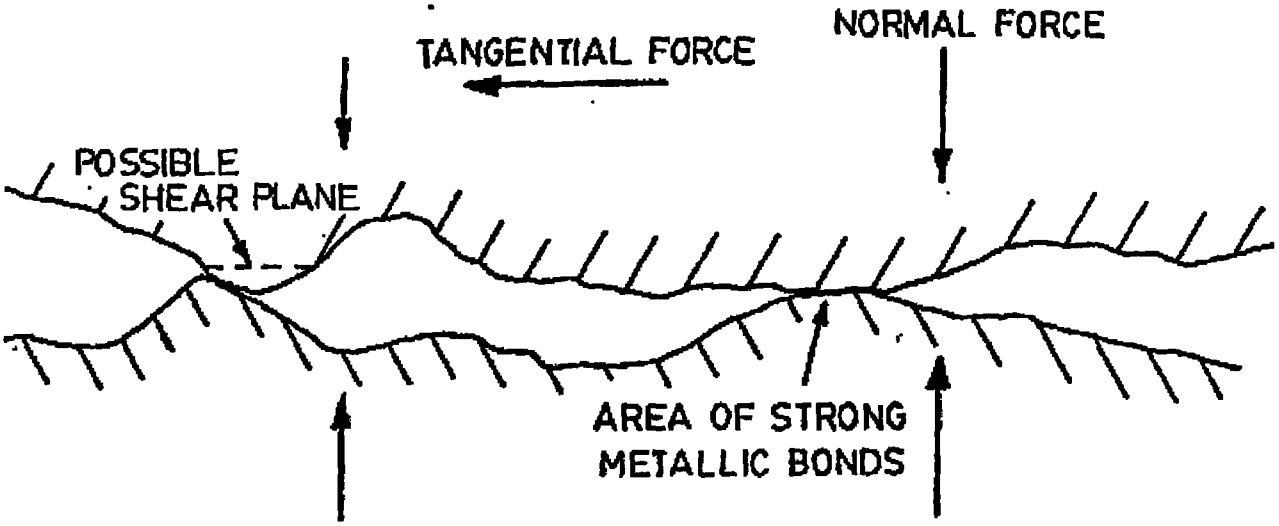

Figure 67 . Phase I Microscopic Model

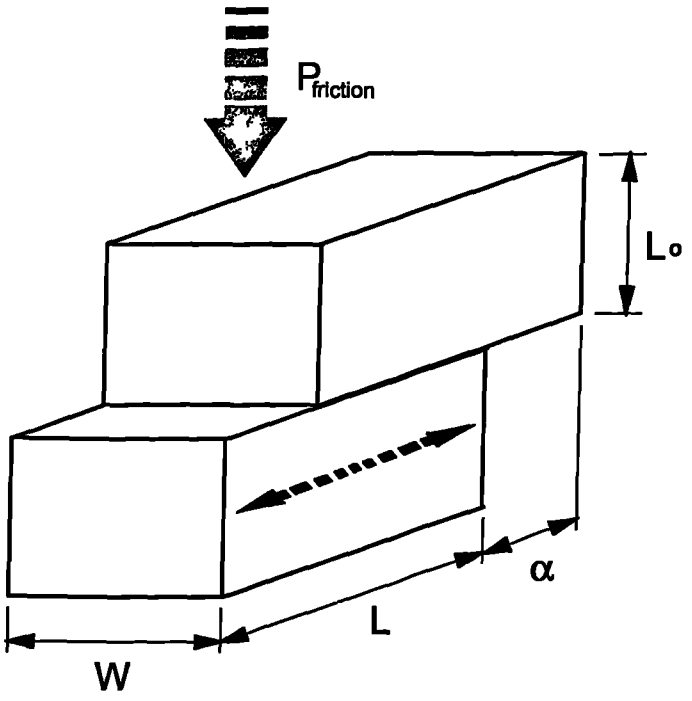

Figure 68 . Analytical Model

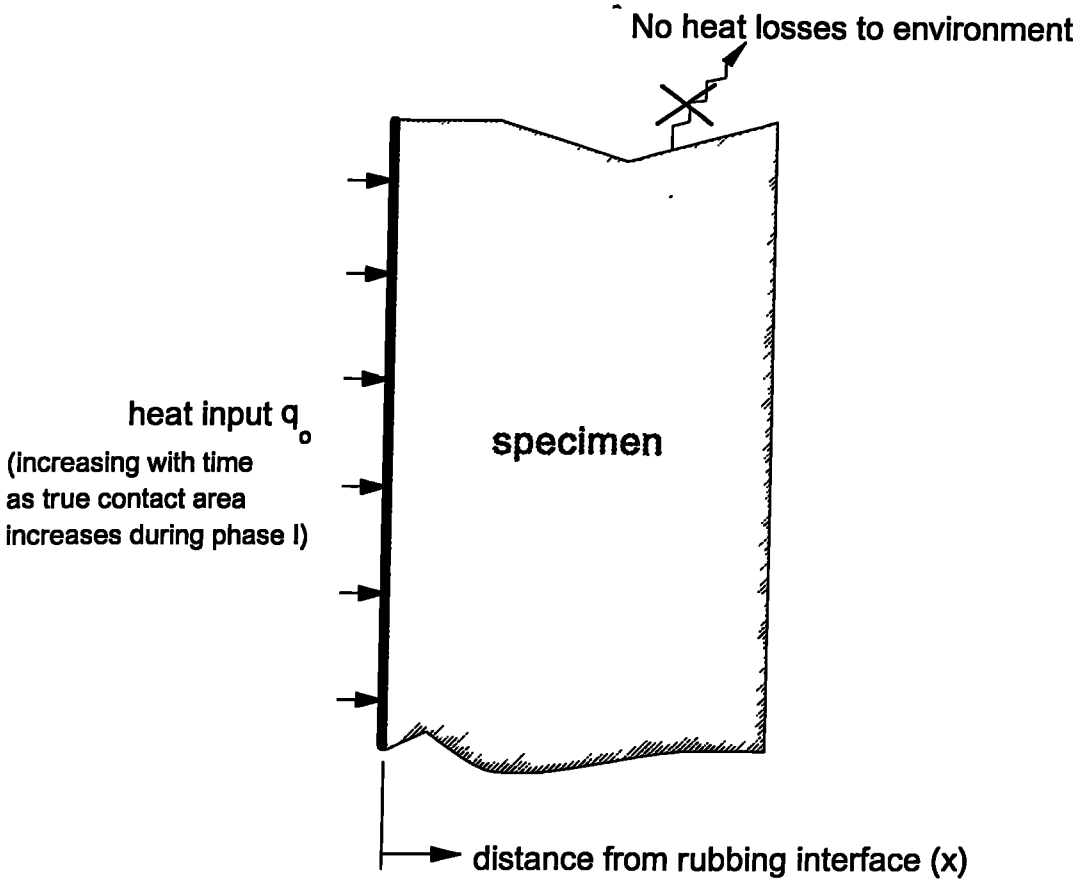

Figure 69 . Heat Flow Model

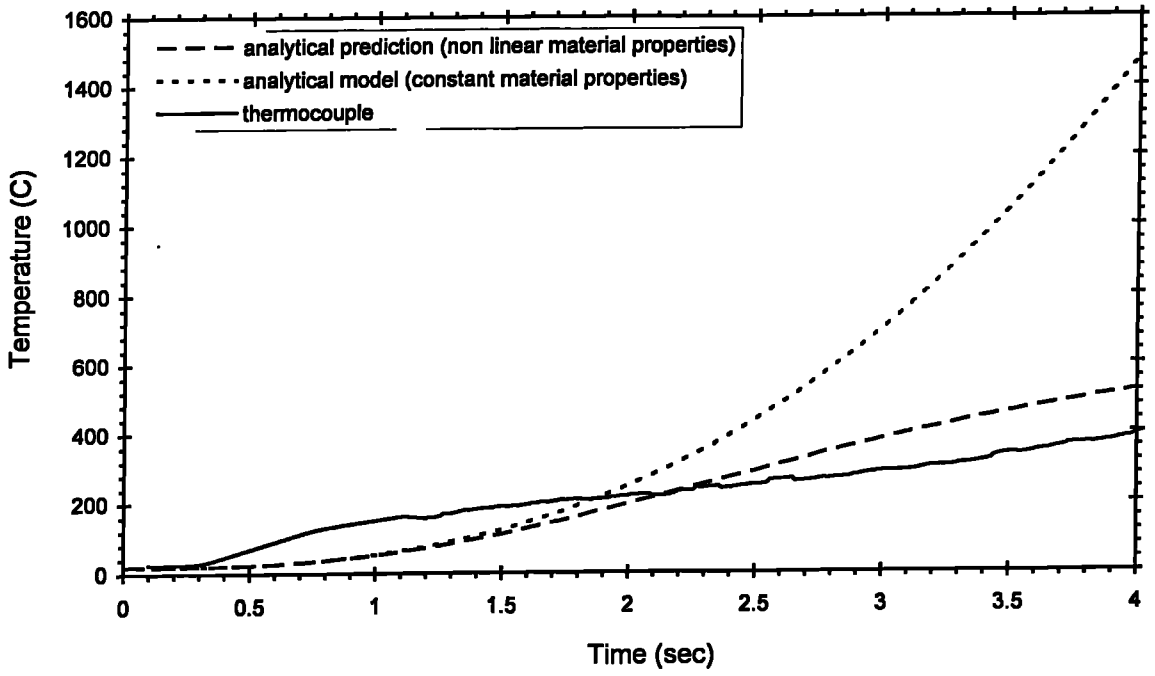

Figure 70 . Comparison Between Experimental And Analytical Model Temperature Data For Initial Phase (Ti 6Al 4V - α : 0.92 mm , f : 30 Hz , P_{fr} : 58.1 MPa -experiment D1)

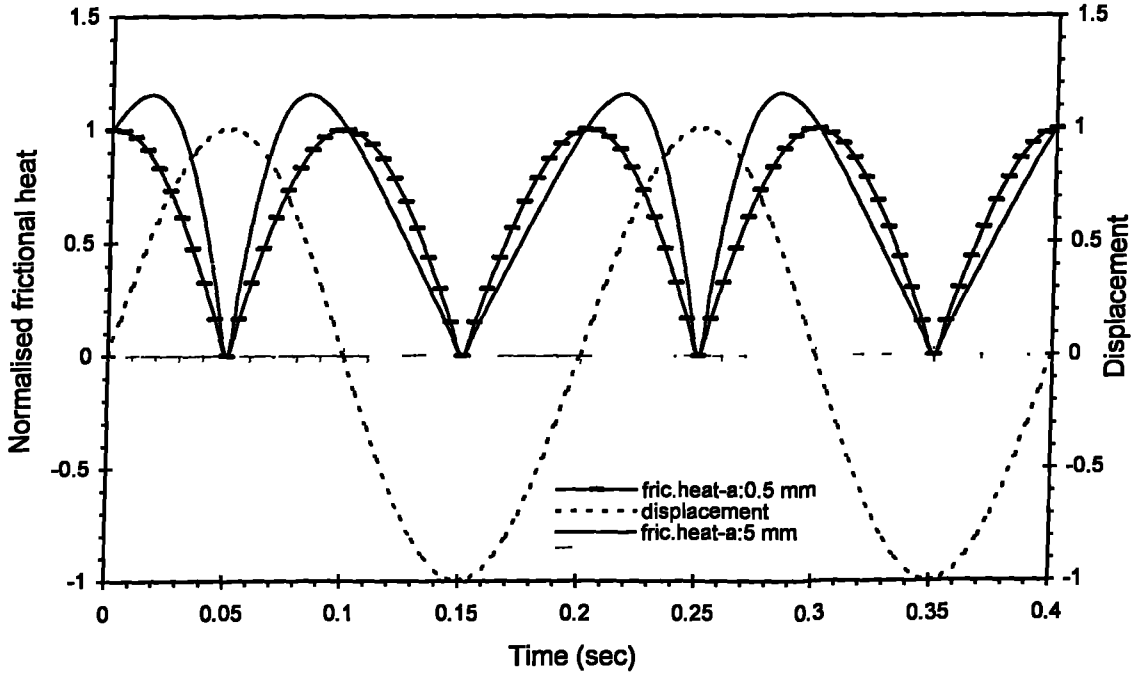

Figure 71 . Instantaneous Frictional Heat Generated During A Cycle (For Two Amplitudes Of Oscillation, f = 5 Hz, Length Of Specimen : 10 mm)

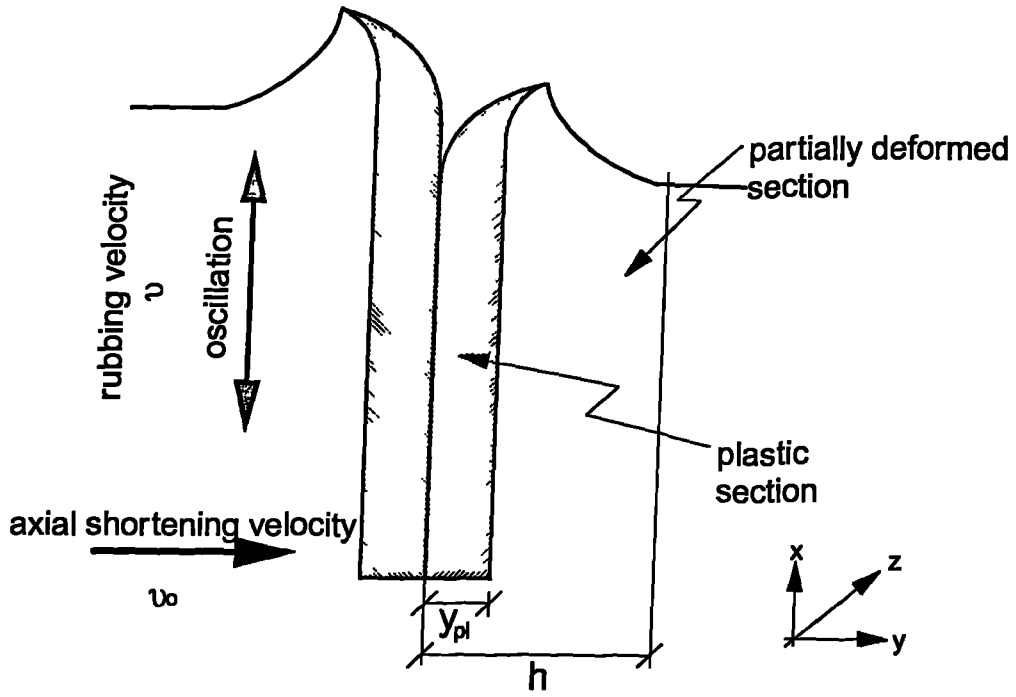

Figure 72 . Material Flow Model

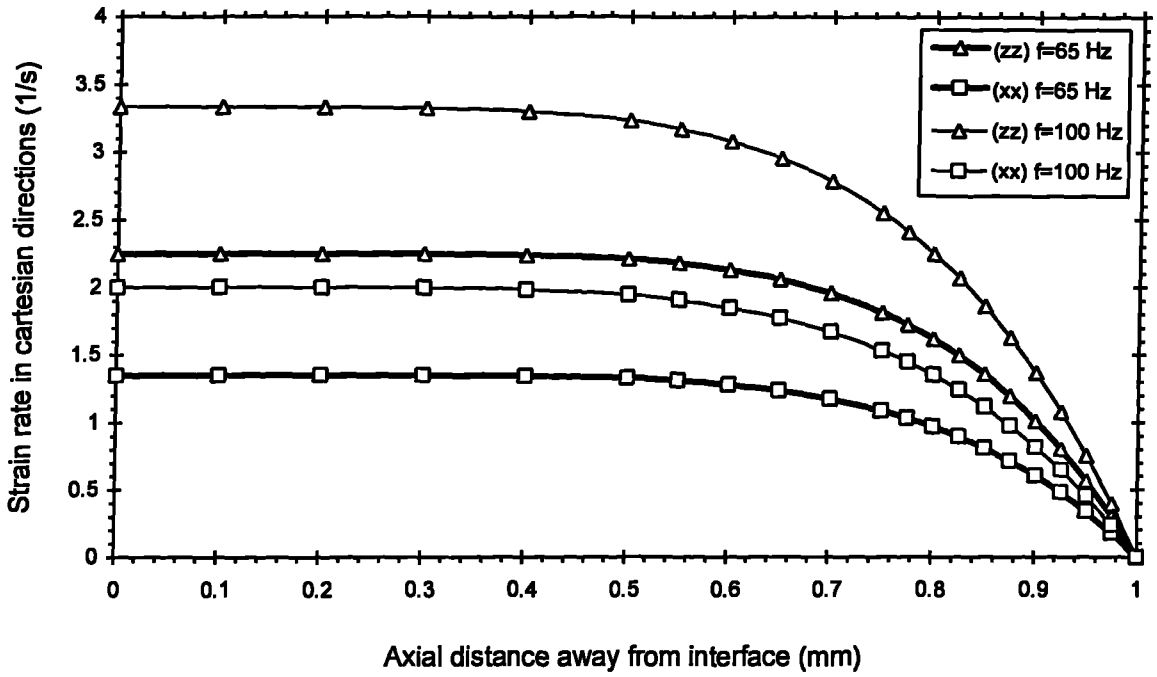

Figure 73 . Predicted HAZ Strain Rate Distribution During Linear Friction Welding Of Ti 6Al 4V (α : 0.92 mm, f : 65 Hz, P_{fr} : 25.9 MPa - experiment D12)

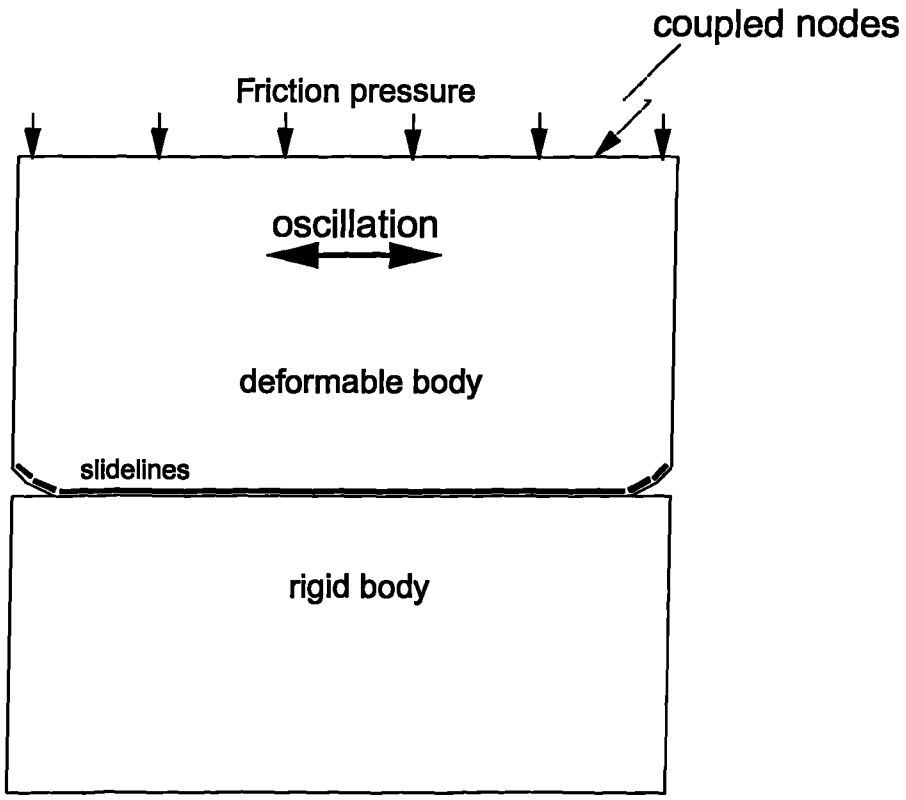

Figure 74 . Finite Element Model Of Linear Friction Welding

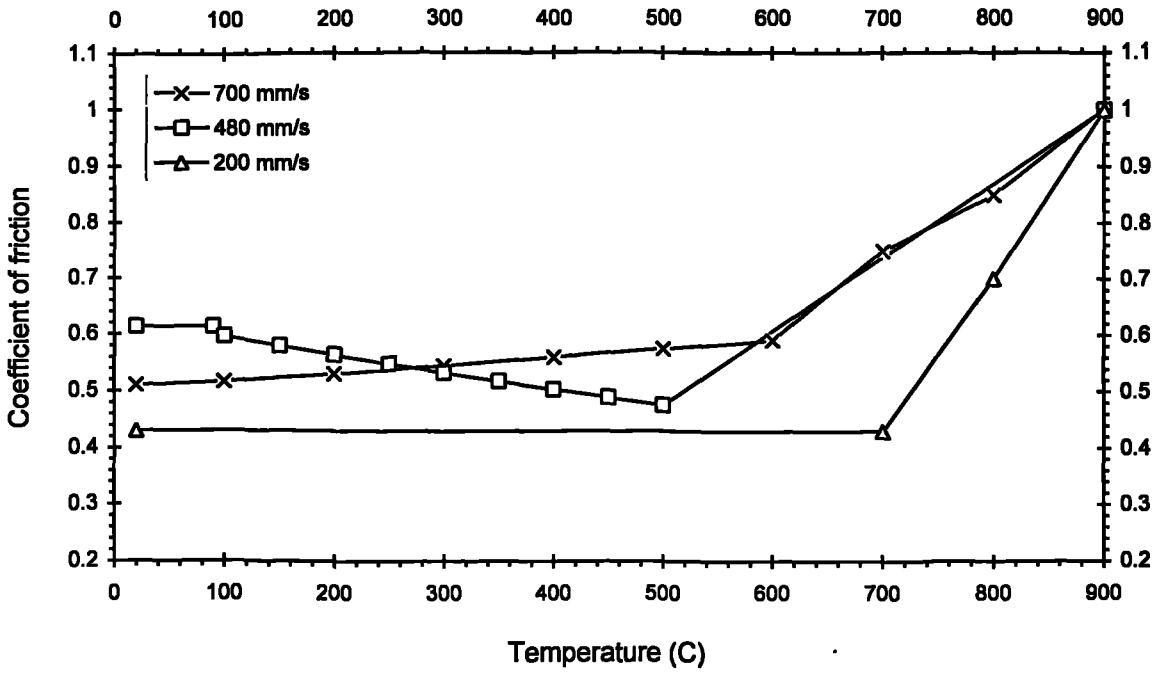

Figure 75 . Friction Coefficient Laws Used In The Finite Element Formulation

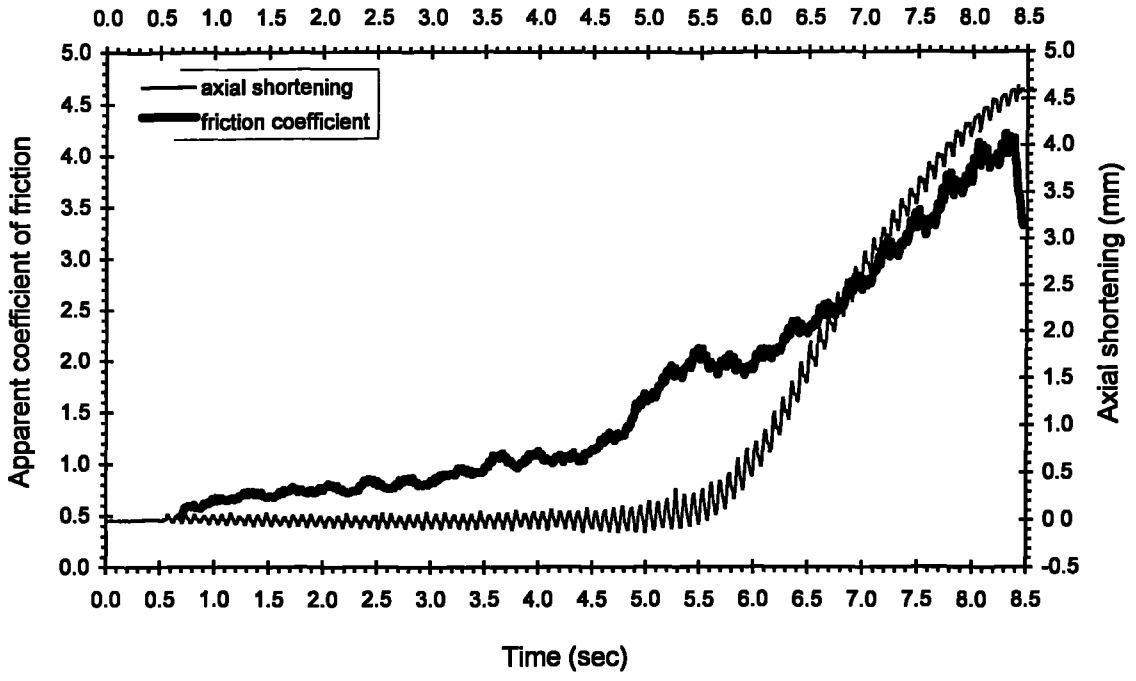

Figure 76 . Apparent friction coefficient and axial displacement history

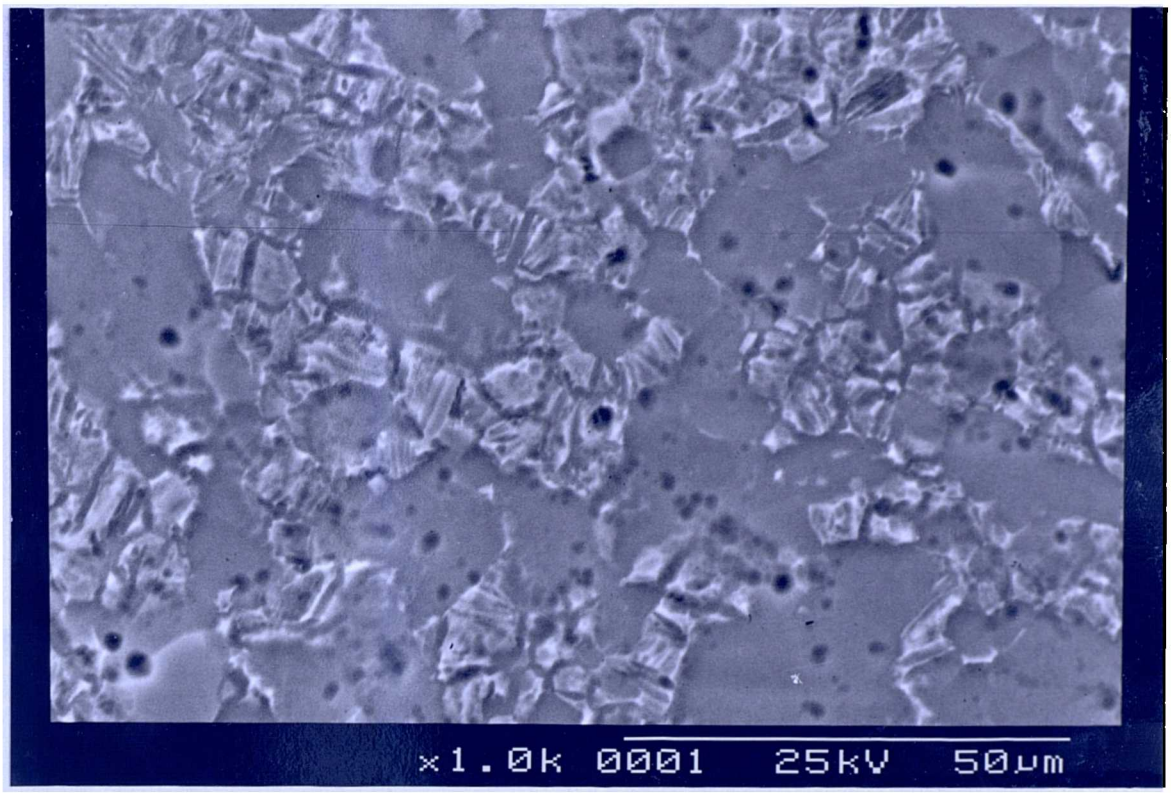

Figure 77 . SEM Micrograph Of Bulk Of Welded Specimen (Ti 6Al 4V)

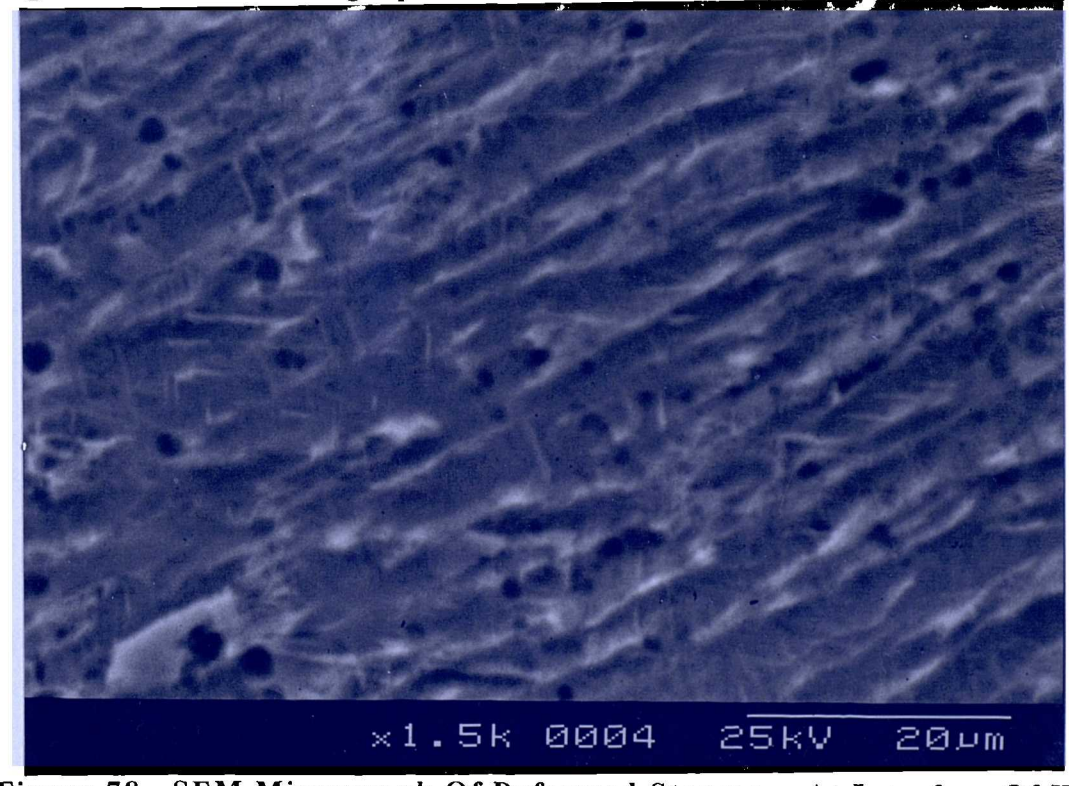

Figure 78 . SEM Micrograph Of Deformed Structure At Interface Of Welded Specimen (Ti 6Al 4V)

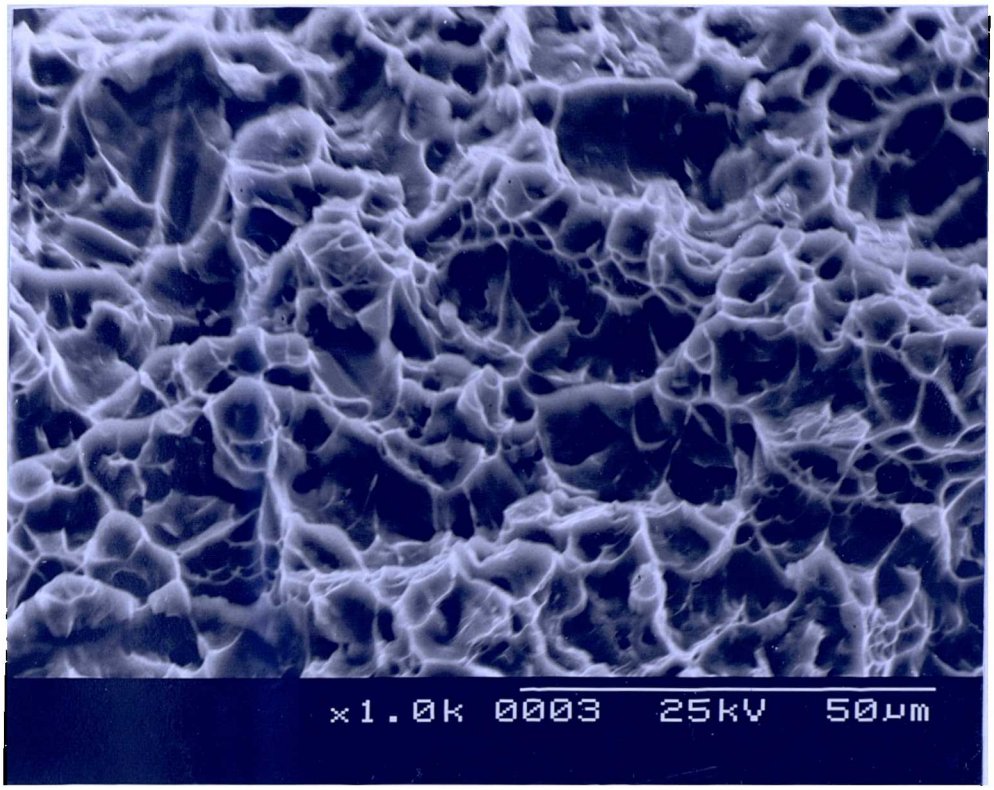

Figure 79 . Fracture Surface Of Weak Weld (α : 0.92 mm, f = 100 Hz, P_{fr} : 50.5 MPa -experiment D16)

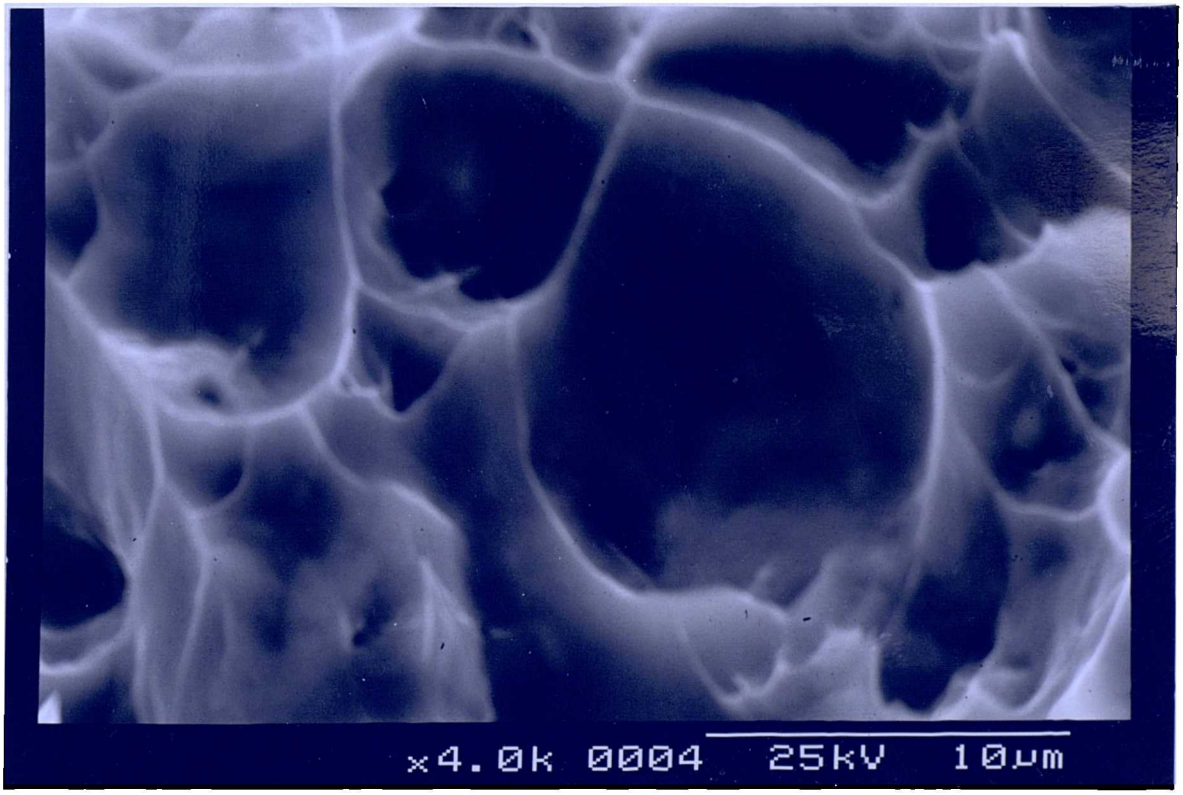

Figure 80 . Fracture Surface Of Weak Weld (α : 0.92 mm, f = 100 Hz, P_{fr} : 50.5 MPa - experiment D16)

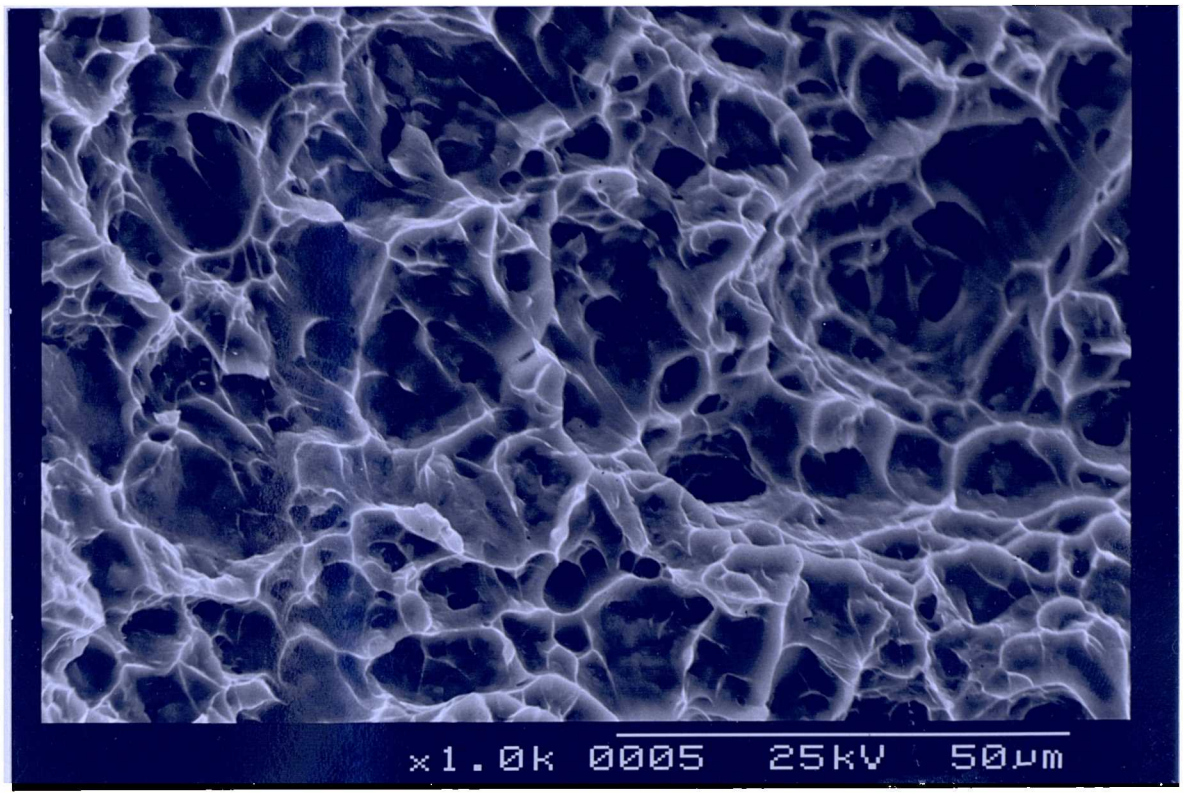

Figure 81 . Fracture Surface Of Weak Weld (α : 0.92 mm, f = 100 Hz, P_{fr} : 50.2 MPa - experiment D17)

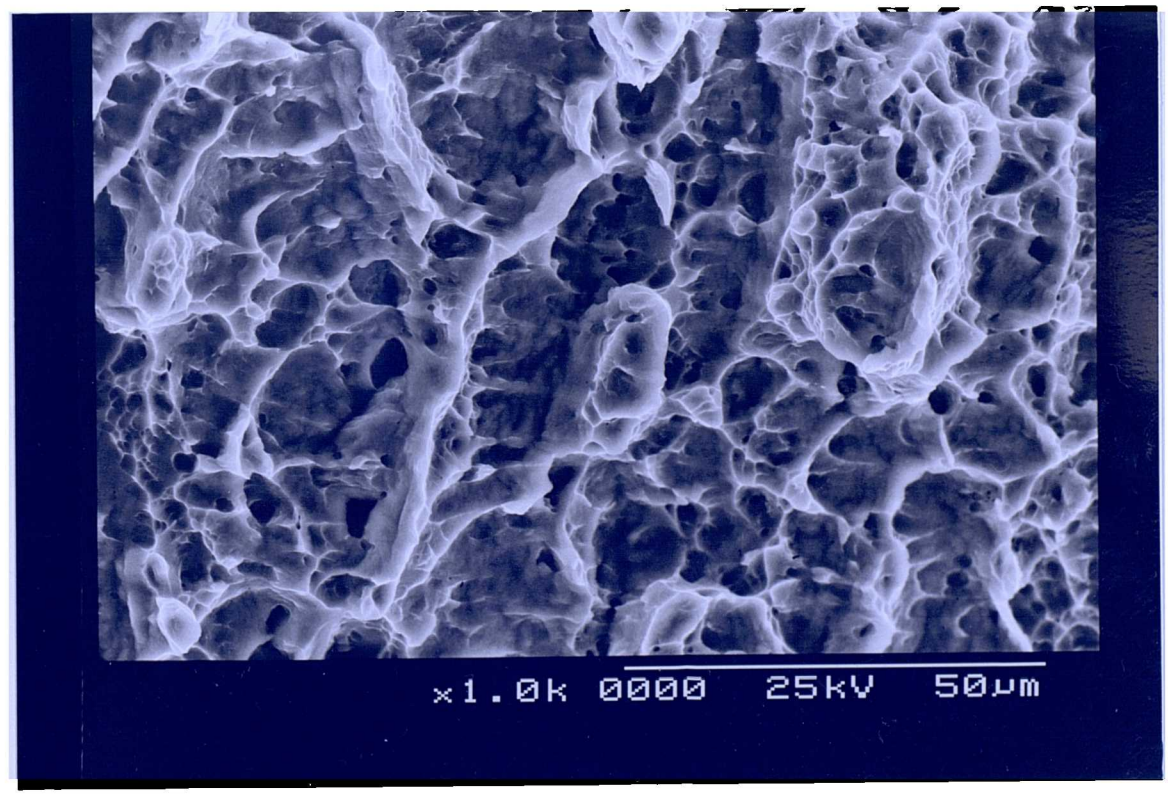

Figure 82 . Fracture Surface Of Weak Weld (α : 3 mm, f = 15 Hz, P_{fr} : 36.3 MPa - experiment A9)

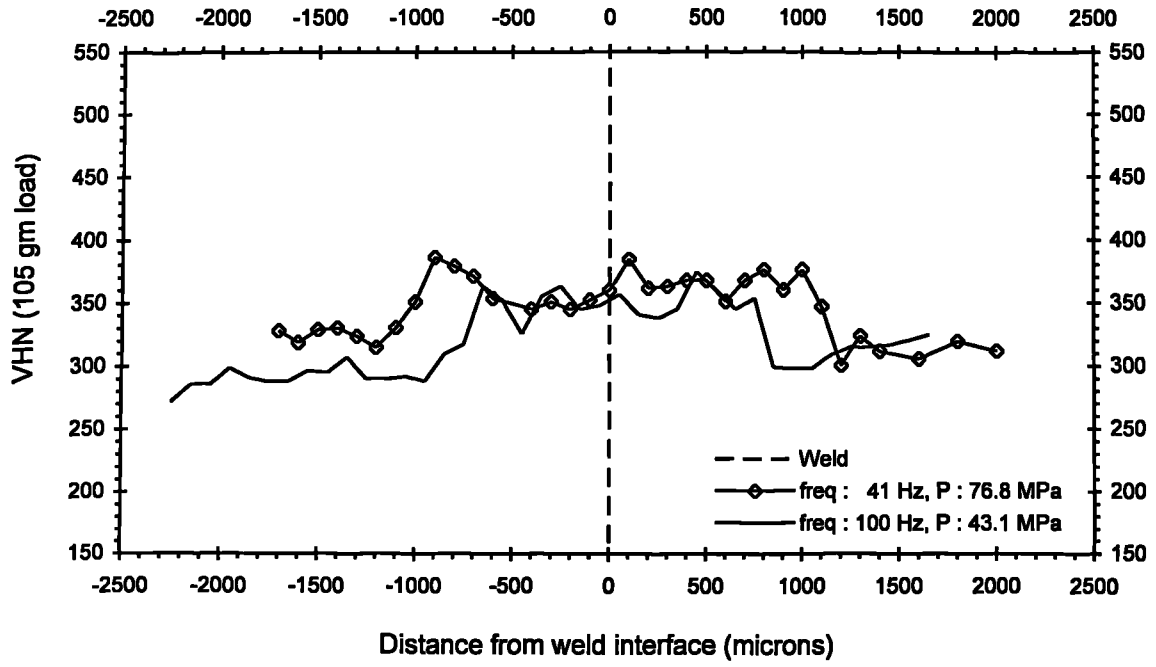

Figure 83 . Vickers Hardness Across Weld (α : 0.92 mm - experiments D3 & D15

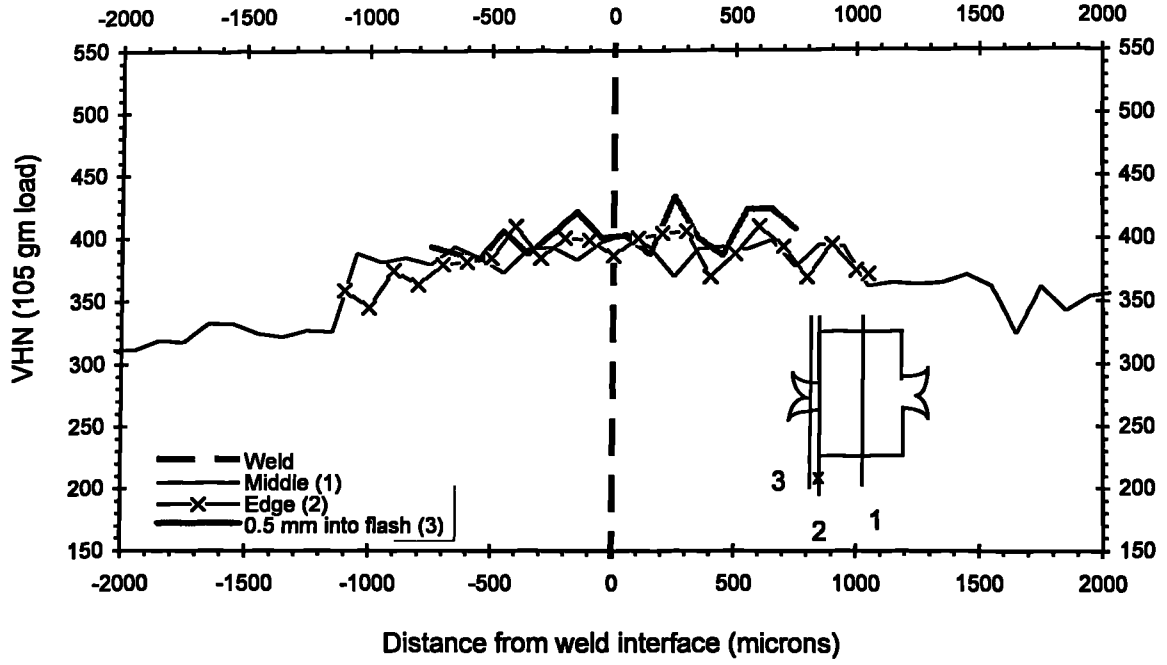

Figure 84 . Vickers Hardness Traverse Across Weld At Various Points Along Weld Line (α : 3 mm, f = 12 Hz, P_{fr} : 61.8 MPa - experiment A8)

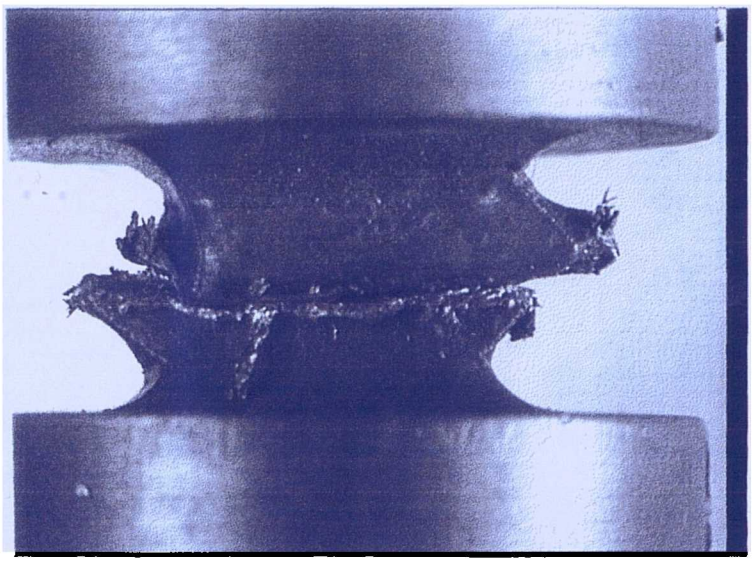

Figure 85 . Linear friction weld of pure lead (99%) (experiment L1)

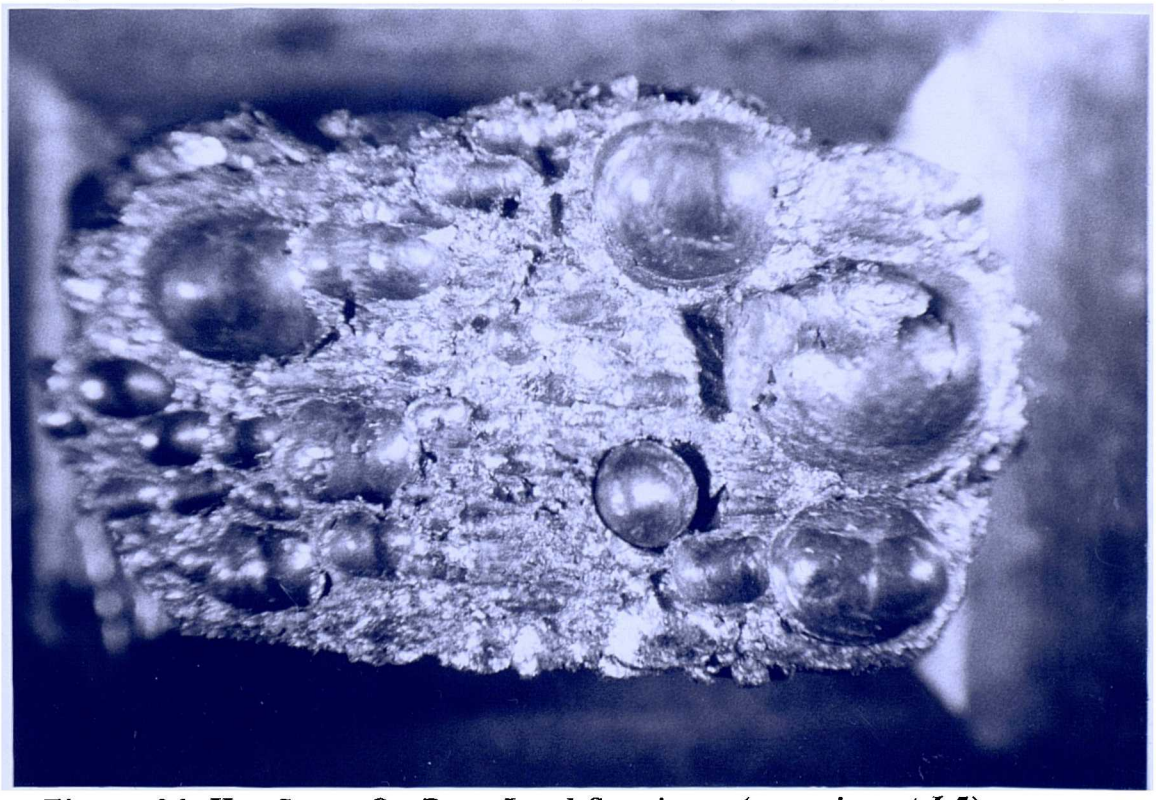

Figure 86. Hot Spots On Pure Lead Specimen (experiment L5)

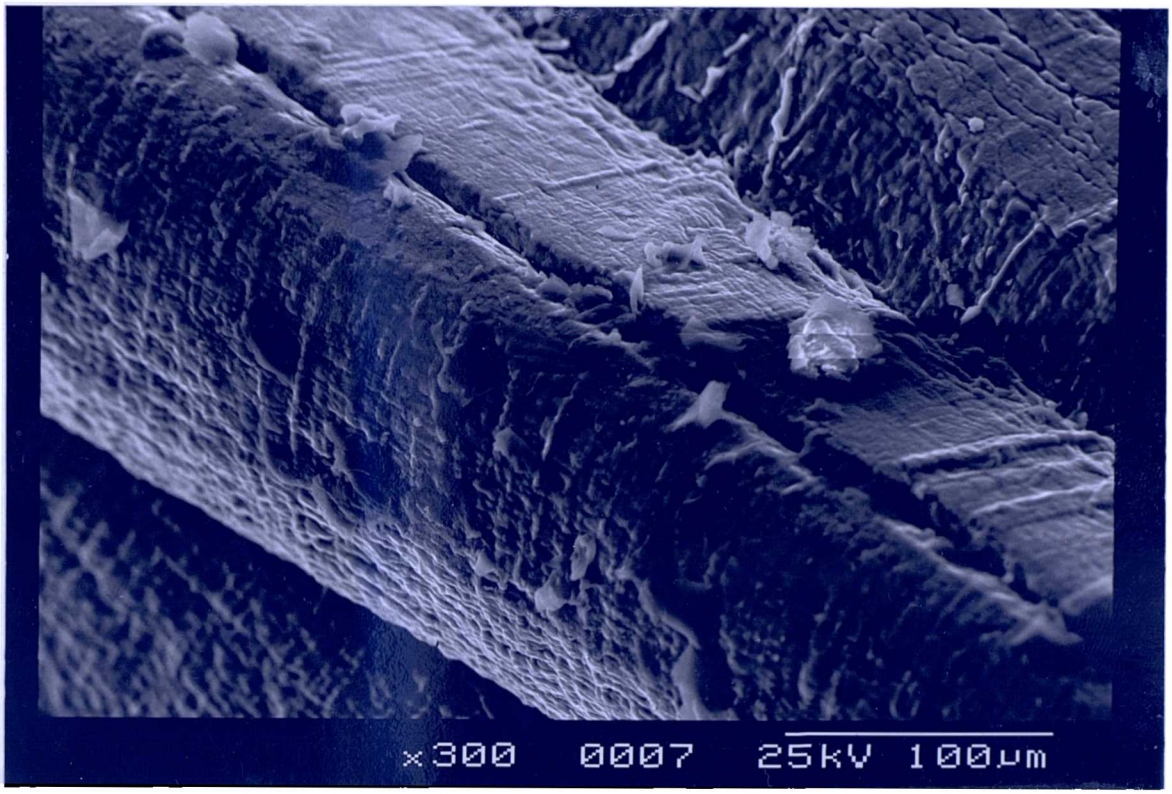

Figure 87 . Detail Of Ridge (Ti 6Al 4V - α : 3 mm, f = 20 Hz, P_{fr} : 44.7 MPa - experiment A20)

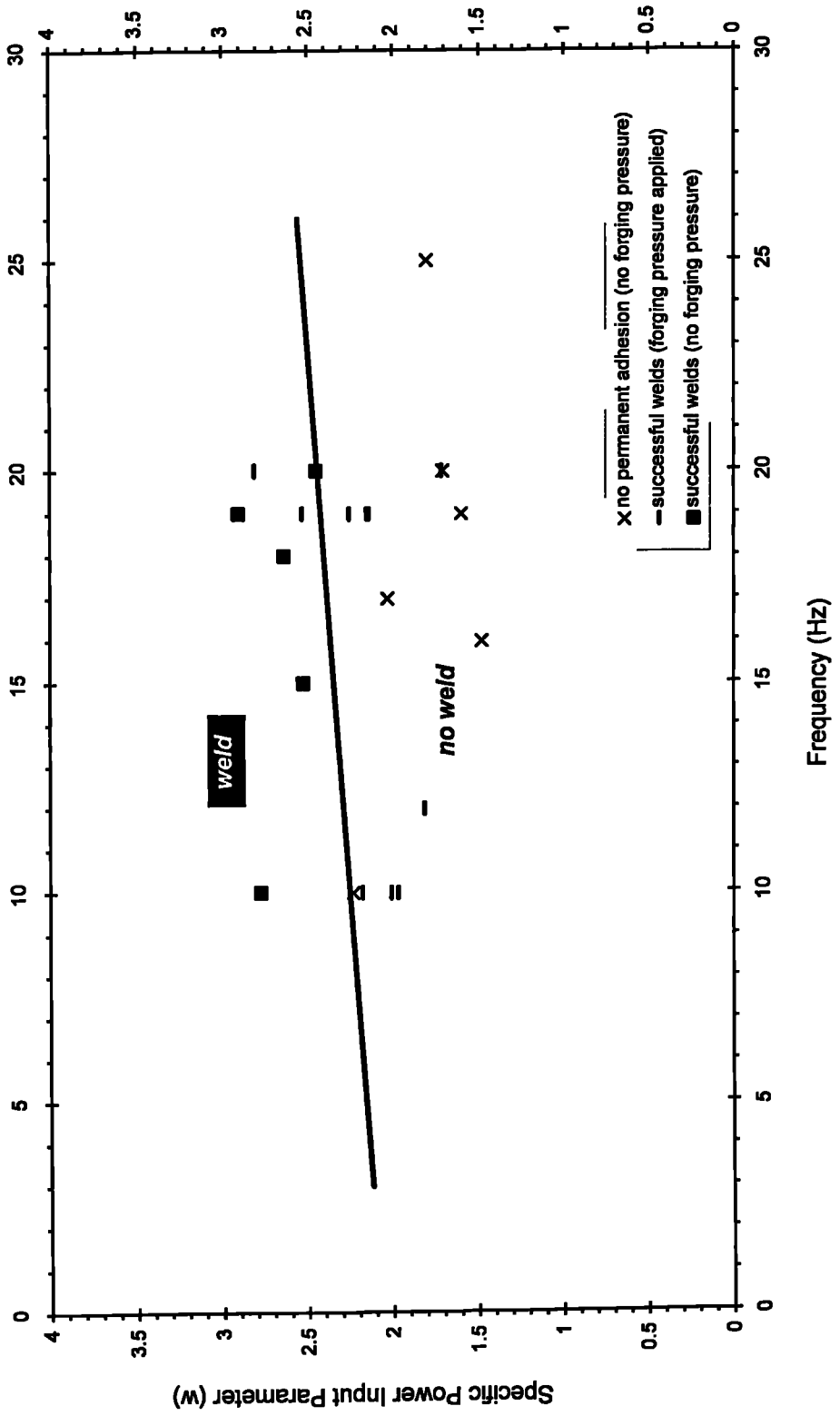

Figure 88 . Effect Of Frequency Of Oscillation On Minimum Specific Power Input Parameter (W) Required To Achieve Weld (α : 3 mm)

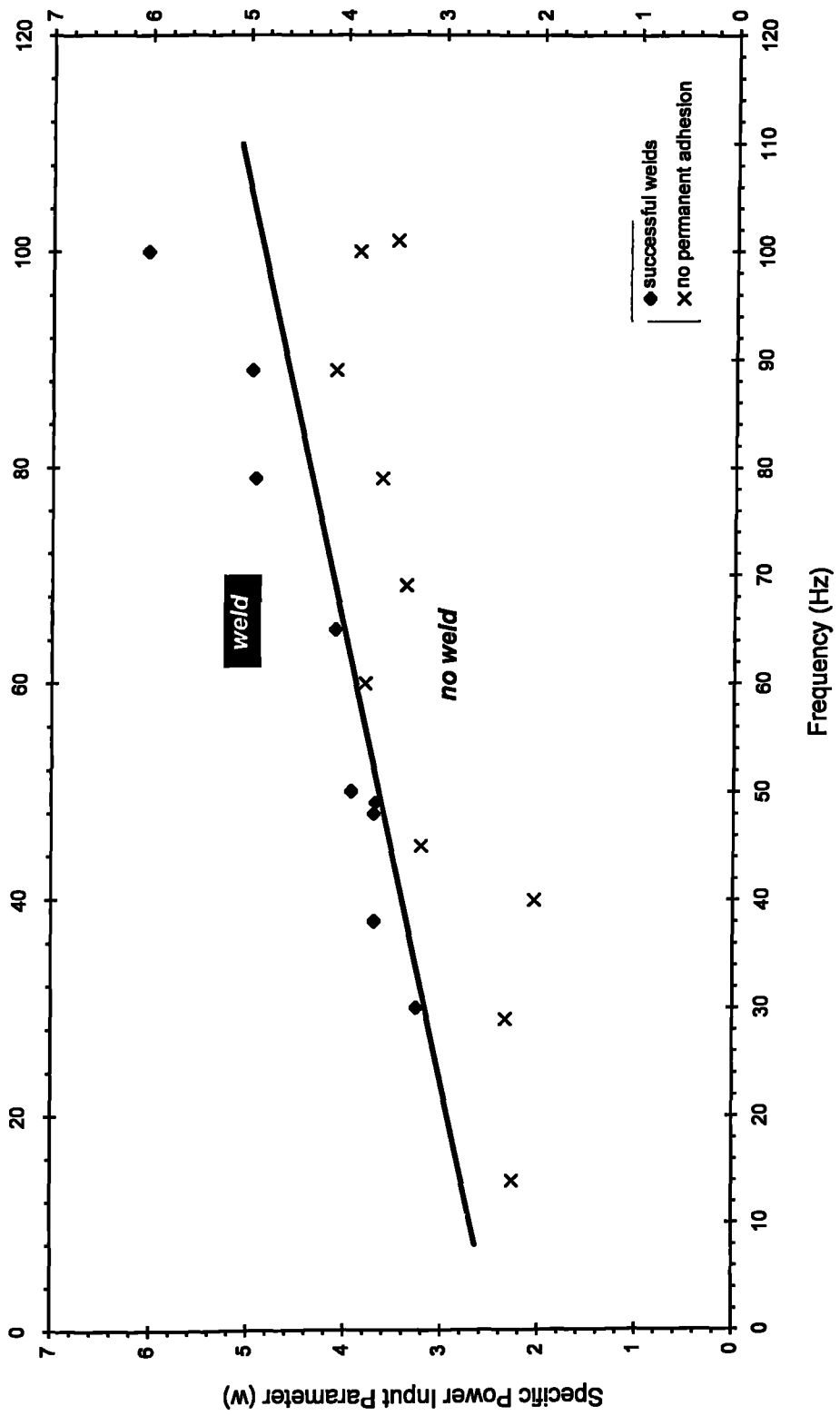

Figure 89 . Effect Of Frequency Of Oscillation On Minimum Specific Power Input Parameter (w) Required To Achieve Weld (α : 0.92 mm)

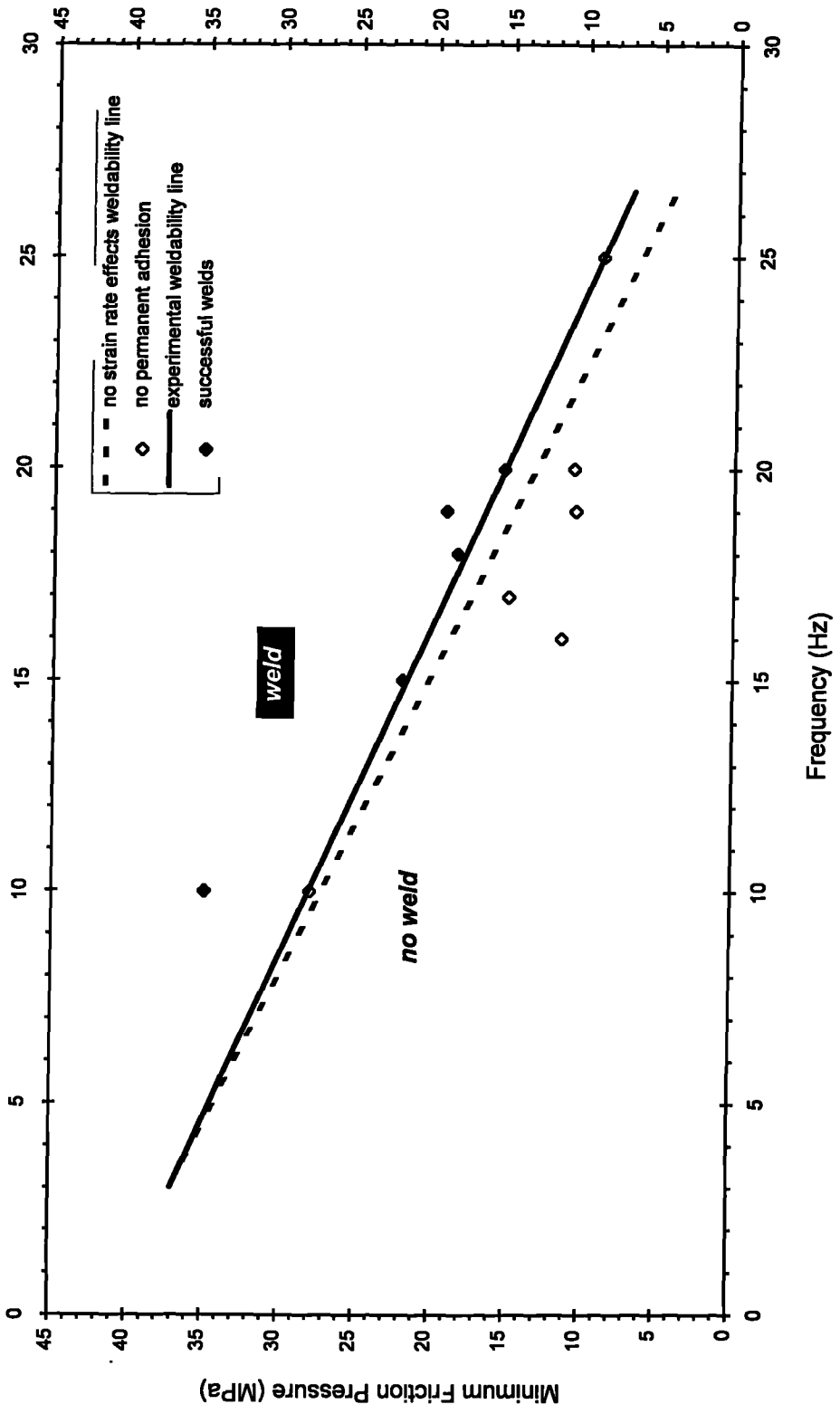

Figure 90 . Effect Of Frequency Of Oscillation On Minimum Friction Pressure Required To Achieve Weld From Experiments As Well As Assuming No Strain Rate Effects(α = 3 mm)

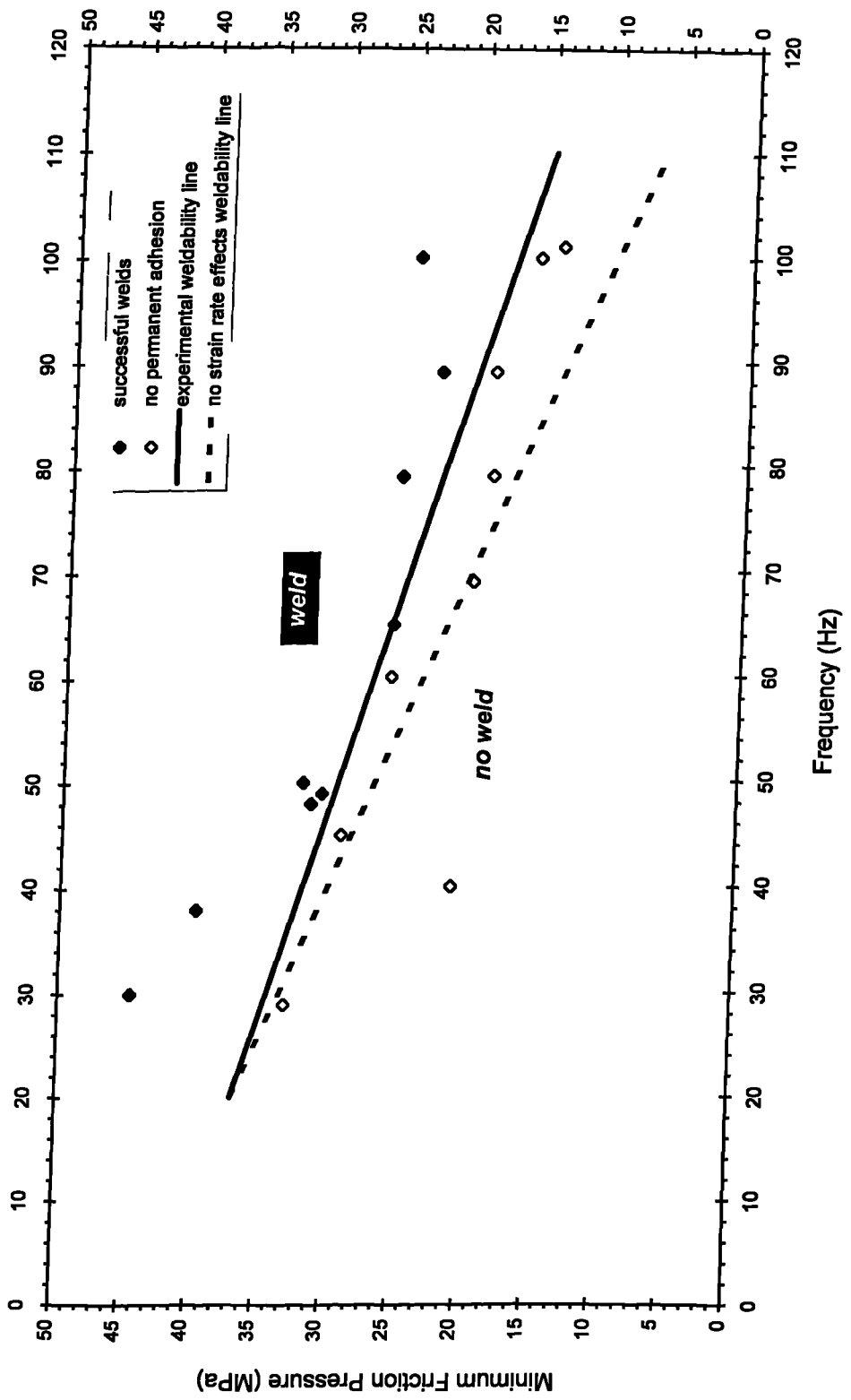

Figure 91 . Effect Of Frequency Of Oscillation On Minimum Friction Pressure Required To Achieve Weld From Experiments As Well As Assuming No Strain Rate Effects (α = 0.92 mm)

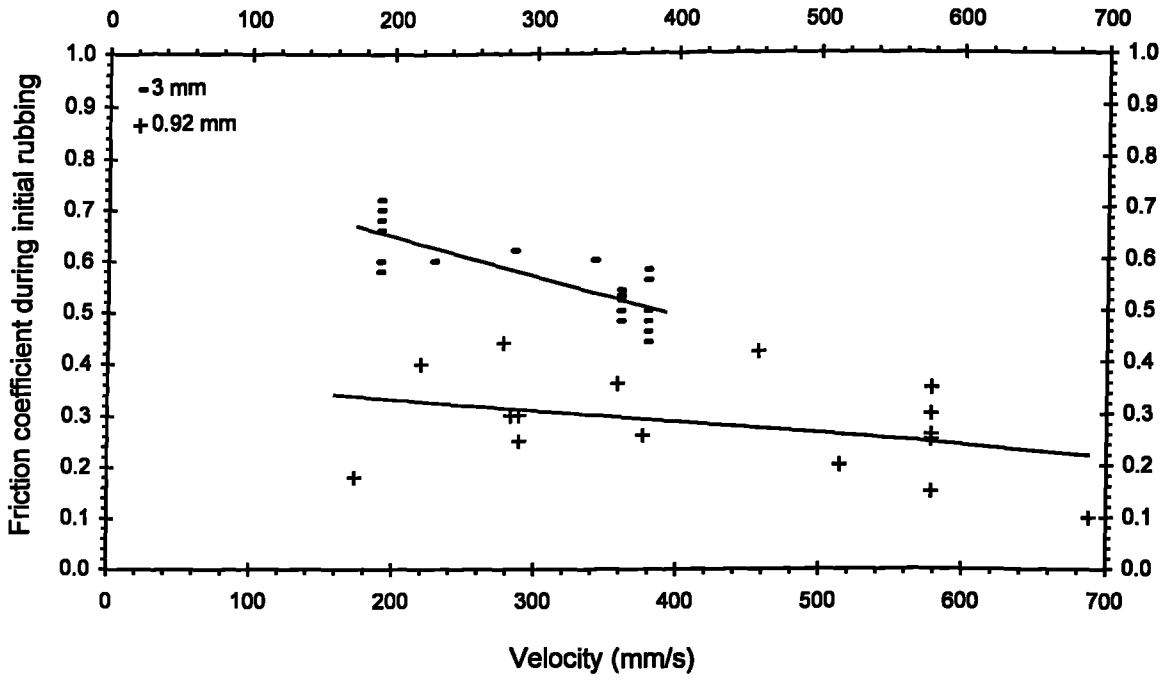

Figure 92 . Effect Of Rubbing Velocity On The Friction Coefficient During Initial Rubbing At Phase I (For Two Amplitudes Of Oscillation)

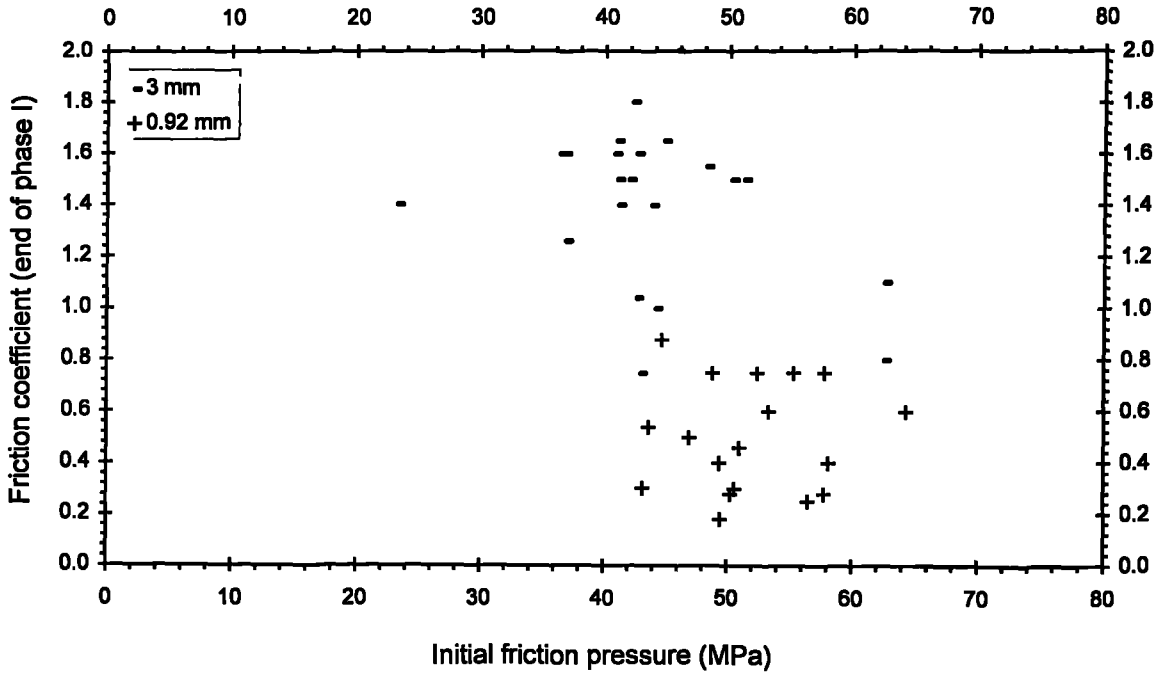

Figure 93 . Effect Of Initial Friction Pressure On The Friction Coefficient During Initial Rubbing At Phase I (For Two Amplitudes Of Oscillation)

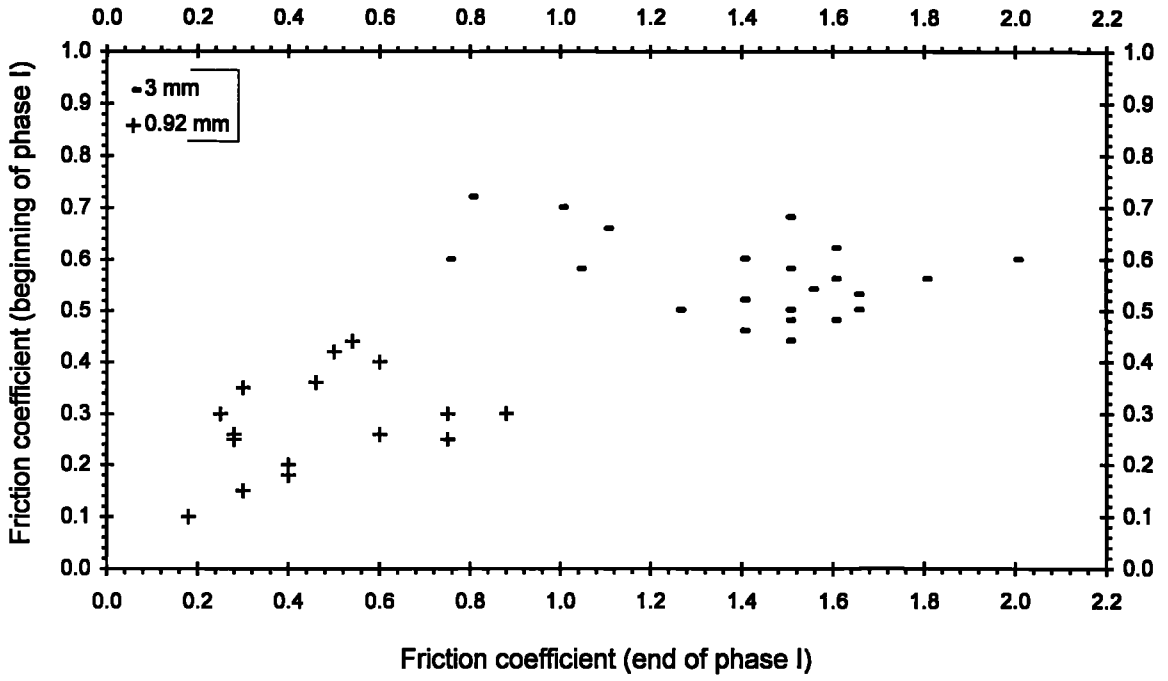

Figure 94 . Association Of Friction Coefficient During Initial Rubbing To The End Of Phase I (For Two Amplitudes Of Oscillation)

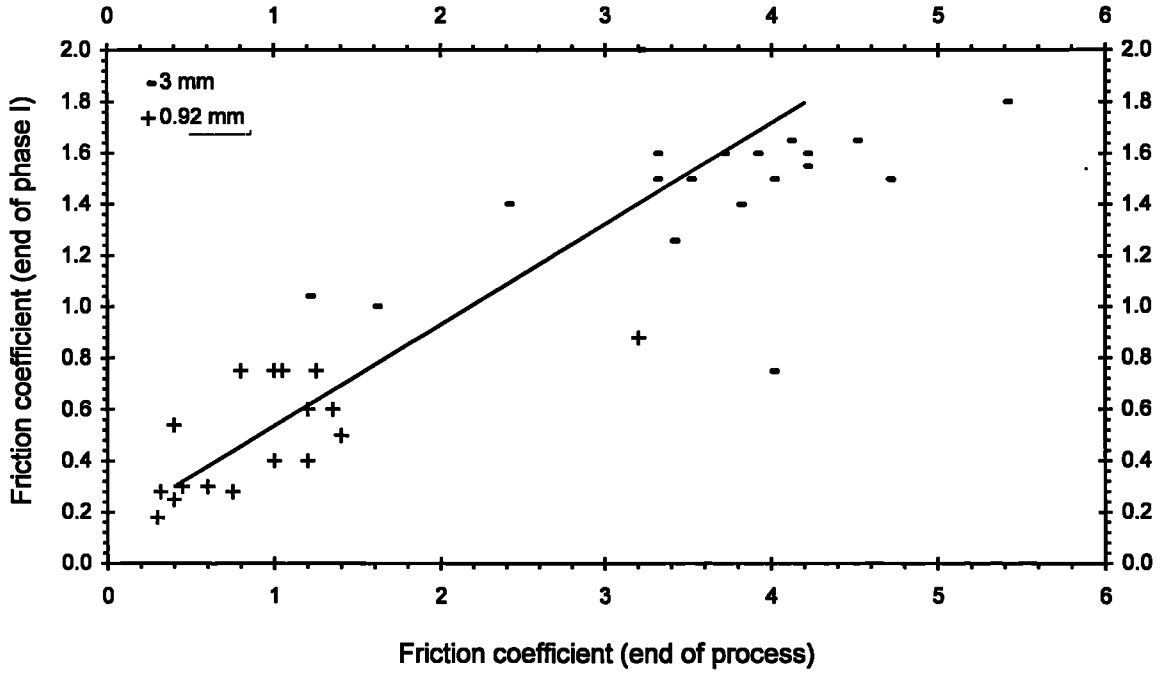

Figure 95 . Association Of Friction Coefficient At The End Of Phase I To That At The End Of The Process (For Two Amplitudes Of Oscillation)

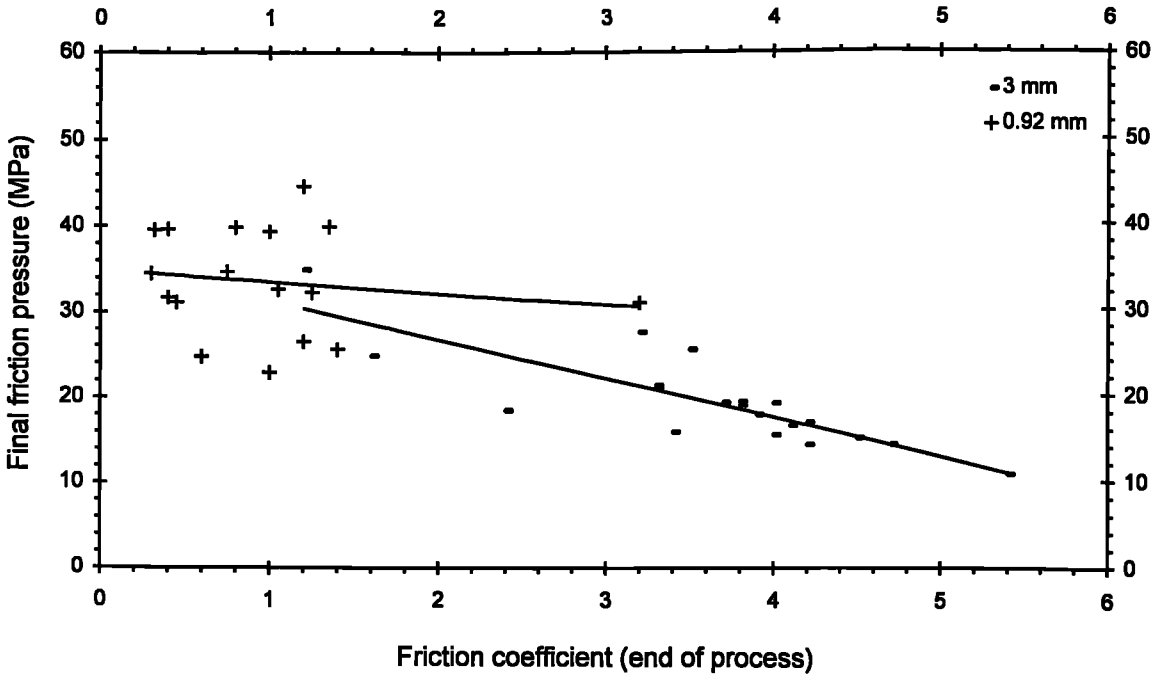

Figure 96 . Effect Of Final Friction Pressure On Friction Coefficient At The End Of The Process (For Two Amplitudes Of Oscillation)

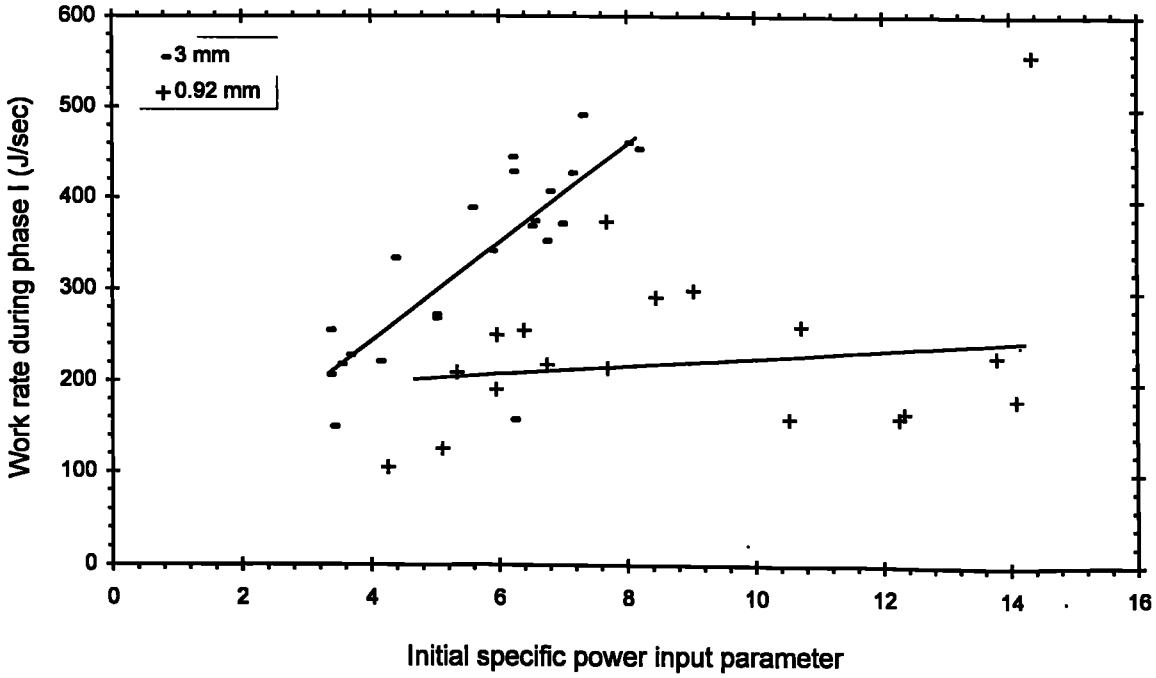

Figure 97 . Effect Of Initial Power Input Parameter On Work Rate During Phase I (For Two Amplitudes Of Oscillation)

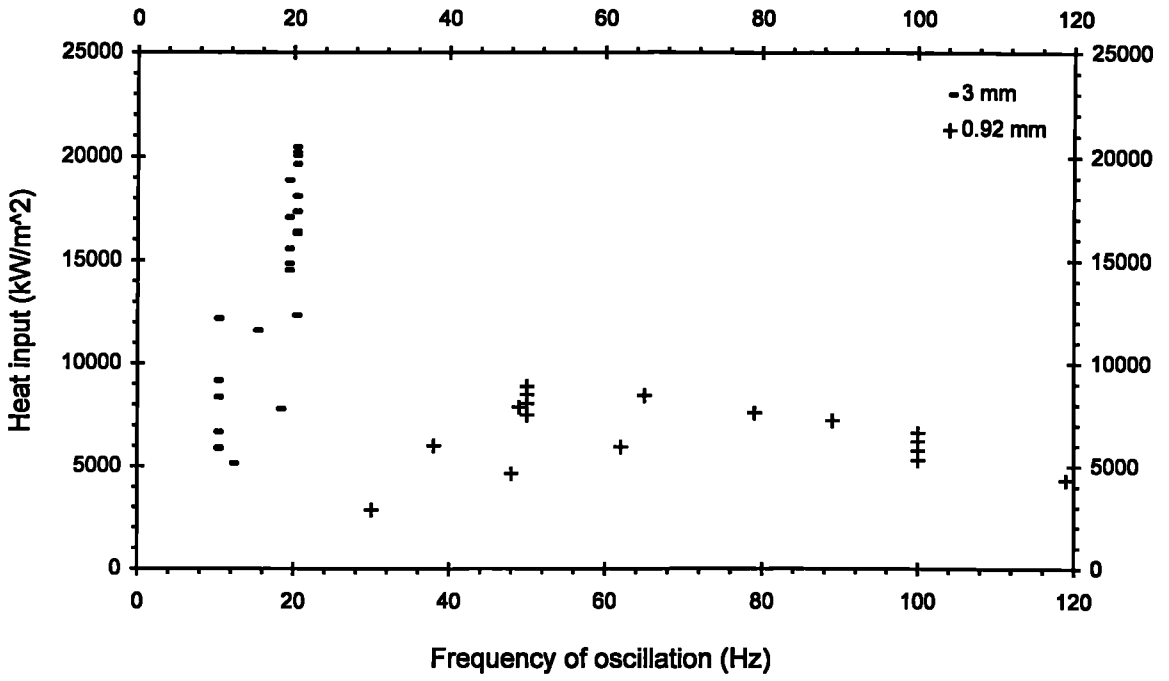

Figure 98 . Effect Of Frequency Of Oscillation On Heat Input During Initial Phase I (For Two Amplitudes Of Oscillation)

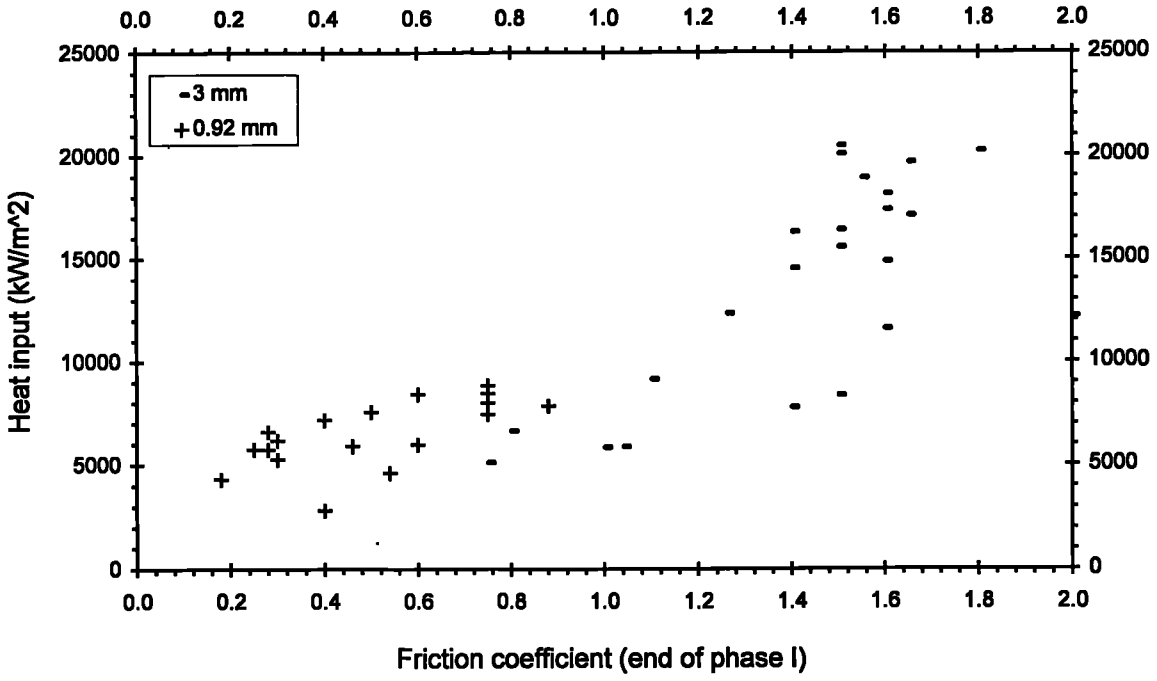

Figure 99 . Effect Of Friction Coefficient At The End Of Phase I On The Heat Input During Phase I (For Two Amplitudes Of Oscillation)

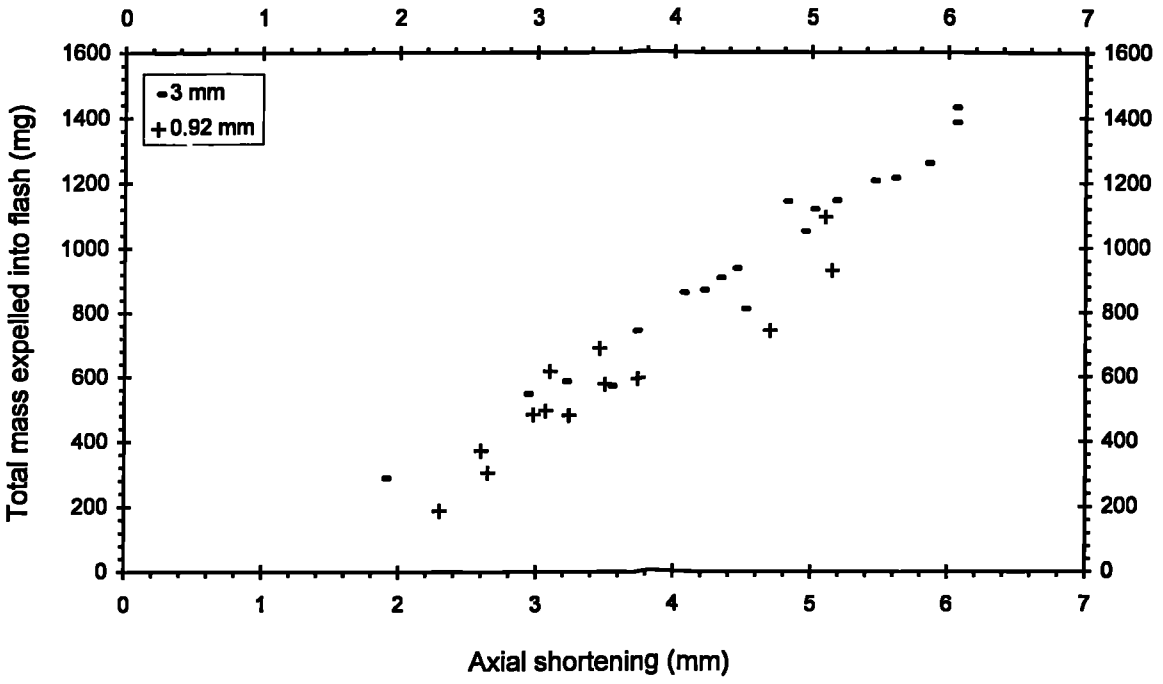

Figure 100 . Effect Of Axial Shortening On Total Mass Expelled Into Flash (For Two Amplitudes Of Oscillation)

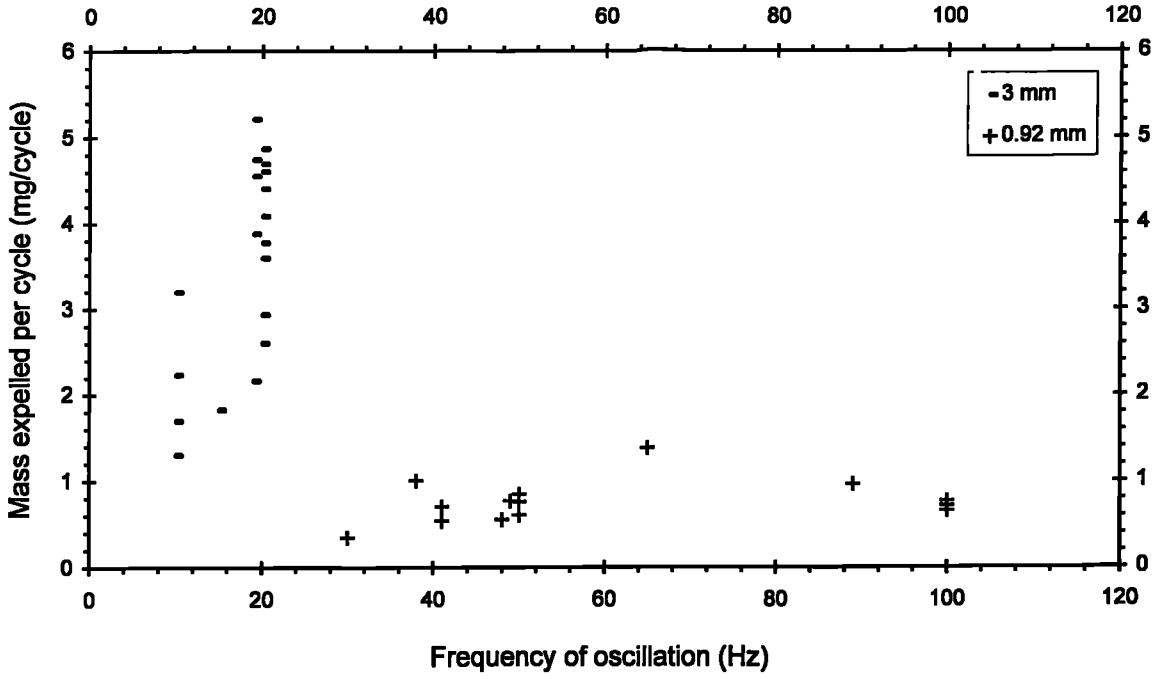

Figure 101 . Effect Of Frequency Of Oscillation On Mass Expelled Into Flash Per Cycle Of Oscillation (For Two Amplitudes Of Oscillation)

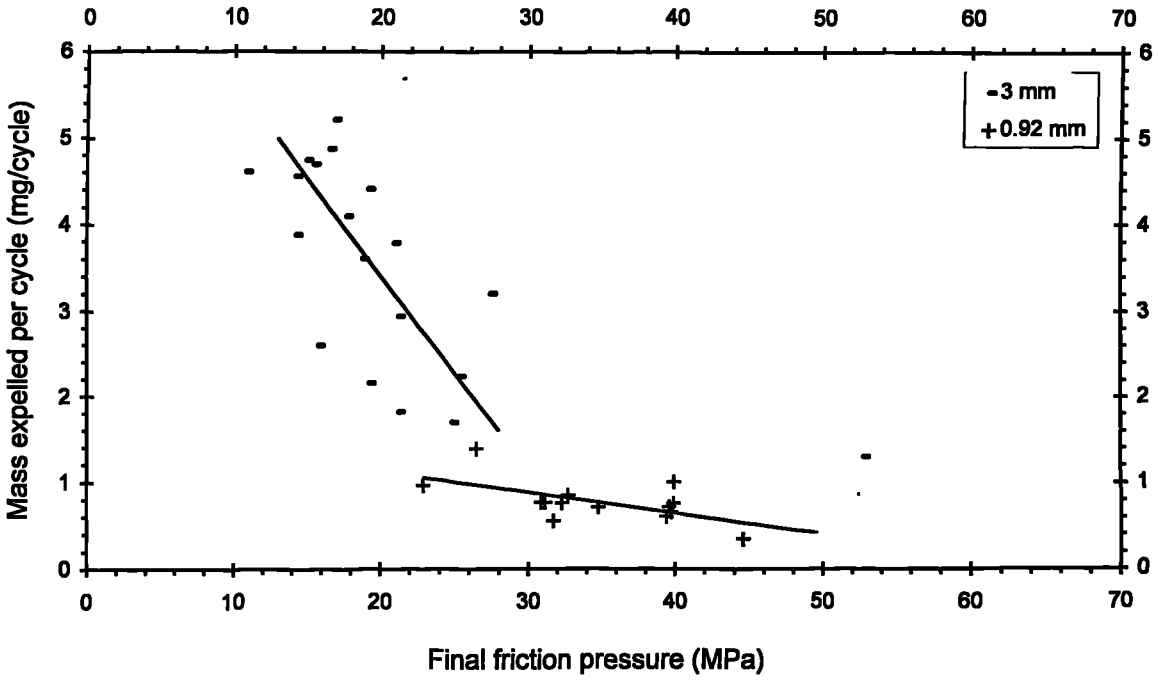

Figure 102 . Effect Of Final Friction Pressure On Mass Expelled Into Flash Per Cycle Of Oscillation (For Two Amplitudes Of Oscillation)

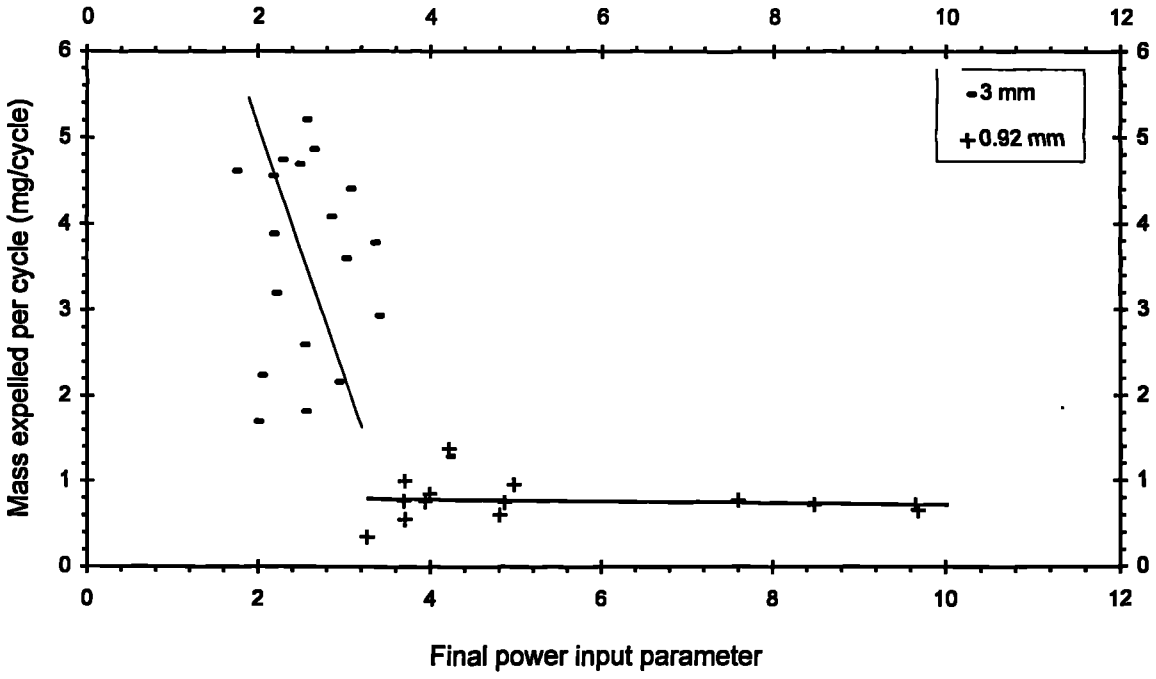

Figure 103 . Effect Of Final Power Input Parameter (w) On Mass Expelled Into Flash Per Cycle Of Oscillation (For Two Amplitudes Of Oscillation)

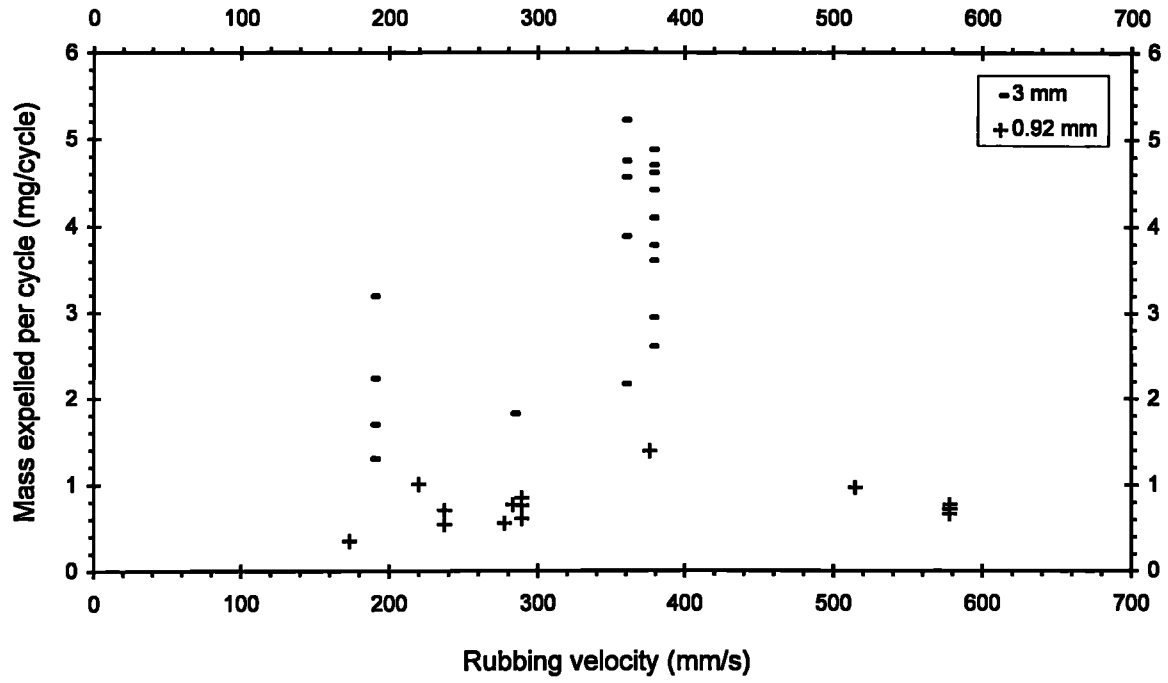

Figure 104 . Effect Of Rubbing Velocity On Mass Expelled Into Flash Per Cycle Of Oscillation (For Two Amplitudes Of Oscillation)

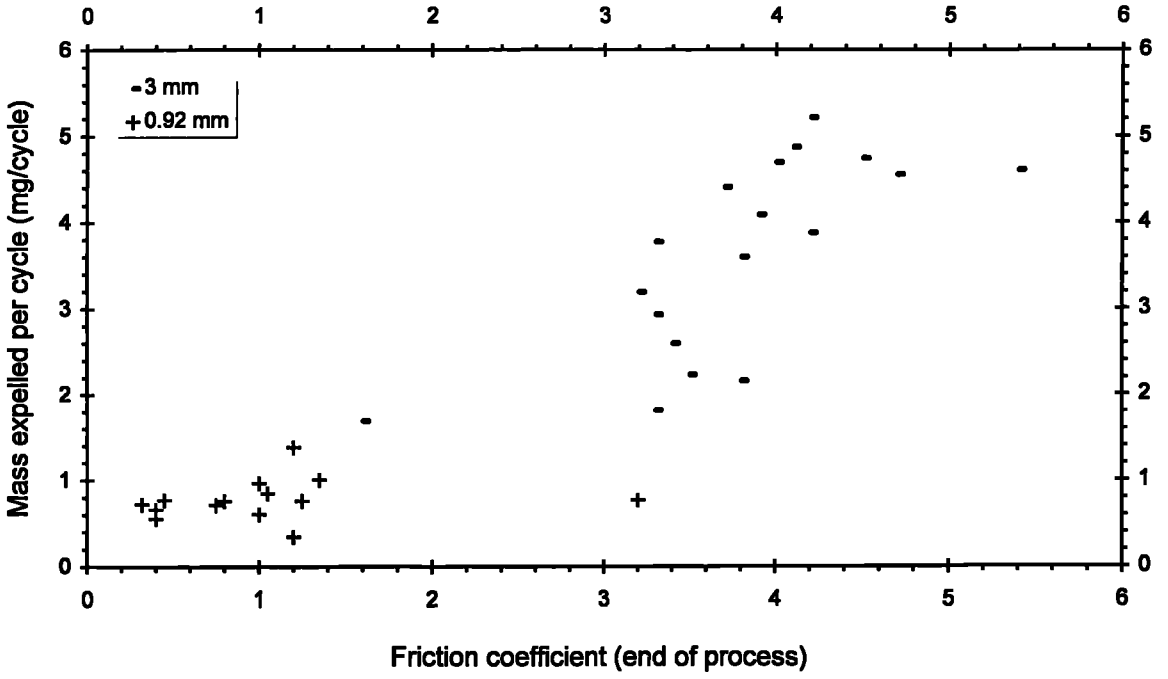

Figure 105 . Effect Of The Friction Coefficient At The End Of The Process On The Mass Extruded Per Cycle (For Two Amplitudes Of Oscillation)

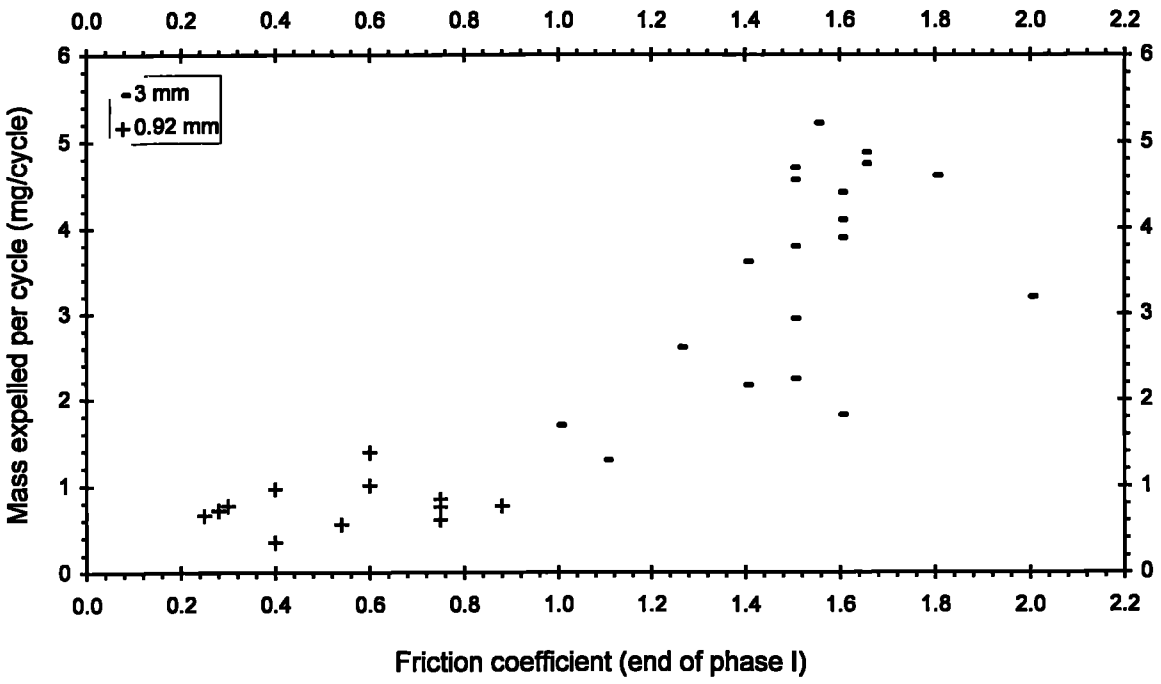

Figure 106 . Effect Of Friction Coefficient During Phase I On The Mass Expelled Into Flash Per Cycle (For Two Amplitudes Of Oscillation)

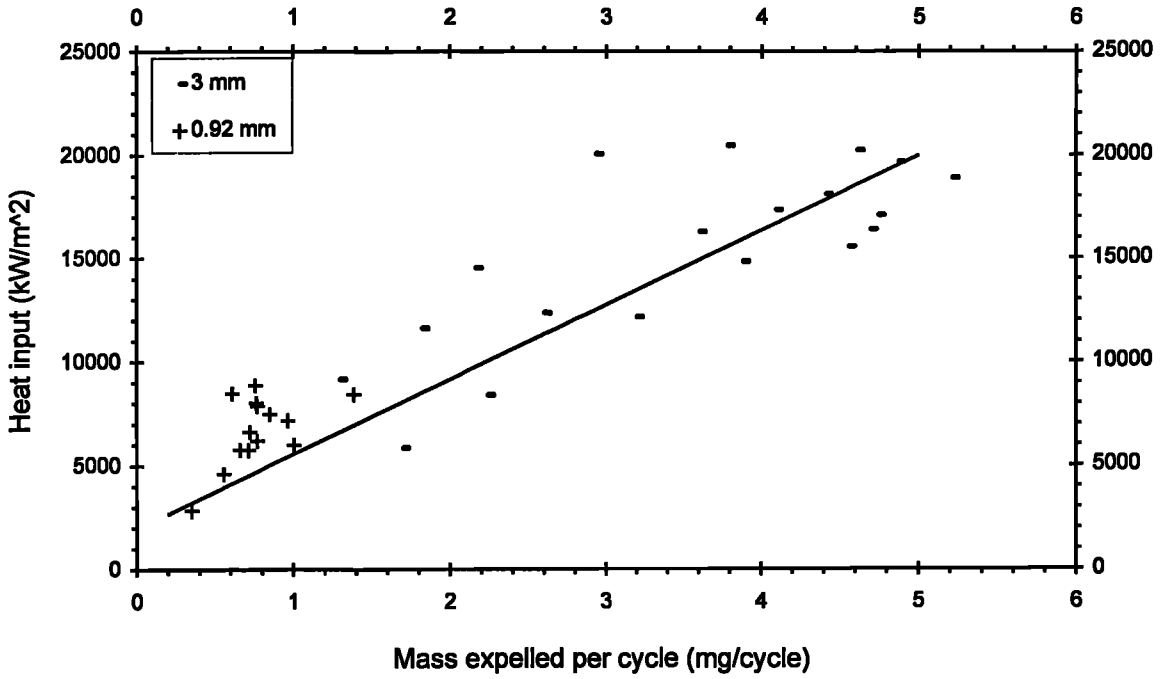

Figure 107 . Effect Of Heat Input During Initial Phase On Mass Expelled Per Cycle I (For Two Amplitudes Of Oscillation)

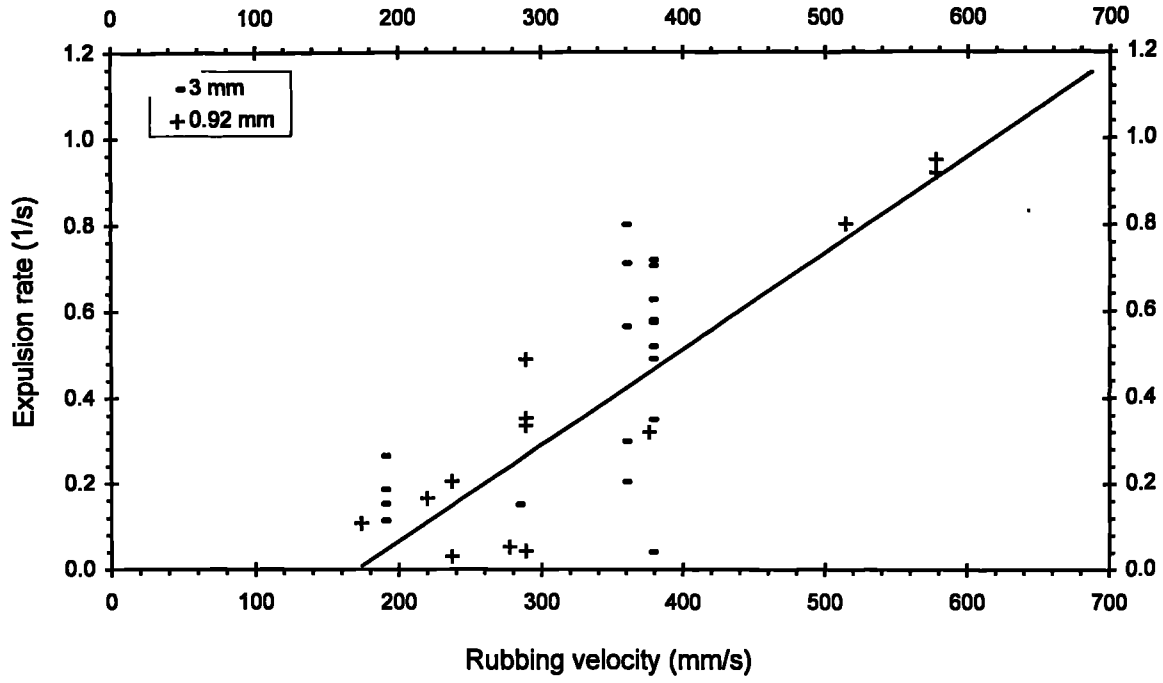

Figure 108 . Effect Of Rubbing Velocity On Expulsion Rate (For Two Amplitudes Of Oscillation)

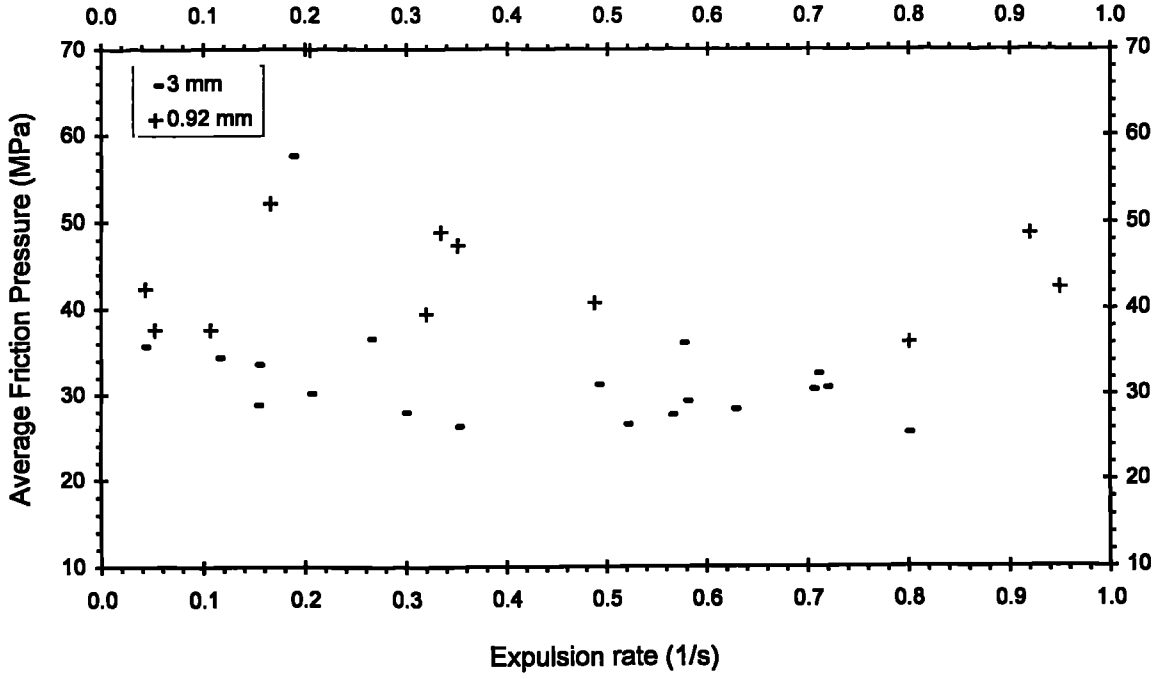

Figure 109 . Effect Of Average Friction Pressure On Expulsion Rate (For Two Amplitudes Of Oscillation)

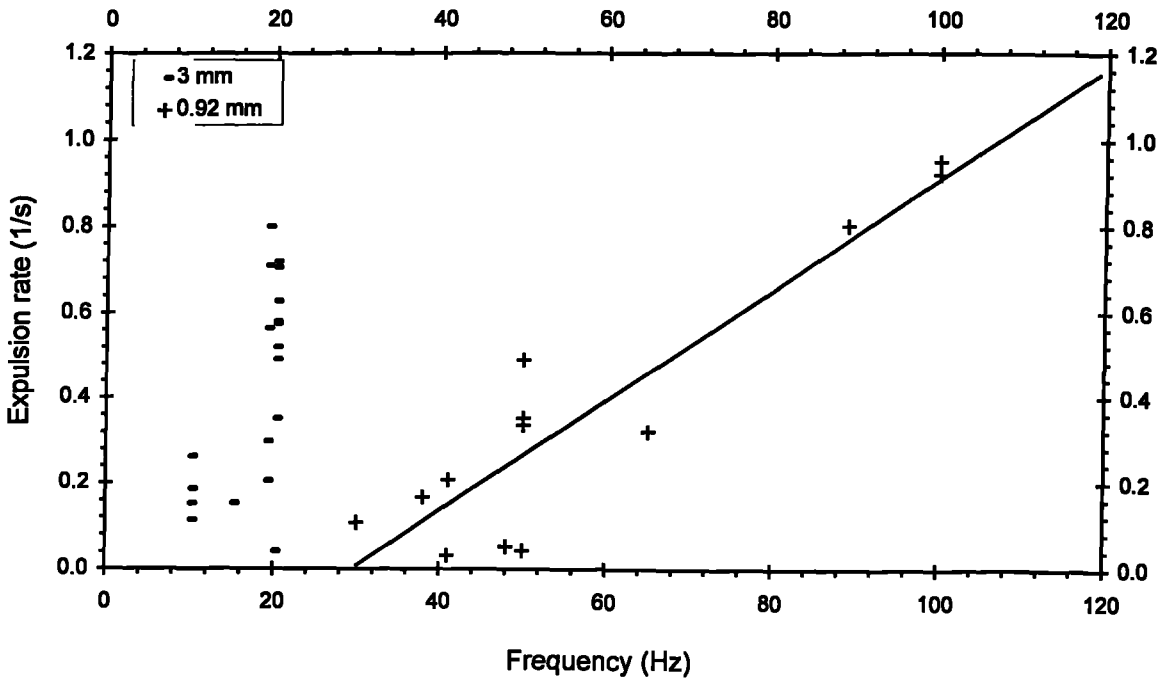

Figure 110 . Effect Of Frequency On Expulsion Rate (For Two Amplitudes Of Oscillation)

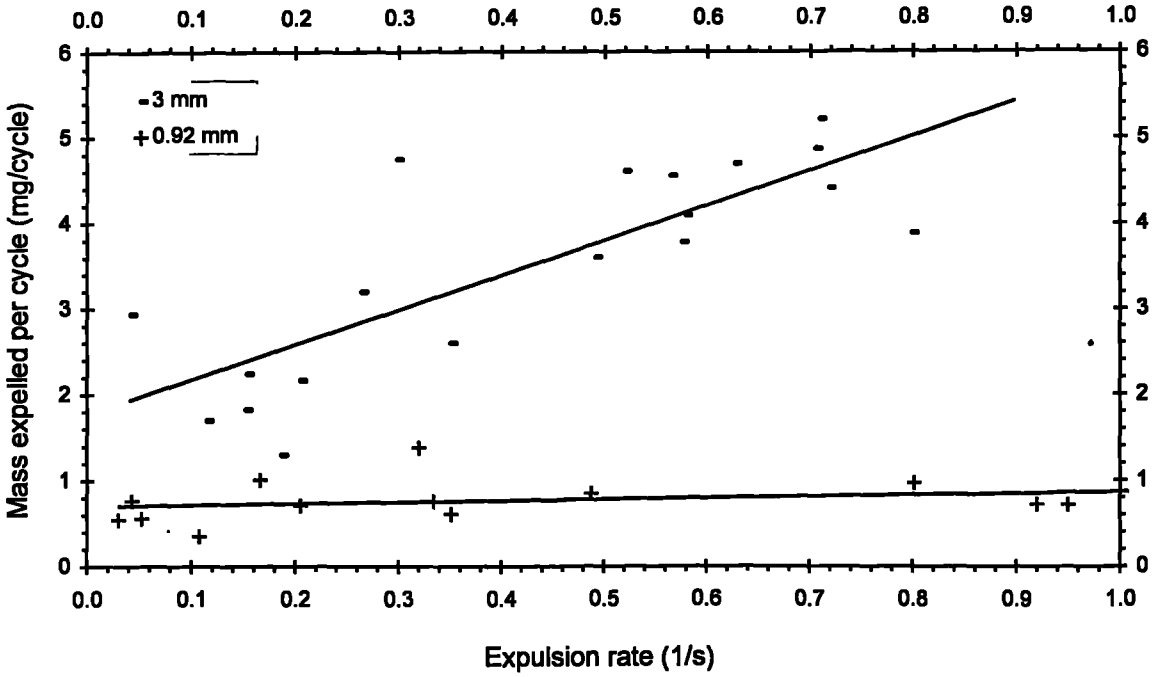

Figure 111 . Effect Of Mass Expelled Into Flash Per Cycle On Expulsion Rate (For Two Amplitudes Of Oscillation)

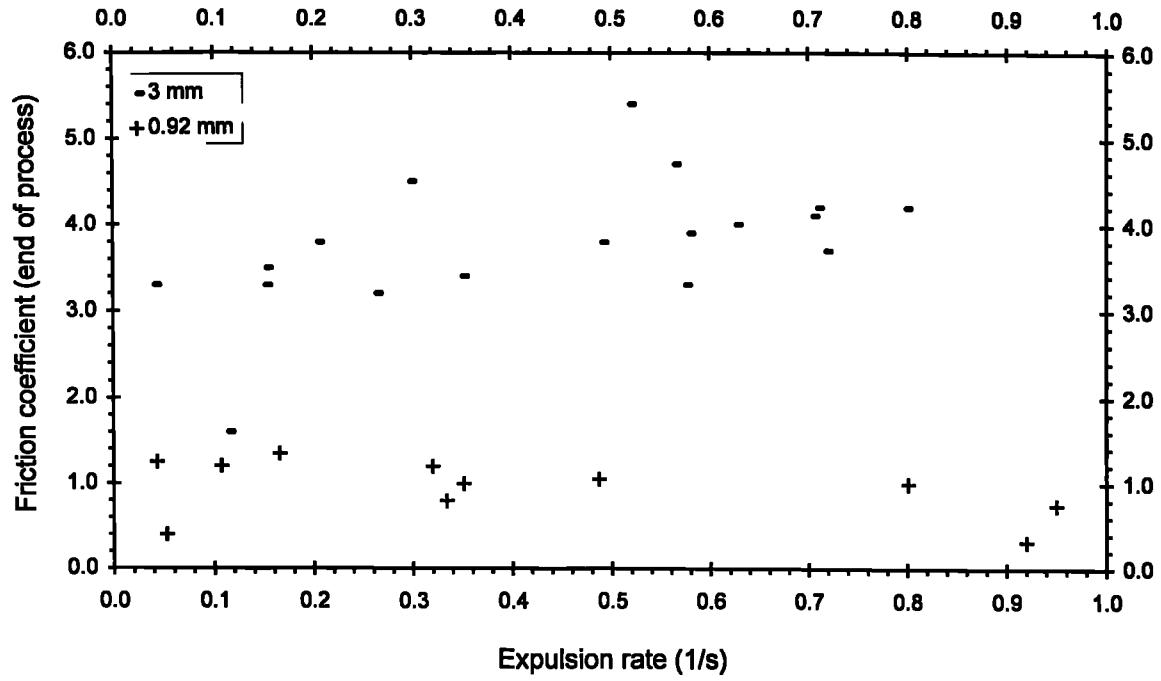

Figure 112 . Effect Of Friction Coefficient At The End Of The Process On The Expulsion Rate (For Two Amplitudes Of Oscillation)

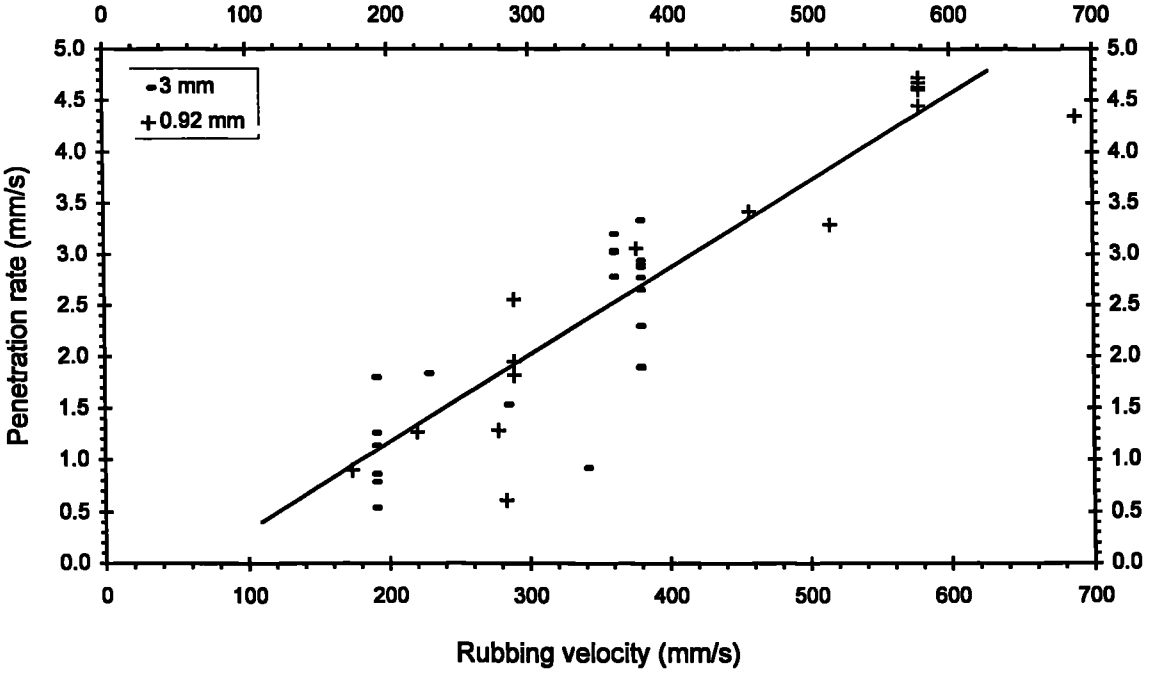

Figure 113 . Effect Of Rubbing Velocity On Penetration Rate During Extrusion (For Two Amplitudes Of Oscillation)

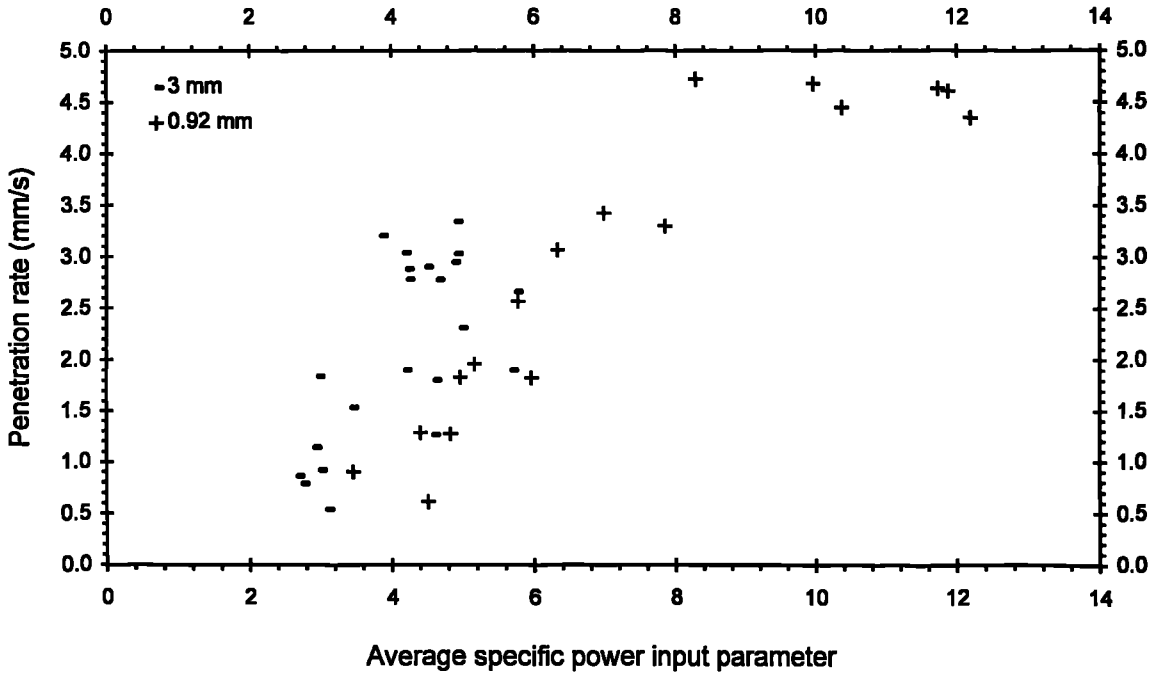

Figure 114 . Effect Of Average Power Input Parameter On Penetration Rate During Extrusion (For Two Amplitudes Of Oscillation)

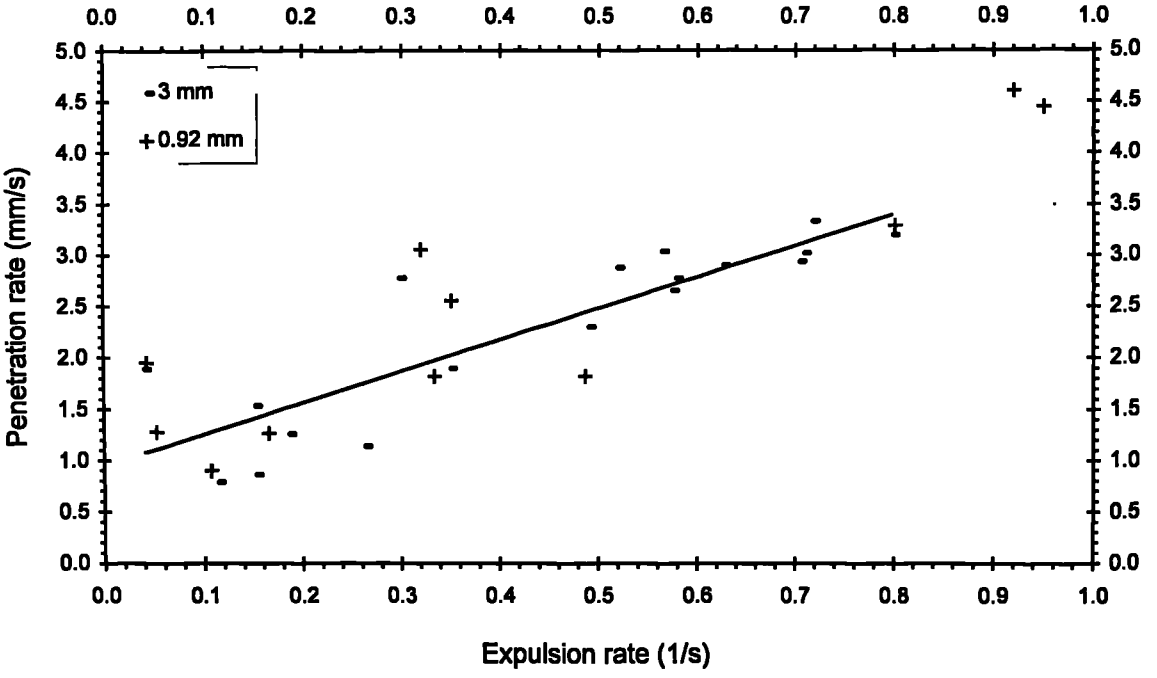

Figure 115 . Effect Of Penetration Rate During Extrusion On Expulsion Rate (For Two Amplitudes Of Oscillation)

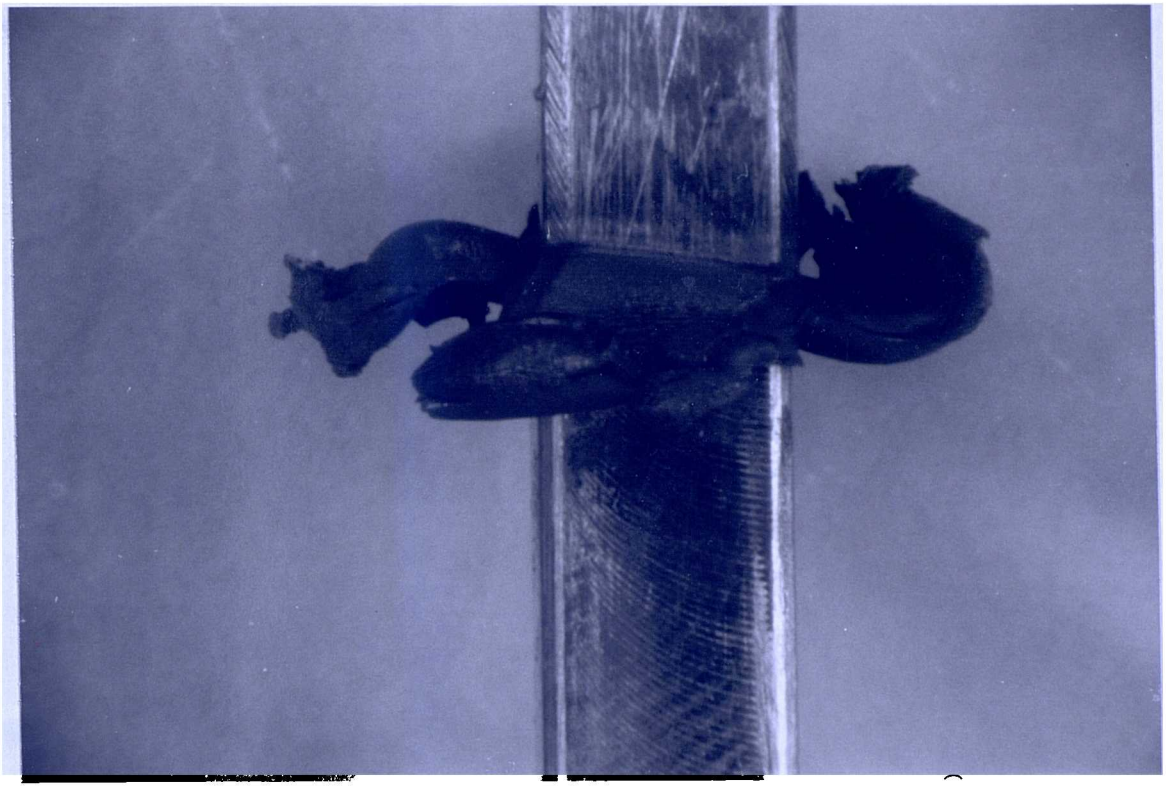

Figure 116 . Typical Linear Friction Weld (Ti 6Al 4V, α : 0.92 mm, f : 62 Hz, P_{fr} : 50.9 MPa - experiment D11)

Figure 117 . Detail Of Ridged Flash Of Linear Friction Weld (Ti 6Al 4V, α : 3 mm, f : 19 Hz, P_{fr} : 40.9 MPa - experiment A13)

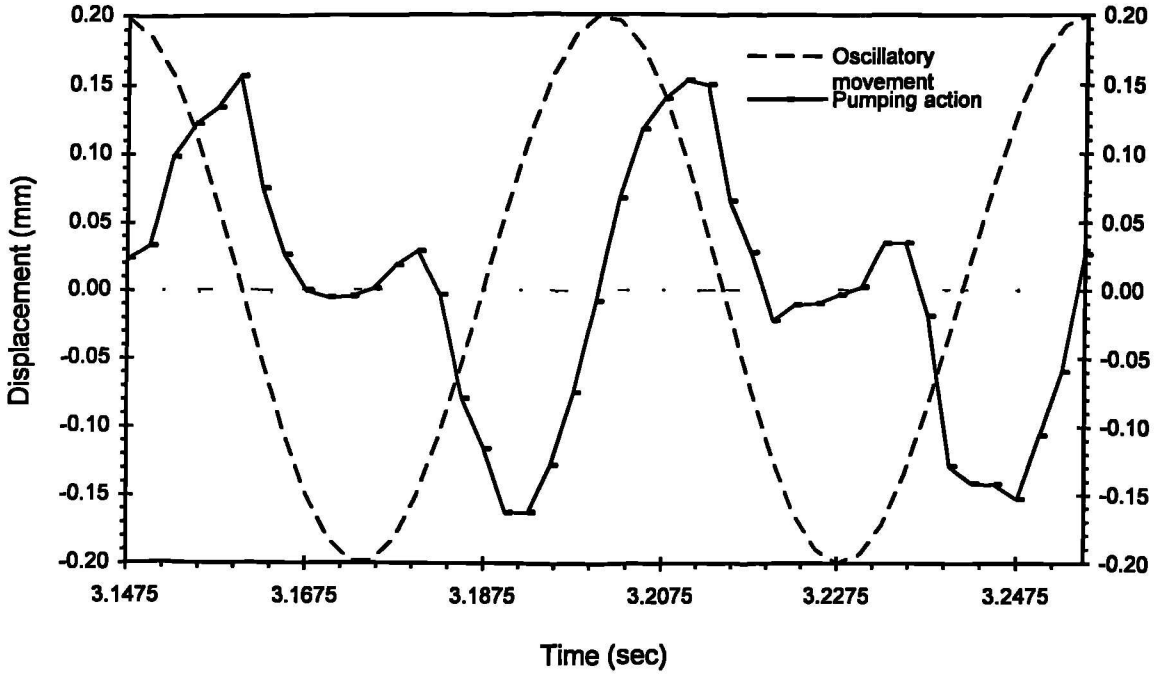

Figure 118 . Vibratory Movement Of Stationary Chuck (Direction : Perpendicular To Movement) (α : 3 mm, f = 19 Hz, P_{fr} : 40.9 MPa - experiment A13)

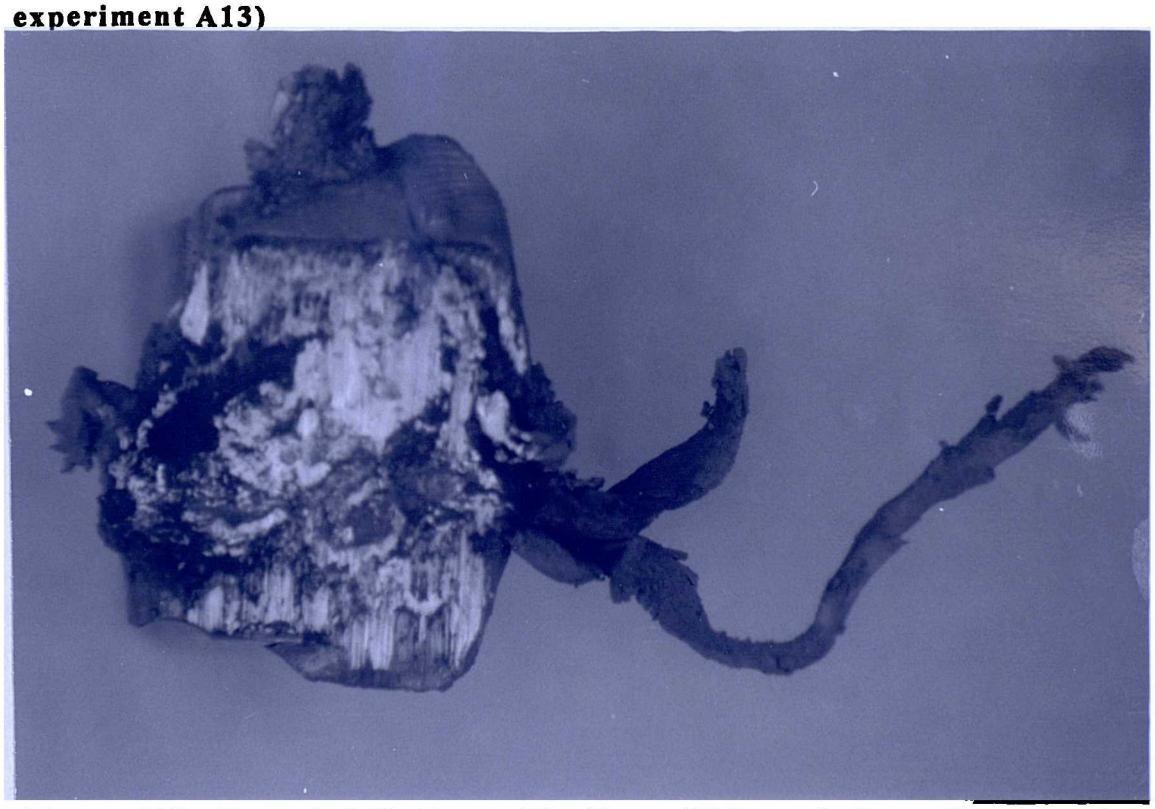

Figure 119 . Extruded Matter In The Form Of Strands From Unsuccessful Linear Friction Welds (Ti 6Al 4V, α : 0.92 mm, f : 29 Hz, P_{fr} : 45.7 MPa - experiment C2)

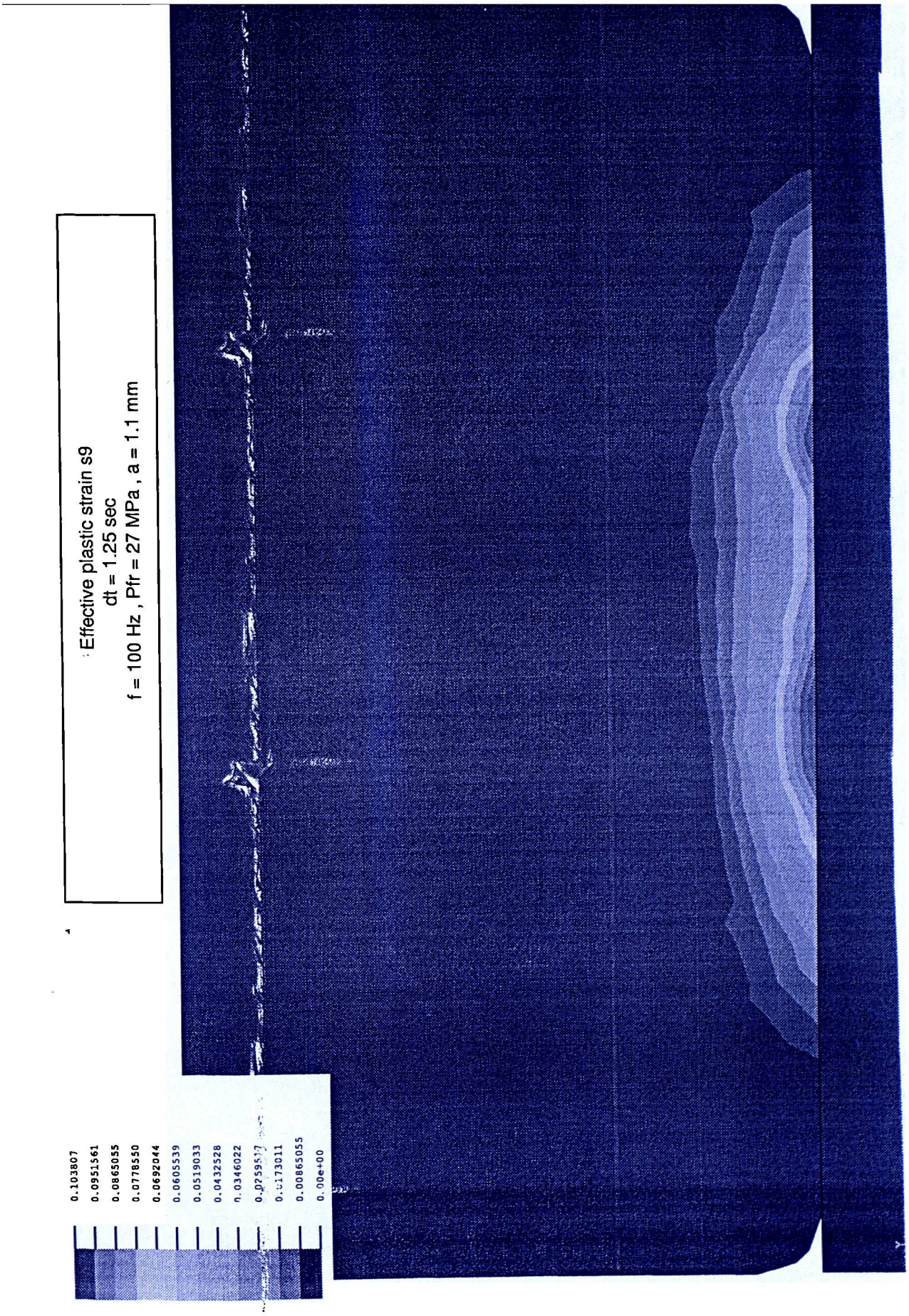

Figure 120 . Conditions Unfavourable To Linear Friction Welding (Finite Element Predictions)

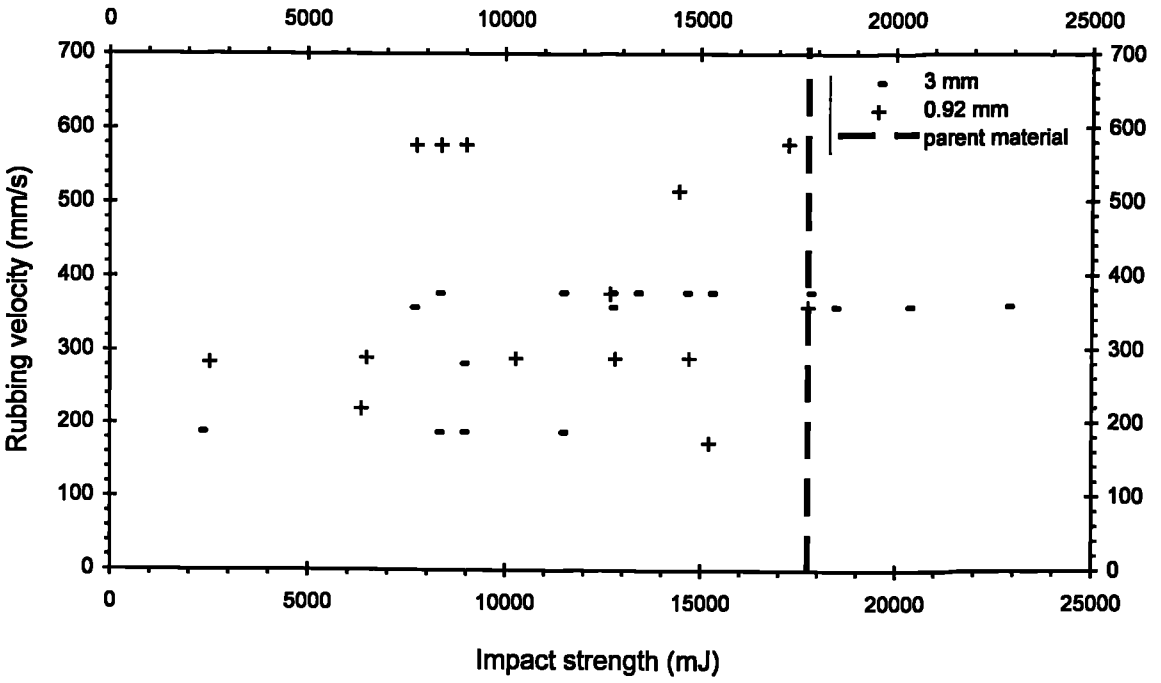

Figure 121 . Effect Of Rubbing Velocity On Impact Strength Of The Weld (For Two Amplitudes Of Oscillation)

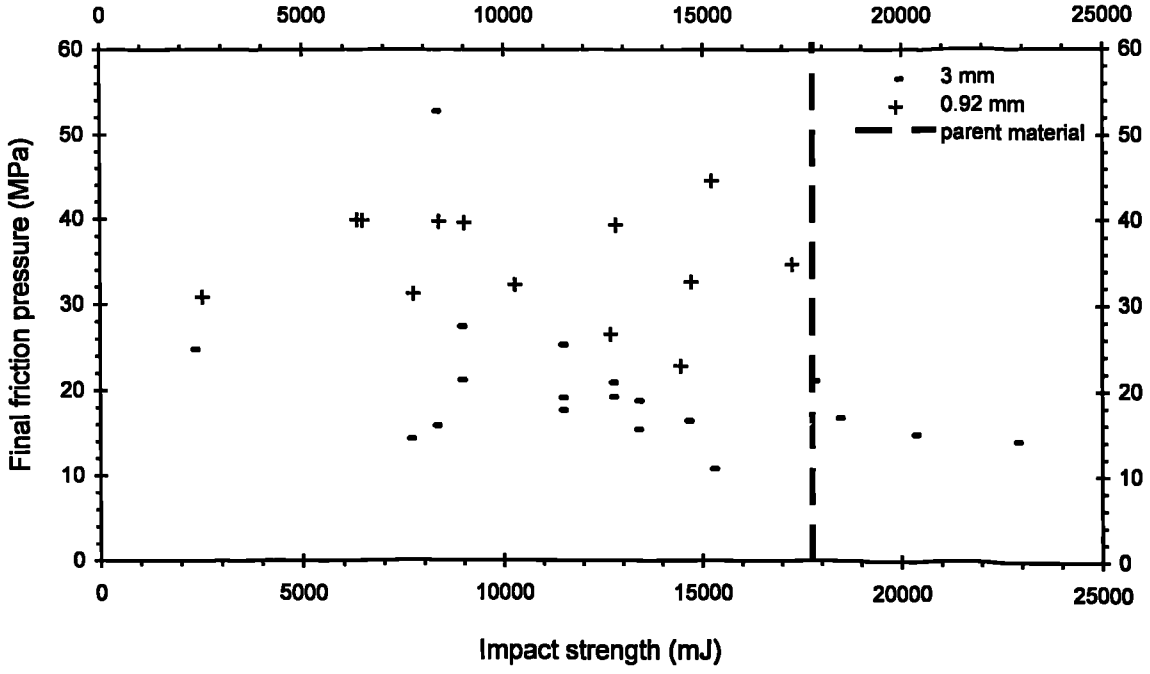

Figure 122 . Effect Of Final Friction Pressure On Impact Strength Of The Weld (For Two Amplitudes Of Oscillation)

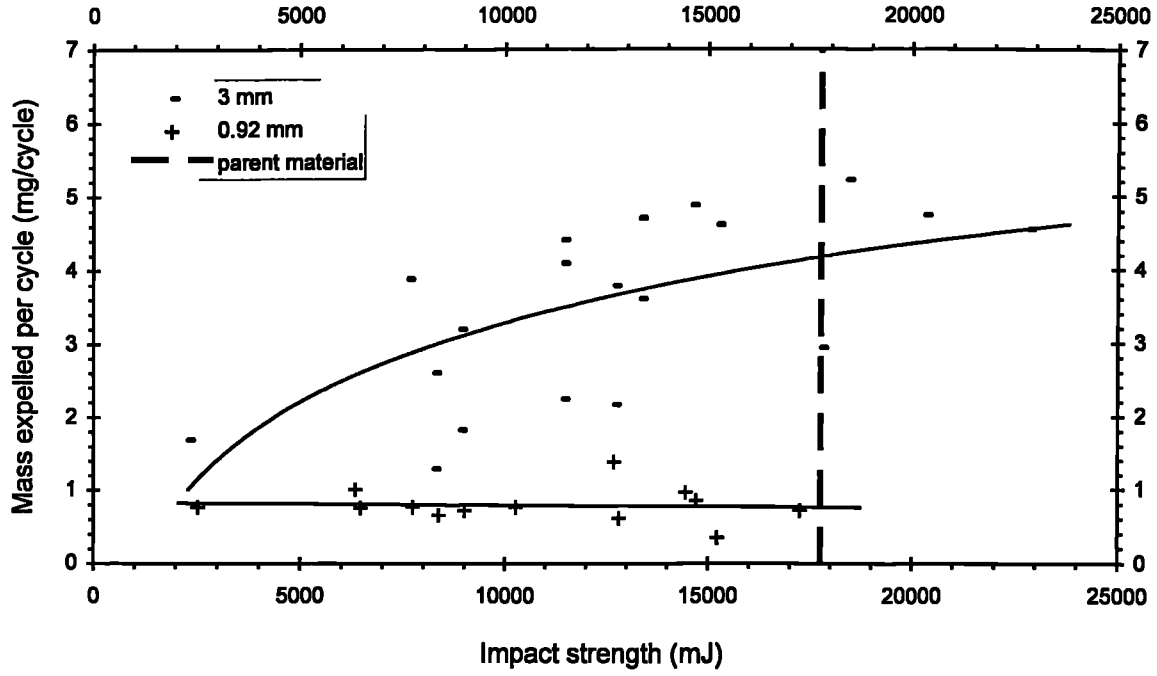

Figure 123 . Effect Of Mass Expelled Per Cycle Of Oscillation On Impact Strength Of The Weld (For Two Amplitudes Of Oscillation)

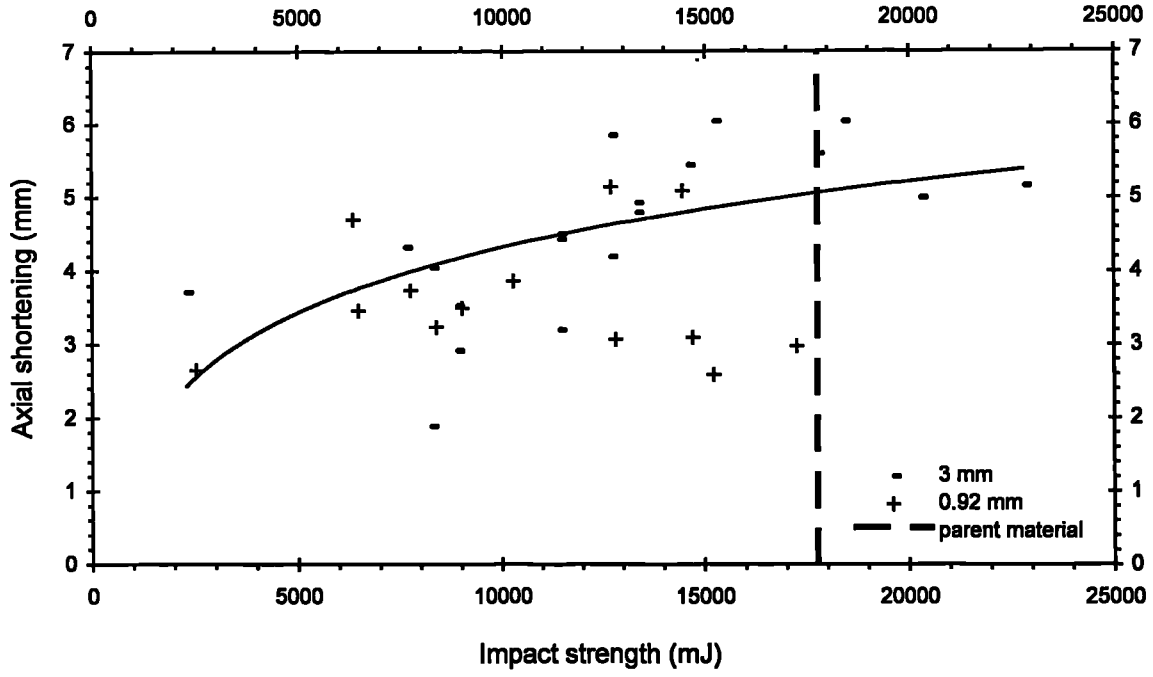

Figure 124 . Effect Of Axial Shortening On Impact Strength Of The Weld (For Two Amplitudes Of Oscillation)

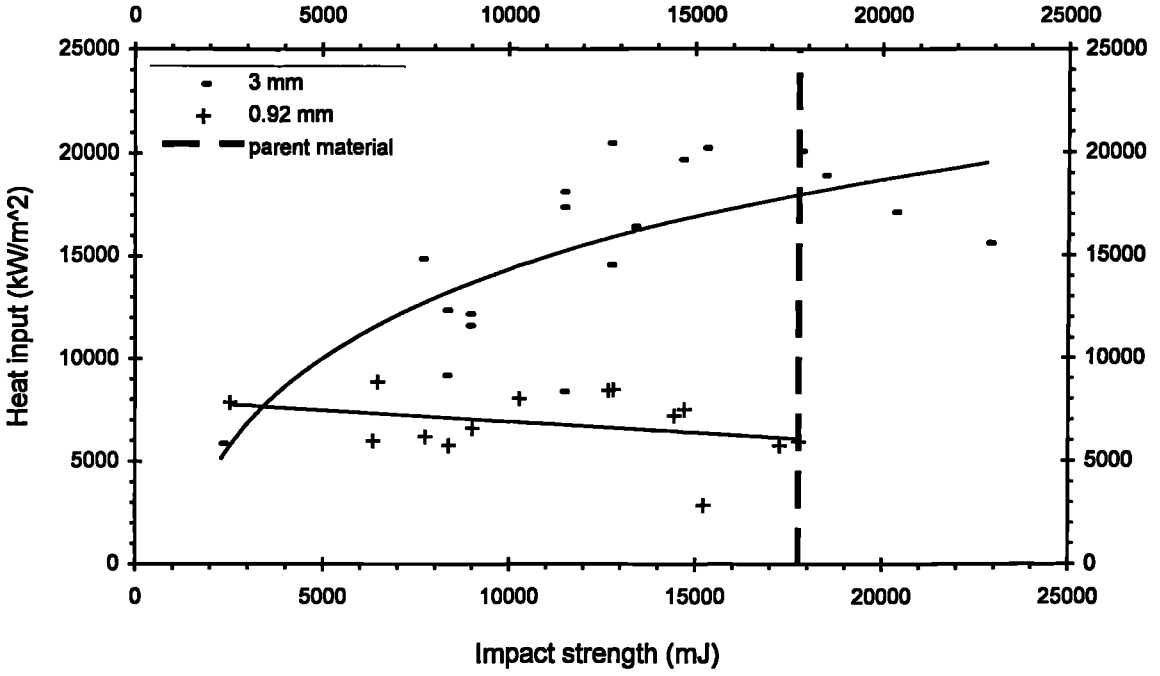

Figure 125 . Effect Of Heat Input During Initial Phase On Impact Strength Of The Weld (For Two Amplitudes Of Oscillation)

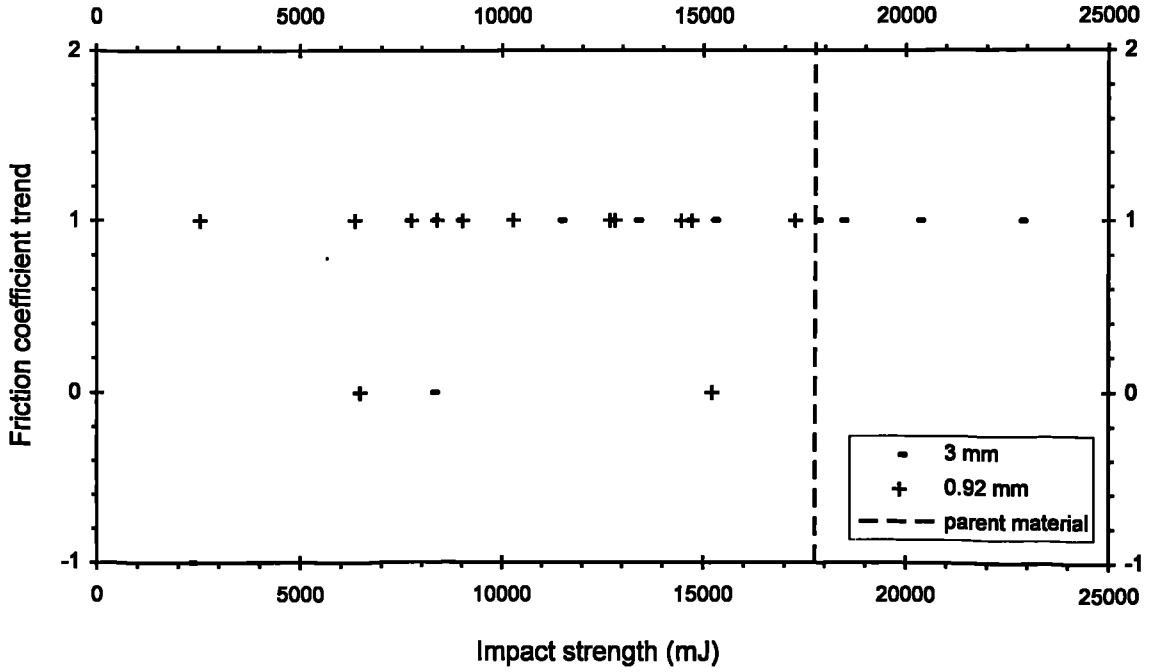

Figure 126 . Effect Of Friction Coefficient Trend During Phase III On Impact Strength Of The Weld (For Two Amplitudes Of Oscillation)

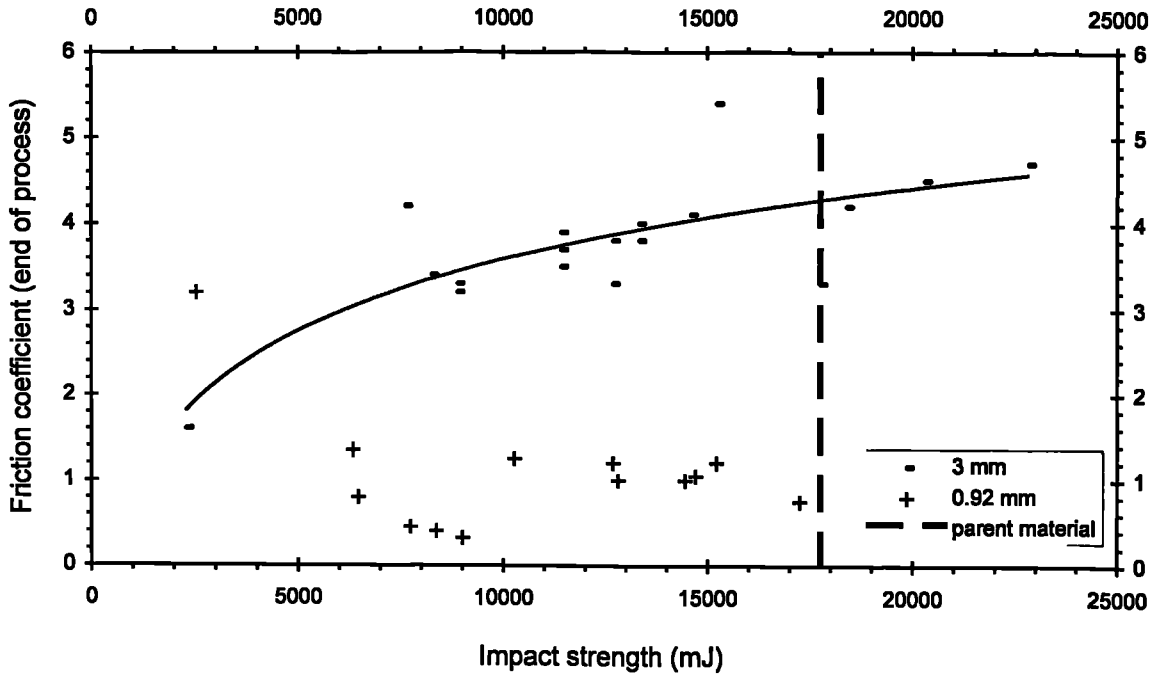

Figure 127 . Effect Of Friction Coefficient At The End Of The Process (End Of Phase III) On Impact Strength Of The Weld (For Two Amplitudes Of Oscillation)

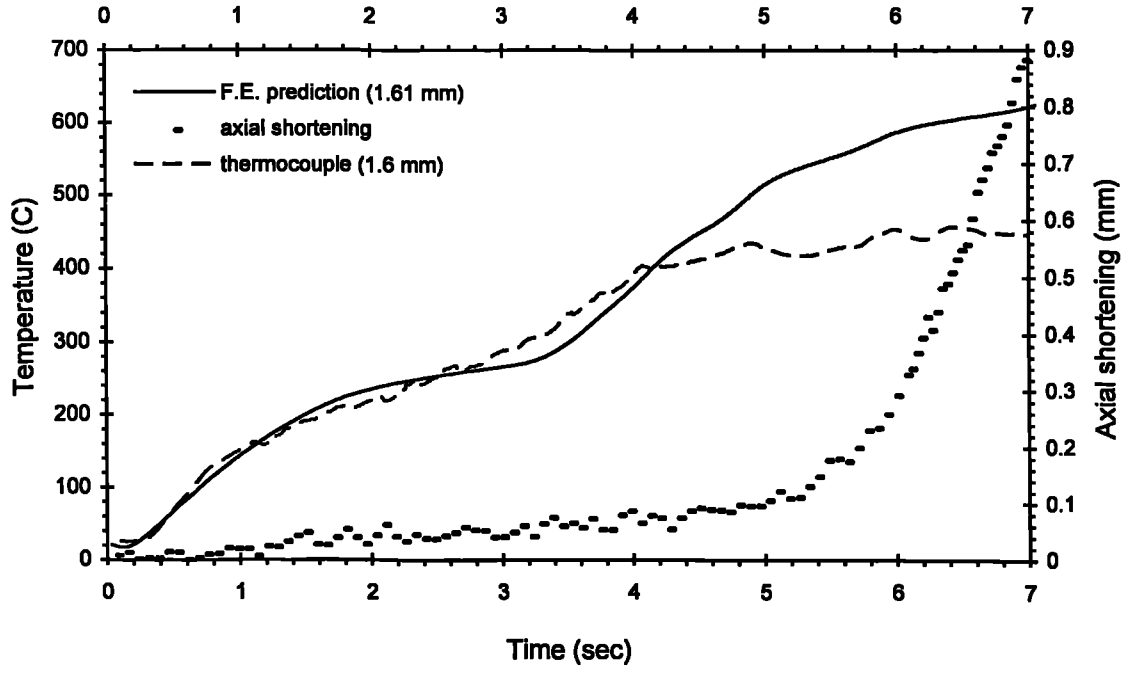

Figure 128 . Comparison Between Experimental And Finite Element Analysis Temperature Data (α = 0.92 mm, f = 30 Hz , P_{fr} = 58.1 MPa - experiment D1)

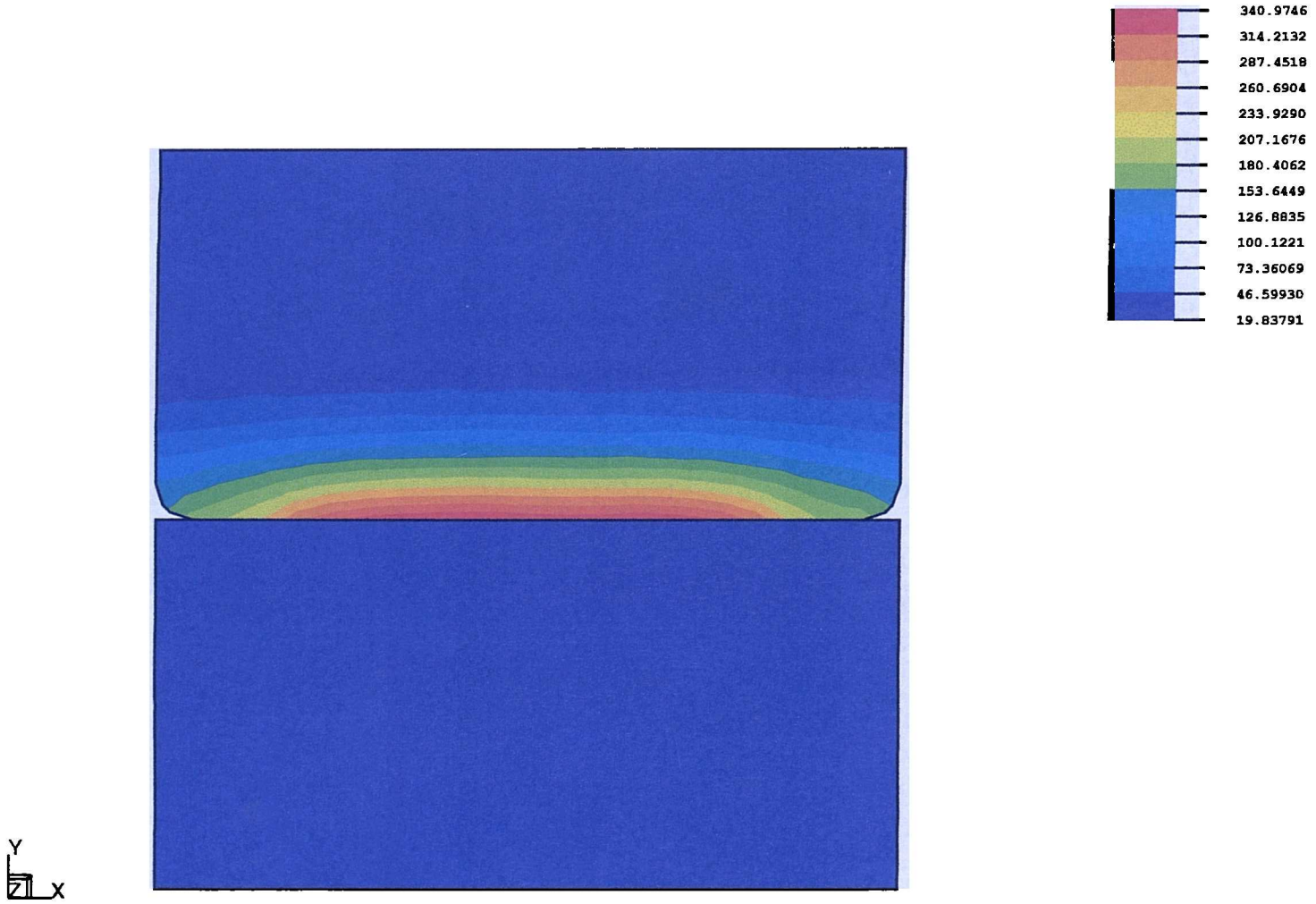

Figure 129. Finite Element Temperature Prediction At Time 1.03 sec
(α = 0.92 mm, f = 30 Hz, P_{fr} = 58.1MPa - experiment D1)

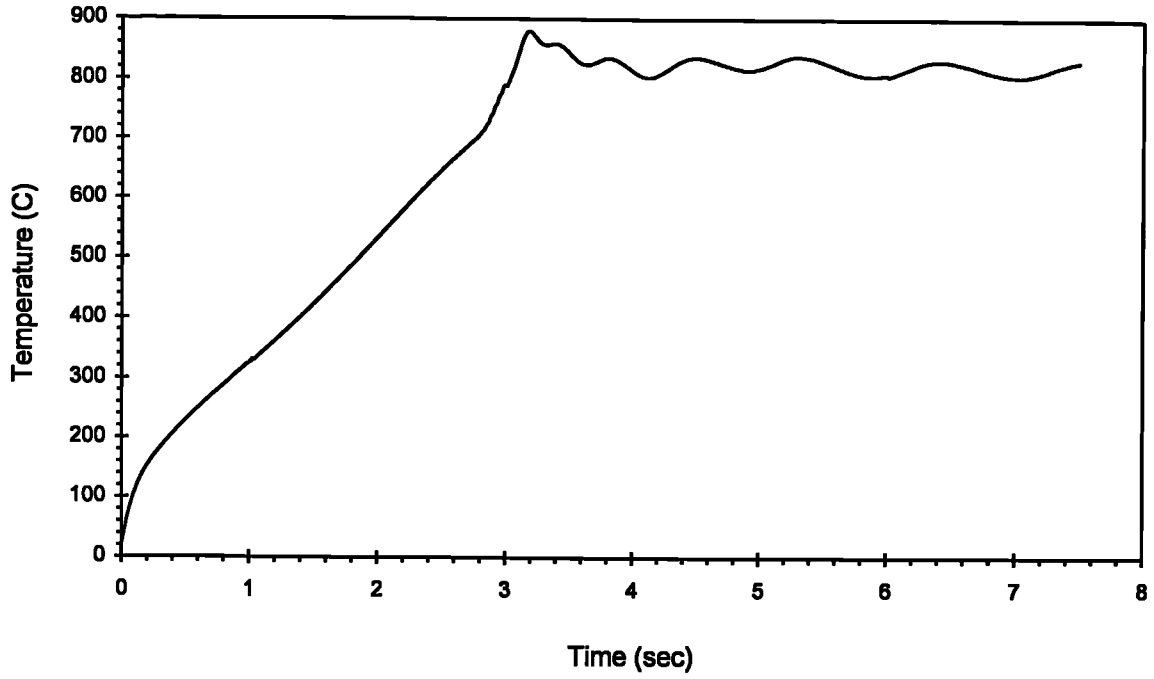

Figure 130 . Finite Element Analysis Temperature Prediction At Rubbing Interface (α = 0.92 mm, f = 30 Hz , P_{fr} = 58.1 MPa - experiment D1)

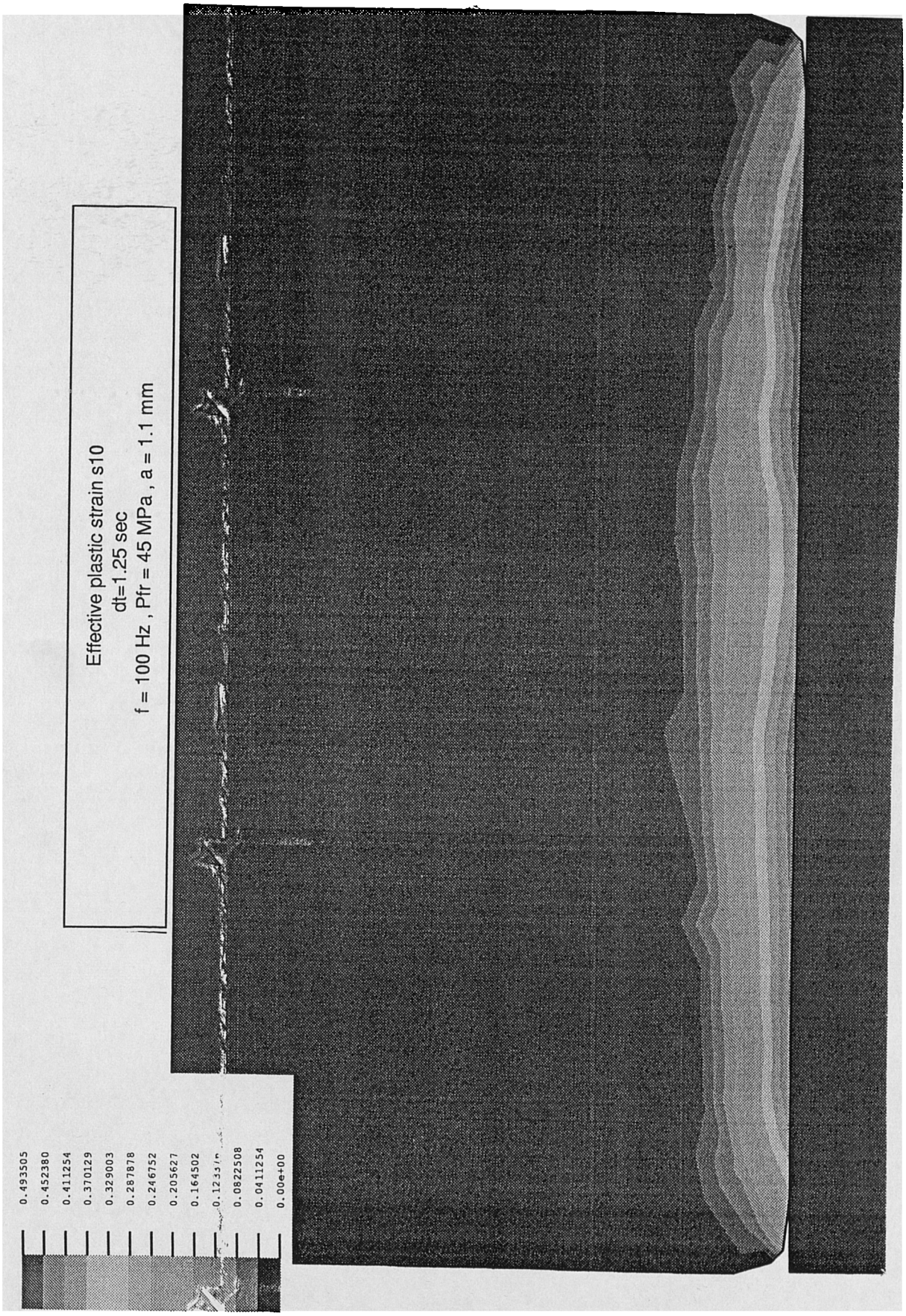

Figure 131 . Conditions Favourable To Linear Friction Welding (Finite Element Predictions)

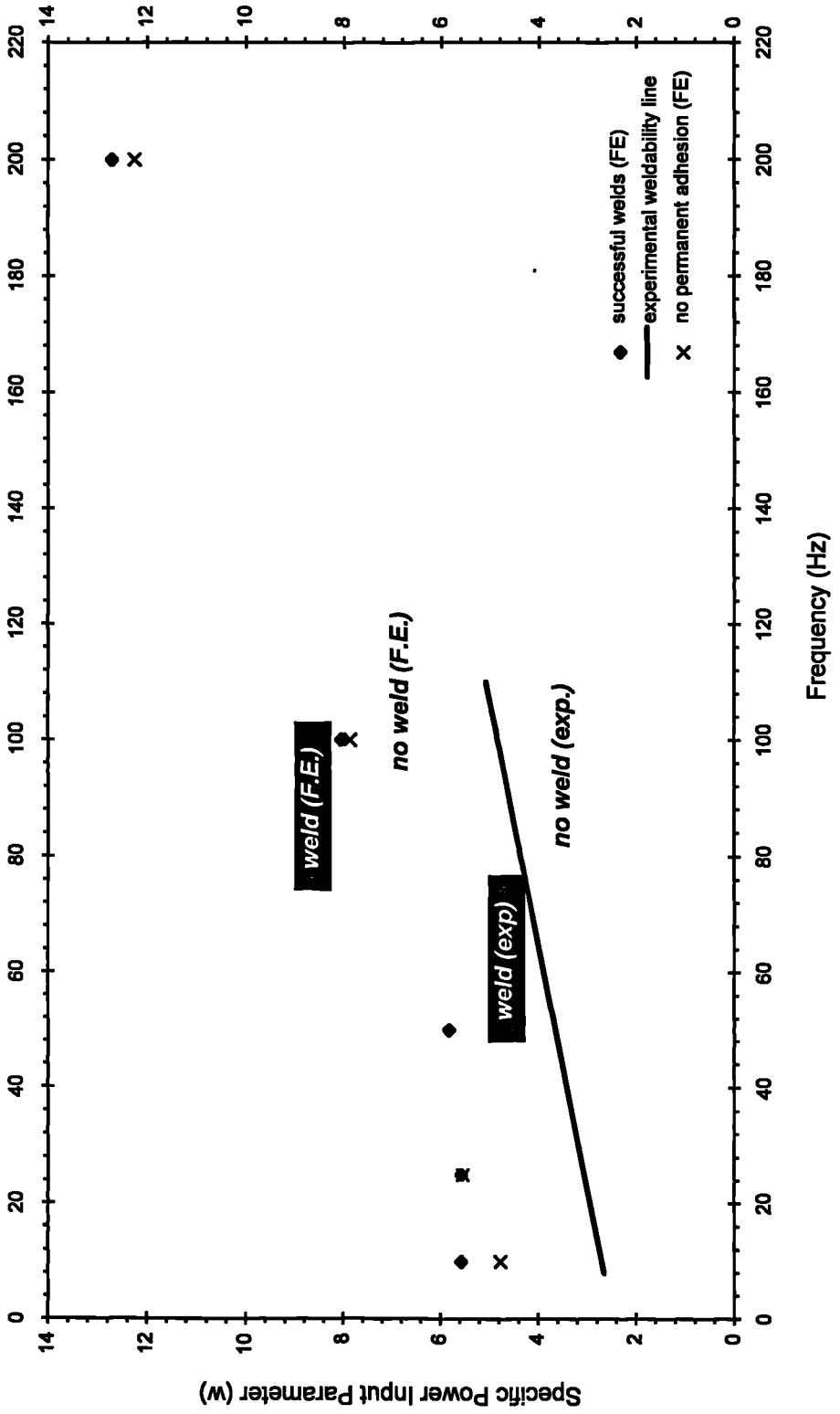

Figure 132 . Effect Of Frequency Of Oscillation On Minimum Power Input Parameter (W) Required To Achieve Welding Conditions (Finite Element Prediction)

$L_4(2^3)$

No.	1	2	3
1	1	1	1
2	1	2	2
3	2	1	2
4	2	2	1
	a	b	a b
Group	1	2	

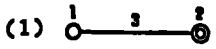

Figure 133 . L_4 Orthogonal Array Used For Fractional Factorial Experimental Designs And Linear Graph To Manipulate It (Taguchi,1986)